

UNCLASSIFIED

AD NUMBER
AD878040
NEW LIMITATION CHANGE
TO Approved for public release, distribution unlimited
FROM Distribution authorized to U.S. Gov't. agencies and their contractors; Critical Technology; OCT 1970. Other requests shall be referred to U.S. Army Aviation Materiel Laboratories, Fort Eustis, VA.
AUTHORITY
USAAMRDL ltr, 10 Sep 1971

THIS PAGE IS UNCLASSIFIED

AD No. _____
REC FILE COPY

AD878040



USAAVLABS TECHNICAL REPORT 70-34

A SMALL AXIAL-CENTRIFUGAL COMPRESSOR MATCHING STUDY PROGRAM

By

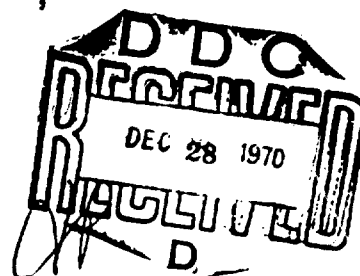
R. C. Pampreen

P. A. Firman

J. R. Erwin

R. W. Dawson

October 1970



**U. S. ARMY AVIATION MATERIEL LABORATORIES
FORT EUSTIS, VIRGINIA**

CONTRACT DAAJ02-69-C-0073...
AIRESEARCH MANUFACTURING COMPANY
DIVISION OF THE GARRETT CORPORATION
PHOENIX, ARIZONA

This document is subject to special export controls, and each transmittal to foreign governments or foreign nationals may be made only with prior approval of U.S. Army Aviation Materiel Laboratories, Fort Eustis, Virginia 23104.



Best Available Copy

DISCLAIMERS

The findings in this report are not to be construed as an official Department of the Army position unless so designated by other authorized documents.

When Government drawings, specifications, or other data are used for any purpose other than in connection with a definitely related Government procurement operation, the United States Government thereby incurs no responsibility nor any obligation whatsoever; and the fact that the Government may have formulated, furnished, or in any way supplied the said drawings, specifications, or other data is not to be regarded by implication or otherwise as in any manner licensing the holder or any other person or corporation, or conveying any rights or permission, to manufacture, use, or sell any patented invention that may in any way be related thereto.

DISPOSITION INSTRUCTIONS

Destroy this report when no longer needed. Do not return it to the originator.

ACCESSION NO.	
CPSTI	WHITE SECTION <input type="checkbox"/>
DOC	DIFF SECTION <input checked="" type="checkbox"/>
ALL	GER. <input type="checkbox"/>
NOTIFICATION	
BY	
DISTRIBUTION/AVAILABILITY CODES	
GENL.	AVAIL. RES. & SPECIAL
2	



DEPARTMENT OF THE ARMY
HEADQUARTERS US ARMY AVIATION MATERIEL LABORATORIES
FORT EUSTIS VIRGINIA 23604

The research described herein was conducted by the AiResearch Manufacturing Company, Phoenix, Arizona, under Contract DAAJ02-69-C-0073. The work was performed under the technical management of David B. Cale, Propulsion Division, U. S. Army Aviation Materiel Laboratories.

Appropriate technical personnel of this Command have reviewed this report and concur with the conclusions and recommendations contained herein.

The findings and recommendations outlined herein will be considered in planning subsequent axial/centrifugal research efforts.

Task 1G162203D14413
Contract DAAJ02-69-C-0073
USAAVLABS Technical Report 70-34
October 1970

A SMALL AXIAL-CENTRIFUGAL COMPRESSOR
MATCHING STUDY PROGRAM

Final Report

by

R. C. Pampreen
P. A. Firman
J. R. Erwin
R. E. Dawson

Prepared by

AiResearch Manufacturing Company
Division of The Garrett Corporation
Phoenix, Arizona

for

U.S. ARMY AVIATION MATERIEL LABORATORIES
FORT EUSTIS, VIRGINIA

This document is subject to special export controls,
and each transmittal to foreign governments or foreign
nationals may be made only with prior approval of U.S.
Army Aviation Materiel Laboratories, Fort Eustis,
Virginia 23604.

ABSTRACT

Engine cycle studies in which compressor component performance anticipated in 1973 was used were conducted to select operating conditions for a 3-pound-per-second front-drive gas turbine optimized for minimum specific fuel consumption (SFC) at 60-percent power. Fixed turbine geometry was assumed. Preliminary matching studies of seven combinations of axial and centrifugal compressor stages were conducted to accomplish cycle requirements for 20-, 30-, 60-, and 100-percent-power operation.

The compressor type selected--two axial stages employing variable inlet guide vanes plus one centrifugal stage--was configured in a preliminary design for application in a preliminary engine layout. Shaft mechanical design problems were encountered because of the small hub diameter of the first axial stage and the shaft length required. A compressor consisting of a single axial stage with variable inlet guide vanes and a fixed-geometry single-stage centrifugal compressor was configured and incorporated in a preliminary engine layout. Component and overall compressor maps were calculated for this configuration. The performance of an engine employing this compressor was calculated over the 20- to 100-percent-power range. Comparisons were made between matched component, compressor, and engine performance with simplified, idealized compressor and engine performance.

The results of this study indicated that a cycle pressure ratio of 10.5:1 at 60-percent power was optimum for a turbo-shaft engine of the above design requirements. The matching problem was concentrated in extending the operating airflow range of the axial compressor, whether single-stage or two-stage. Variable inlet guide vanes provide the best solution to the matching problem. The matching problem was unaffected by the choice of maximum turbine inlet temperature, so 2500°F was selected on the basis of minimum SFC and maximum specific power. An engine having a single-stage axial and a single-stage centrifugal as the compressor combination offers an SFC of 0.492 at 60-percent power (475 horsepower). With a two-stage axial and a single-stage centrifugal as the compressor combination, the calculated SFC at 60-percent power is 0.479.

FOREWORD

The study program reported herein was performed under contract to the U.S. Army Aviation Materiel Laboratories (USAAVLABS), Contract DAAJ02-69-C-0073 (Task 1G162203D14413). The program was conducted by the AiResearch Manufacturing Company, a division of The Garrett Corporation, during the period of June 1, 1969, to December 31, 1969.

Mr. David Cale was the technical representative for USAAVLABS.

The responsibility of the co-authors was as delineated below. Mr. R. C. Pamphreen, senior engineering specialist, served as the principal aerodynamic investigator and performed the compressor preliminary design and matching computations. Mr. P. A. Firman, senior engineering specialist, served as an aerodynamic investigator and performed the engine cycle studies. Mr. J. R. Erwin supervised the aerodynamic activities and performed the inlet guide vane analysis. Mr. R. E. Dawson, assistant project engineer, served as the program manager.

The authors wish to acknowledge the following AiResearch personnel:

Mr. F. Weber, project engineer, who contributed direction and support to the program as supervisor of advanced technology, Aircraft Propulsion Engines.

Mr. R. O. Bullock, chief of Aero/Thermo, who contributed guidance and support to the program.

Mr. J. G. Castor, project engineer, who contributed direction and support during the final phases of the program.

TABLE OF CONTENTS

	<u>Page</u>
ABSTRACT	iii
FOREWORD	v
LIST OF ILLUSTRATIONS	xi
LIST OF TABLES	xvi
LIST OF SYMBOLS	xviii
 1. INTRODUCTION	 1
1.1 General	1
1.2 Assumed Engine	1
1.3 Program Logic	1
1.3.1 Task IA - Engine Cycle Analysis, Tentative	 2
1.3.2 Task IIA - Compressor Design and Matching, Tentative	 2
1.3.3 Task IB - Engine Cycle Analysis	2
1.3.4 Task IIB - Compressor Design and Matching	 2
1.3.5 Task III - Compressor Performance Predictions	 2
1.3.6 Task IV - Engine Performance Predictions	 3
 2. TASK IA, ENGINE CYCLE ANALYSIS (TENTATIVE)	 4
2.1 General	4
2.2 Design-Point Cycle Assumptions	4
2.2.1 Compressor Performance Estimates (Design-Point)	 4
2.2.1.1 Single-Stage Axial Compressors	 7
2.2.1.2 Two-Stage Axial Compressors	 9
2.2.1.3 Single-Stage Centrifugal Compressors	 9

TABLE OF CONTENTS (Contd)

	<u>Page</u>
2.2.1.4 Multistage Axial-Centrifugal Compressors	13
2.2.2 Tentative Compressor Selection, AA + C Versus A + C	16
2.3 Design-Point Analysis	21
2.4 Off-Design Cycle Assumptions	26
2.5 Off-Design Analysis	27
3. TASK IIA, PRELIMINARY DESIGN AND MATCHING (TENTATIVE)	33
3.1 General	33
3.2 Preliminary Design of Axial and Centrifugal Compressors	33
3.2.1 Two-Stage Axial Compressor Design, $P_3/P_1 = 2.02:1$	35
3.2.2 Centrifugal Compressor Design, $P_4/P_3 = 5.1:1$	36
3.3 Compressor Matching Studies, AA + C, $P_4/P_1 = 9.5:1$	38
3.3.1 Initial Studies	38
3.3.2 Evaluation of Matching Schemes	44
3.3.2.1 Single Spool, AAFG + CFG	46
3.3.2.2 Single Spool, AAFG + CVDV	51
3.3.2.3 Single Spool, AAFG + CVIGV.	52
3.3.2.4 Single Spool, AAVIGV + CFG.	61
3.3.2.5 Single Spool, AAVIGV + CVIGV.	69
3.3.2.6 Single Spool, AAVIGV + C (VIGV + VDV).	74
3.3.2.7 Twin Spool, AAFG + CFG	81
3.3.2.8 Selection of Matching Scheme.	86
3.4 Compressor Design and Matching, AAVIGV + CFG, $P_4/P_1 = 10.5:1$	87
3.5 Compressor Design and Matching, AAVIGV + CFG, $P_4/P_1 = 11.5:1$	88
4. TASK IB, ENGINE CYCLE ANALYSIS	
4.1 General	93
4.2 Cycle Assumptions	93

TABLE OF CONTENTS (Contd)

	<u>Page</u>
4.3 Compressor Matching Studies, $P_4/P_1 = 9.5:1$	93
4.4 Selection of Optimum Cycle Pressure Ratio . . .	97
4.5 Estimated Engine Operating Line	98
5. TASK IIB, COMPRESSOR DESIGN AND MATCHING	103
5.1 General	103
5.2 Aerodynamic Design and Matching, AAVIGV + CFG ($P_4/P_1 = 10.5:1$)	103
5.2.1 Two-Stage Axial Compressor Matching . .	104
5.2.2 Preswirl Angle Estimation	105
5.2.3 Two-Stage Axial Compressor Design ($P_3/P_1 = 2.05:1$)	107
5.2.4 Centrifugal Compressor Design ($P_4/P_3 = 5.1:1$)	111
5.2.5 Compressor Matching	114
5.2.6 Engine Conceptual Design Considerations	115
5.3 Cycle Considerations for A + C Compressor	116
5.3.1 Aerodynamic Design Requirements, A + C Compressor	116
5.3.1.1 Validation Analyses for A + C Compressor, $P_4/P_1 = 10.5:1$. .	117
5.3.2 Matching Scheme, A + C Compressor . . .	117
5.4 Aerodynamic Design and Matching, AVIGV + CFG ($P_4/P_1 = 10.5:1$)	120
5.4.1 Preswirl Angle Estimation	120
5.4.2 Single-Stage Axial Compressor Design ($P_3/P_1 = 1.48$)	120
5.4.3 Centrifugal Compressor Design ($P_4/P_3 = 7.1:1$)	121
5.4.4 Compressor Matching, AVIGV + CFG	124
5.5 Conceptual Design of Compressor and Engine . .	124
5.5.1 Mechanical Analyses for Compressor Rotors	129

TABLE OF CONTENTS (Contd)

	Page
5.5.2 Mechanical Analyses for Engine Shafting	129
6. TASK III, COMPRESSOR PERFORMANCE PREDICTION	137
6.1 Data Display.	137
6.2 Discussion	137
7. TASK IV, ENGINE PERFORMANCE PREDICTION	150
7.1 General	150
7.2 Calculation Procedure	150
7.3 Overall Compressor Performance	151
7.4 Gasifier Turbine Performance	151
7.5 Power Turbine Performance	152
7.6 Engine Performance	152
8. CONCLUSIONS AND RECOMMENDATIONS	155
8.1 General	155
8.2 Conclusions	155
8.3 Recommendations	157
9. LITERATURE CITED	158
 APPENDIX I -- CYCLE ASSUMPTIONS FOR ENGINE DESIGN-POINT ANALYSIS	 159
APPENDIX II -- CYCLE ASSUMPTIONS FOR ENGINE OFF-DESIGN ANALYSIS	 161
APPENDIX III -- ENGINE CYCLE RELATIONSHIPS	167
APPENDIX IV -- INLET GUIDE VANE ANALYSIS	181
DISTRIBUTION	183

LIST OF ILLUSTRATIONS

<u>Figure</u>		<u>Page</u>
1	Program Logic Diagram	5
2	Single-Stage Axial Compressor Efficiency Estimates	8
3	Two-Stage Axial Compressor Efficiency Estimates	10
4	Single-Stage Centrifugal Compressor Polytropic Efficiency Estimates	11
5	Variation of Overall Efficiency and Work Split for Two-Stage Axial Plus Single-Stage Centrifugal Compressor, Current Technology	15
6	Single-Stage Axial Plus Single-Stage Centrifugal Compressor Efficiency Estimates .	17
7	Two-Stage Axial Plus Single-Stage Centrifugal Compressor Efficiency Estimates	19
8	Design-Point Engine Performance, 0-Percent Cooling Flow	22
9	Design-Point Engine Performance, 3-Percent Cooling Flow	23
10	Design-Point Engine Performance, 6-Percent Cooling Flow	24
11	Design-Point Engine Performance, 9-Percent Cooling Flow	25
12	Engine Off-Design Performance: Speed and Flow Versus Design Pressure Ratio	28
13	Engine Off-Design Performance: Pressure Ratio Versus Design Pressure Ratio	29
14	Engine Off-Design Performance: Turbine Inlet Temperature and Specific Fuel Consumption Versus Design Pressure Ratio	30

LIST OF ILLUSTRATIONS (Contd)

<u>Figure</u>		<u>Page</u>
15	Engine Operating Lines (Tentative Compressor Requirements)	32
16	Design Study for Centrifugal Stage of 9.5:1-Pressure-Ratio Compressor: Blade Exit Angle, Stage Efficiency, and Diffusion Factor	37
17	Design Study for Centrifugal Stage of 9.5:1-Pressure-Ratio Compressor: Clearance Loss, Rotor Tip Radius, and Rotor Exit Width	39
18	Illustration of Match Points on Compressor Maps	41
19	Estimated Performance Characteristics, Two-Stage Axial Plus Centrifugal Compressor (Includes No Efficiency Degradation), AAFG + CFG	47
20	Estimated Performance Characteristics, Two-Stage Axial Plus Centrifugal Compressor (Includes No Efficiency Degradation Due to CVDV's), AAFG + CVDV	53
21	Estimated Performance Characteristics, Two-Stage Axial Plus Centrifugal Compressor (No Efficiency Degradation Due to CVIGV), AAFG + CVIGV	57
22	Estimated Performance Characteristics, Two-Stage Axial Plus Centrifugal Compressor (Includes Efficiency Degradation Due to CVIGV), AAFG + CVIGV	59
23	Estimated Performance Characteristics, Two-Stage Axial Plus Centrifugal Compressor (Includes No Efficiency Degradation Due to AAVIGV), AAVIGV + CFG	63
24	Estimated Performance Characteristics, Two-Stage Axial Plus Centrifugal Compressor (Includes Efficiency Degradation Due to AAVIGV), AAVIGV + CFG	67

LIST OF ILLUSTRATIONS (Contd)

<u>Figure</u>		<u>Page</u>
25	Estimated Performance Characteristics, Two-Stage Axial Plus Centrifugal Compressor (Includes No Efficiency Degradation Due to AAVIGV and CVIGV), AAVIGV + CVIGV	71
26	Estimated Performance Characteristics, Two-Stage Axial Plus Centrifugal Compressor (Includes Efficiency Degradation Due to AAVIGV and CVIGV), AAVIGV + CVIGV	75
27	Estimated Performance Characteristics, Two-Stage Axial Plus Centrifugal Compressor (Includes Efficiency Degradation Due to AAVIGV + CVIGV), AAVIGV + CVIGV + CVDV	79
28	Estimated Performance Characteristics, Two-Stage Axial Plus Centrifugal Compressor, (Includes No Efficiency Degradation), Twin Spool - AAFG + CFG	83
29	Estimated Performance Characteristics, Two-Stage Axial Plus Centrifugal Compressor. Design-Point Overall Pressure Ratio = 10.5 (No Efficiency Degradation Due to AAVIGV), AAVIGV + CFG	89
30	Estimated Performance Characteristics, Two-Stage Axial Plus Centrifugal Compressor. Design-Point Overall Pressure Ratio = 11.5 (No Efficiency Degradation Due to AAVIGV), AAVIGV + CFG	91
31	Engine Off-Design Performance: Specific Fuel Consumption and Turbine Inlet Temperature Versus Design Pressure Ratio	101
32	Engine Operating Line (Tentative Compressor Requirements).	102
33	Pressure-Ratio/Flow-Ratio Characteristics for Various Amounts of Preswirl	108
34	First-Stage Stator Hub Inlet Vector Diagram Comparison	110

LIST OF ILLUSTRATIONS (Contd)

<u>Figure</u>		<u>Page</u>
35	Compressor Flow Path, Two-Stage Axial Plus Centrifugal Compressor, AAVIGV + CFG . .	113
36	Idealized Compressor Map, Nondimensionalized From A + C Data	118
37	Engine Off-Design Performance: Comparison With A + C and AA + C Compressors	119
38	Compressor Flow Path, Single-Stage Axial Plus Centrifugal Compressor, AVIGV + CFG	123
39	Engine Conceptual Layout	127
40	Elemental Model of Axial and Centrifugal Compressor Rotors	130
41	Power-Shaft Dynamic Analysis	133
42	Power-Shaft Radial Spline and Bearing Loads .	135
43	Compressor Flow Path, Single-Stage Axial Plus Centrifugal Compressor, AVIGV + CFG . . .	138
44	Estimated Performance Characteristics, One-Stage Axial Plus Centrifugal Compressor, AVIGV + CFG.	139
45	Compressor Vector Diagrams, 30-Percent Power	141
46	Compressor Vector Diagrams, 60-Percent Power	143
47	Compressor Vector Diagrams, 100-Percent Power	145
48	Compressor Map Comparison	148
49	Engine Performance Parametric Plots	153
50	Turbine Design-Point Efficiency Versus Engine Cycle Pressure Ratio	160

LIST OF ILLUSTRATIONS (Concluded)

<u>Figure</u>		<u>Page</u>
51	Gasifier Turbine Map	162
52	Power Turbine Map	163
53	Idealized Compressor Map, Nondimensionalized From AA + C Data.	164
54	Combustion Efficiency Map, Nondimensionalized	166
55	Typical Turbine Efficiency/ Pressure-Ratio Characteristic	169
56	Variation of the Ratio $c \cdot \text{Power}$ Turbine Work Ratio at $T_g = 2000^\circ\text{F}$ to Work Ratio at $T_g = X$ With Design Point Turbine Inlet Temperature for $1600^\circ\text{F} < x < 2200^\circ\text{F}$	179

LIST OF TABLES

<u>TABLE</u>		<u>Page</u>
I	Qualitative Comparison of Axial-Centrifugal Compressors, AA + C Versus A + C	16
II	Comparison of Compressor Performance (A + C Versus AA + C)	34
III	AAFG + CFG Compressor	50
IV	AAFG + CFG Compressor (Reduced T_5)	50
V	AAFG + CVDV Compressor	52
VI	AAFG + CVIGV Compressor ($\eta_C = \eta_{C, \text{DESIGN}}$)	56
VII	AAFG + CVIGV Compressor ($\eta_{CC} = 0.945 \eta_{CC, \text{DESIGN}}$ for CVIGV $\neq 0^\circ$)	61
VIII	AAVIGV + CFG Compressor ($\eta_C = \eta_{C, \text{DESIGN}}$)	65
IX	AAVIGV + CFG Compressor ($\eta_{AX} = 0.945 \eta_{AX, \text{DESIGN}}$ for AAVIGV $\neq 0^\circ$)	69
X	AAVIGV + CVIGV Compressor ($\eta_C = \eta_{C, \text{DESIGN}}$)	73
XI	AAVIGV + CVIGV Compressor ($\eta_{AX-CC} = 0.945 \eta_{AX-CC, \text{DESIGN}}$ for AAVIGV + CVIGV $\neq 0^\circ$)	74
XII	AAVIGV + C (VIGV + VDV) Compressor ($\eta_{AX-CC} = 0.945 \eta_{AX-CC, \text{DESIGN}}$ for AAVIGV, CVIGV, and CVDV $\neq 0^\circ$)	78
XIII	Twin-Spool Compressor, AAFG + CFG ($\eta_{HPT} = \eta_{LPT} = \eta_{GT, \text{DESIGN}}$)	82
XIV	Twin-Spool Compressor, AAFG + CFG ($\eta_{HPT} = \eta_{GT, \text{DESIGN}}$; $\eta_{LPT} = 0.96 \eta_{GT, \text{DESIGN}}$)	85
XV	Engine Cycle Data (Calculated) Compressor Matching Studies	95

LIST OF TABLES (Contd)

<u>TABLE</u>		<u>Page</u>
XVI	Engine Cycle Data (Calculated) Cycle Pressure- Ratio Study	99
XVII	Summary of Design Matching Results (AAVIGV)	105
XVIII	Aerodynamic Data Summary for Two-Stage Axial Compressor	112
XIX	Aerodynamic Data Summary for a Centrifugal Compressor Designed To Match With a Two- Stage Axial Compressor	114
XX	Aerodynamic Data Summary for One-Stage Axial Compressor	122
XXI	Aerodynamic Data Summary for Centrifugal Compressor Designed To Match With One- Stage Axial Compressor	124
XXII	Engine Cycle Data (Calculated), AAVIGV + CFG Compressor Matching Results	125
XXIII	Mechanical Analysis for Compressor Rotors . .	131
XIV	Mechanical Analysis Data for Selected Elements of Compressor Rotors	132

LIST OF SYMBOLS

- A - area, sq ft
- C - constant of proportionality
- C_p - specific heat at constant pressure, Btu per lb per °R
- g - gravitational acceleration, ft per sec²
- h - static enthalpy, Btu per lb
- H - stagnation enthalpy, Btu per lb
- ΔH - actual enthalpy rise, Btu per lb
- $\Delta H'$ - ideal enthalpy rise, Btu per lb
- J - mechanical equivalent of heat, ft-lb per Btu
- K - work coefficient
- N - rotational speed, rpm
- N_s - specific speed, old definition (rev per min)
(ft^{3/4} per sec^{1/2})*
- N'_s - specific speed, new definition (rev per min)
(ft^{3/4} per sec^{1/2})*
- P - total pressure, lb per sq ft
- p - static pressure, lb per sq ft
- Q - volume flow rate, cu ft per sec
- R - radius, ft
- s - entropy, Btu per lb per °R
- t - static temperature, °R
- T' - temperature for ideal enthalpy rise, °R
- T - total temperature, °R

*The dimension of specific speed is a result of the mass unit for ΔH per lb being pounds weight instead of slugs. If slug mass units were used, specific speed would be dimensionless.

LIST OF SYMBOLS (Contd)

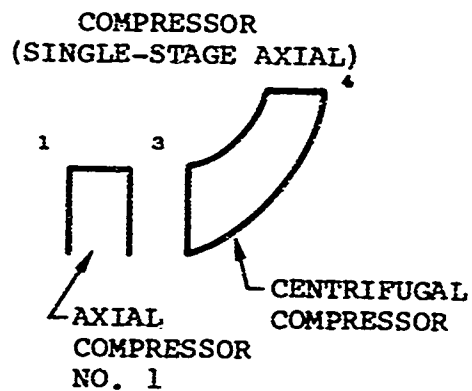
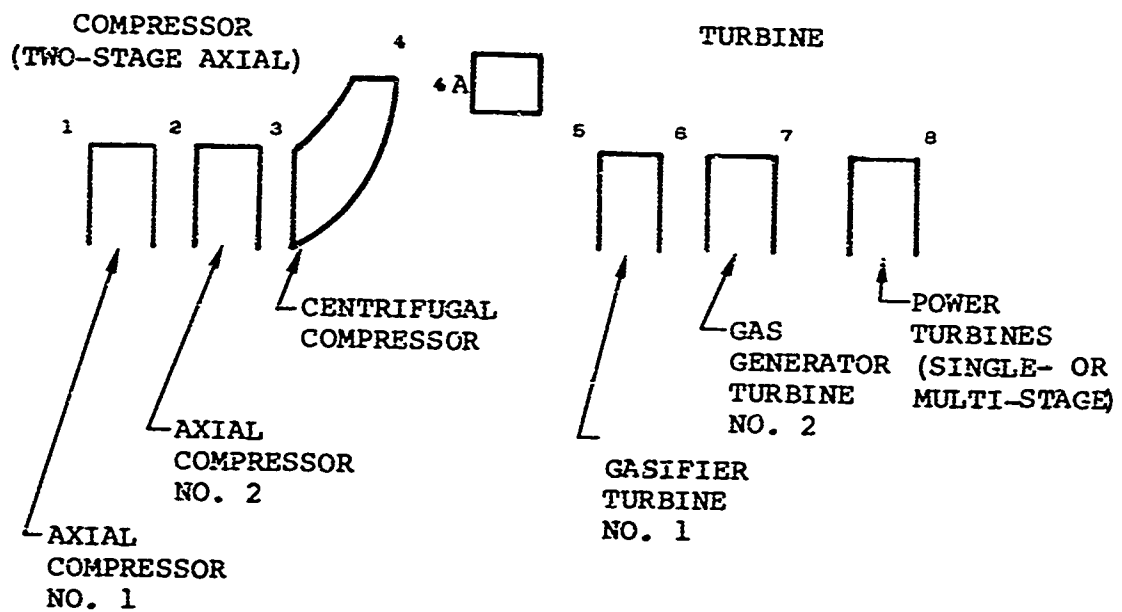
U - peripheral velocity, ft per sec
 V - absolute velocity, ft per sec
 W - flow rate, lb per sec
 W' - relative velocity, ft per sec
 β_g - preswirl angle, deg
 β - relative air angle, deg
 γ - ratio of specific heat, C_p/C_v
 δ - P/P_1
 η_C - compressor adiabatic efficiency
 η_T - turbine adiabatic efficiency
 η_P - polytropic efficiency based on stagnation properties
 η_P^s - polytropic efficiency based on static properties
 η_{CP} - compressor polytropic efficiency
 η_{TP} - turbine polytropic efficiency
 θ - T/T_1
 λ - blockage
 μ - slip factor
 ρ' - density, slugs per cu ft
 ρ - specific weight, lb per cu ft

Subscripts

100 - 100% power	L - leakage
60 - 50% power	LF - low-pressure spool
30 - 30% power	PT - power turbine
20 - 20% power	r - radial direction
acc - accessory	s - static
AX - axial compressor	st ₁ - stage one
C - compressor	st ₂ - stage two
CC - centrifugal compressor	T - turbine
DP - design point	t - total
GT - gasifier turbine	z - axial direction
HP - high-pressure spool	θ - tangential direction

LIST OF SYMBOLS (Contd)

STATION IDENTIFICATION



1. INTRODUCTION

1.1 GENERAL

This report describes the work accomplished and the analytical results achieved on a small axial-centrifugal compressor matching study program. This matching program was conducted to achieve a useful combination of advanced axial-centrifugal compressor stages for maximum efficiency operation at conditions representing engine part load. The analytical results of this program as reported herein better define the nature of the axial-centrifugal compressor matching problem, identify promising matching schemes, and determine the optimum cycle parameters for an assumed engine.

1.2 ASSUMED ENGINE

To provide a basis for this matching study, an engine was defined and can be summarized as a front-drive turboshaft engine, with advanced components reflecting performance levels considered to be achievable within a 3-year development period. The engine was sized for 3-pound-per-second airflow, and the turbine inlet temperature for 100-percent power was selected to be 2500°F. The turbine employs fixed geometry and includes an air-cooled gasifier section and a free-power-turbine section. All engine components, including the axial/centrifugal compressors, were configured to achieve minimum specific fuel consumption for 60-percent power (first priority) and 30-percent power (second priority).

1.3 PROGRAM LOGIC

This program has been conducted in four tasks, I through IV. Tasks I and II included major efforts of an iterative nature for tentative analyses, A, and for final analyses, B, for a total of six major program activities. These program activities were conducted and are reported as outlined below and as shown on the program logic diagram, Figure 1.

TASK IA - ENGINE CYCLE ANALYSIS - TENTATIVE
TASK IIA - COMPRESSOR DESIGN AND MATCHING - TENTATIVE
TASK IB - ENGINE CYCLE ANALYSIS
TASK IIB - COMPRESSOR DESIGN AND MATCHING
TASK III - COMPRESSOR PERFORMANCE PREDICTION
TASK IV - ENGINE PERFORMANCE PREDICTION

A brief description of these tasks is presented in the following subparagraphs.

1.3.1 Task IA - Engine Cycle Analysis, Tentative

Design-point cycle assumptions, including axial-centrifugal compressor efficiencies, were projected 3 years. Design-point analysis was conducted and selection was made for off-design analyses (P_4/P_1 at 60-percent power = 9:1, 10:1, 11:1, 12:1, 13:1, and 14:1).

An idealized compressor map and component maps were estimated. Off-design analyses were conducted. Design-point pressure ratios were tentatively selected to be 9.5:1, 10.5:1, and 11.5:1. Compressor cycle requirements were estimated for these cases.

1.3.2 Task IIA - Compressor Design and Matching, Tentative

Aerodynamic design and compressor matching studies were conducted for 9.5:1 two-stage axial (AA) and single-stage centrifugal compressors (C). Seven matching combinations were compared, and the best was tentatively selected to be a single-spool compressor (SS) with variable inlet guide vanes (VIGV) for axial compressor and fixed geometry (FG) for a centrifugal compressor (AAVIGV + CFG). Aerodynamic design and compressor matching were conducted for 10.5:1 and 11.5:1 compressors with the selected AAVIGV + CFG matching combination.

1.3.3 Task IB - Engine Cycle Analysis

Engine cycle analysis was conducted based on cycle assumptions from Task IA, except that compressor performance is from Task IIA. Optimum design-point pressure ratio was selected to be $P_4/P_1 = 10.5:1$ and compressor cycle requirements were estimated.

1.3.4 Task IIB - Compressor Design and Matching

Pursuant to the design of the selected compressor (AAVIGV + CFG, P_4/P_1 at 60-percent power = 10.5:1), initial iterations were conducted to establish the aerodynamic design, matching, and mechanical configuration. Based on the results of these initial design iterations, a design redirection was determined to finalize the design of an AVIGV + CFG compressor (P_4/P_1 at 60-percent power = 10.5:1).

1.3.5 Task III - Compressor Performance Predictions

Compressor performance predictions for the final compressor are displayed; axial and centrifugal tip-velocity triangles are shown for 30-, 60-, and 100-percent-power points.

1.3.6 Task IV - Engine Performance Predictions

Engine cycle analysis was conducted based on cycle assumptions from Task IA and final compressor design ($P_4/P_1 = 10.5$, AVICV + CFG). Data are displayed as listed in Figure 1.

2. TASK 1A, ENGINE CYCLE ANALYSIS (TENTATIVE)

2.1 GENERAL

Engine cycle analyses were conducted to select the best combination of cycle pressure ratio and turbine inlet temperature for minimum SFC at the 60-percent-power (first priority) and 30-percent-power (second priority) points. Analyses included design and off-design operation for an assumed engine with advanced components.

The engine configuration selected for study was a front-drive turboshaft engine with a free turbine. Fixed turbine geometry was assumed. The engine was sized for 3.0 pounds per second airflow at the 60-percent-power point designated for this study as the design point. The 100-percent-power point was defined for operation at 2500°F turbine inlet temperature (TIT).

2.2 DESIGN-POINT CYCLE ASSUMPTIONS

Design-point cycle assumptions were estimated to reflect advanced technology achievable within a 3-year development period.

Component and overall compressor performance estimates for design-point operation were made as reported in Paragraph 2.2.1. All other cycle assumptions were made as summarized in Appendix I of this report. Together, these estimates form the basis of the design-point analyses conducted for this program.

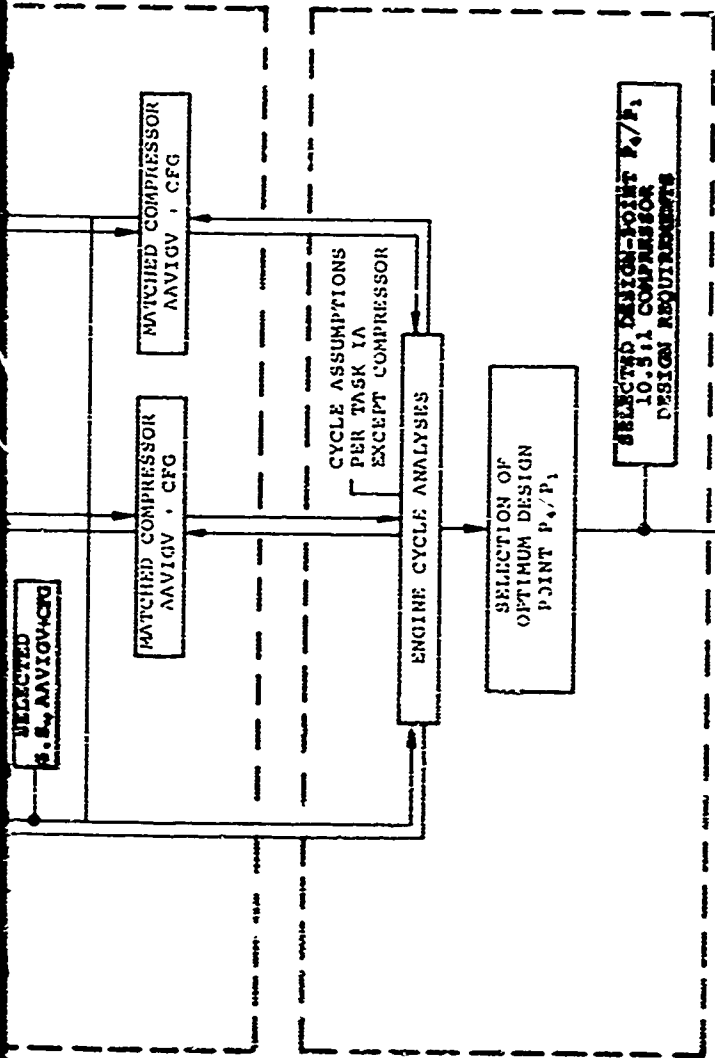
2.2.1 Compressor Performance Estimates (Design-Point)

Overall compressor efficiency estimates were made based on current technology and on advanced technology projection considered to be achievable within a 3-year development period. This study was completed for the two multistage compressor configurations of interest in this program--a single-stage axial plus single-stage centrifugal configuration, and a two-stage axial plus single-stage centrifugal configuration. The component performance estimates are based on examination of test data and advanced technology projections for single-stage axial, two-stage axial, and single-stage centrifugal compressors, as reported in the following subparagraphs. The overall compressor efficiency levels are based on the axial and centrifugal compressor predictions, with optimum matching assumed for peak efficiency operation of all compressor stages for all design-point pressure ratios considered.

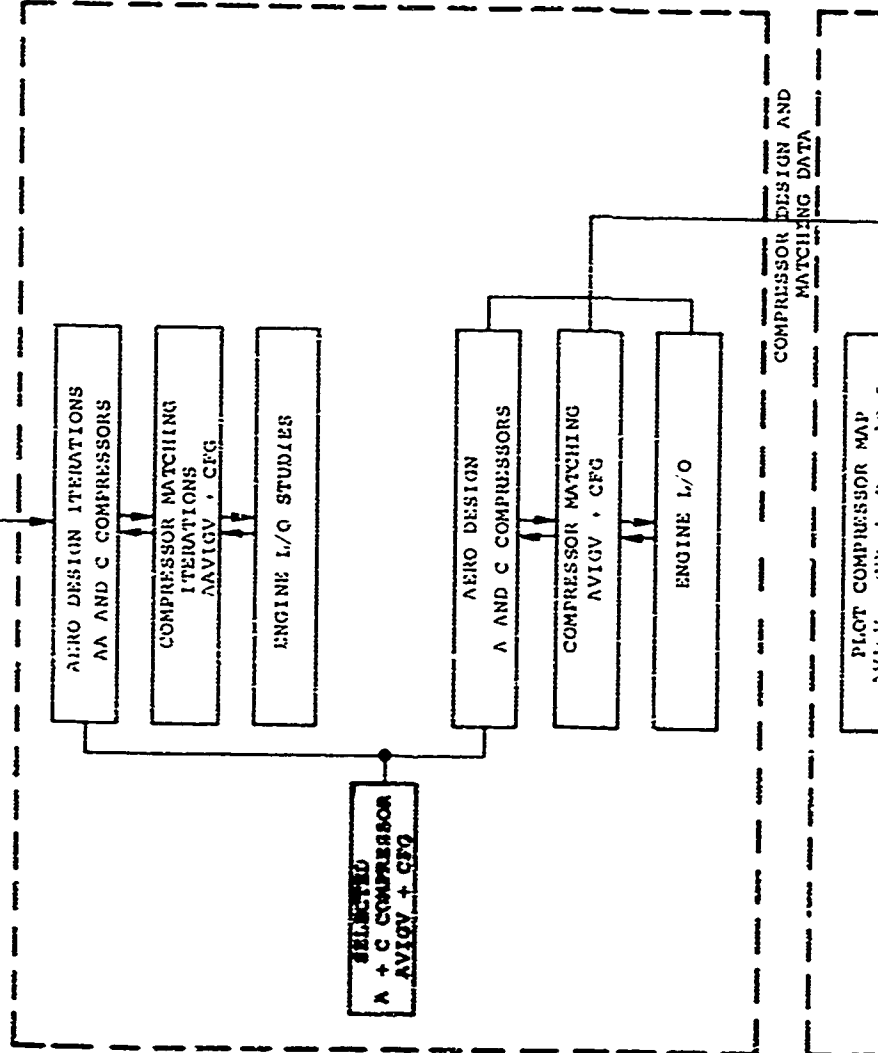
5

B

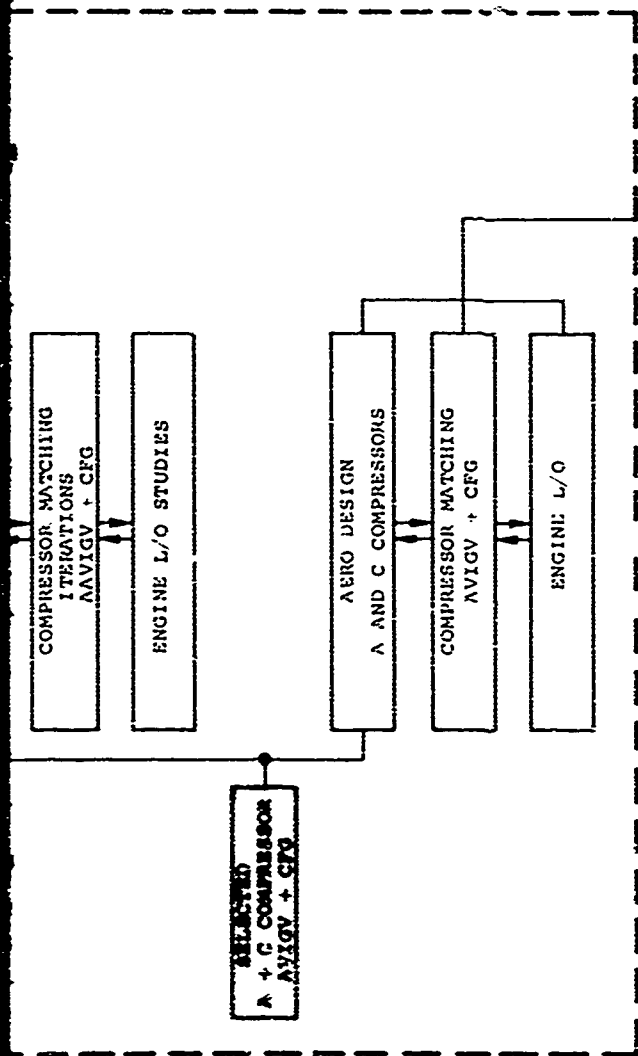
TASK 1B
ENGINE CYCLE ANALYSIS



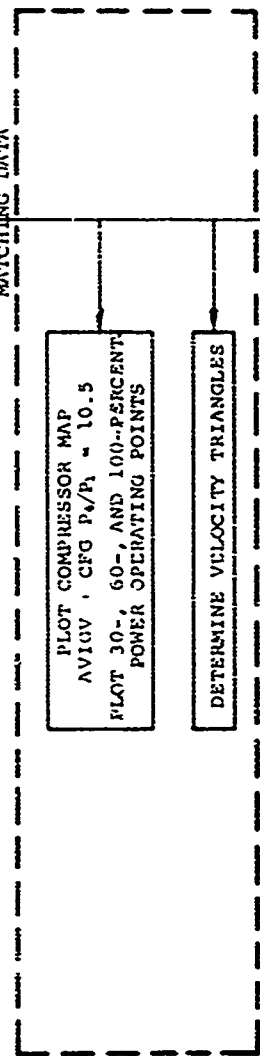
TASK 11D
COMPRESSOR DESIGN AND MATCHING



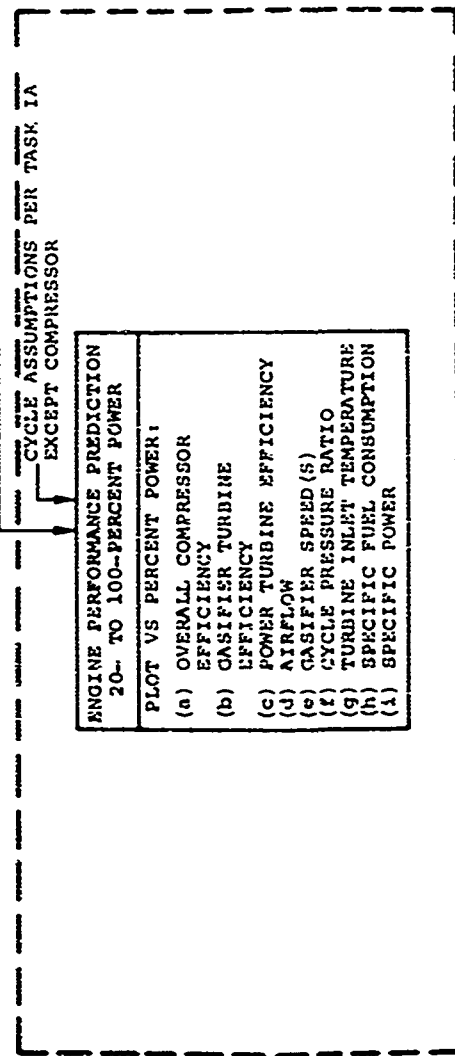
TASK IIB
COMPRESSOR DESIGN
AND MATCHING



TASK III
COMPRESSOR PERFORMANCE
PREDICTION



TASK IV
ENGINE PERFORMANCE
PREDICTION



- ENGINE PERFORMANCE PREDICTION
20- TO 100-PERCENT POWER
- PLOT VS PERCENT POWER:
- (a) OVERALL COMPRESSOR EFFICIENCY
 - (b) GASIFIER TURBINE EFFICIENCY
 - (c) POWER TURBINE EFFICIENCY
 - (d) AIRFLOW
 - (e) GASIFIER SPEED (S)
 - (f) CYCLE PRESSURE RATIO
 - (g) TURBINE INLET TEMPERATURE
 - (h) SPECIFIC FUEL CONSUMPTION
 - (i) SPECIFIC POWER

2.2.1.1 Single-Stage Axial Compressors

The data for nine single-stage axial compressors examined included stage efficiency, pressure ratio, surge margin, and tip speed as displayed in Figure 2. The data included maximum efficiencies observed at design speed and at some off-design speeds as noted. The data displayed were reported from 1961 through 1968 and include the results of the advanced technology compressor developed under contract to USAAVLABS and reported in Reference 1.

Figure 2 contains the values of efficiency versus pressure ratio and surge margin versus tip speed for the various data and displays the current and projected efficiency levels versus pressure ratio. The envelope of the data is used to define design-point efficiency levels for current technology.

For axial compressors used to supercharge centrifugal compressors, efficiency increases over the current level indicated in Figure 2 will probably come from loss reductions at supersonic Mach numbers and at high diffusion factors. As tip speed is increased to accommodate present D-factor limits, the rotor hub/tip ratio increases. This increase in hub-tip ratio is limited by the amount of interstage duct distortion between the axial and centrifugal stages. As a consequence, rotor tip and rotor and stator hub D-factor limits must be met with increasing blade number and/or chord length as single-stage pressure ratio increases. Either approach increases wetted area and wake sizes. As chord length increases, blade aspect ratio decreases. This is a direction toward decreased efficiency. Limiting the increase in hub/tip ratio results in lower rotor tip speeds than might otherwise be chosen, but tip relative Mach numbers of 1.5 or over will still have to be accepted at stage pressure ratios from 2.5 to 3.0.

A 3-year efficiency improvement line has been projected as shown in Figure 2. No efficiency gain is expected at single-stage pressure ratios of 1.7:1 or lower. The greatest improvement is expected at pressure ratios greater than 2.0:1, where Mach-number and D-factor limits are taxed the most. Benefits will more probably be

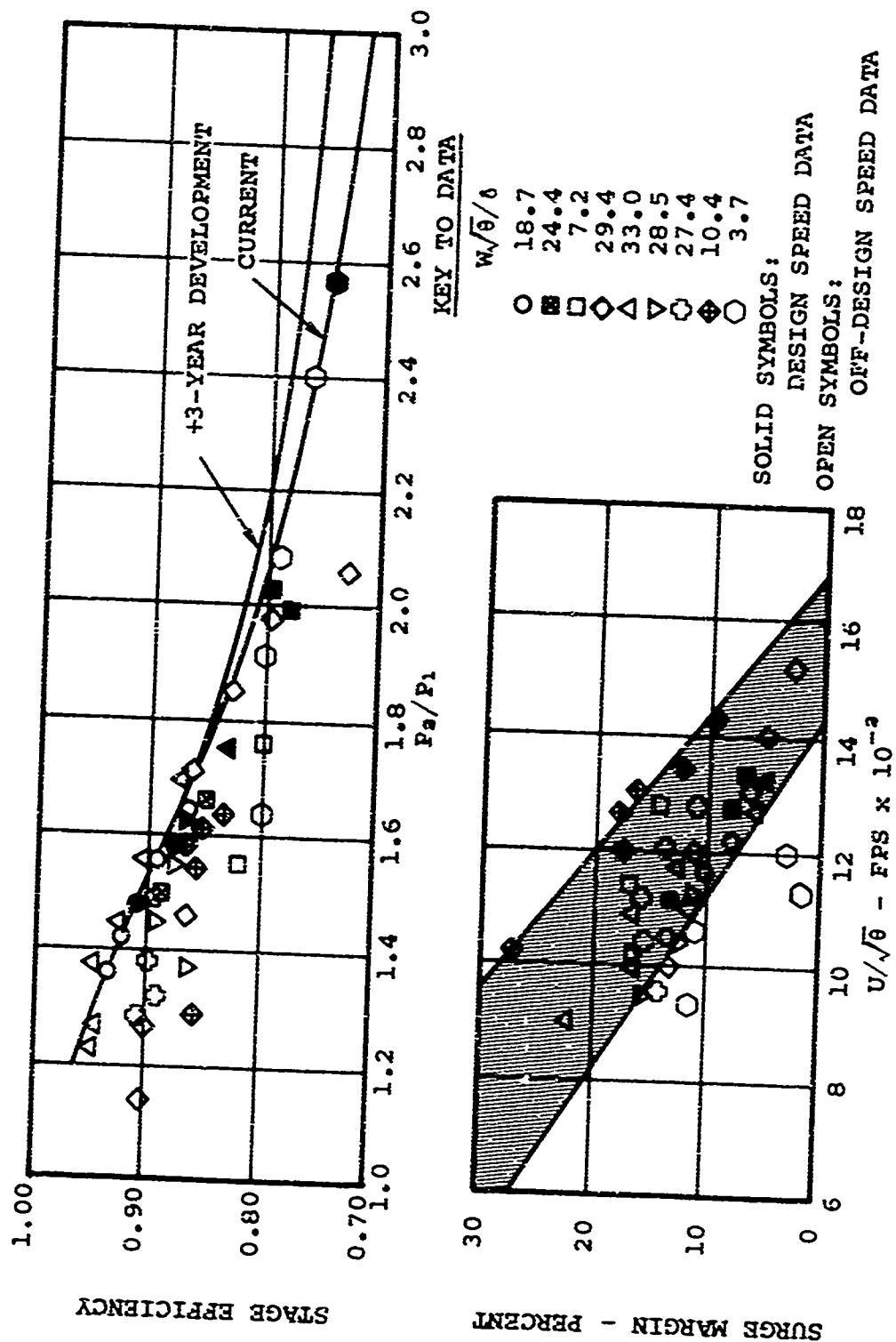


Figure 2. Single-Stage Axial Compressor Efficiency Estimates.

derived from extending Mach-number/D-factor limits than from reducing minimum loss. Some success has been shown with tandem cascades in extending the D-factor limit. New supersonic blade sections and new design approaches could possibly be conceived to reduce shock losses.

2.2.1.2 Two-Stage Axial Compressors

Test data were examined for five two-stage axial compressors and included stage efficiency, pressure ratio, surge margin, and tip speed as displayed in Figure 3. The data for the two-stage axial compressors included maximum efficiencies observed at design speed and at some off-design speeds as noted.

Figure 3 displays the values of efficiency versus pressure ratio and surge margin versus tip speed for the various data and displays the current and projected efficiency levels versus pressure ratio. The envelope of the data points is used to define design-point efficiency levels for current technology.

The two-stage axial compressor efficiency levels projected for advanced technology, achievable within a 3-year period, are not expected to change. The two-stage axial compressor consists of stages with individual pressure ratios from 1.5 to 2.0. Little improvement in single-stage efficiency level is expected in this range, as reported above. The gain for the two-stage compressor is expected to come from improved matching to achieve the current efficiency levels with increased surge margin for the peak efficiency operating points.

2.2.1.3 Single-Stage Centrifugal Compressors

Test data were examined for various single-stage centrifugal compressors as obtained from 32 separate tests. The data included the results of the advanced technology compressors developed under contract to USAAVLABS and reported in Reference 2.

Figure 4 displays the values of polytropic efficiency versus specific speed. Because of the wide range of possible design-point pressure ratios (5:1 to 10:1),

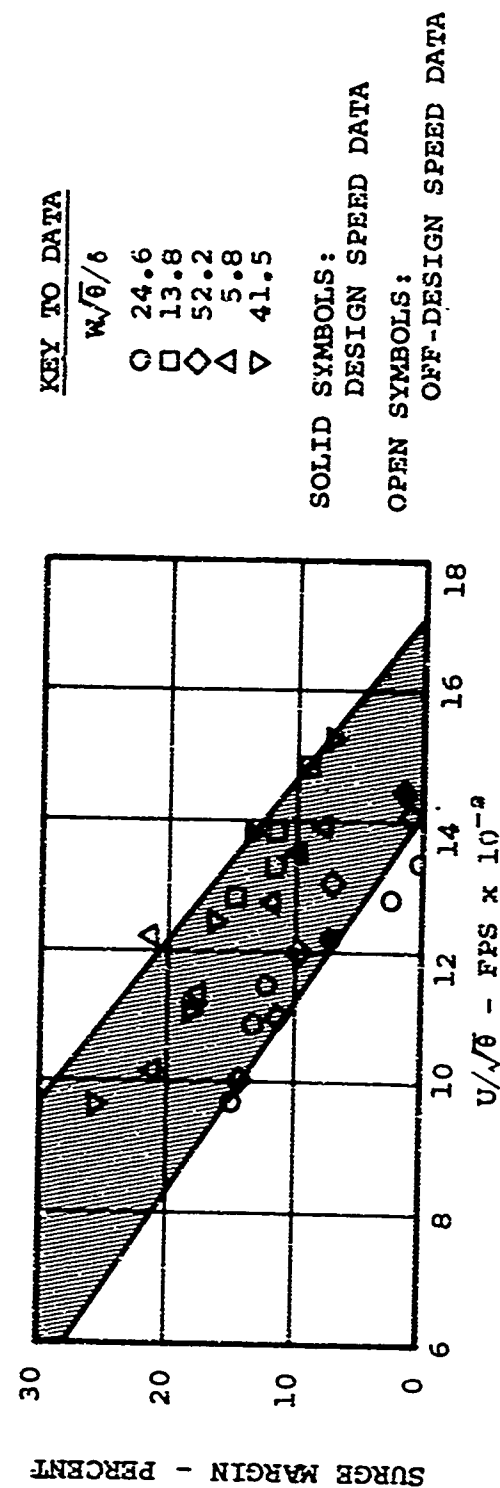
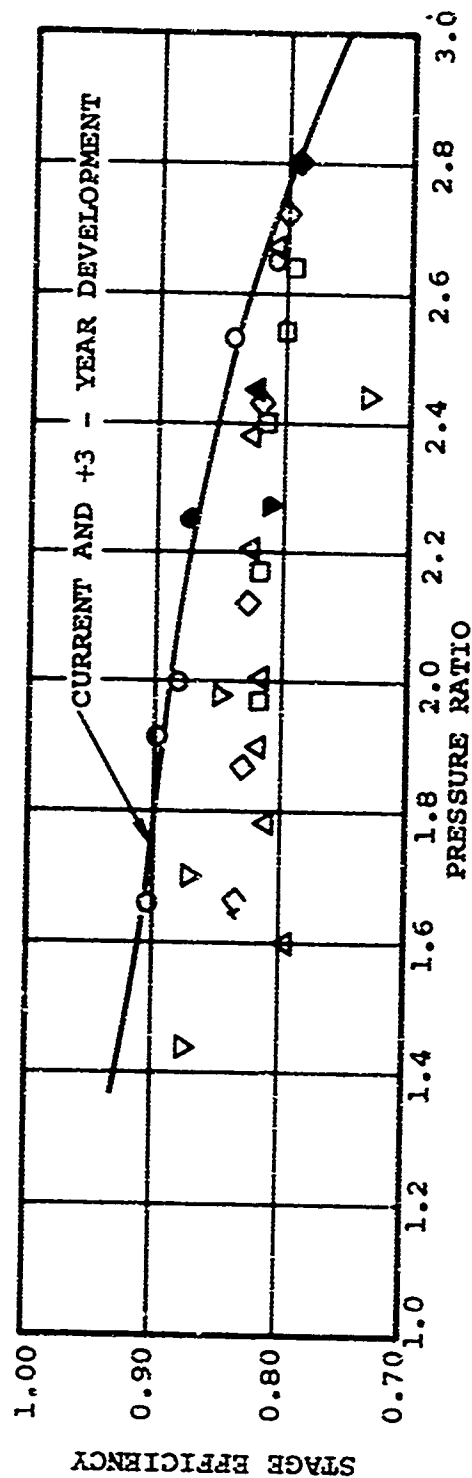


Figure 3. Two-Stage Axial Compressor Efficiency Estimates.

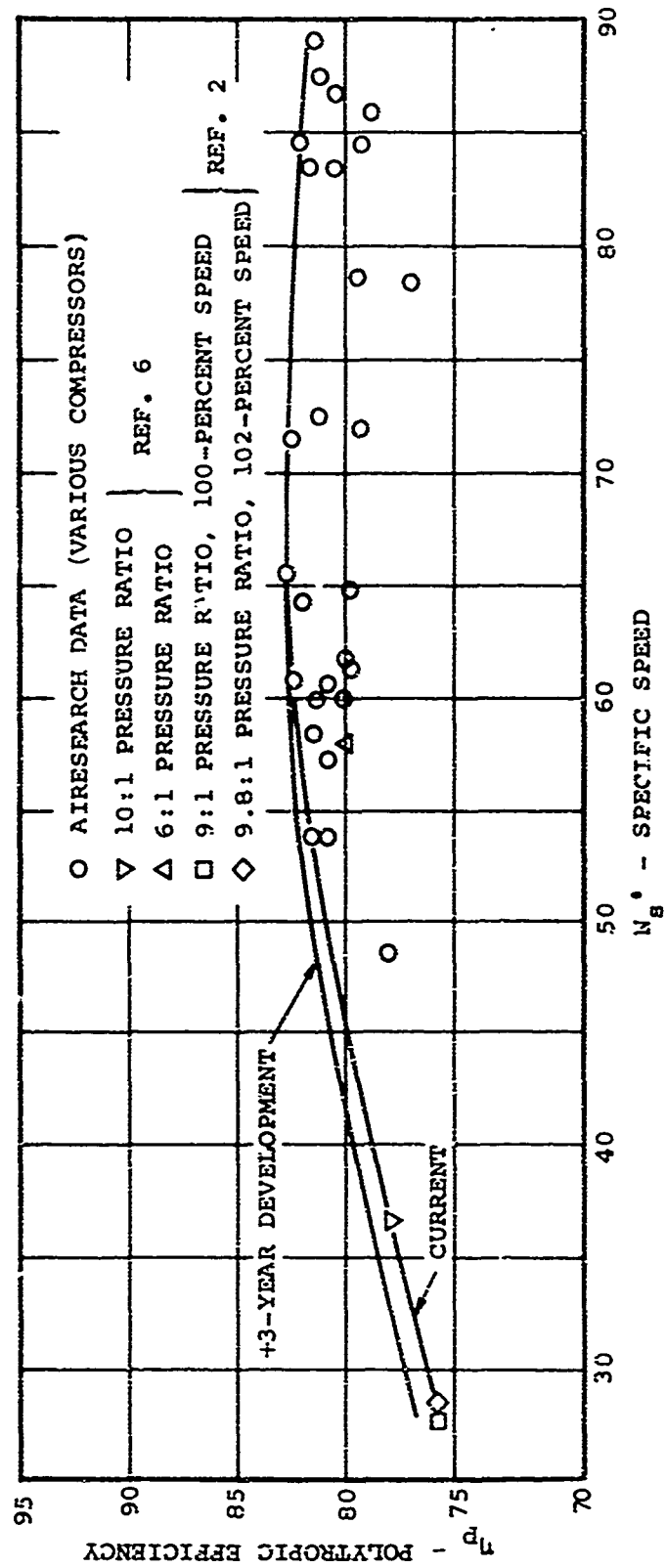


Figure 4. Single-Stage Centrifugal Compressor Polytropic Efficiency Estimates.

polytropic efficiency is a better reference of the state of the art than is adiabatic efficiency, since it is more indicative of aerodynamic losses. Specific speed has been chosen as the independent variable, since centrifugal compressor efficiency depends on rotational speed and flow rate as well as pressure ratio. The envelope of the data points is used to define design-point efficiency levels for current technology. This envelope is partially determined by the USAAVLABS advanced technology compressor data, as noted in Figure 4, for specific speeds up to 50 (N_s').

Advanced technology efficiency levels are also shown in Figure 4. These efficiency levels are expected to be achieved by minimizing the rotor and vaneless diffuser combined loss.

Polytropic efficiency has been used since it is a direct measure of fluid mechanic losses. Adiabatic efficiency rates the work done by the compressor to an equivalent isentropic process. This is not a measure of fluid mechanic losses, but only an indication that they exist. From the simple energy equation,

$$dh = tds + \frac{1}{\rho} dp \quad (1)$$

Polytropic efficiency is defined from static properties as follows:

$$\eta_p = \frac{\frac{1}{\rho} dp}{dh} \quad (2)$$

However, stagnation properties are widely used to evaluate the polytropic efficiencies of compressors. Adding the change in kinetic energy to both sides of the simple energy equation,

$$dh + d \frac{V^2}{2} = dH = tds + \frac{1}{\rho} dp + d \frac{V^2}{2} \quad (3)$$

Polytropic efficiency based on stagnation properties as commonly used for turbomachinery is then

$$\eta_p = \frac{\frac{1}{\rho} dp + d \frac{V^2}{2}}{dH} \quad (4)$$

Equation 4 shows that polytropic efficiency is a measure of change in static pressure and kinetic energy actually achieved for the thermodynamic energy supplied. A constant polytropic efficiency over a pressure ratio range from 5:1 to 10:1 indicates that aerodynamic losses are proportional to the compressor work. A drop in polytropic efficiency indicates proportionately higher losses as compressor work increases.

As used here, specific speed is defined with the volume flow represented by the square root of the product of the compressor inlet and outlet volume flow rates, namely,

$$Q = \sqrt{\frac{W_C}{\rho_1} \cdot \frac{W_C}{\rho_2}} = \frac{W_C}{\rho_1} \sqrt{\frac{\rho_1}{\rho_2}} = \frac{W_C}{\rho_1} \sqrt{\frac{\theta_2}{\delta_2}} \quad (5)$$

Also, the compressor input head is used instead of the output head. The full definition, in terms of the familiar specific speed, is

$$N'_S = \frac{N\sqrt{Q}}{(\Delta H)^{3/4}} = \frac{N\sqrt{W_C \rho_1}}{(\Delta H')^{3/4}} \left(\frac{\theta_2}{\delta_2}\right)^{1/4} \left(\eta_C\right)^{3/4}$$

$$N'_S = N_S \left(\frac{\theta_2}{\delta_2}\right)^{1/4} \left(\eta_C\right)^{3/4} \quad (6)$$

2.2.1.4 Multistage Axial-Centrifugal Compressors

Based on the above studies of current and advanced compressor stage performance, multistage axial-centrifugal compressor efficiency estimates were made for design-point operation. An optimum stage match for maximum efficiency of the compressor stages was assumed at all design-point pressure ratios considered (6:1 through 24:1). Estimates were completed for the following multistage compressors:

1. Single-stage axial plus centrifugal, current technology
2. Single-stage axial plus centrifugal, advanced technology

3. Two-stage axial plus centrifugal, current technology
4. Two-stage axial plus centrifugal, advanced technology

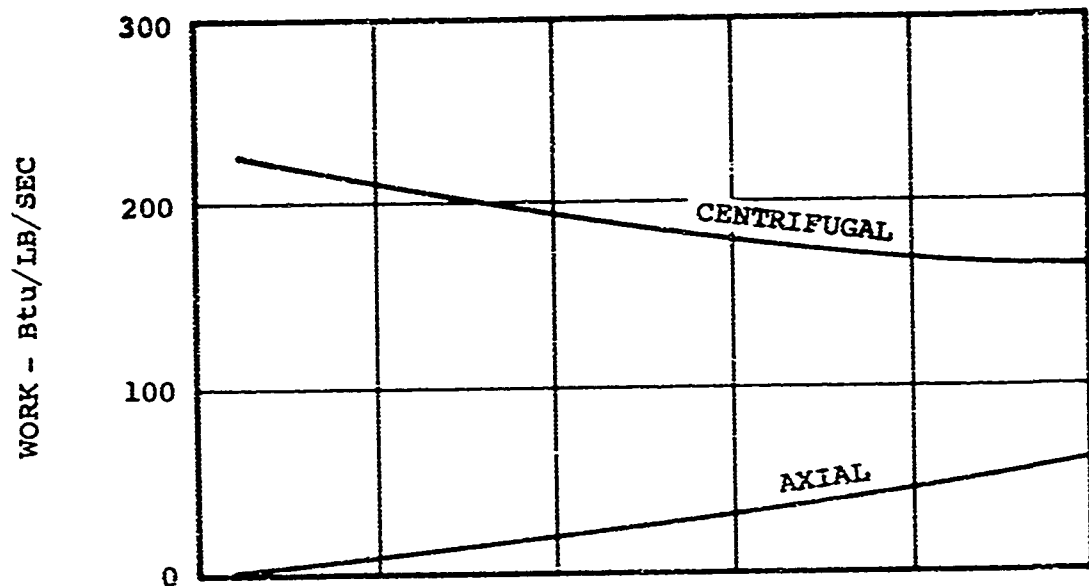
The overall compressor efficiency was maximized by iterative calculations for assumed work splits between the axial and centrifugal components. Calculations were made for selected design-point pressure ratios of 6, 12, 18, and 24. Results were plotted to display axial compressor work, centrifugal compressor work, and overall compressor efficiency versus axial compressor pressure ratio. A typical working plot is shown in Figure 5 for the selected design-point pressure ratio of 18:1 and 60,000 rpm. For this case the maximum overall compressor efficiency occurs at an axial compressor pressure ratio of 2.27:1. This results in 81 percent of the work being done in the centrifugal compressor, which shows the domination of this stage on the overall compressor performance characteristics.

Since no single compressor speed can be selected for the broad range of design-point pressure ratios being considered here (6:1 to 24:1), calculations were made for speeds of 50,000, 60,000, and 70,000 rpm. These speeds were selected for this 3.0-pound-per-second compressor to bracket the optimum speed that might be selected for any design-point pressure ratio in the range of interest.

The results of these calculations based on the single-stage axial, two-stage axial, and single-stage centrifugal compressor estimates reported in the paragraphs above are displayed in Figures 6 and 7, and represent the design-point compressor performance estimates as noted.

These results show that the maximum overall compressor efficiency decreases with increasing pressure ratio for a given speed, due in part to the resulting decreases in centrifugal compressor specific speed. For a given design-point pressure ratio, the overall compressor efficiency is higher for higher speeds because of the resulting higher specific speed of the centrifugal compressor.

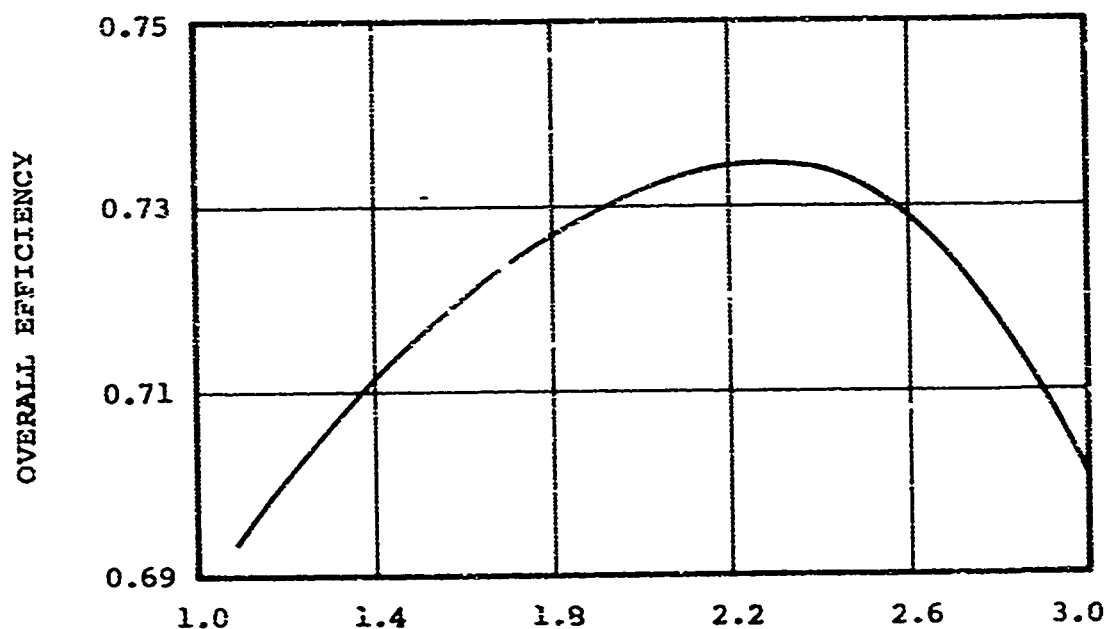
It should be noted that increases in the centrifugal compressor efficiency levels above those shown would effect the optimum work split to decrease the pressure ratio of the axial compressor for maximum overall compressor efficiency. Similarly, increases in the axial



$N/\sqrt{\theta_1} = 60,000$ RPM

$W/\sqrt{\theta_1}/\theta_1 = 3.0$ LB/SEC

PRESSURE RATIO = 18:1 $P_4/P_1 = 18:1$



AXIAL COMPRESSOR PRESSURE RATIO - P_3/P_1

Figure 5. Variation of Overall Efficiency and Work Split for Two-Stage Axial Plus Single-Stage Centrifugal Compressor, Current Technology.

compressor efficiency levels above that shown would effect an increase in the axial compressor pressure ratio for maximum overall compressor efficiency.

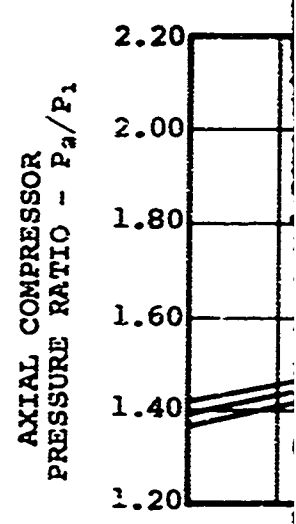
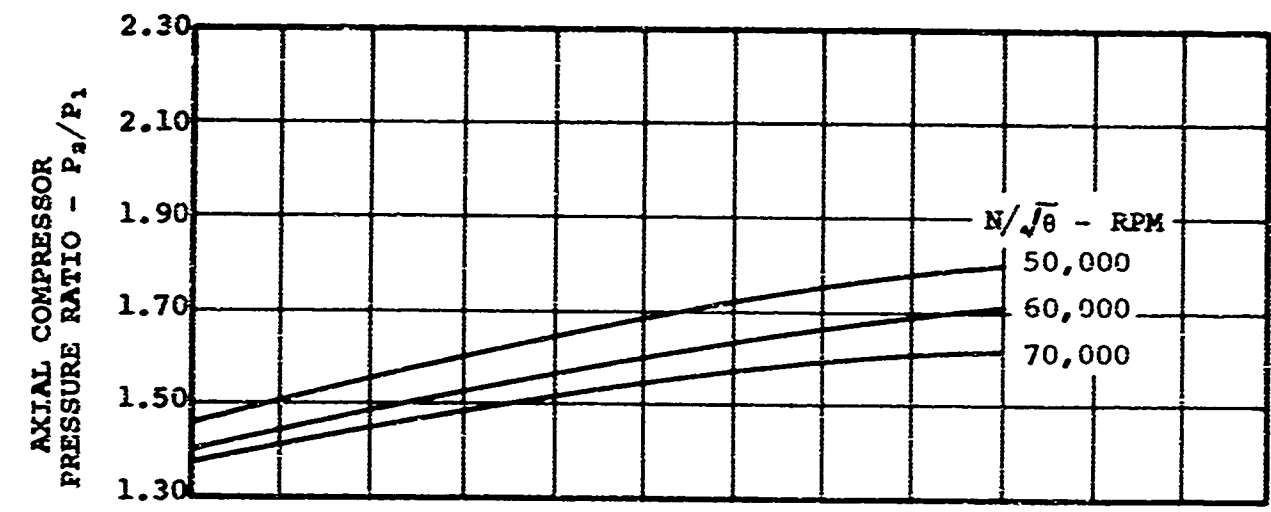
An effect similar to this is evidenced in Figures 6 and 7 by observing the reduction in axial compressor work for higher selected rotational speeds. The higher rotational speeds result in higher specific speeds and, hence, higher efficiencies for the centrifugal compressor, thereby affecting the work split toward increased work in the centrifugal compressor.

2.2.2 Tentative Compressor Selection, AA+C Versus A+C

In order to make a tentative selection of one versus two axial plus centrifugal compressor configuration, a qualitative examination was made of the relative merits for the two approaches. Table I presents a comparison of some of the more important engine parameters.

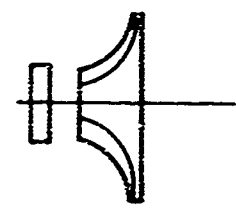
TABLE I. QUALITATIVE COMPARISON OF AXIAL-CENTRIFUGAL COMPRESSORS, AA + C VERSUS A + C			
Engine Parameter		AA + C	A + C
Performance	SFC	+	
	η_c	+	
	Power	+	
	Response, polar moment of inertia	+	
Weight		0	0
Envelope	Diameter	+	
	Length		+
Reliability (Mechanical)			+
Cost			+
+ = advantage 0 = standoff			

A

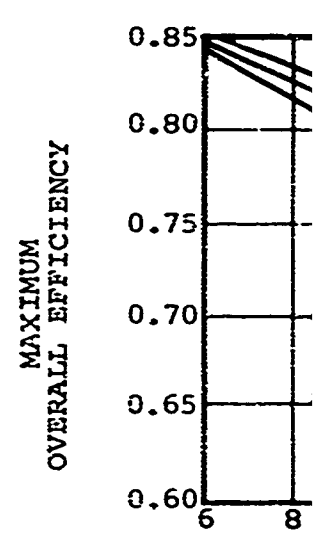
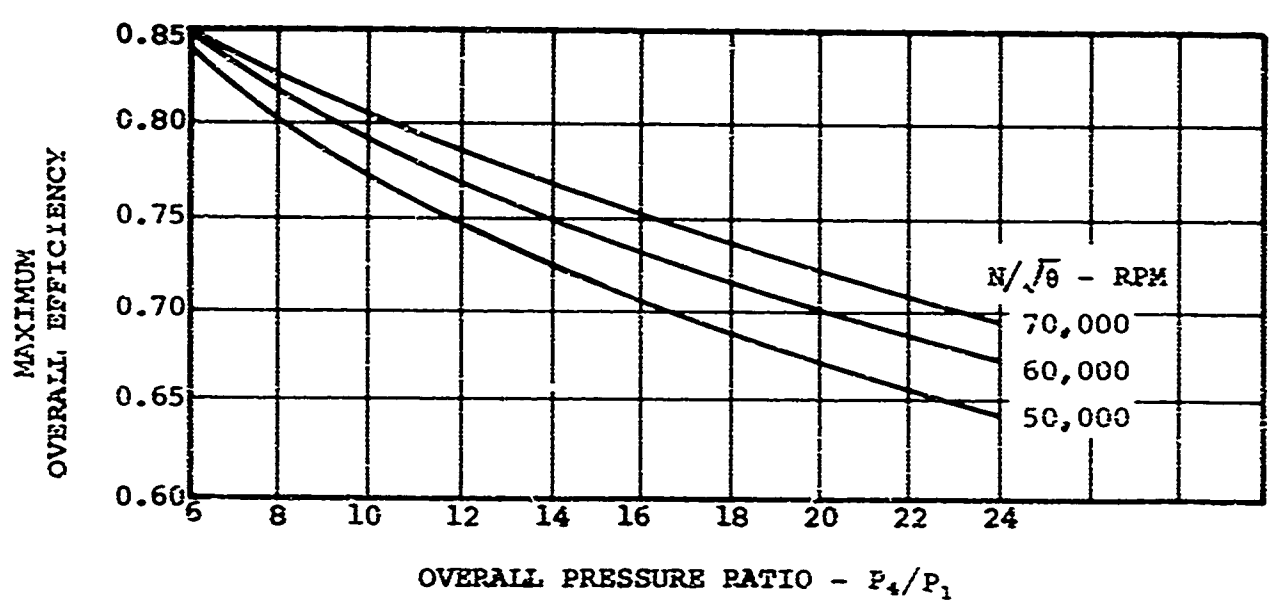


$W_a \sqrt{\theta}/\delta = 3.0$ LB/SEC

CURRENT TECHNOLOGY



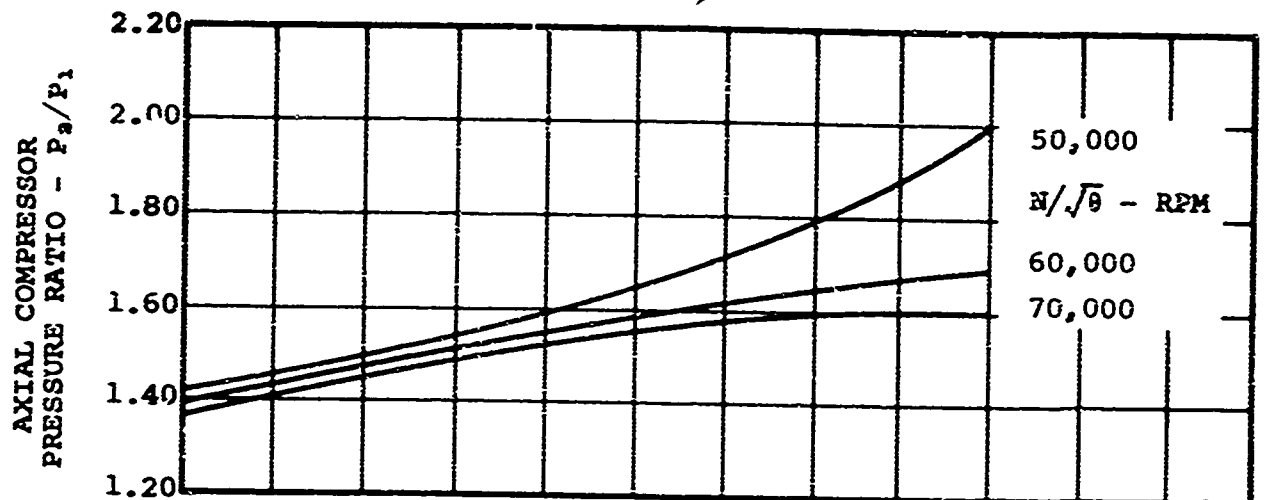
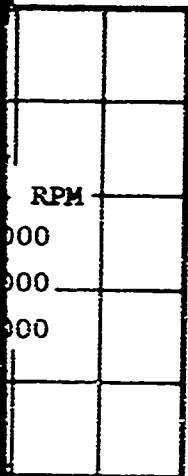
$W_a \sqrt{\theta}/\delta$



(A) CURRENT TECHNOLOGY

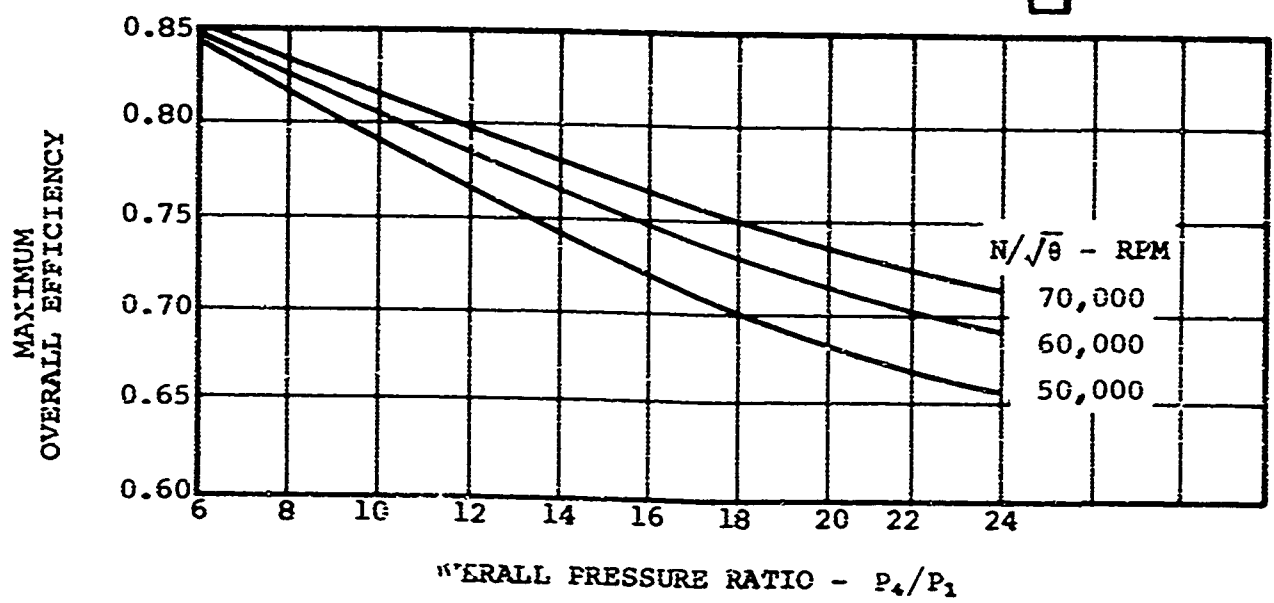
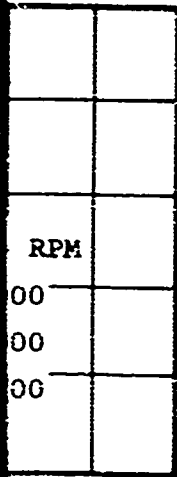
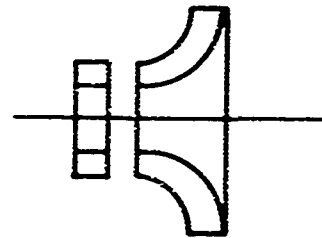
Figure 5. Single-Stage Axial Plus Single-Stage Centrifugal Compressor Efficiency Estimates.

B



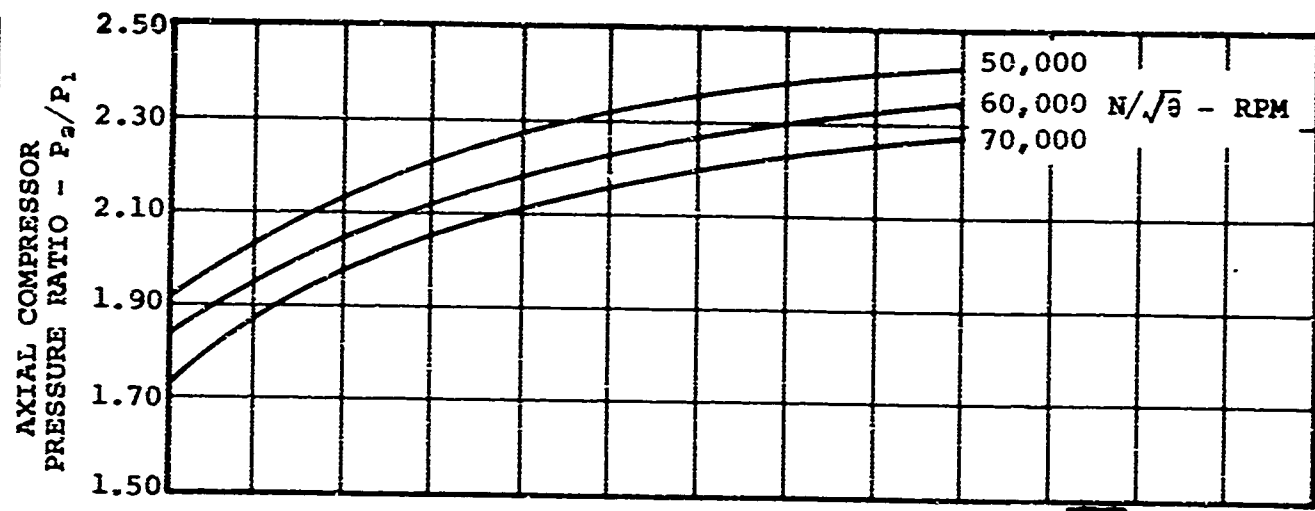
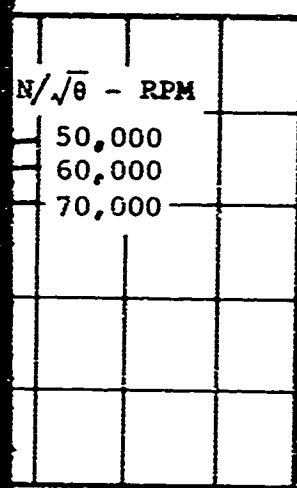
$W_a \sqrt{\theta}/\delta = 3.0 \text{ LB/SEC}$

ADVANCED
TECHNOLOGY



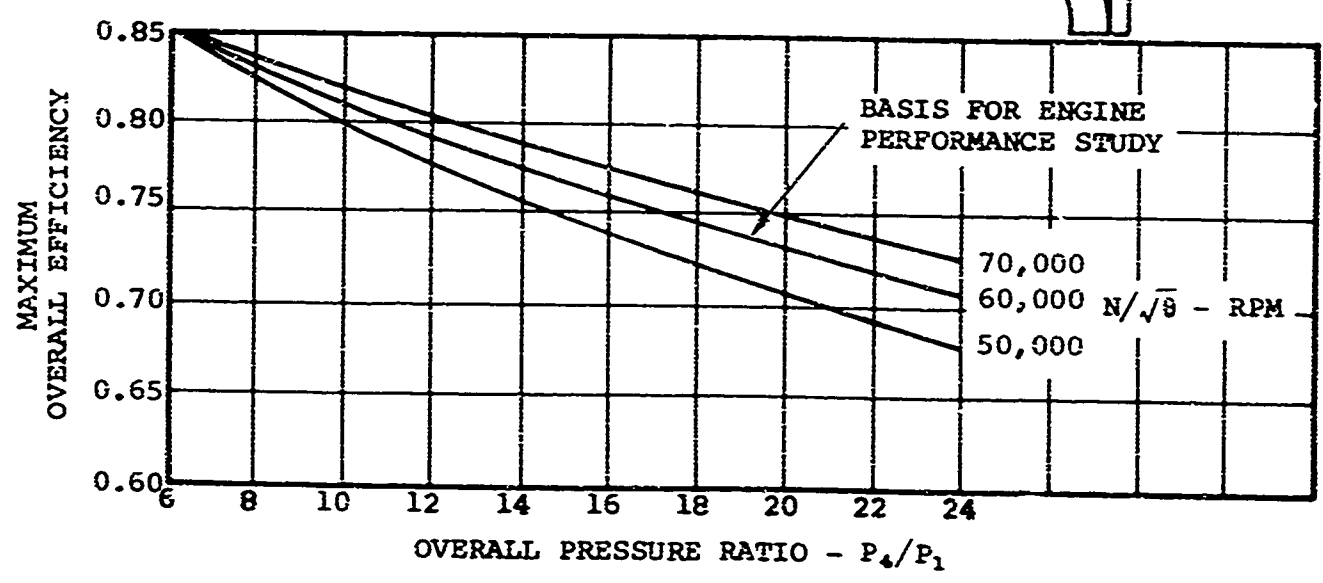
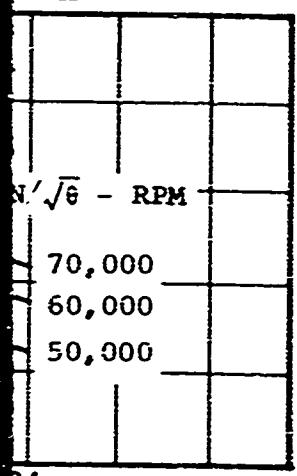
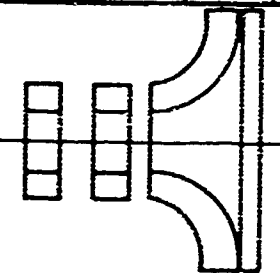
(B) ADVANCED TECHNOLOGY

B



$W_a \sqrt{\theta}/\delta = 3.0$ LB/SEC

ADVANCED TECHNOLOGY



(B) ADVANCED TECHNOLOGY

These comparative results show that, based on performance considerations the AA+C combination shows an advantage over the A+C compressor. Considerations of envelope, reliability, and cost show an advantage for the A+C compressor. In order to achieve a useful compressor with the best possible performance, the AA+C compressor configuration was chosen for tentative evaluation. Clearly this is a marginal choice, since the benefits of the AA+C compressor must be compared against the length, cost, and simplicity penalties resulting from the added stage.

This was intended to be a tentative selection, subject to re-examination as additional information becomes available. Re-examination of this choice was made as reported in Paragraphs 3.2 and 5.3, and ultimately resulted in the final configuration of an A+C compressor for this program.

2.3 DESIGN-POINT ANALYSIS

The design-point analysis was conducted based on the cycle assumptions established to be representative of advanced engine component performance levels as reported in Paragraph 2.2 and Appendix I of this report.

Gasifier cooling airflows were treated as a parameter in this study to better determine the effect of this variable on engine performance and on selection of optimum design-point pressure ratio. Cooling-flow values included in the analysis were 0, 3, 6, and 9 percent of the compressor airflow.

The design-point analysis was completed for cycle pressure ratios of 8:1 to 20:1 and for TIT of 1600°F to 2500°F. The results are displayed in Figures 8 through 11 and show the relationship of specific power and SFC versus cycle pressure ratio for 0-, 3-, 6-, and 9-percent cooling airflows, respectively.

These plots show a relatively flat characteristic of SFC versus compressor pressure ratio due to cycle, accounting for compressor and gasifier turbine efficiency degradation with increasing cycle pressure ratio. Comparison of Figure 11 with Figure 8 shows the effect of 9-percent cooling airflow on the SFC levels and on the compressor pressure ratio selection for minimum SFC. Values for 2100°F operation with 9-percent cooling flow are: minimum SFC = 0.480 at 10.5:1 compared to 0-percent cooling flow values of minimum SFC = 0.448 at 12:1.

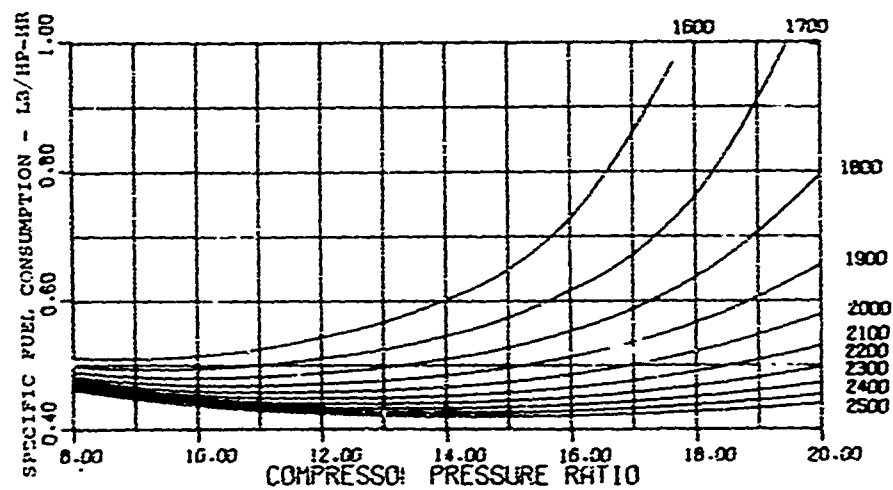
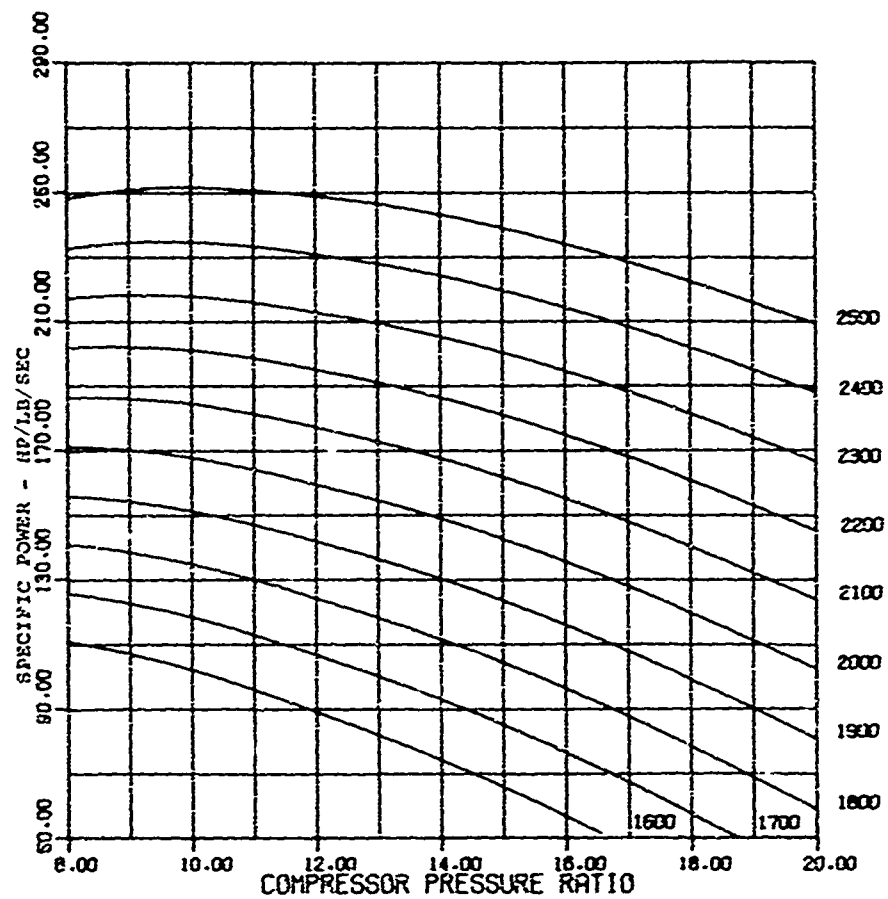


Figure 8. Design-Point Engine Performance, 0-Percent Cooling Flow.

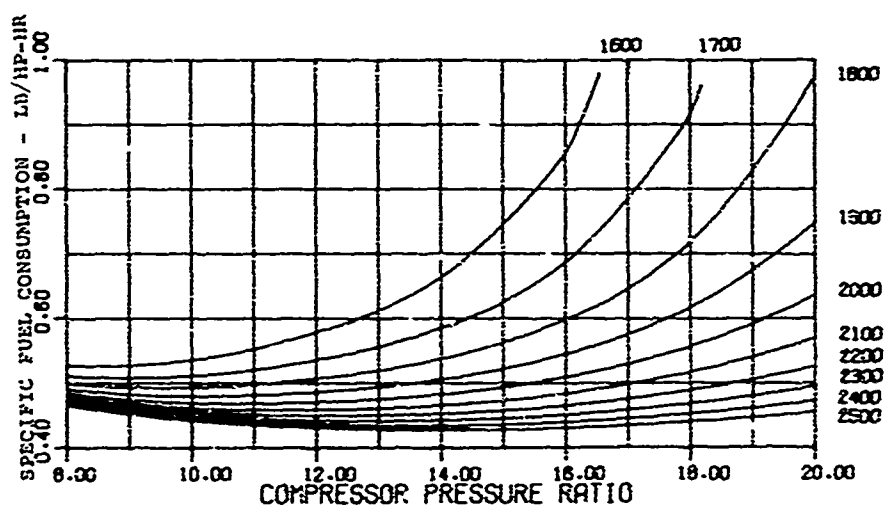
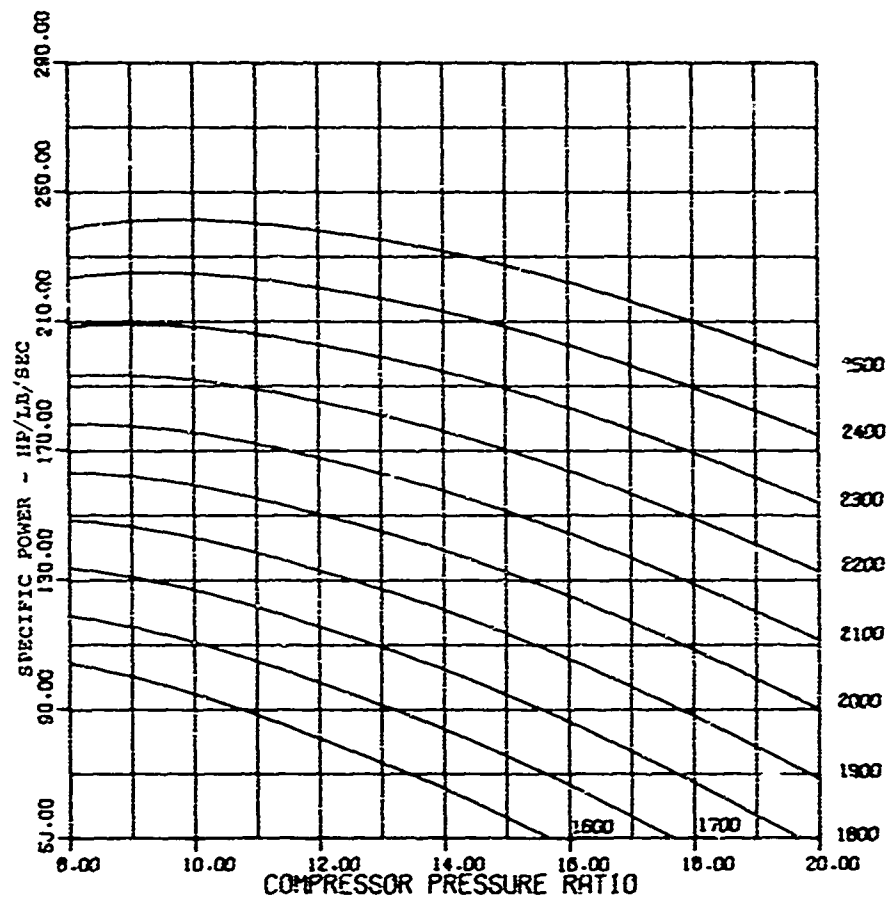


Figure 9. Design-Point Engine Performance, 3-Percent Cooling Flow.

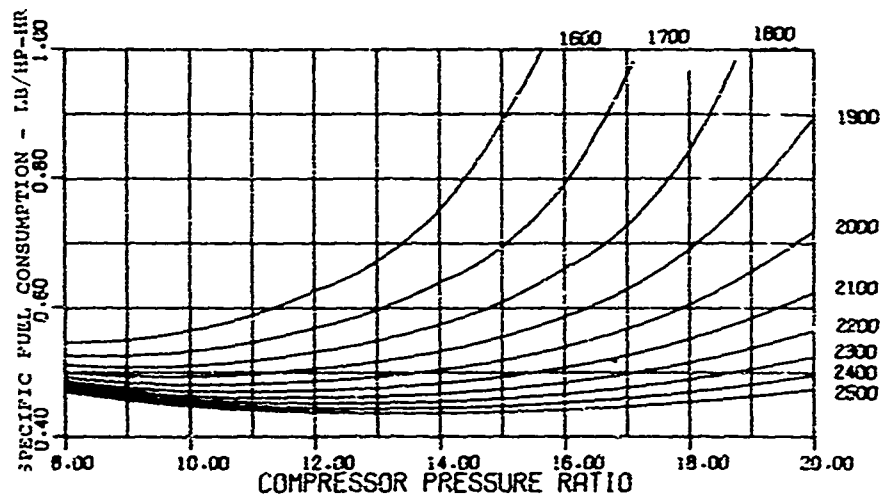
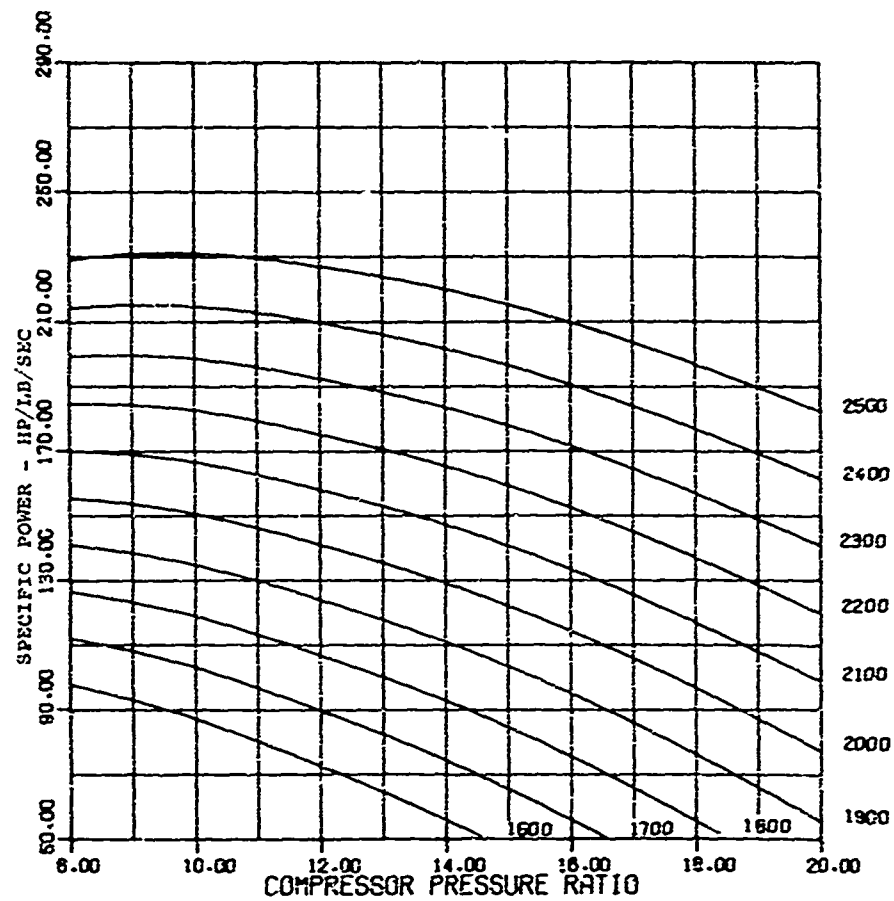


Figure 10. Design-Point Engine Performance, 6-Percent Cooling Flow.

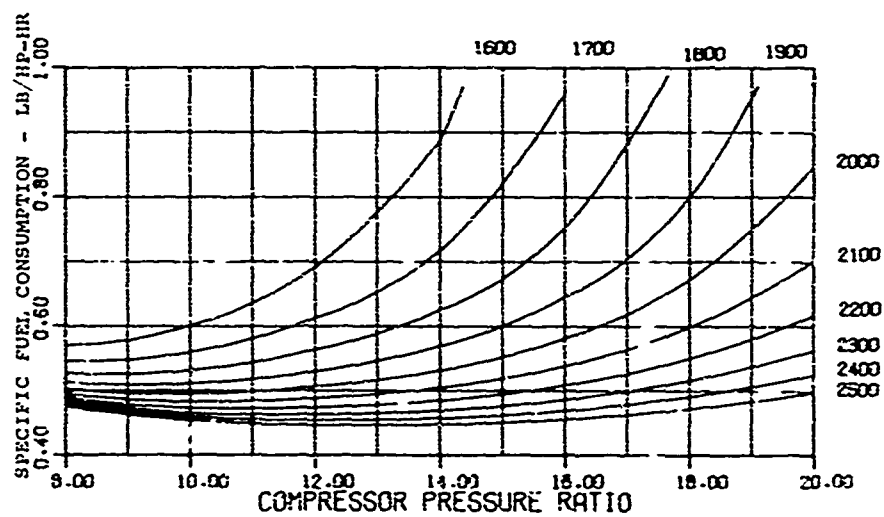
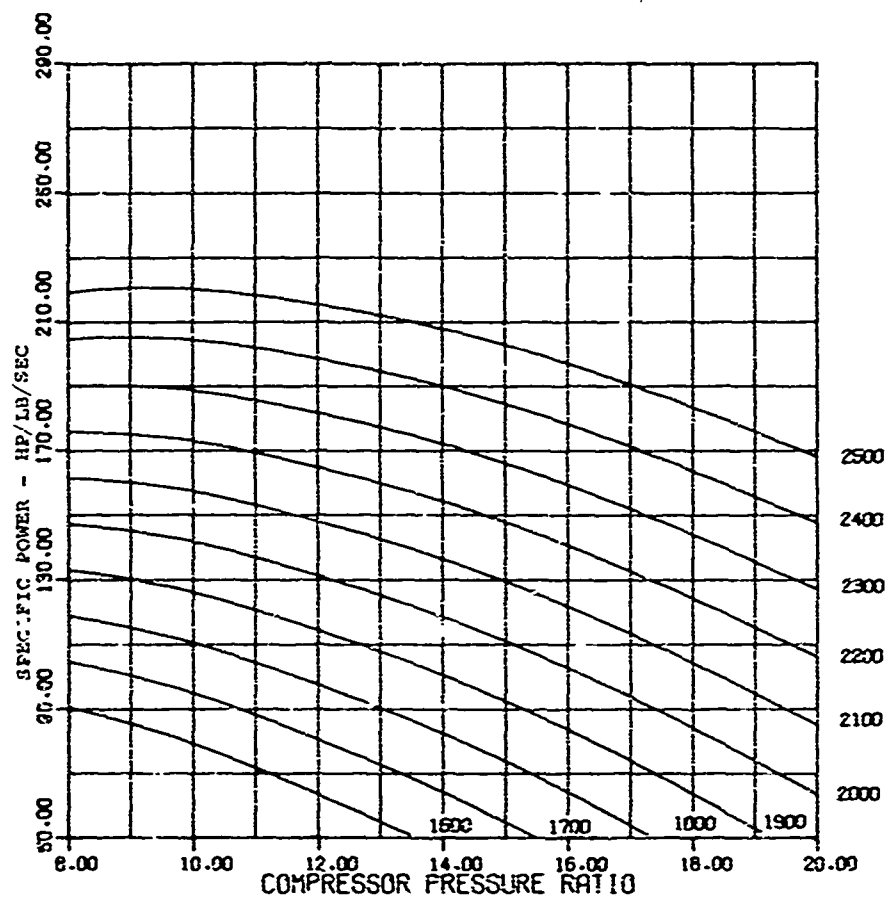


Figure 11. Design-Point Engine Performance, 9-Percent Cooling Flow.

Since the engine configuration selected for this study is a free power turbine with fixed turbine geometry sized for 2500°F TIT at 100-percent power, it was estimated that 60-percent power would be achieved at approximately 2100°F TIT. Furthermore, it was projected that 9-percent cooling flow for a gasifier turbine, of the approximate description considered here, would be achievable within a 3-year development period. Based on this, a tentative selection for design-point pressure ratio was made for 10.5:1, and a preliminary target for SFC was established as 0.460 for the case of no design-point compressor efficiency degradation due to matching.

These values include only a preliminary accounting for the effect of off-design component efficiencies (at 100-percent power) on the design point TIT, and no accounting for the off-design component efficiencies on SFC at 30-percent power (second priority). Therefore, selection was made of several design-point pressure ratios to bracket the 10.5:1 choice. The design-point pressure ratios selected for off-design analyses are 9:1, 10:1, 11:1, 12:1, 13:1, and 14:1.

2.4 OFF-DESIGN CYCLE ASSUMPTIONS

The engine cycle analysis for off-design performance was based on advanced component performance levels as estimated for the design-point analysis, reported in Paragraph 2.2, and on component off-design characteristics as estimated for this task and reported herein. The component off-design characteristics estimated for this study include nondimensionalized gasifier and power turbine maps and an idealized compressor map.

The idealized compressor map includes no surge or choke limits but provides a nondimensionalized schedule of compressor efficiency and pressure rise with speed.

These component maps and all other estimated off-design characteristics are reported in Appendix II of this report and, along with the design-point cycle assumptions reported in Paragraph 2.2, form the basis of the off-design analysis reported in Paragraph 2.5.

2.5 OFF-DESIGN ANALYSIS

Engine cycle analyses for off-design performance were conducted for the cases selected from the design-point study. The selected cases were for design-point pressure ratios of 9:1, 10:1, 11:1, 12:1, 13:1, and 14:1. For each selected design-point pressure ratio, iteration was conducted to achieve 2500°F TIT for 100-percent power. The plotted results are presented in Figures 12, 13, and 14.

Figure 12 shows the relationship of gasifier speed/gasifier design-point speed, and corrected flow versus design-point pressure ratio. Both are constant for each selected power condition as follows:

100-percent power - 108.4-percent speed - 3.64 lb per sec

60-percent power - 100-percent-speed - 3.0 lb per sec

30-percent power - 94.0-percent speed - 2.35 lb per sec

20-percent power - 88.4-percent speed - 2.09 lb per sec

Figure 13 shows the relationship of pressure ratio versus design-point pressure ratio for each selected power condition, as follows:

100-percent power - $(P_4/P_1)_{100} = 1.31 (P_4/P_1)_{DP}$

60-percent power - $(P_4/P_1)_{60} = 1.00 (P_4/P_1)_{DP}$

30-percent power - $(P_4/P_1)_{30} = 0.735 (P_4/P_1)_{DP}$

20-percent power - $(P_4/P_1)_{20} = 0.67 (P_4/P_1)_{DP}$

Figure 14 shows the relationship of TIT (°F) and of SFC to design-point pressure ratio. Inspection of this figure shows that the minimum SFC for 60-percent power occurs at a design-point pressure ratio of 10.75:1. Further, the minimum SFC for 30-percent power (second priority) occurs at a design-point pressure ratio of 10.0:1. Based on this and the relatively flat characteristic of the SFC for 60-percent power near the minimum value, a design-point pressure ratio of 10.5:1 was tentatively selected.

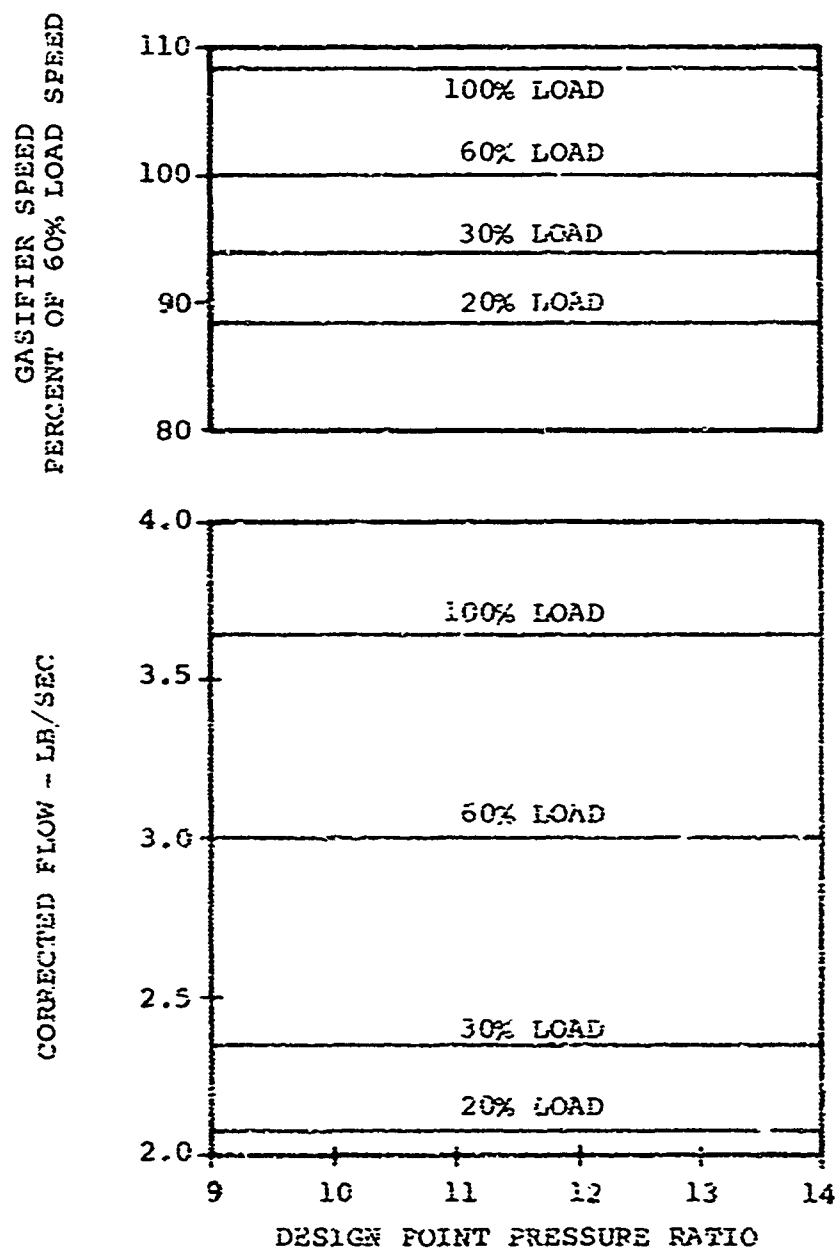


Figure 12. Engine Off-Design Performance: Speed and Flow Versus Design Pressure Ratio.

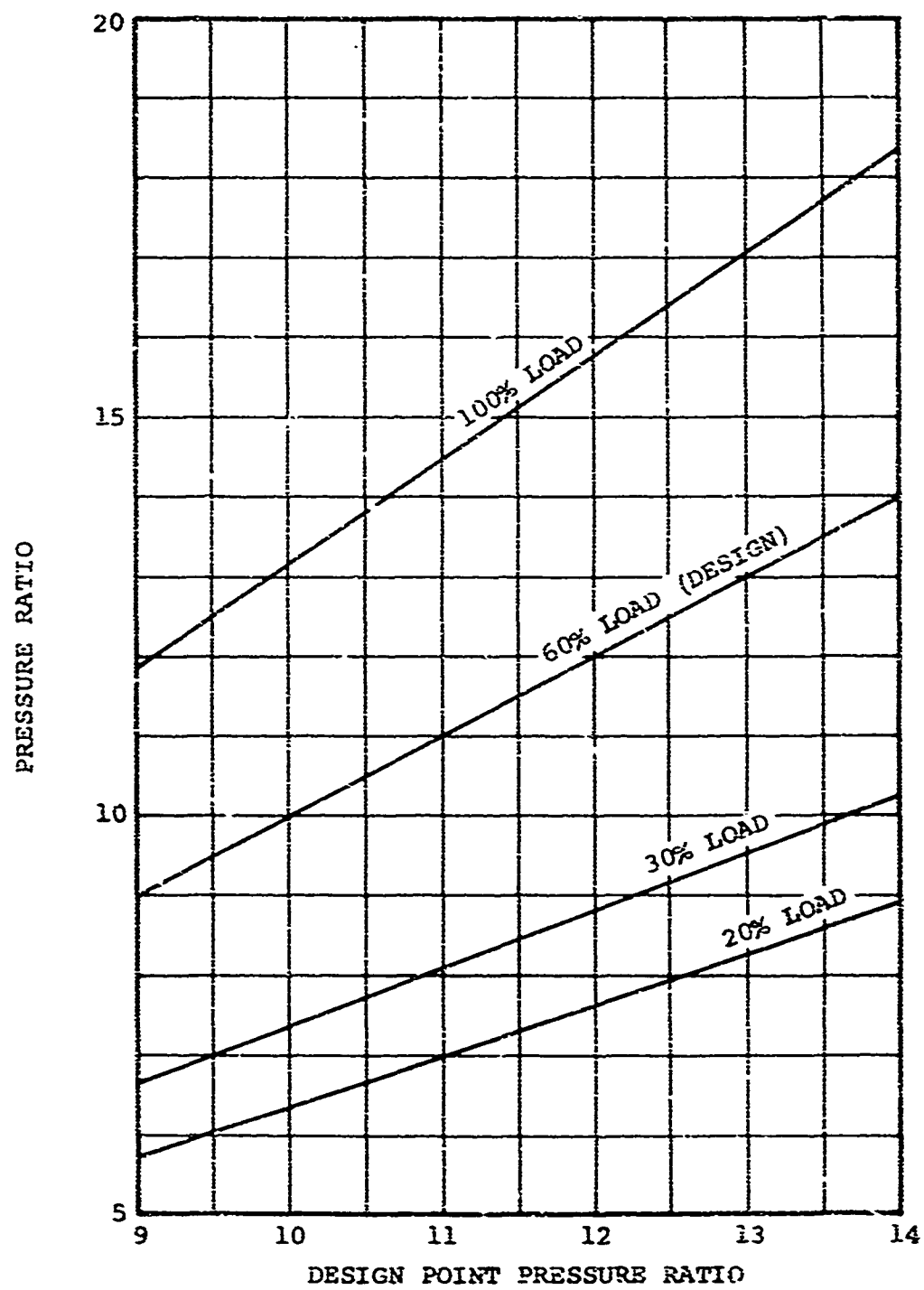


Figure 13. Engine Off-Design Performance:
Pressure Ratio Versus Design
Pressure Ratio.

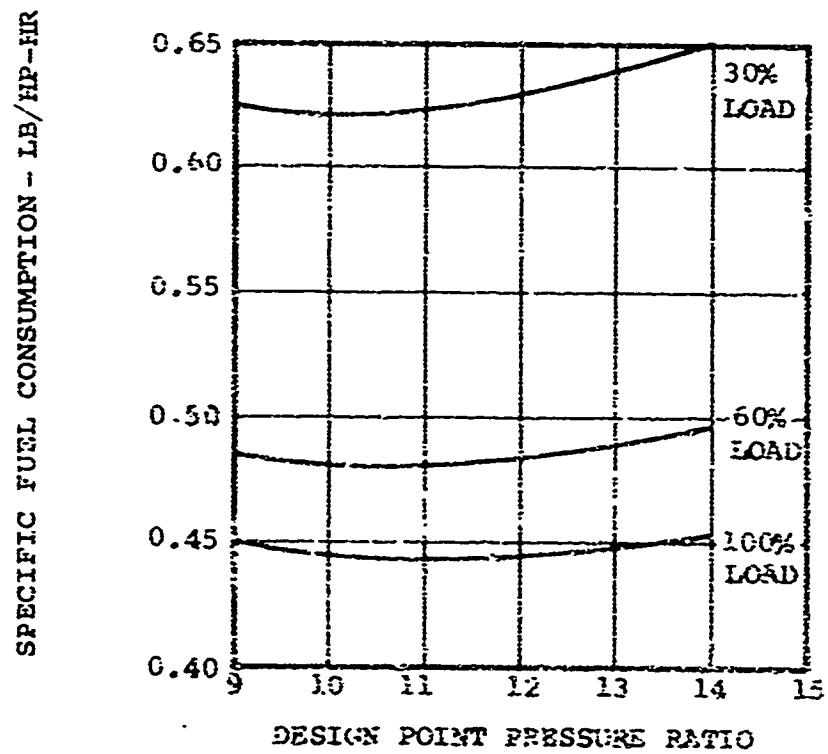
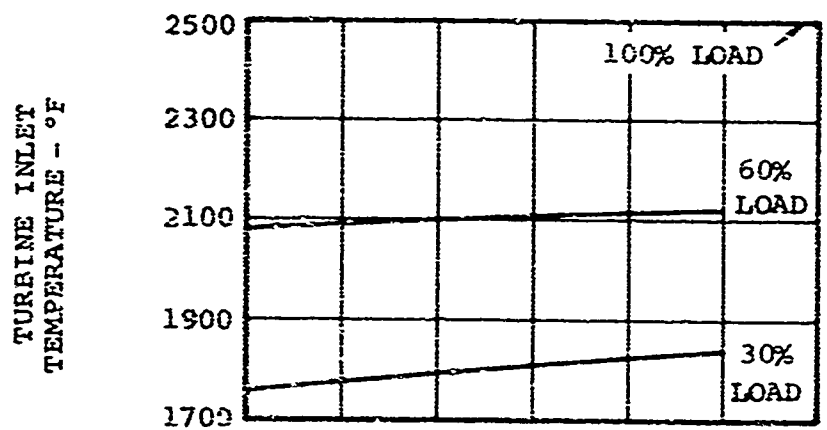


Figure 14. Engine Off-Design Performance: Turbine Inlet Temperature and SFC Versus Design Pressure Ratio.

Clearly, this selection, based on the preliminary data of this phase, is subject to uncertainty due to approximations that are inherent in the idealized compressor map. For this reason, neighboring design-point pressure ratios were also selected for further study in order to facilitate a firmer selection of an optimum design-point pressure ratio and to better estimate compressor design requirements for Task IIB.

Final selection from this phase activity was made for 9.5:1, 10.5:1, and 11.5:1 design-point pressure ratios. A plot showing compressor pressure ratio versus corrected flow for these three cases is presented in Figure 15. These three preliminary engine operating lines display the compressor design requirements for the tentative compressor design and matching studies of Task IIA.

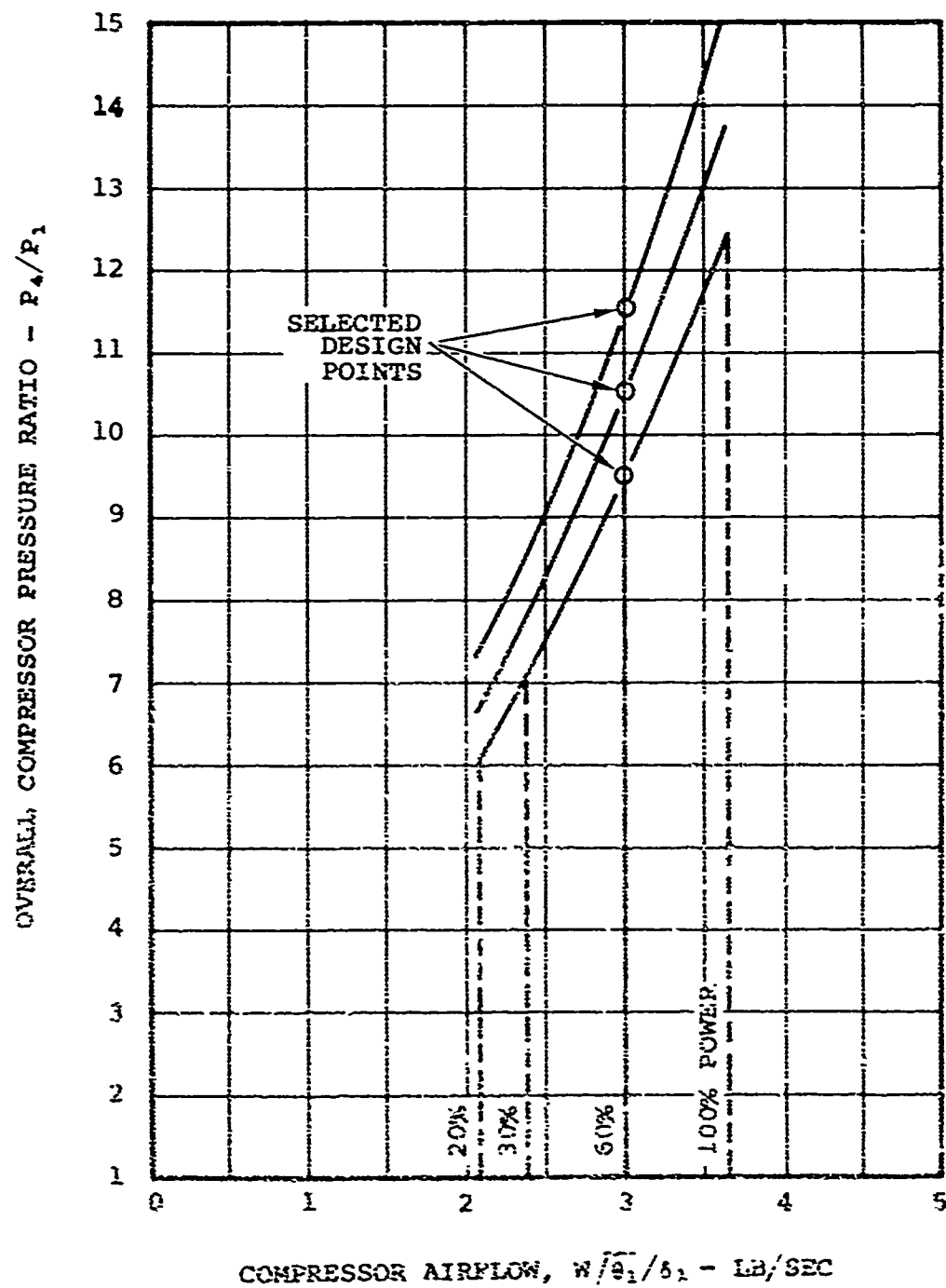


Figure 15. Engine Operating Lines
(Tentative Compressor Requirements).

3. TASK IIA, PRELIMINARY DESIGN AND MATCHING (TENTATIVE)

3.1 GENERAL

This section presents the results of compressor preliminary design and matching studies conducted to select the best compressor combination for the engine cycle identified in Task IA and discussed in the previous section. Certain relationships between compressor operation at design speed and power, and at other operating conditions, govern important factors of the compressor matching problem. These relations are derived in Appendix III, and their effect on compressor component operation is developed. Seven compressor combinations are then analyzed and their performance is compared.

3.2 PRELIMINARY DESIGN OF AXIAL AND CENTRIFUGAL COMPRESSORS

Preliminary design was conducted for axial and centrifugal compressors and was based upon the compressor design requirements as established by the tentative engine cycle analysis of Task IA, Section 2.0, and as displayed in Figure 5. These compressor design requirements are estimates based on the idealized compressor map employed in Task IA and on the selected design-point pressure ratios of 9.5:1, 10.5:1, and 11.5:1.

In order to reexamine the choice of one versus two axial plus centrifugal compressor configurations (refer to Paragraph 2.2.2), a comparison was made for the selected design-point pressure ratios. Results are presented in Table II.

Table II shows that a two-stage axial plus one-stage centrifugal (AA + C) compressor can be expected to yield a higher design-point compressor efficiency, by 0.5 to 0.9 point (depending on the final design-point pressure ratio), than that expected from a one-stage axial plus one-stage centrifugal (A + C). Furthermore, the off-design compressor efficiency at 100-percent power for the AA + C compressor versus the A + C compressor can be expected to be 1.0 to 2.0 points higher. This will yield a higher design-point cycle temperature for the AA + C compressor for the given constraint of 2500°F (TIT) at 100-percent power.

TABLE II. COMPARISON OF COMPRESSOR PERFORMANCE (A + C VERSUS AA + C)						
Design-Point Pressure Ratio (from Task IA)						
Description	9.5		10.5		11.5	
	Axial Com- ponent P_3/P_1	Overall η_C	Axial Com- ponent P_3/P_1	Overall η_C	Axial Com- ponent P_3/P_1	Overall η_C
1 Axial + 1 centrifugal	1.46	80.8	1.48	79.7	1.50	78.6
2 Axial + 1 centrifugal	2.02	81.3	2.05	80.4	2.09	79.5
$\Delta \eta_C = \eta_C(2 \text{ axial})$ $- \eta_C(1 \text{ axial})$	-	0.5	-	0.7	-	0.9

In addition to the foregoing, qualitative evaluation for these pressure ratios indicates that the AA + C compressor (5.1:1 centrifugal stage for 10.5:1 overall) will be smaller in diameter and slightly lighter in weight than a shorter A + C compressor (7.1:1 centrifugal stage for 10.5:1 overall).

Based on this, the choice for the AA + C compressor configuration was substantiated for these tentative compressor design and matching studies.

Further selection was made at this point to limit initial design and matching studies to the case of 9.5:1 design-point pressure ratio. This case was selected for rigorous evaluation of matching schemes. The cases of 10.5:1 and 11.5:1 were conducted later, based on the matching evaluation, and are reported in Paragraphs 3.4 and 3.5.

3.2.1 Two-Stage Axial Compressor Design, $P_3/P_1 = 2.02:1$

The performance characteristics of the two-stage axial compressor were taken from the data of a reference two-stage compressor of the GTCP660 engine. The particular compressor selected was chosen because of the complete knowledge of its aerodynamic design and its test results. It was intended that the compressor designed for this task be as aerodynamically similar to the reference compressor as possible. However, the geometry was expected to be different from that of the reference compressor because of the difference in the design conditions of the two compressors. Consequently, before the matching studies of Task IIA were begun, a preliminary design was performed for the axial compressor. The purpose of the calculation was to yield a design whose aerodynamic parameters, such as diffusion-factor and Mach-number levels, were commensurate with those of the reference compressor or good design practice, whichever was applicable.

The design flow of the axial compressor is 3.0 pounds per second, and the rotational speed is 60,000 rpm. The flow is a program specification. The rotational speed is a result of obtaining a satisfactory combination of inlet axial Mach number, first rotor tip speed, and inlet hub/tip ratio. An inlet Mach number of 0.55 and a hub/tip ratio of 0.5 were tentatively selected. The first rotor tip speed was selected to be close to that of the reference compressor and compatible with Figure 3 for good range. This was reconsidered in Task IIB when the range requirements became fully defined by the variable-geometry selection. This flow/speed combination was different enough from the reference compressor to prevent a direct scale.

Another design feature was the specification of zero rotor hub exit swirl. This specification was intended to minimize the distortion of the transition section between the axial and centrifugal stages.

The preliminary design calculation proceeded under the assumption of simple radial equilibrium. Radially constant stagnation energy and loss were assumed at each calculation station. Streamline slope and curvature, entropy gradient, and energy gradient are considered in Task IIB. The design effort in this task was to establish through this simplified procedure the feasibility of designing under the condition of zero rotor hub exit relative swirl while not exceeding established limits of certain aerodynamic criteria. The design results showed reasonable Mach-number, air-turning-angle, and diffusion-factor levels.

3.2.2 Centrifugal Compressor Design, $P_4/P_3 = 5.1:1$

The centrifugal compressor was designed with a computer-programmed procedure that determines the rotor and diffuser geometry. The rotor is designed from empirical correlations for surge, choke, slip factor, and efficiency for centrifugal compressors, with arbitrary values of blade exit angle relative to the radial direction. Data have been correlated for blade exit angle up to 42° . The vaneless diffuser uses the conventional pipe flow analogy with an empirical friction coefficient. The vaned diffuser is treated as a cascade and uses cascade loss and turning-angle correlations to obtain overall stage performance.

The design configuration was established through a parametric study involving several aerodynamic parameters. For a given rotor exit absolute air angle, the performance correlations contained in the program provide the variation of blade exit angle with shroud-line relative velocity ratio. This is the ratio of the rotor outlet/inlet relative velocity at the shroud. At each relative velocity ratio, the vaneless diffuser gap was varied to obtain maximum overall stage efficiency. The variation of maximum efficiency with shroud-line relative velocity ratio was then obtained for three values of absolute exit air angle.

The results are summarized in Figure 16. The maximum efficiency of the stage increases as the air angle decreases from 75° to 69° . The efficiency variation for each air angle tends to approach a peak value, but then increases linearly. The reason for this is that the design value of impeller efficiency has not been penalized for impeller rear-disk friction. As blade exit angle increases, the rotor diameter increases and exit width decreases. The clearance penalty has been accounted for, but not the increase in disk friction at the back of the rotor. Consequently, the curves should probably reach a maximum.

It was believed that 50° of blade angle represents a realistic advance in the state of the art. This is only 8° higher than the maximum for which data has been accumulated, and the disk friction correction should be small. At 50° , the air-angle value of 69° has the highest stage efficiency. Lower values of air angle were not examined, since it appeared that, at 50° of blade exit angle, the efficiency is close to maximum.

The diffusion factor of the second row of the tandem cascade is shown for reference, since it is the more highly loaded of

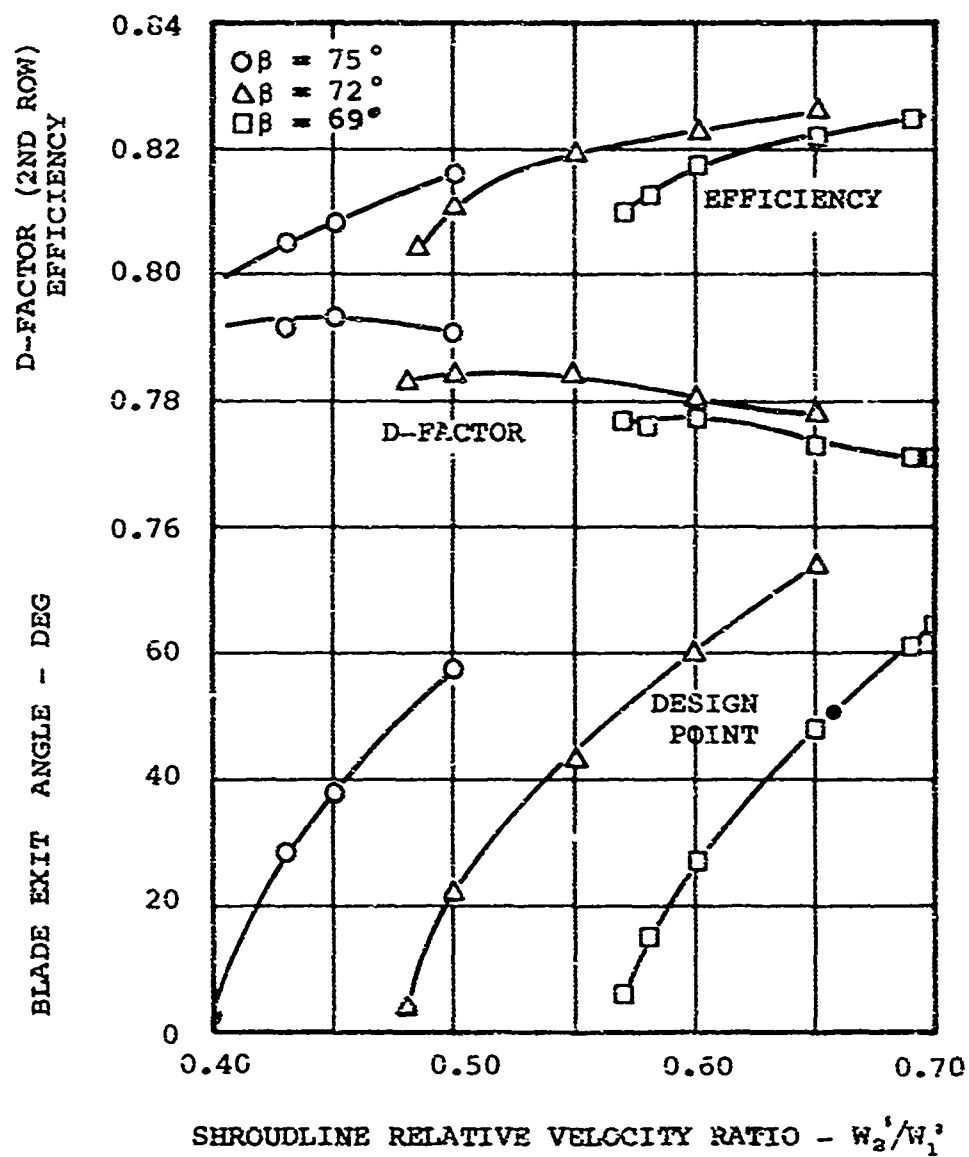


Figure 16. Design Study for Centrifugal Stage of 9.5:1-Pressure-Ratio Compressor: Blade Exit Angle, Stage Efficiency, and Diffusion Factor.

the two rows. The diffusion factor decreases as rotor exit absolute air angle decreases.

Figure 17 shows the variation of rotor tip radius, rotor exit width, and clearance efficiency penalty as functions of shroud-line relative velocity ratio and absolute exit air angle. The exit width decreases as the air angle decreases and, to a lesser degree, as shroud-line relative velocity ratio increases. These give consequent increases in clearance penalty.

Upon completion of the design, the program uses the geometry to compute the complete performance characteristics from surge to choke at all speeds of interest. Correlations are included in the program for efficiency degradation due to Reynolds number as well as clearance. Both the design and off-design calculations account for these influences. Only the clearance penalty was significant; Reynolds number was too high to contribute to loss.

3.3 COMPRESSOR MATCHING STUDIES, $AA + C, P_4/P_1 = 9.5:1$

Axial-centrifugal compressor matching studies were conducted based on the axial and centrifugal compressor designs conducted for this task and reported in Paragraph 3.2 above. The detailed preliminary design for these compressors produced estimated efficiency levels slightly higher than those predicted in Task IA and produce an overall compressor peak efficiency (with no degradation for matching) of 0.834.

The objective of these compressor matching studies was to identify the axial-centrifugal compressor matching scheme that would hopefully yield this peak efficiency coincident with the design operating point (60-percent power) and provide satisfactory operation over the range of 20- to 100-percent power.

3.3.1 Initial Studies

Initial matching attempts were intended to scale the axial and centrifugal compressors for peak efficiency match at design flow and employ variable compressor geometry as required for off-design surge margin and off-design efficiency. However, the matching iterations conducted in the preliminary design of the axial and centrifugal compressors showed the major problem to be one of achieving a design point match at part power such as to realize near maximum efficiency in the axial compressor. This results from the characteristics of

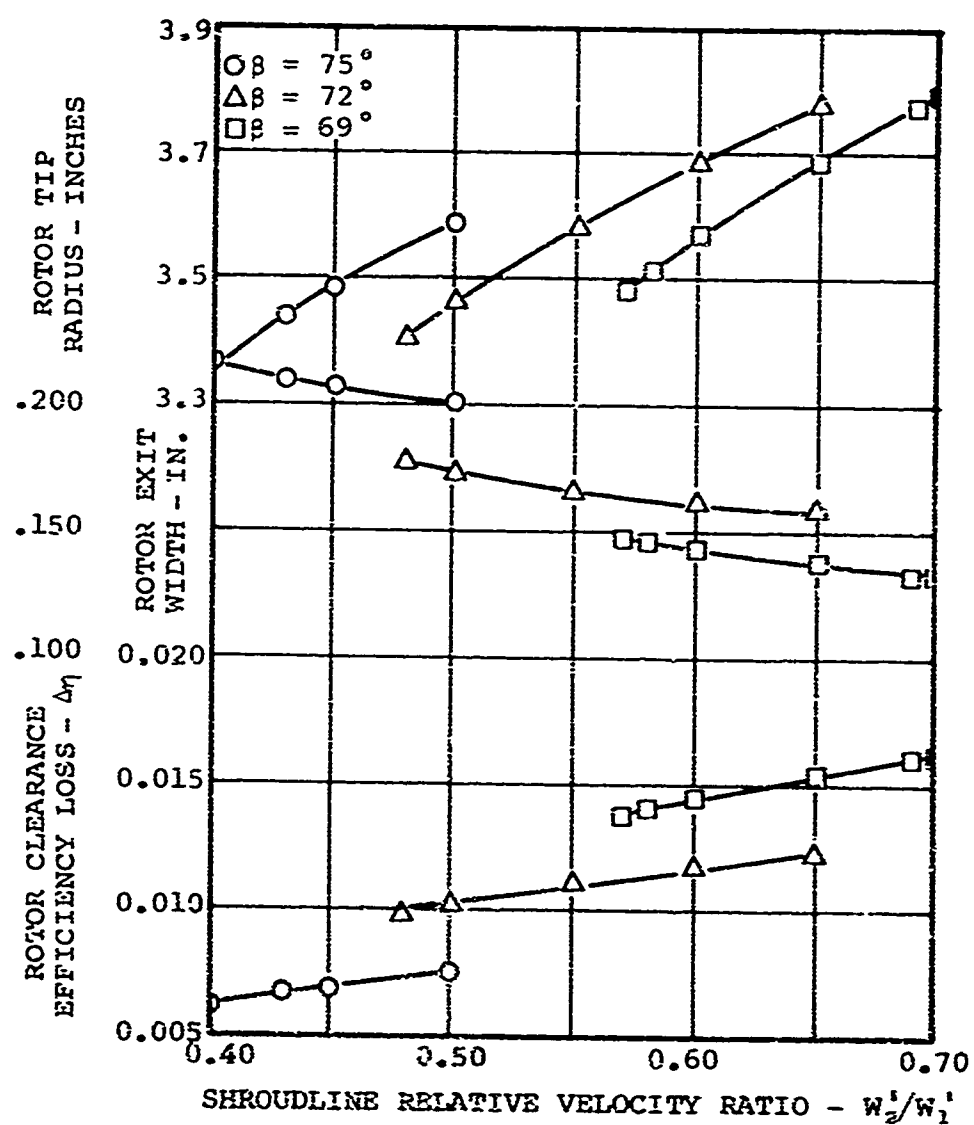


Figure 17. Design Study for Centrifugal Stage of 9.5:1-Pressure-Ratio Compressor: Clearance Loss, Rotor Tip Radius, and Rotor Exit Width.

the gasifier and power turbines (choked nozzles) in relating the compressor flows, pressure ratios, and speeds for the various power points, especially 100- and 60-percent power. This relationship is developed in Appendix III and is illustrated in the following example.

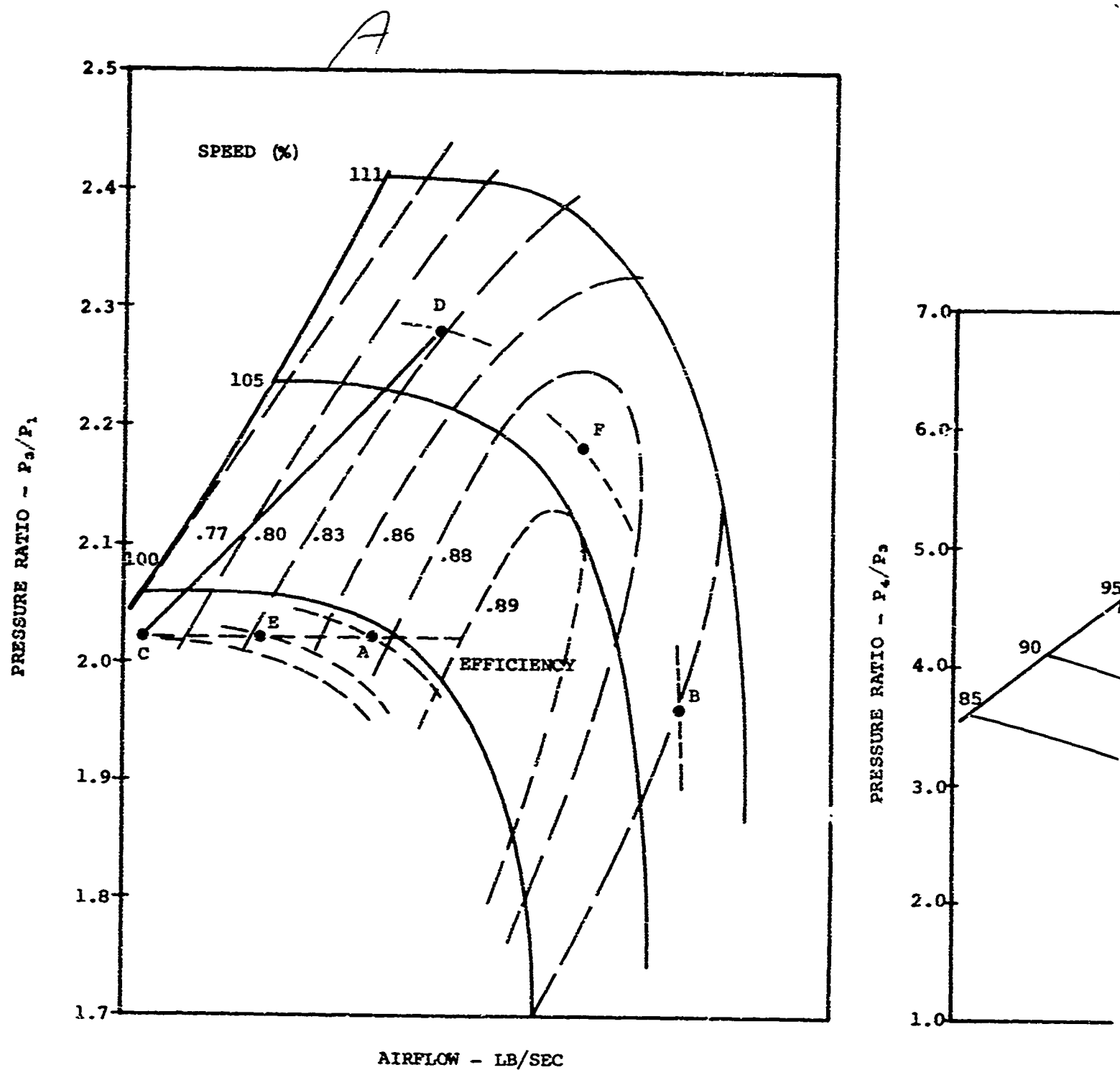
Iterative matching attempts were conducted for representative axial and centrifugal compressors to achieve near peak efficiency operation at the 60-percent-power point while meeting the off-design compressor requirements of pressure ratio, efficiency, and flow for 20-, 30-, and 100-percent-power points. For the case of fixed turbine geometry (and choked nozzle), the gasifier turbine temperature ratio for off-design to design-point operation is fixed and, consequently, the gasifier spool-speed ratio for off-design to design-point operation is fixed. From Task IA, the 100-percent power requirements are compared to the 60-percent power requirements and are repeated here for clarity:

$$\frac{W_{C,100}}{W_{C,60}} = 1.21 \quad \frac{P_4/P_1]_{100}}{P_4/P_1]_{60}} = 1.31 \quad \frac{N_C/\sqrt{\theta_1}]_{100}}{N_C/\sqrt{\theta_1}]_{60}} = 108.4$$

A compressor match based on these required relationships, and on a fixed compressor geometry was achieved for an assumed TIT (maximum) of 2500°F. Results are displayed on Figure 18, which shows that the design-point operation, illustrated as Point C, of the axial compressor is approximately 11 points below peak efficiency (0.89 minus 0.78).

While this match results in operation of the axial compressor near stall at the design point, it is more important to observe the poor match-point efficiency.

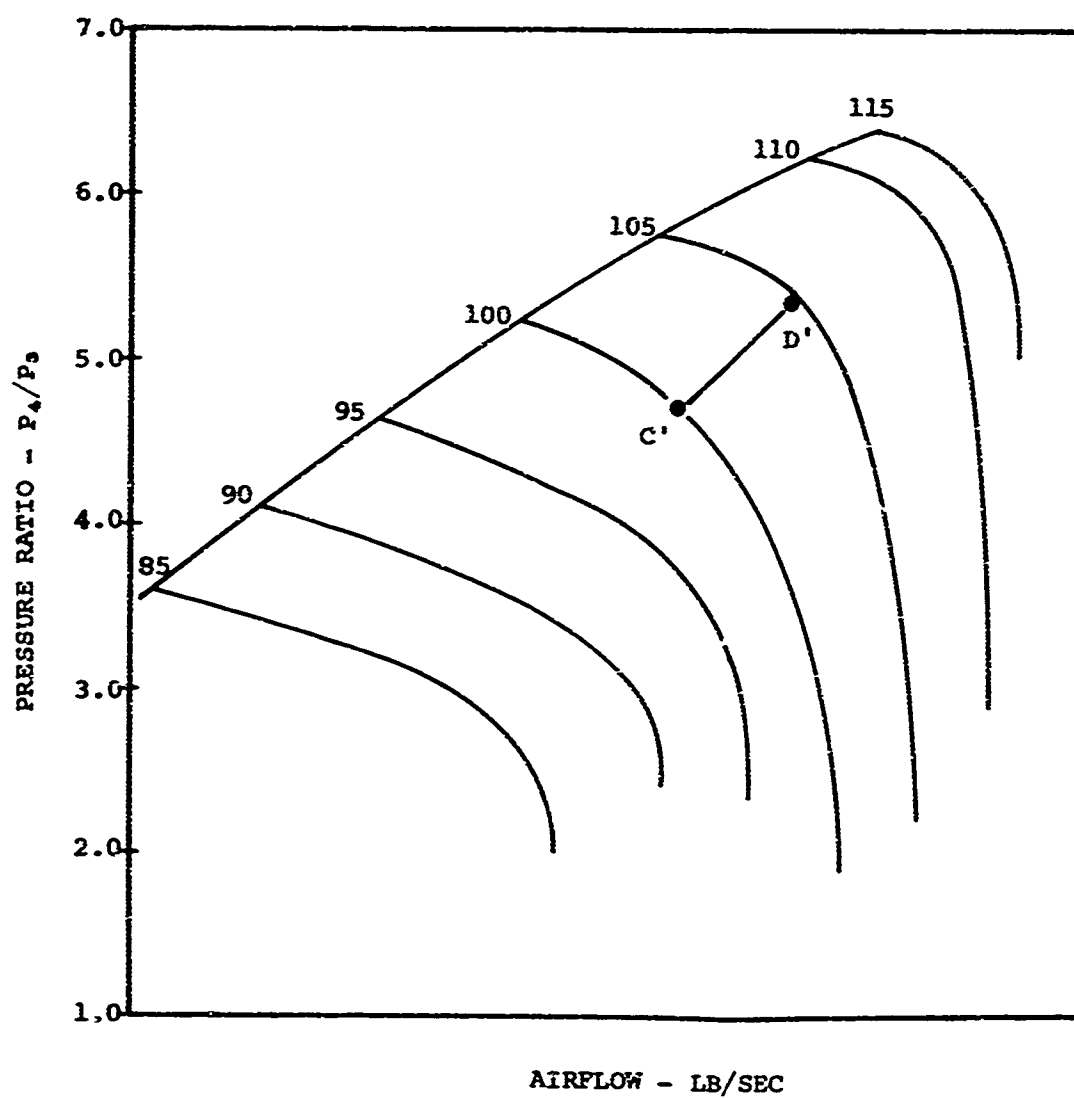
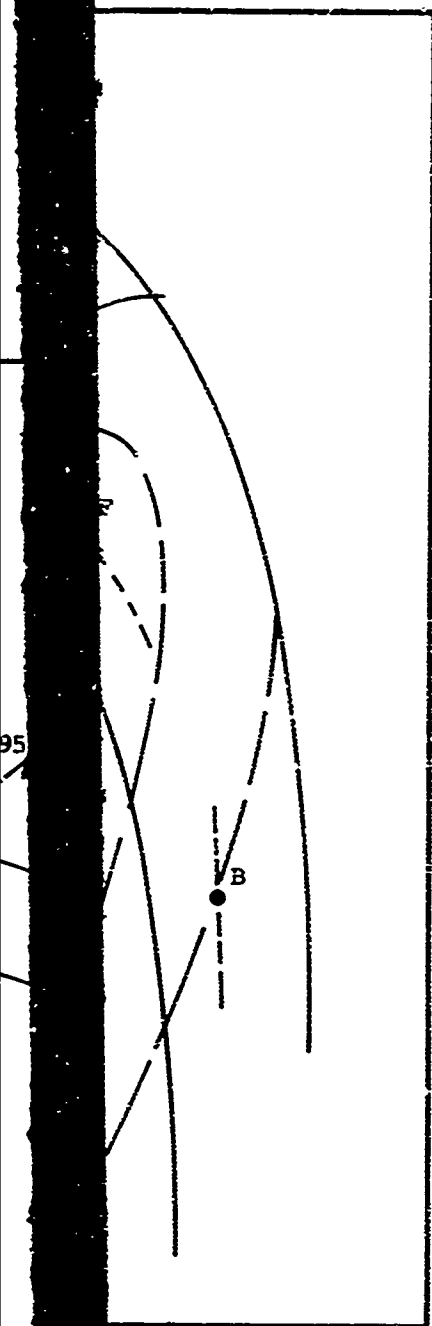
The poor match results from the fact that the required match point on the axial compressor component is forced to a lower flow than that coincident with peak efficiency for the design speed. This is a direct result of the relationship of the compressor requirements for 100- and 60-percent power points as determined by the engine cycle analysis in Task IA, and repeated above.



(A) AXIAL COMPRESSOR MAP

Figure 18. Illustration of Match Points on Compressor Maps.

B



(B) CENTRIFUGAL COMPRESSOR MAP

nts

From the axial compressor map, the ratio of choke flows between design speed and a speed that is 1.085 of design speed is 1.10. This is not a peculiar feature of the map, but it can be shown to be typical. To arrive at the required 1.21:1 flow ratio, it is necessary to select a flow at design speed that is about 10 percent from design-speed choke flow. This would locate the 100-percent-power point on choke flow at 1.085 speed ratio. Points A and B on Figure 18 show this. However, since design pressure ratio is 2.02:1, Point A must fall on a speed line less than the one identified as 1.0. This then becomes the design speed if Point B combines the pressure ratio of its centrifugal compressor match point to give the required overall pressure ratio at 100-percent power. The match shows that the overall pressure ratio is too low. To arrive at the axial/centrifugal pressure ratio at 100-percent power, the axial pressure ratio at a speed ratio of 1.085 must increase. As it does, the flow moves off to choke and, to maintain the 1.21:1 flow ratio, the flow at design speed moves further from choke flow. At some point, the speed and flow ratio requirements are met, together with the overall pressure ratios required at the 60- and 100-percent-power points. This case is illustrated on Figure 18 as Points C and D.

Note that, since peak axial compressor efficiency is near choke flow, the operating line characteristic forces the design point to be far from the peak efficiency of the axial compressor at design speed. To achieve a better design-point match and meet the off-design compressor requirements, some form of variable compressor geometry or twin spooling is required.

One case to be considered would be inlet guide vanes (IGV's) ahead of the axial compressor. Actuating IGV's opposite to the rotor rotation at 100-percent power shifts the compressor characteristics toward higher flows and pressure ratios relative to the design speed characteristics. This would move the match point toward the peak efficiency by increasing the choke flow ratio $(W_{C,100}]choke / W_{C,60}]choke)$ for the fixed speed ratio.

Another approach would be inlet guide vanes ahead of the centrifugal compressor. Actuation against rotation of these IGV's at 100-percent power would increase the pressure ratio and flow so that the overall compressor requirements at 100-percent power would be met at a higher flow and lower pressure ratio for the axial compressor. From part A of Figure 18, Point D would then move to F, and consequently C to E.

A third approach to be considered is variable diffuser vanes (VDV's) for the centrifugal stage. Actuation of VDV's at 100-percent power would increase flow and allow the overall compressor requirements to be met at a higher flow in the axial compressor.

Based on these observations, the major advantage to be derived from variable compressor geometry is modification of the pressure ratio and flow characteristics of the overall compressor to allow match-point selection on the axial compressor nearer to choke and hence nearer to peak efficiency. It is not clear from this example how combinations of these variable-geometry cases might behave; therefore, they were evaluated and are discussed in the following paragraphs. The best variable matching scheme would then have to be compared to twin spooling to make a selection.

3.3.2 Evaluation of Matching Schemes

Based on the observations made in the initial matching studies, seven matching schemes were selected for evaluation. Off-design surge margin was a secondary consideration for these studies.

Since the preliminary designs for the two-stage axial and single-stage centrifugal compressors used in these studies are essentially identical, the differences in overall compressor efficiency and engine SFC that are reported in the paragraphs that follow are attributable to the effects of the compressor matching variation studied. All values except as noted are based on matching for 2500°F TIT at 100-percent power. The seven schemes studied were for the combinations of compressors shown on the following page.

Two-Stage
Axial Compressor
(AA)

Single-Stage
Centrifugal Compressor
(C)

Single Spool

- | | |
|--------------------------------------|--|
| 1. Fixed geometry (FG) | Fixed geometry (FG) |
| 2. Fixed geometry (FG) | Variable diffuser vanes (VDV) |
| 3. Fixed geometry (FG) | Variable inlet guide vanes (VIGV) |
| 4. Variable inlet guide vanes (VIGV) | Fixed geometry (FG) |
| 5. Variable inlet guide vanes (VIGV) | Variable inlet guide vanes (VIGV) |
| 6. Variable inlet guide vanes (VIGV) | Variable inlet guide vanes plus variable diffuser vanes (VIGV + VDV) |

Twin Spool

- | | |
|------------------------|---------------------|
| 7. Fixed geometry (FG) | Fixed geometry (FG) |
|------------------------|---------------------|

For each of these combinations, several matching iterations were made by use of existing computer programs for compressor matching and for engine cycle performance. Iterations were based on compressor matching data and engine cycle data to effect satisfactory matches for minimum SFC for design-point operation (60-percent power).

The results of these compressor matching studies are discussed in the following paragraphs. Compressor and compressor-component maps are included and display the estimated compressor design requirements as determined in Task IA and the actual engine operating points as determined by engine cycle analysis (Task IB) based on the respective compressor maps as reported below.

Based on these matching studies, a "best" matching scheme was selected for further evaluation.

3.3.2.1 Single Spool, AAFG + CFG

A match was achieved for this combination, consisting of:

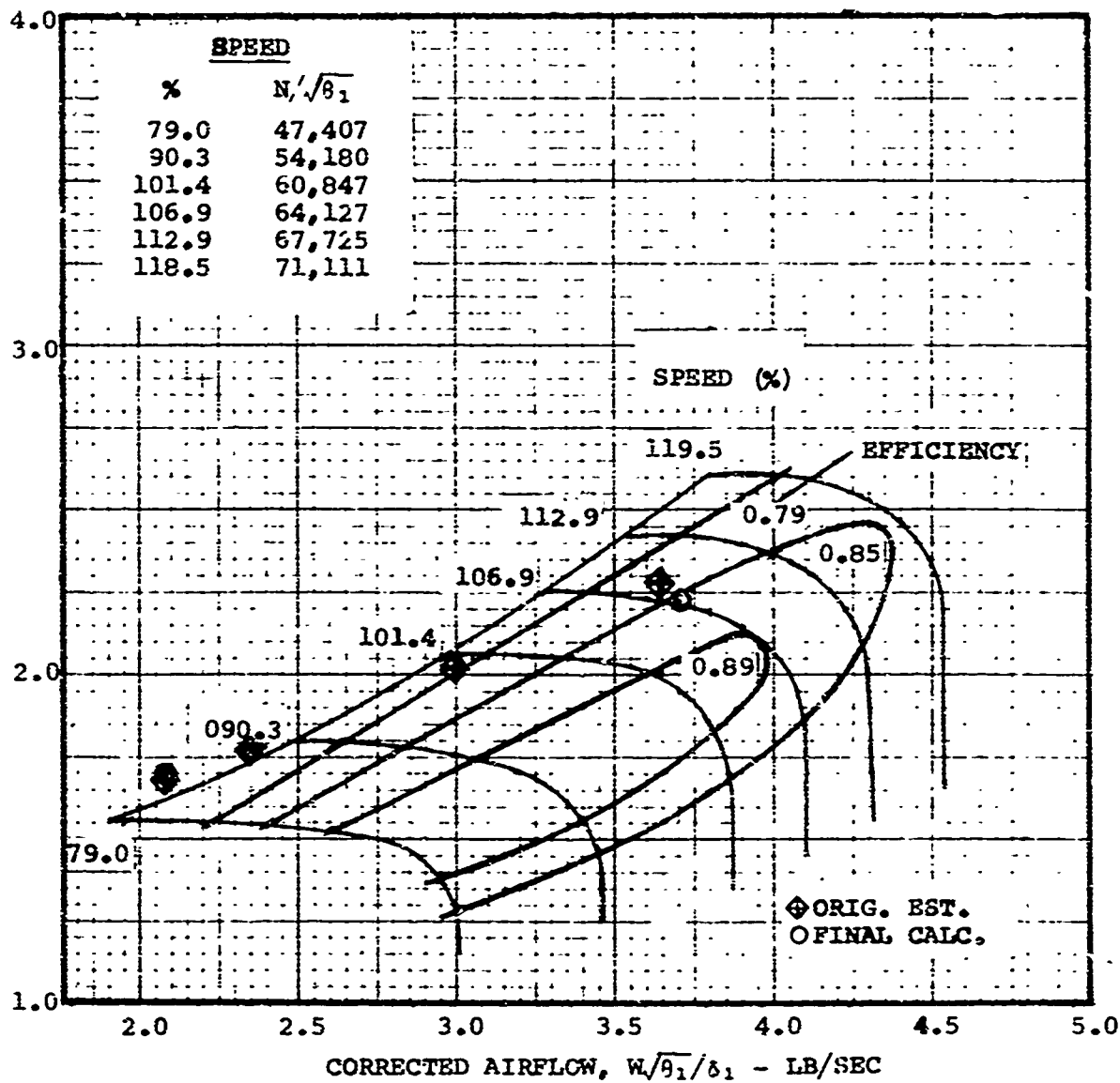
1. Two-stage axial compressor component, fixed geometry (AAFG)
2. Single-stage centrifugal compressor component, fixed geometry (CFG)

The results of this study show that the axial compressor operates far from peak efficiency over the range of 20- to 100-percent power. Furthermore, the axial compressor operates in the stall regime at reduced power levels. The poor match resulting from this combination is evidenced by an overall compressor peak efficiency of approximately 0.795. This data provides quantitative evidence of the conclusions made in the preliminary matching studies. The data for this study are displayed in the three compressor maps of Figure 19.

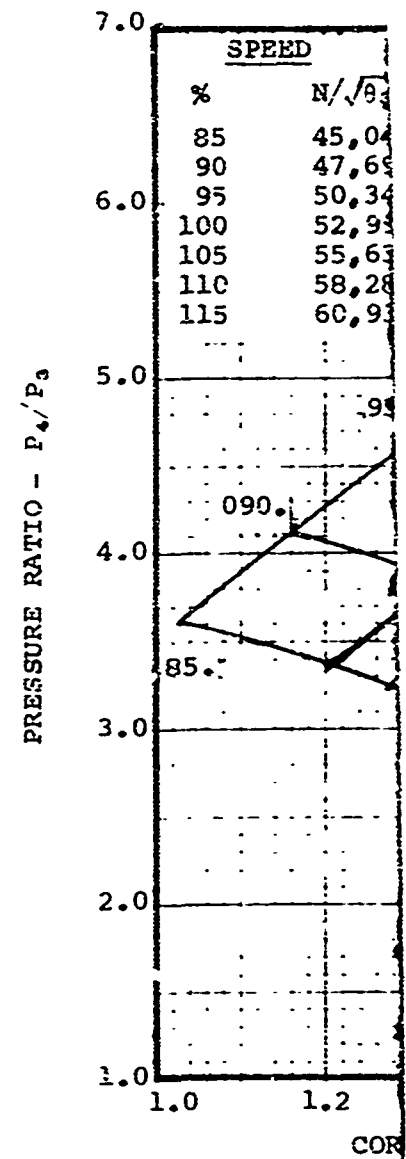
The axial and centrifugal compressor efficiency levels assumed for this study are as estimated by preliminary design and include no efficiency degradation ($\eta_C = \eta_{C, \text{DESIGN}}$).

Parts A and B of Figure 19 display the performance characteristics of the axial and centrifugal compressors as they would be obtained from individual component rig tests for these compressors. Part C of Figure 19 displays the performance characteristics of the multistage compressor obtained from the individual performance characteristics of Parts A and B. The surge line of the axial compressor is also included on Figure 19C. It passes between the 30- and 60-percent power points. Off-design operation to the left of the surge line of the inlet stages is a familiar experience in multistage axial compressors. The presence of a centrifugal compressor instead of many more axial stages has not changed this.

On axial-centrifugal combinations, however, multistage instability has been experienced at the axial compressor surge line. This instability occurs over a small range of flow at any given speed. The reason for this can be shown in Figure 19D.



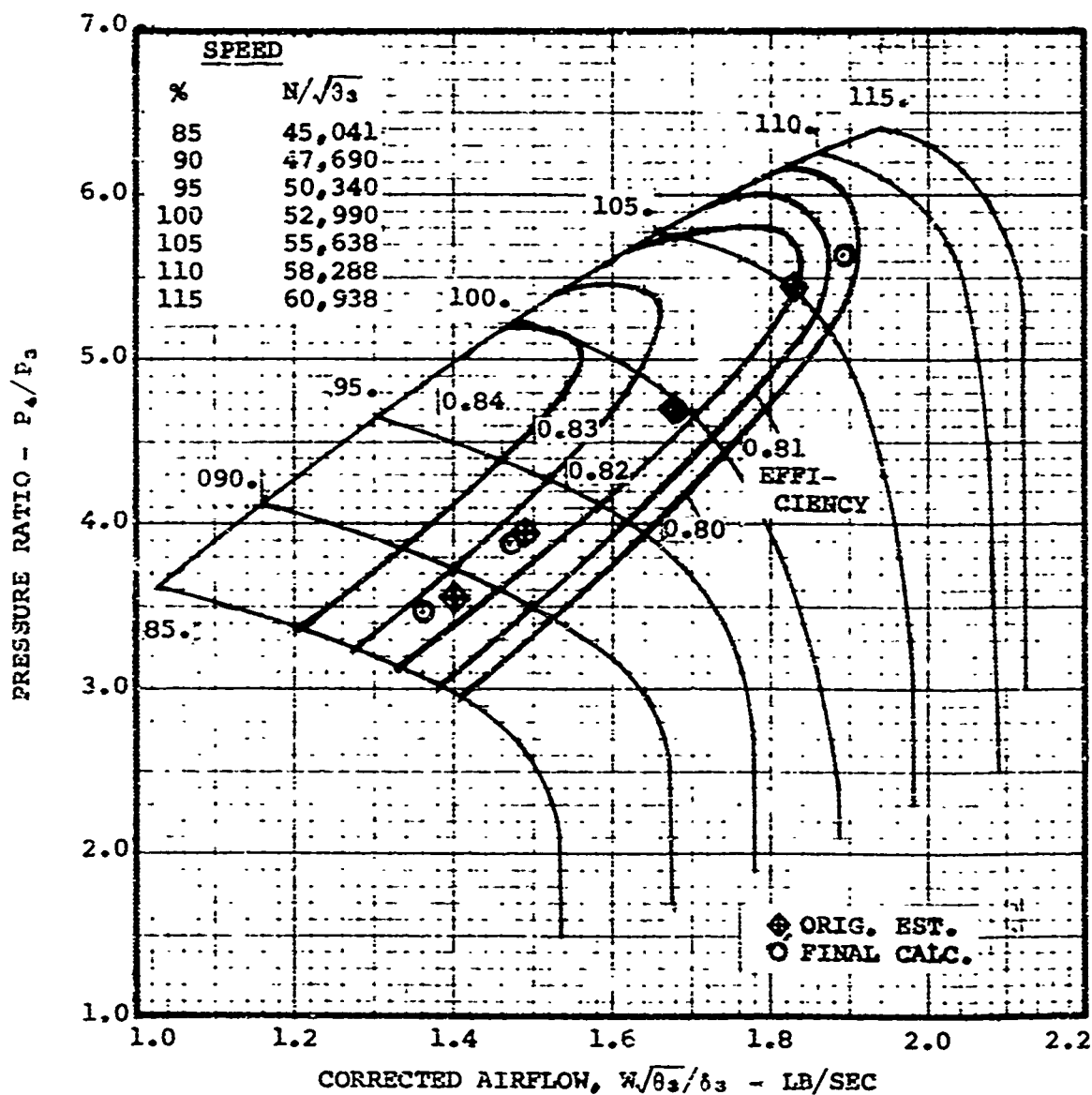
(A) AXIAL COMPRESSOR COMPONENT: FIXED GEOMETRY



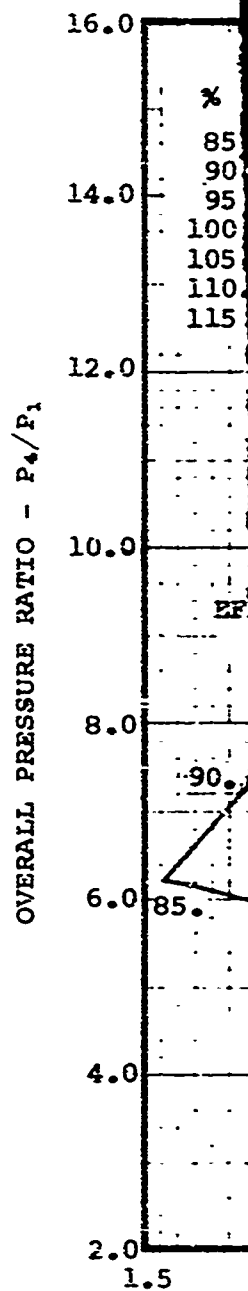
(B) CENTRIFUGAL COMPRESSOR COMPONENT: FIXED GEOMETRY

Figure 19. Estimated Performance Characteristics, Two-Stage Axial Plus Centrifugal Compressor (Includes No Efficiency Degradation), AAFG + CFG.

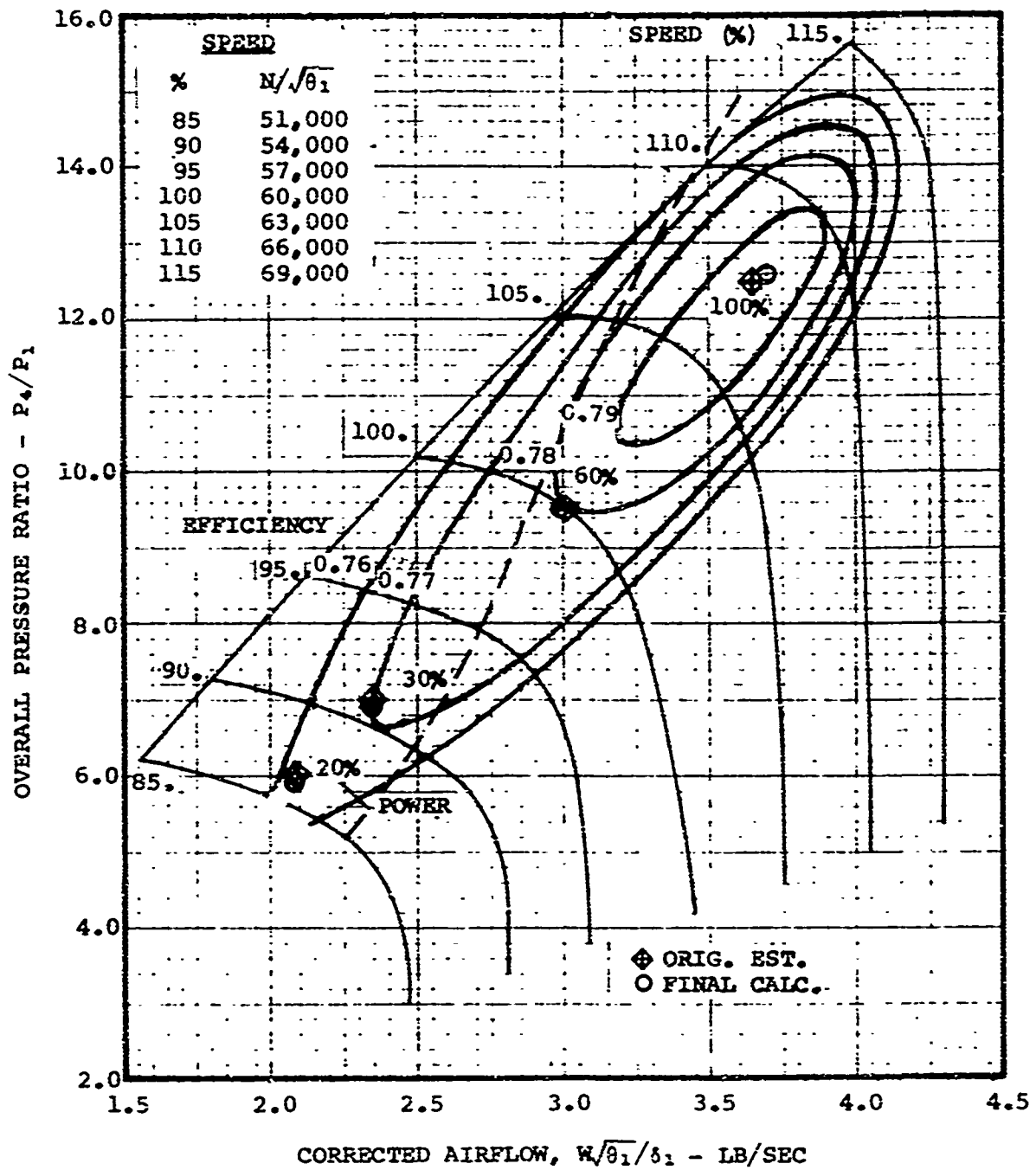
13



(B) CENTRIFUGAL COMPRESSOR COMPONENT: FIXED GEOMETRY

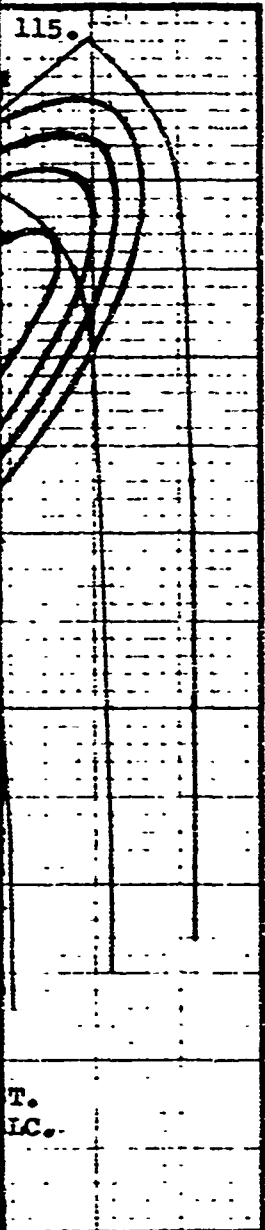


C



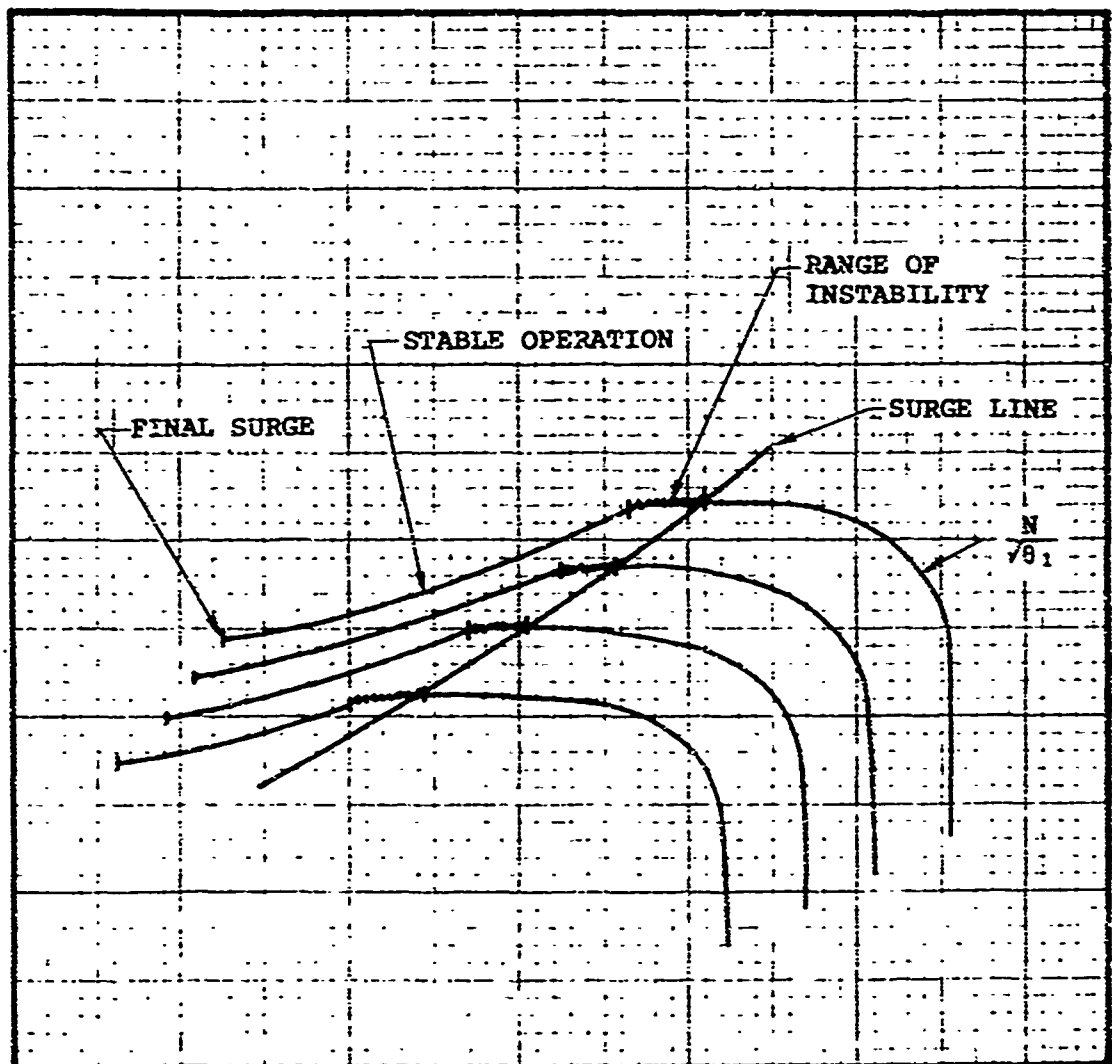
(C) OVERALL COMPRESSOR

D



4.0 4.5

PRESSURE RATIO - P_3/P_1



CORRECTED AIRFLOW, $W\sqrt{\theta_1}/6$ - LB/SEC

(D) AXIAL COMPRESSOR OPERATING REGIMES

On a rig test of the axial compressor, the performance characteristics are usually obtained from choke to the surge line. Continued throttling will reveal that the compressor can be brought out of surge and that stable operation can exist to the left of the usual surge line. However, the surge line is not a line, but is a small range of flow that exists before stable operation can be achieved with continued throttling. This range of flow acts as a range of instability for the axial-centrifugal combination. The multistage compressor will not surge, but a rig test would reveal an inability to acquire data within this instability range.

Similarly, it will not be possible for an engine to have a steady-state operating point within this range. From the proximity of the 20- and 30-percent power points to the axial compressor surge line in Figures 19A and 19C, it is conceivable that these power points and, in fact, all power points below about 50 percent would fall within the width of the range of instability. For engine operation which would accelerate across the axial compressor surge line, this instability is not a problem; for engine operation which demands steady-state power delivery, it is a problem. Clearly, besides better efficiency matching, a definite amount of margin from axial compressor surge is needed. Both of these parameters, overall efficiency and surge margin from axial compressor surge, will be referred to in the performance displays through the rest of this report.

Since data to the left of surge is not usually acquired on test and because of the paucity of data that is available, a simplified model for the axial compressor performance to the left of surge was assumed in order to match with the centrifugal compressor and compute the multistage performance. Pressure ratio characteristics were extended at a constant value which was taken as the surge value. Temperature rise ratio was extrapolated nearly linearly, concomitant with checks with efficiency to yield a smooth variation of efficiency with flow at any given speed. With the axial compressor performance characteristics thus extended, the overall performance was computed with centrifugal compressor surge used to define the surge of the multistage compressor.

Part A of Figure 19 indicates a design-point efficiency of 0.77 (3 pounds per second) compared to 0.896 (3.75 pounds per second) at peak efficiency for design speed. This shows, as did the initial matching studies, the

desirability of moving the design point toward choked flow for improved efficiency over the operating range.

Part B of Figure 19 indicates a design-point efficiency of 0.823 compared to 0.83 at 10-percent surge margin. Additional matching iterations could effect relocation of the design point on this map to achieve the peak efficiency but is unwarranted for this preliminary study.

Part C of Figure 19 indicates a design-point efficiency of 0.78 with adequate multistage surge margin over the operating range. Note that the compressor operating line falls on the maximum efficiency for each speed line. However, due to the poor component efficiency match, the maximum efficiency levels are significantly lower than the potential.

The compressor and engine SFC data for this combination are shown in Table III.

TABLE III. AAFG + CFG COMPRESSOR					
Percent Power	$W \sqrt{\theta}/\delta$ (lb/sec)	P_4/P_1	$\eta_{4,1}$	T_5 (°F)	SFC
100.0	3.698	12.57	0.793	2500	0.450
60.0	2.989	9.50	0.780	2150	0.497
29.0	2.351	6.93	0.768	1800	0.649
18.5	2.080	5.92	0.762	1650	0.816

Additional matching runs were made for lower selected TIT levels to evaluate this effect on matching. Results showed no effect on compressor component matching and showed higher SFC's as predictable for the lower cycle temperatures. The compressor and engine cycle data points are shown in Table IV for the case of 2250°F TIT at 100-percent power.

TABLE IV. AAFG + CFG COMPRESSOR (REDUCED T_5)					
Percent Power	$W \sqrt{\theta}/\delta$ (lb/sec)	P_4/P_1	$\eta_{4,1}$	T_5 (°F)	SFC
100.0	3.725	12.61	0.793	2250	0.471
59.7	3.014	9.57	0.780	1940	0.526
29.5	2.391	7.10	0.769	1650	0.694
21.0	2.170	6.30	0.763	1550	0.839

3.3.2.2 Single Spool, AAFG + CVDV

A match was achieved for this combination, consisting of:

1. Two-stage axial compressor component, fixed geometry (AAFG)
2. Single-stage centrifugal compressor component, variable diffuser vanes (CVDV)

The results of this study show improvement in the operating characteristics of the axial compressor compared to the fixed-geometry combination (AAFG + CFG). However, the axial compressor for this combination operates at lower than optimum flows over most of the speed range and near stall at the lower power points. This match yields an overall compressor peak efficiency of approximately 0.81 near the 100-percent-power point.

The axial and centrifugal compressor efficiency levels assumed for this study are as estimated by preliminary design and include no efficiency degradation for CVDV ($\eta_C = \eta_{C,DESIGN}$).

Based on matching iterations for this combination, CVDV angle settings were selected to be 0° for speeds up to and including 100-percent design speed, and -2° for speeds above 100 percent. Note that negative setting angles denote adjustment to reduce the vane angle with respect to the radial direction and thereby increase flow. The data for this study are displayed in the three composite compressor maps (0° and -2° CVDV setting angles) of Figure 20.

Part A of Figure 20 displays axial compressor characteristics and reflects the improved compressor match by the closer proximity of the operating line to the peak efficiency region of the axial component. An improvement in surge margin is also evidenced by this map, and actuation of the diffuser vanes at the lower power settings could be considered to achieve additional surge margin for the low power points.

Part B of Figure 20 displays the centrifugal compressor characteristics and shows a narrow surge margin at the 100-percent-power point. This would prevent a rematch to move the 60- and 30-percent-power points nearer to the peak efficiency operating regime that exists nearer to surge.

Part C of Figure 20 displays the overall compressor characteristics and shows that the operating line falls very near to the peak efficiencies for the speed lines over the operating range. Also, the efficiency islands display higher efficiency levels than were achieved with the fixed-geometry combination, reflecting substantial improvement in the compressor match.

The compressor and engine SFC data for this combination are given in Table V.

TABLE V. AAFG + CVDV COMPRESSOR					
Percent Power	$W \sqrt{\theta}/\delta$ (lb/sec)	P_4/P_1	η_{41}	T_5 (°F)	SFC
100.0	3.690	12.60	0.809	2500	0.444
60.0	2.988	9.51	0.801	2130	0.487
30.8	2.389	7.08	0.788	1800	0.616
19.5	2.096	6.00	0.778	1650	0.770

3.3.2.3 Single Spool, AAFG + CVIGV

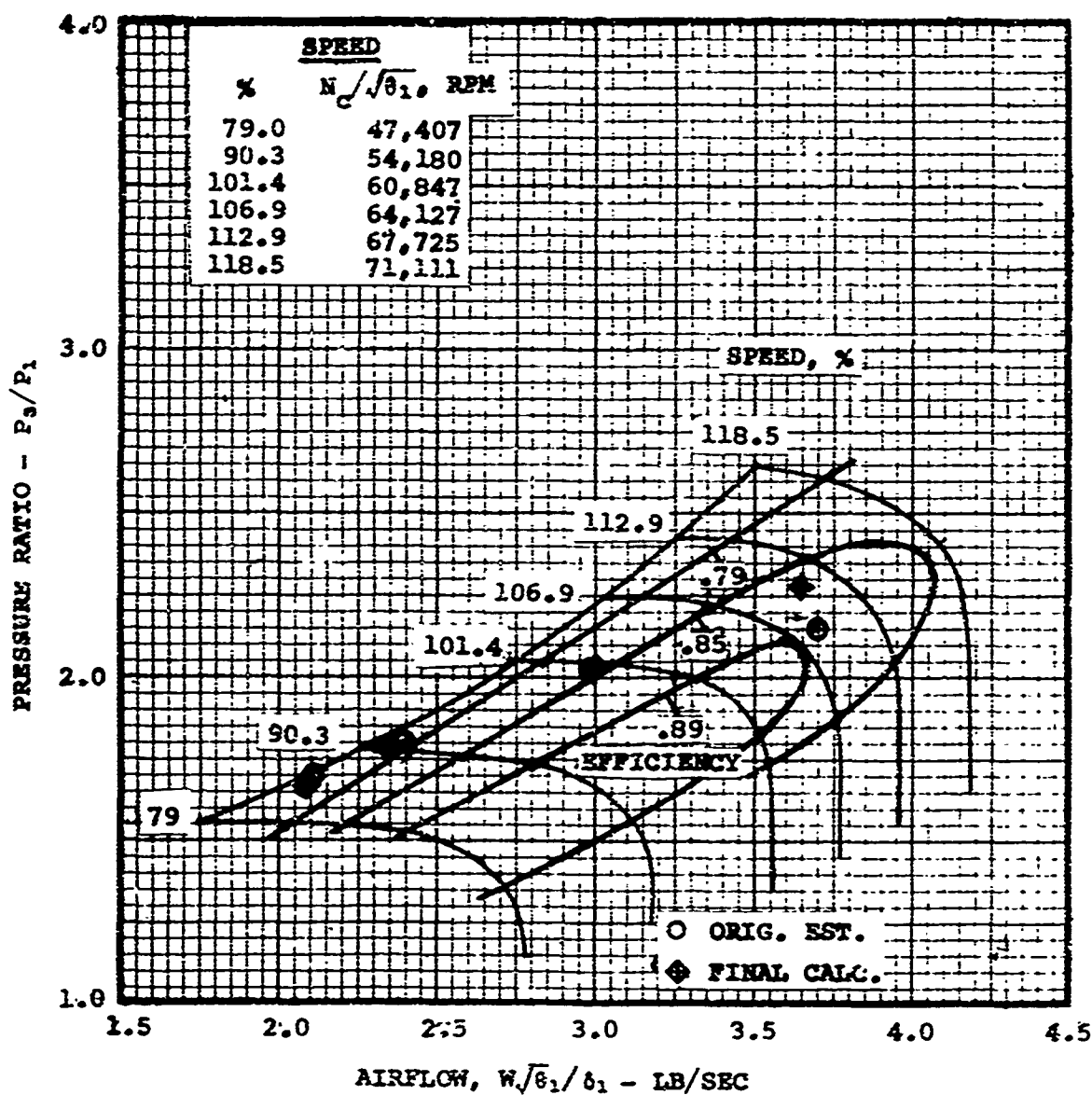
A match was achieved for this case, consisting of:

1. Two-stage axial compressor component, fixed geometry (AAFG)
2. Single-stage centrifugal compressor component, variable inlet guide vanes (CVIGV)

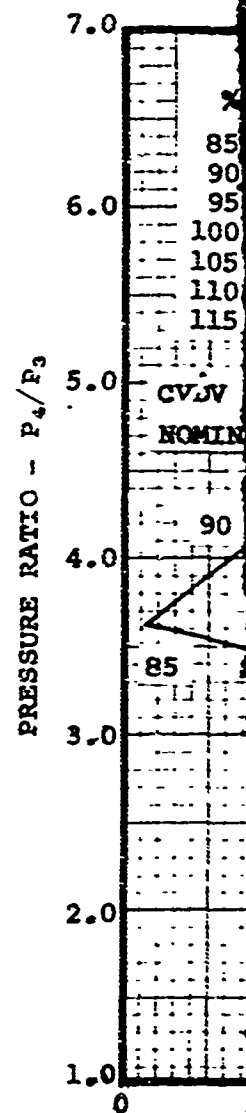
The results of this study show improvement in the match of the axial compressor compared to the fixed-geometry combination (AAFG + CFG) but no significant improvement compared to the combination with variable diffuser vanes (AAFG + CVDV). The axial compressor operates at lower than optimum flows over most of the speed range and near stall at the lower power points.

The axial and centrifugal compressor efficiencies assumed for this study are as follows:

1. Compressor efficiencies are as estimated by the compressor preliminary design
($\eta_C = \eta_{C, \text{DESIGN}}$).



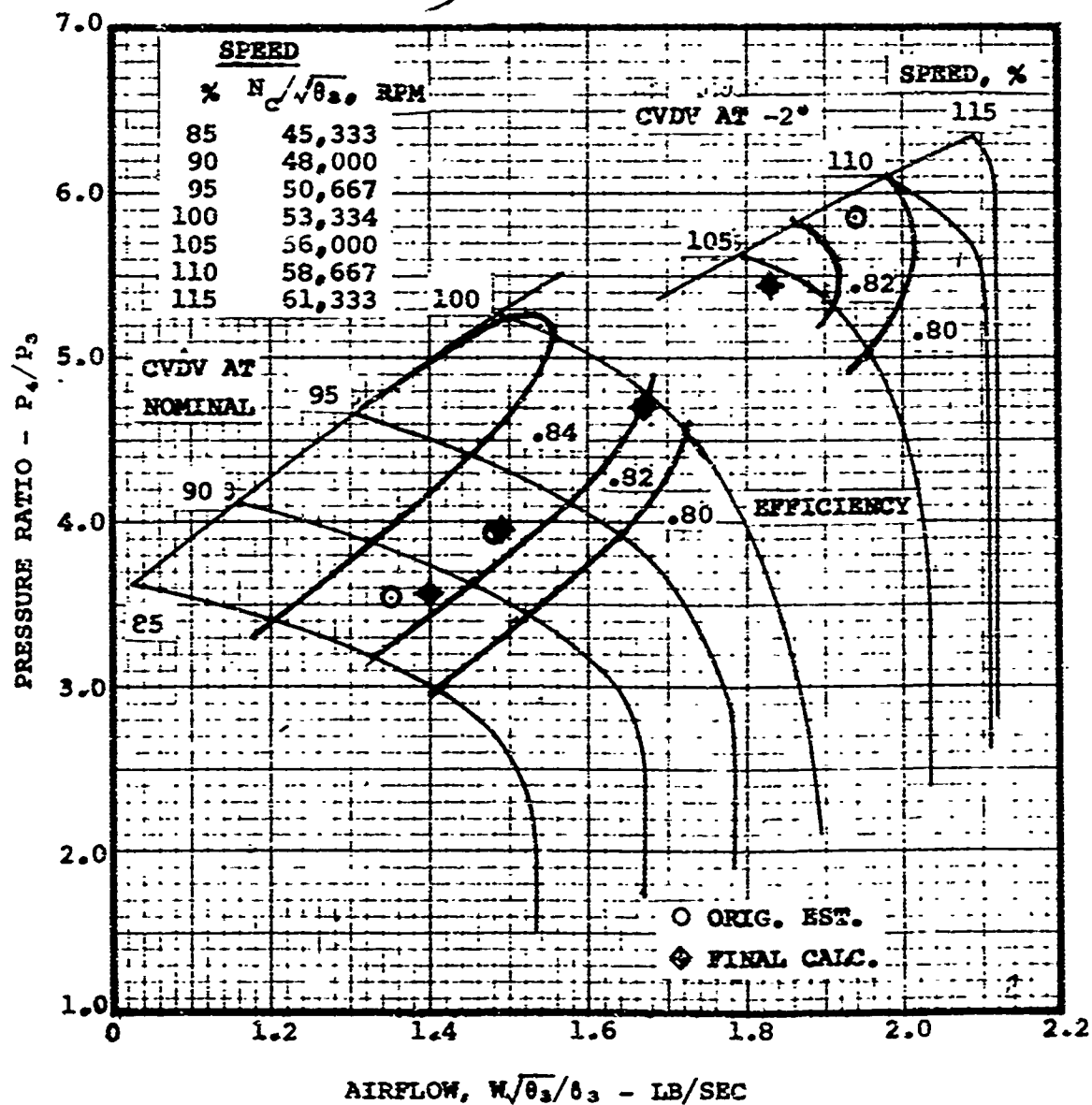
(A) AXIAL COMPRESSOR: FIXED GEOMETRY



(B)

Figure 20. Estimated Performance Characteristics, Two-Stage Axial Plus Centrifugal Compressor (Includes No Efficiency Degradation Due to CVDV's), AAFG + CVDV.

B

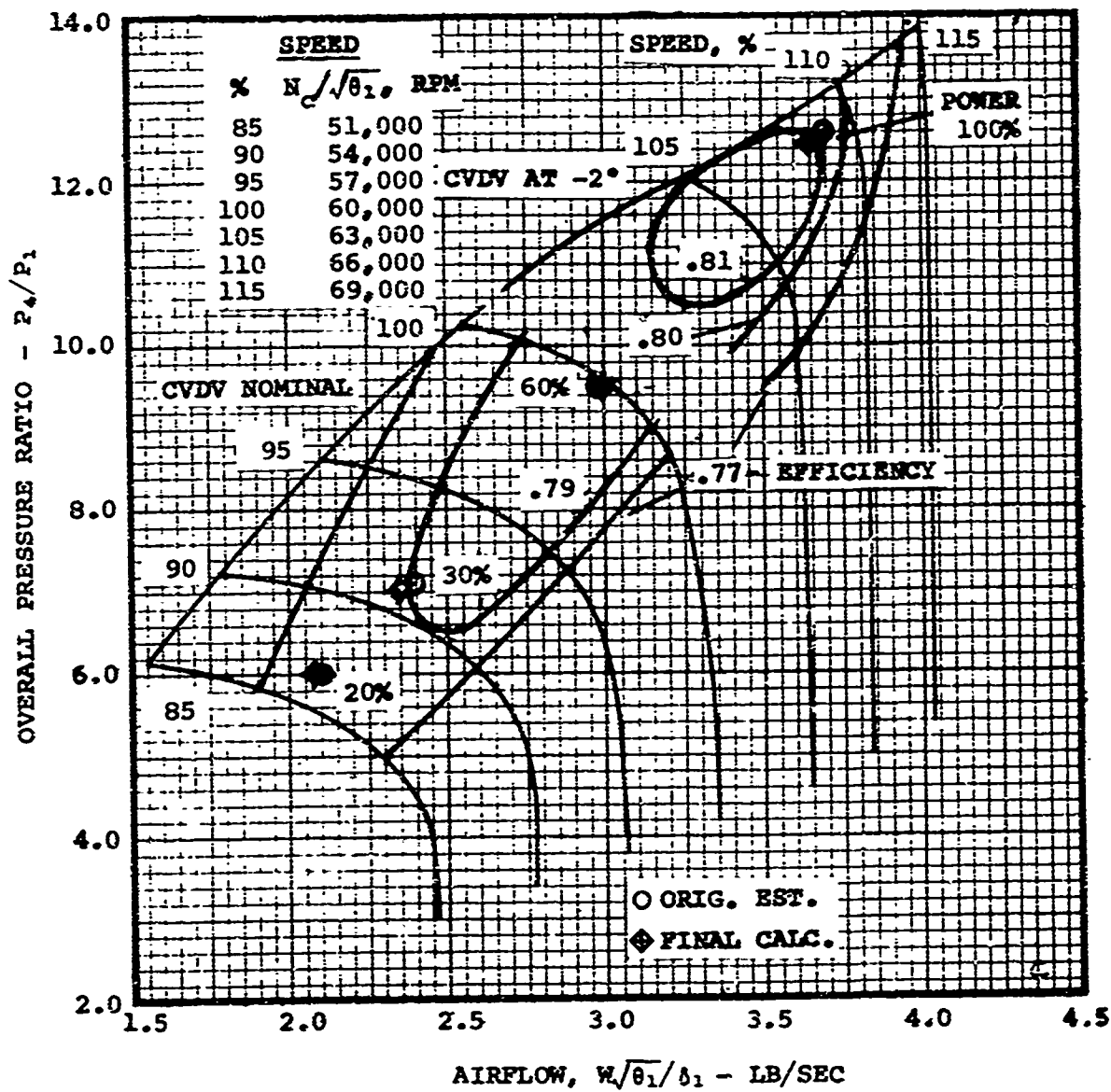
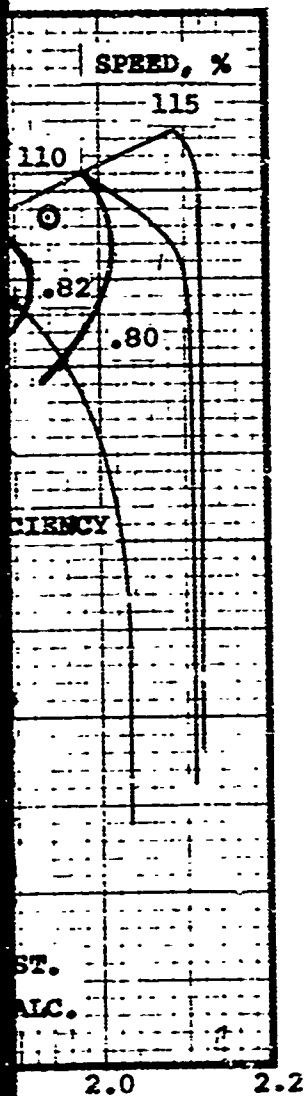


(B) CENTRIFUGAL COMPONENT: VARIABLE DIFFUSER GEOMETRY, NOMINAL AND -2° SETTING ANGLE

OVERALL PRESSURE RATIO - P_4/P_3

Two-
to

C



(C) OVERALL COMPRESSOR

FUSER
GLE

2. Compressor efficiencies are as estimated by the compressor preliminary design except that the centrifugal compressor efficiency is degraded to 0.945 of the design values for operating point(s) with CVIGV's actuated off 0° setting angle ($\eta_{CC} = 0.945 \eta_{CC, \text{DESIGN}}$ for CVIGV $\neq 0^\circ$).

Based on matching iterations for this combination, CVIGV angle settings were selected to be 0° for speeds up to and including 100-percent design speed, and -15° for speeds above 100 percent. Note that negative setting angles effect swirl in the direction opposite to rotor rotation.

1. $\eta_C = \eta_{C, \text{DESIGN}}$ The match for this case yields an overall compressor peak efficiency over 0.81 near the 100-percent-power point. The data are displayed in the three composite compressor maps (0° and -15° CVIGV setting angles) of Figure 21.

Part A of Figure 21 displays the axial compressor characteristics and shows that the match is less than optimum, as evidenced by the location of the operating line with respect to the efficiency islands and to the surge line at the low power points. Design-point operation is achieved at 0.85 efficiency--approximately 4 points below the peak efficiency for this stage.

Part B of Figure 21 displays the centrifugal compressor characteristics and shows that the operating line provides for adequate surge margin for this stage. The pressure ratio for this stage at 100-percent power is substantially increased by the CVIGV's (6.04 versus 5.63) and results in a reduced efficiency for this point.

Part C of Figure 21 displays the overall compressor characteristics and shows that the operating line falls near the peak efficiency points for the various speed lines with adequate surge margin over the operating range. Also, the efficiency levels are approximately 3 points higher than those achieved with fixed geometry.

This match results in a significant improvement in design-point SFC compared to the fixed-geometry case. However, the results are obviously optimistic, since no efficiency degradation for the presence of CVIGV's has been included here. The narrow surge margin observed for the axial component may result in axial component stall; but as in the case of the fixed-geometry compressor, overall compressor surge would not be expected.

The compressor and engine SFC data for this case are given in Table VI.

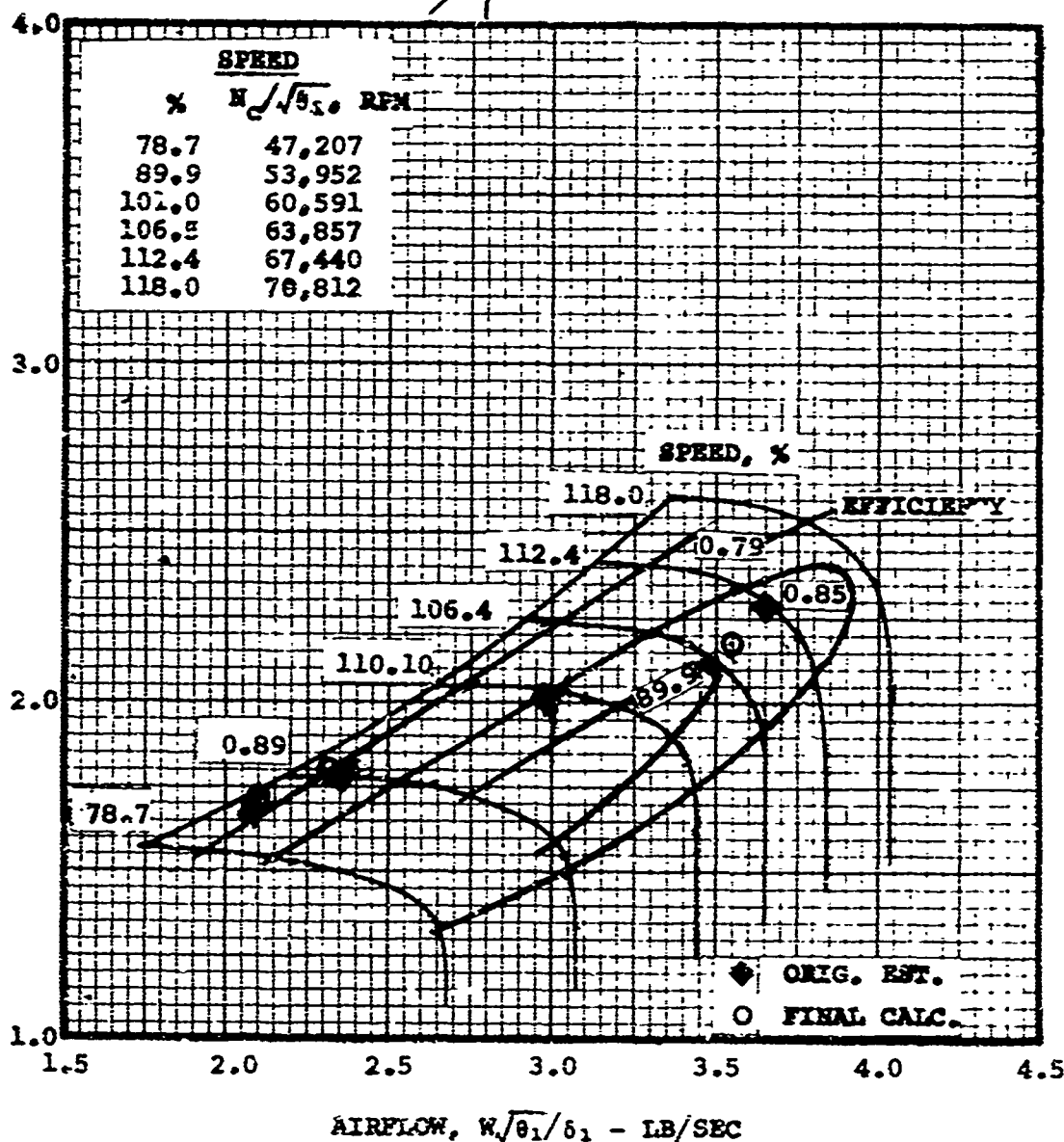
TABLE VI. AAFG + CVIGV COMPRESSOR ($\eta_c = \eta_{c, \text{DESIGN}}$)					
Percent Power	$W/\sqrt{\theta}/\delta$ (lb/sec)	P_4/P_1	$\eta_{h,1}$	T_5 (°F)	SFC
100.0	3.644	12.53	0.802	2500	0.447
59.5	2.983	9.48	0.808	2090	0.486
28.6	2.337	6.90	0.793	1750	0.636
20.9	2.135	6.15	0.785	1650	0.744

2. $\eta_{CC} = 0.945 \eta_{CC, \text{DESIGN}}$ FOR CVIGV $\neq 0^\circ$:

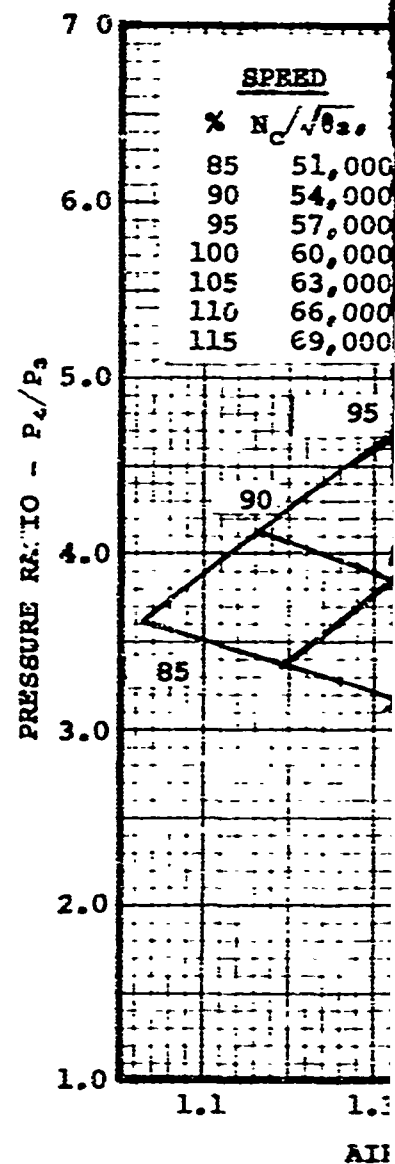
The efficiency degradation for this case was selected to show sensitivity to this parameter and is considered to be representative of losses that may be expected for this configuration.

The match for this case yields an overall compressor peak efficiency over 0.80 at the design point. The data are displayed in the three composite compressor maps (0° and -15° CVIGV setting angles) of Figure 22.

Part A of Figure 22 displays the axial compressor characteristics. Comparison with Part A of Figure 20 shows the effect on the 20-, 30-, 60-, and 100-percent-power points for the efficiency degradation assumed for this case.



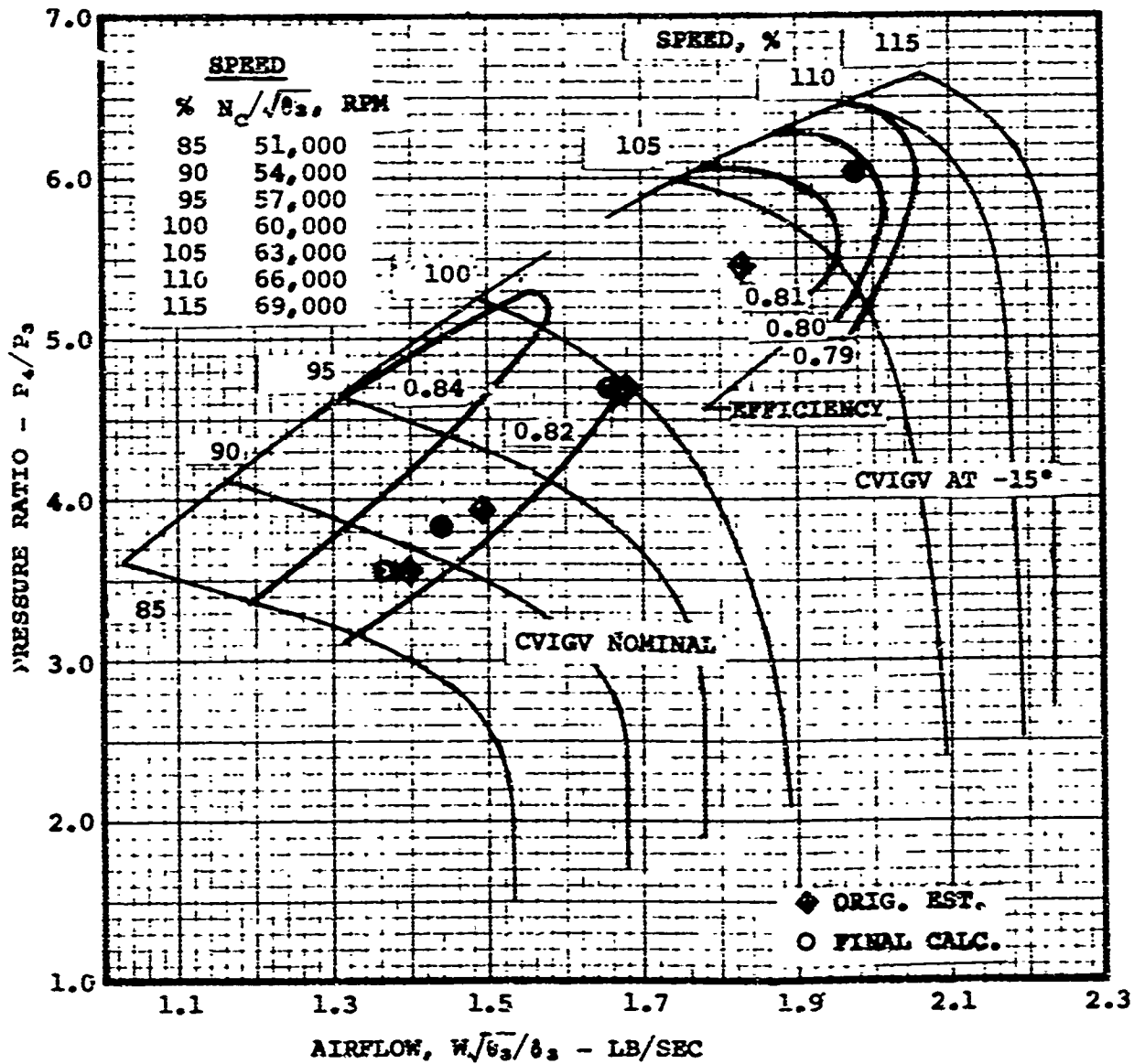
(A) AXIAL COMPRESSOR: FIXED GEOMETRY



(B) CENTRIFUGAL COMPRESSOR

Figure 21. Estimated Performance Characteristics, Two-Stage Axial Plus Centrifugal Compressor (No Efficiency Degradation Due to CVIGV), AAFG + CVIGV.

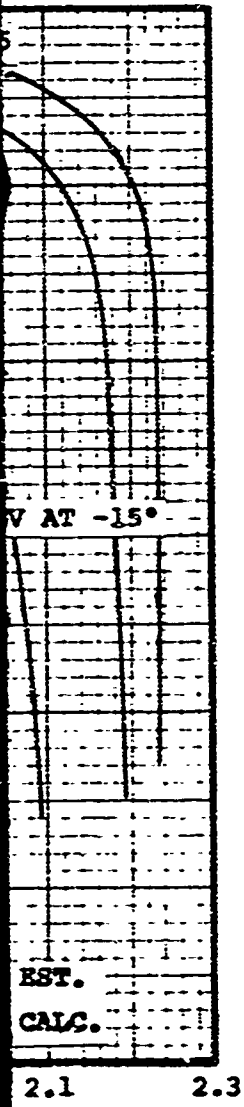
B



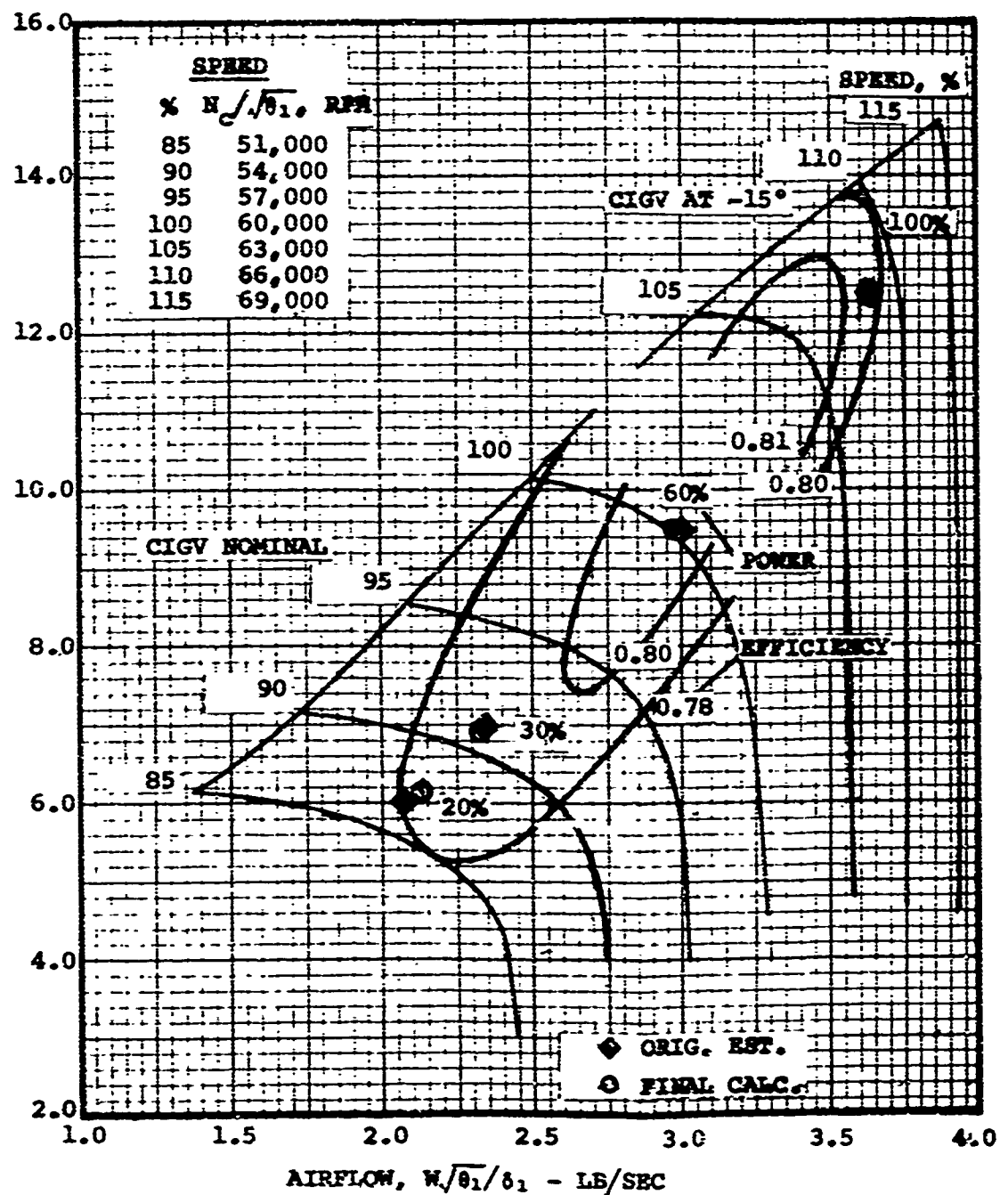
OVERALL PRESSURE RATIO - P_4/P_3

(B) CENTRIFUGAL COMPRESSOR: VARIABLE INLET GUIDE VANES, 0° AND -15°

C

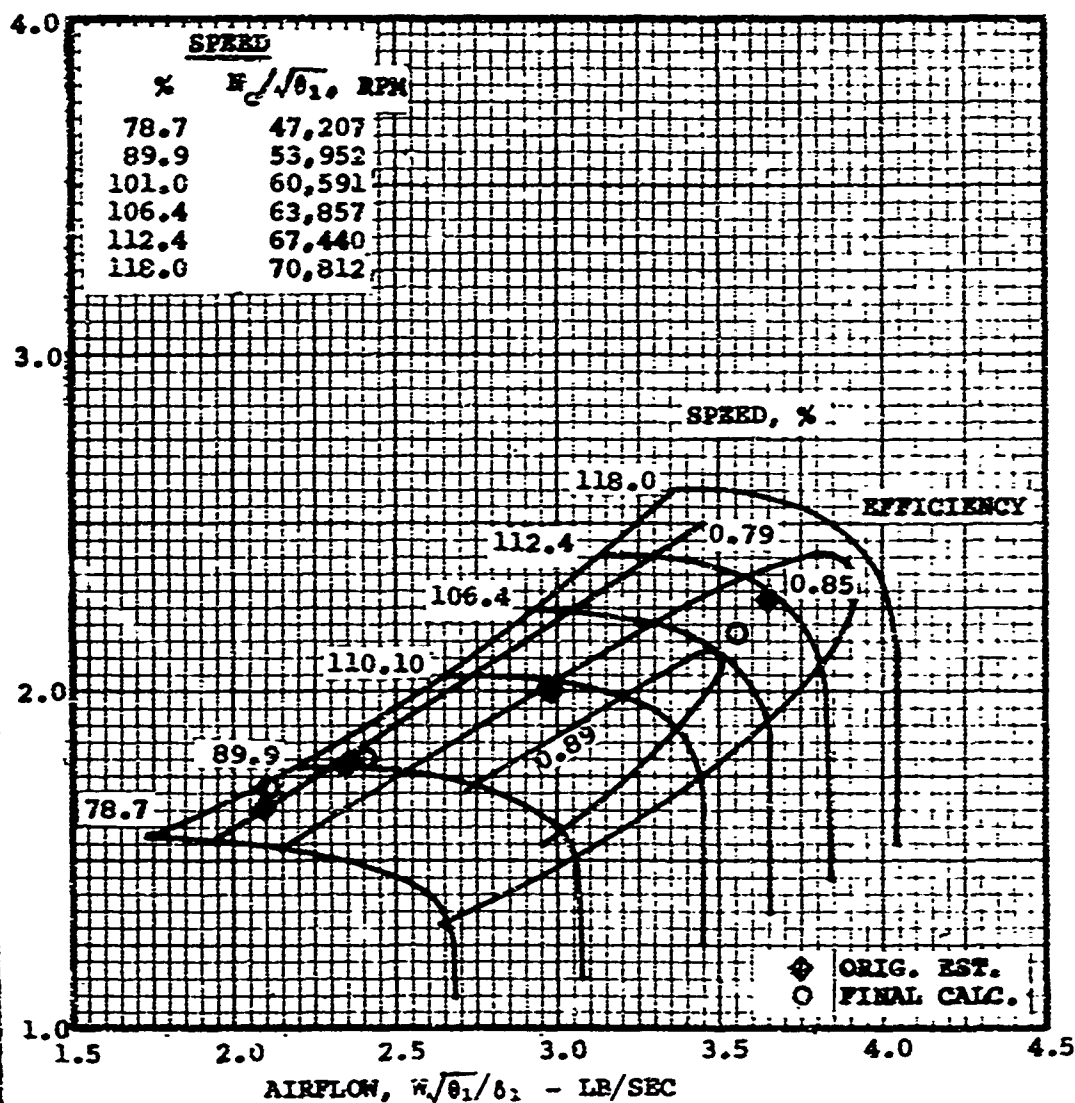


OVERALL PRESSURE RATIO - P_4/P_1

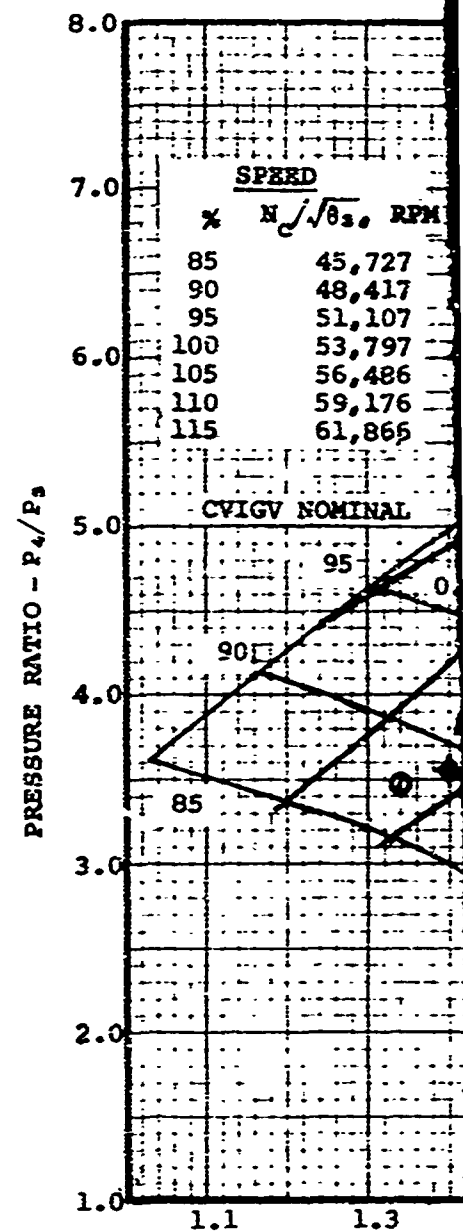


(C) OVERALL COMPRESSOR

A



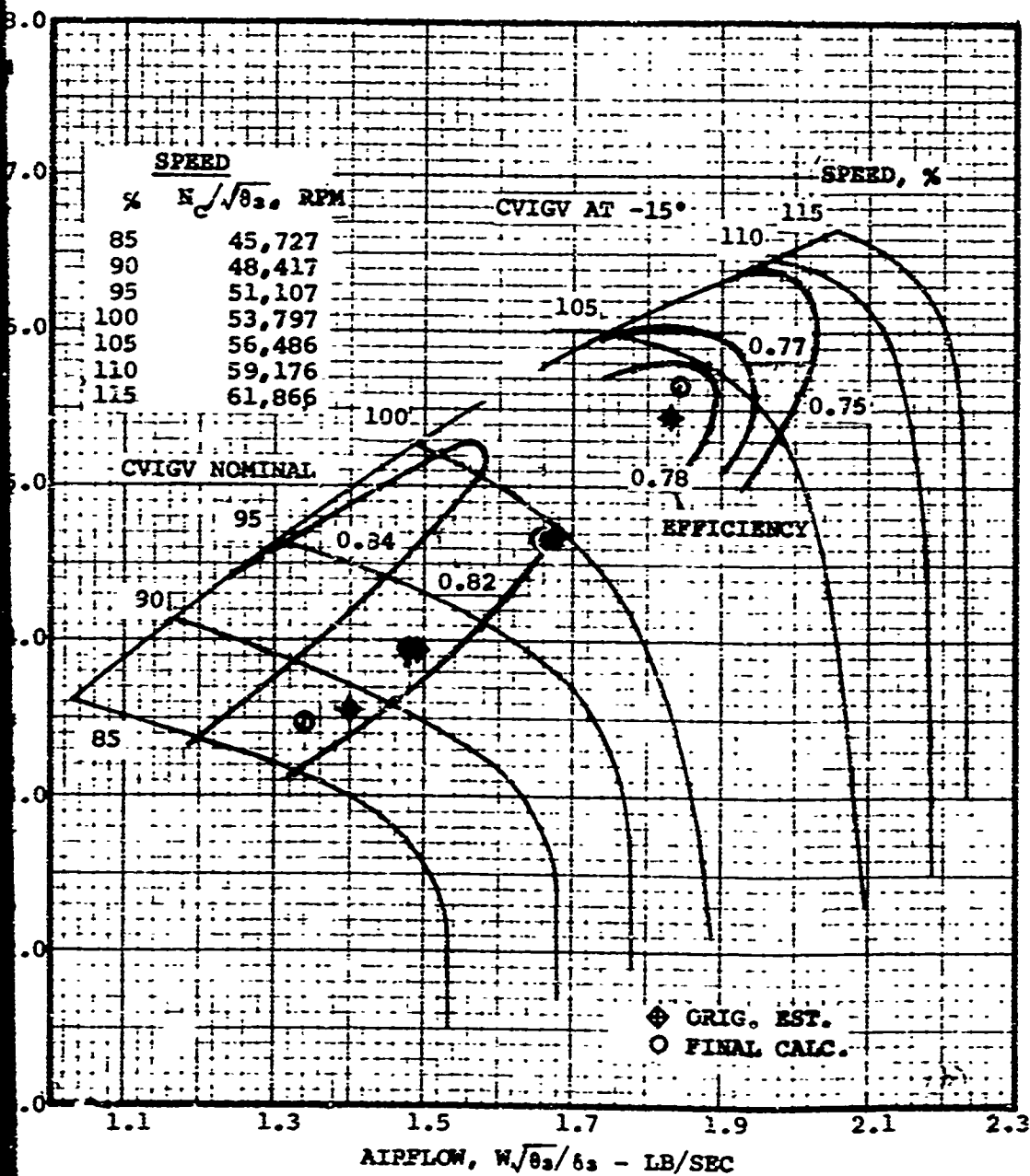
(A) AXIAL COMPRESSOR: FIXED GEOMETRY



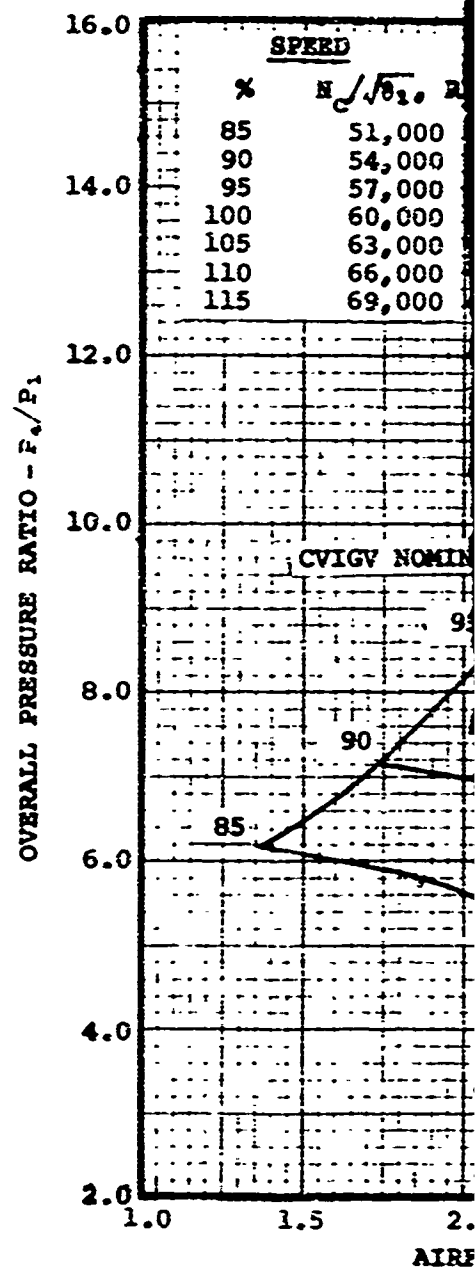
(B) CENTR. INLET
(η_{CC})

Figure 22. Estimated Performance Characteristics, Two-Stage Axial Plus Centrifugal Compressor (Includes Efficiency Degradation Due to CVIGV), AAFG + CVIGV.

B

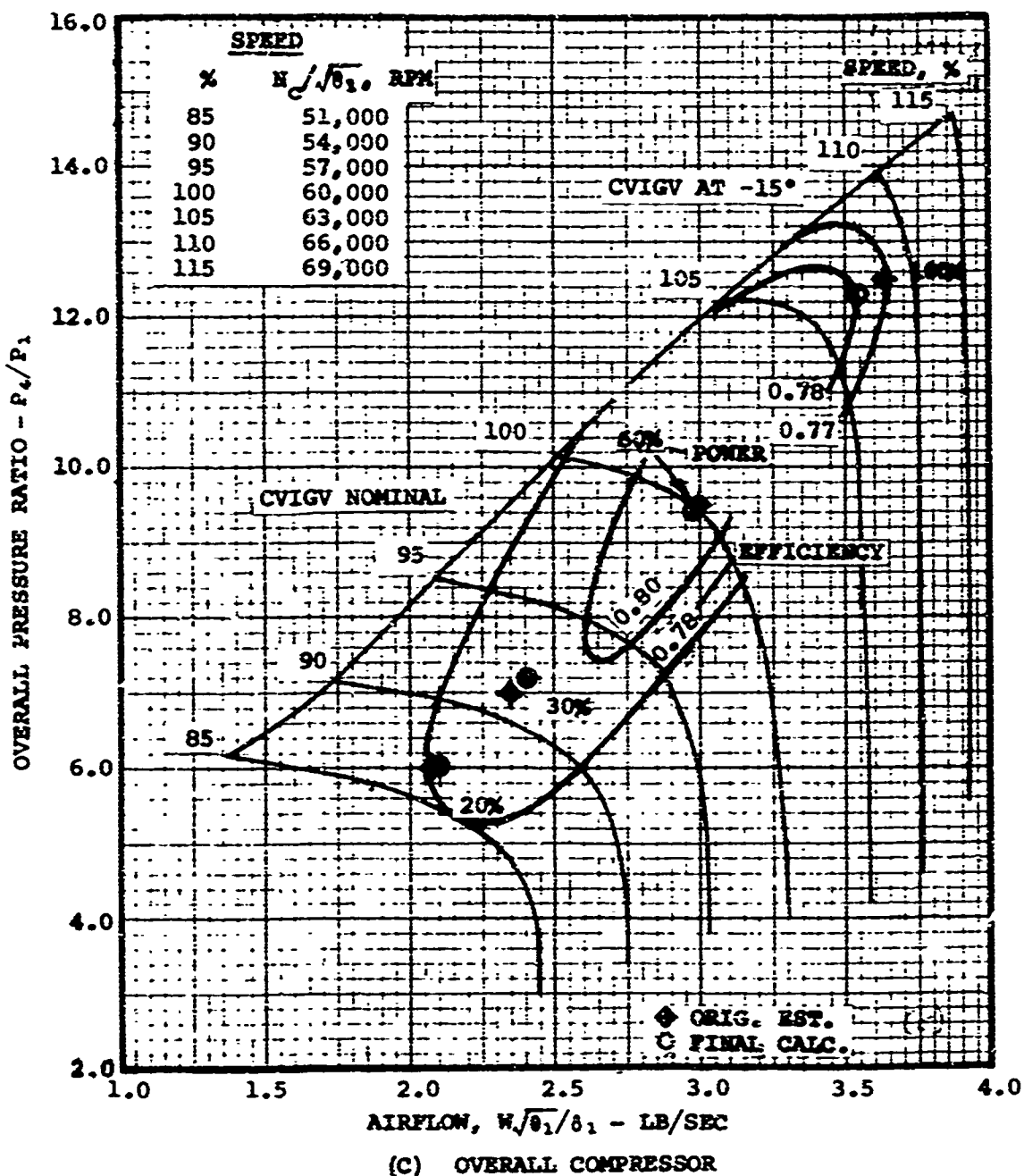
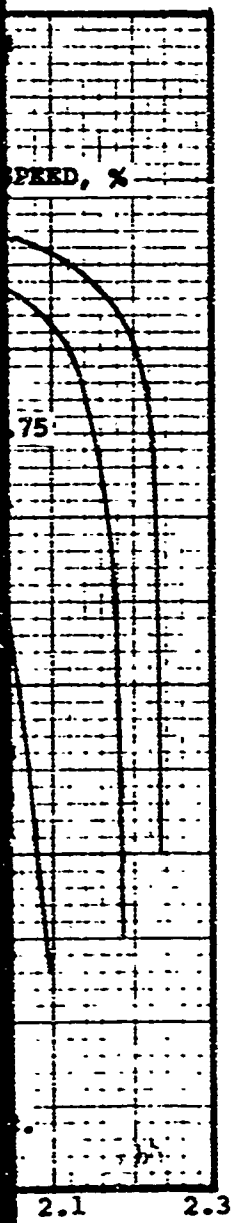


(B) CENTRIFUGAL COMPRESSOR: VARIABLE
INLET GUIDE VANES, 0° AND -15°
($\eta_{CC} = 0.945 \eta_{CC'} \text{ DESIGN FOR CIGV AT } -15^\circ$)



(C)

C



-15°)

Part B of Figure 22 displays the centrifugal compressor characteristics and shows the effect on the 100-percent-power point of the efficiency degradation assumed for this study. Compared to Part B of Figure 20, the efficiency, pressure ratio, flow, and corrected speed are all reduced.

Part A of Figure 22 shows the effects of a representative efficiency degradation assigned for this study to the centrifugal stage for the presence of CVIGV's at -15° setting angle (100-percent power). The composite maps are predictably similar except for the efficiency levels where the CVIGV's are actuated to -15° setting angle.

The compressor and engine SFC data for this case are given in Table VII.

TABLE VII. AAFG + CVIGV COMPRESSOR ($\eta_{CC} = 0.945 \eta_{CC, \text{DESIGN}}$ FOR CVIGV $\neq 0^\circ$)					
Percent Power	$W/\sqrt{\theta}/\delta$ (lb/sec)	P_4/P_1	η_{41}	T_6 ($^\circ\text{F}$)	SFC
100.0	3.542	12.29	0.780	2500	0.460
59.9	2.970	9.44	0.808	2040	0.493
32.1	2.408	7.18	0.796	1750	0.615
19.9	2.095	6.02	0.783	1600	0.781

3.3.2.4 Single Spool, AAVIGV + CFG

A match was achieved for this case, consisting of:

1. Two-stage axial compressor component, variable inlet guide vanes (AAVIGV)
2. Single-stage centrifugal compressor component, fixed geometry (CFG)

The results of this study show a significant improvement in the compressor match and yield efficiency levels near the full potential for the compressors as designed. The axial compressor operates at lower than optimum flows for the reduced power points, but operation at 60- and 100-percent power is near the peak efficiency points for the respective speeds. The axial

compressor operates with 5- to 7-percent surge margin at the 20-percent-power point, and additional surge margin could be gained for acceleration by actuation of the AAVIGV's at reduced power.

The axial and centrifugal compressor efficiencies assumed for this study are as follows:

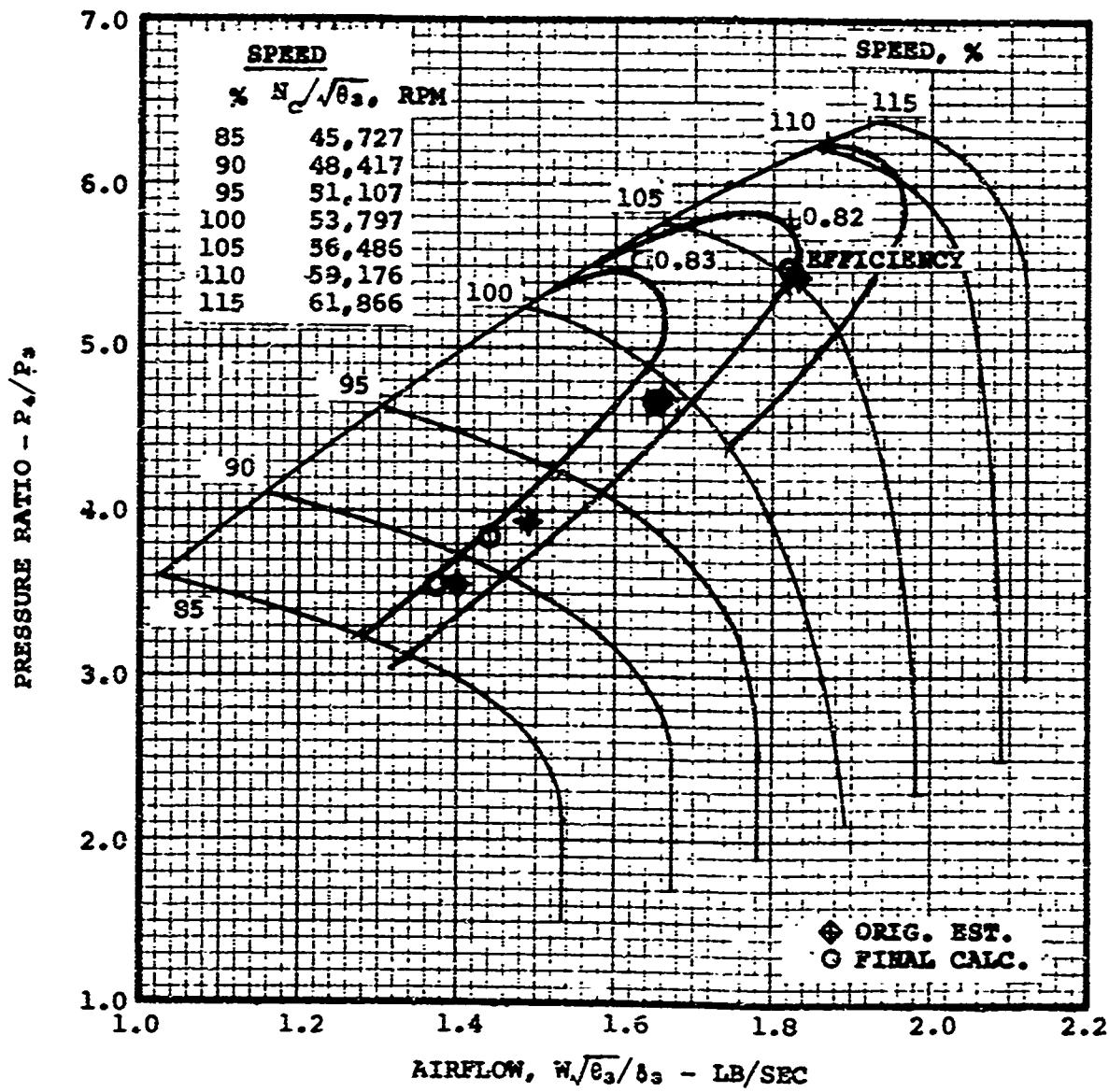
1. Compressor efficiencies are as estimated by the compressor preliminary design
 $(\eta_C = \eta_{C, \text{DESIGN}})$.
2. Compressor efficiencies are as estimated by the compressor preliminary design except that the axial compressor efficiency is degraded to 0.945 of the design values for operating point(s) with AAVIGV's actuated off 0° setting angle
 $(\eta_{AX} = 0.945 \eta_{AX, \text{DESIGN}} \text{ for AAVIGV} \neq 0^\circ)$.

Based on matching iterations for this combination, AAVIGV angle settings were selected to be 0° for speeds up to and including 100-percent design speed, and -15° for speeds above 100 percent. Note that negative setting angles effect swirl in the direction opposite to rotor rotation.

1. $\eta_C = \eta_{C, \text{DESIGN}}$: The match for this case yields an overall compressor peak efficiency of approximately 0.82 near the design point (60-percent power). The data are displayed in the three composite compressor maps (0° and -15° AAVIGV setting angles) of Figure 23.

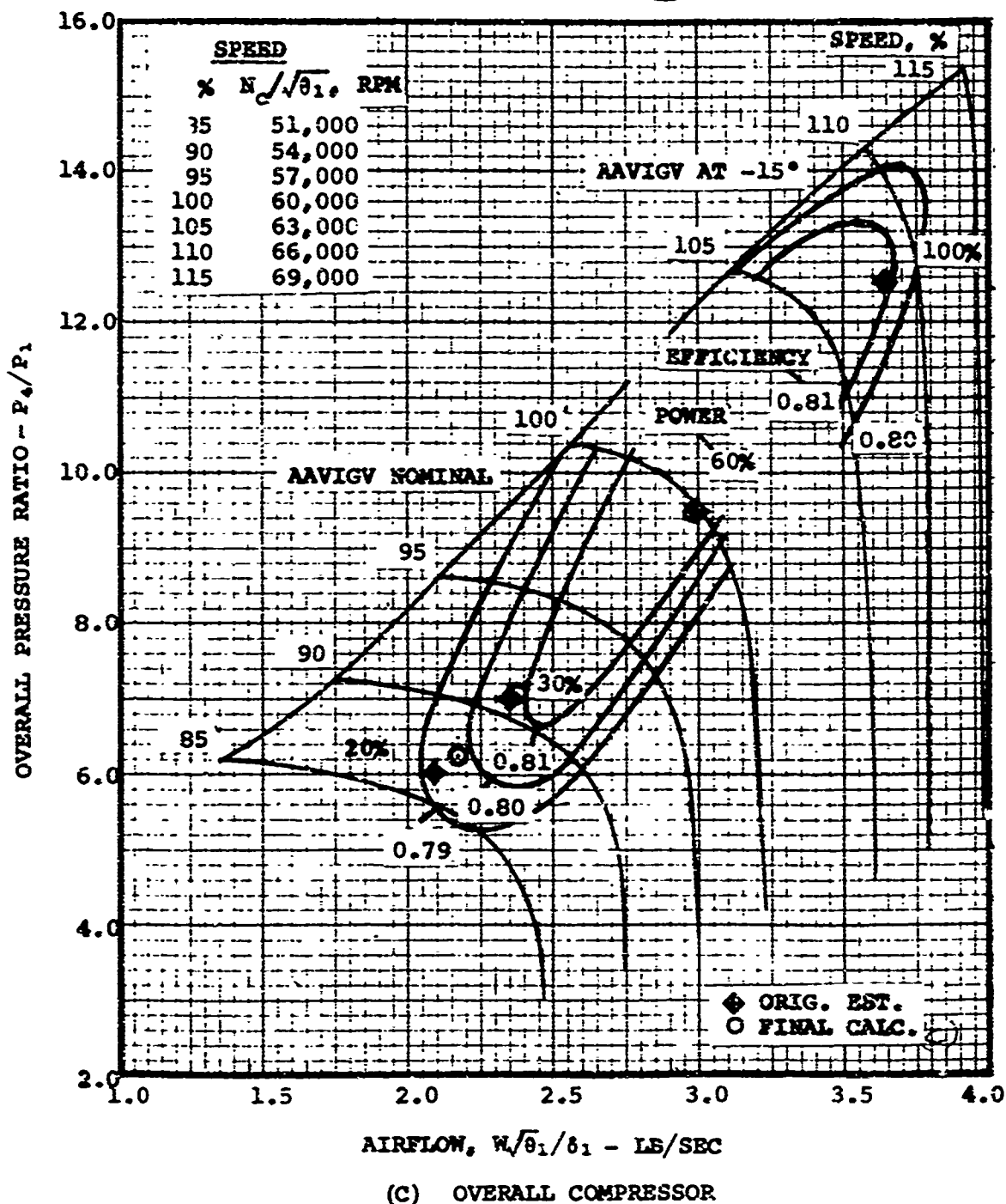
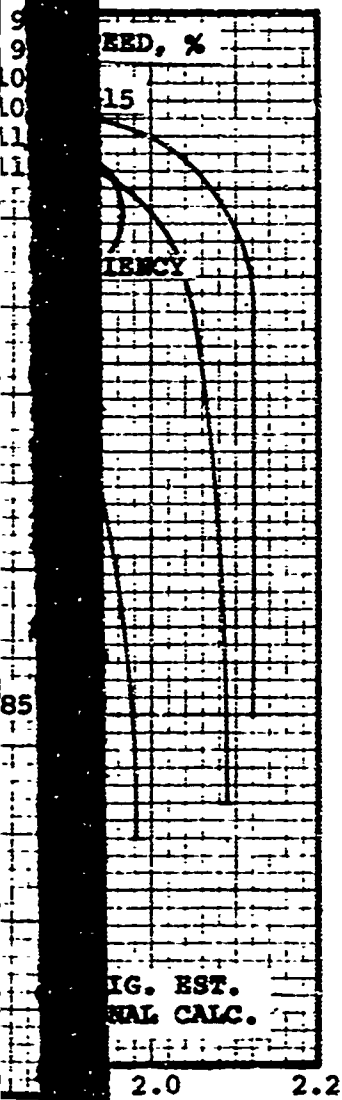
Part A of Figure 23 displays the axial compressor characteristics and shows that the match is still slightly less than ideal, as evidenced by the 0.878 design-point efficiency compared to the 0.89+ peak efficiency. Also, the narrow surge margin at the low power points may require actuation of the AAVIGV's at these power levels for adequate surge margin. This could be accomplished without complication but may slightly increase the operating SFC's for these low power points.

B



OVERALL PRESSURE RATIO - P_4/P_3

(B) CENTRIFUGAL COMPRESSOR: FIXED GEOMETRY



Part B of Figure 23 displays the centrifugal compressor characteristics and shows that the operating line provides for adequate surge margin for this stage and is very close to the peak efficiency operation. However, comparison with Part B of Figure 14 shows that the operating line on the centrifugal compressor map differs only slightly from that determined for the fixed-geometry combination (AAFG + CFG).

Part C of Figure 23 displays the overall compressor characteristics. From this it can be seen that the operating line falls near the peak efficiency points for the various speed lines with adequate surge margin over the operating range. Also, the design-point efficiency is approximately 0.819, which represents the best match achieved in these matching studies.

The compressor and engine SFC data for this case are given in Table VIII. These results are the best achieved in these tentative matching studies, but are clearly optimistic due to the assumption of no compressor efficiency degradation due to AAVIGV's.

TABLE VIII. AAVIGV + CFG COMPRESSOR ($\eta_C = \eta_{C, \text{DESIGN}}$)					
Percent Power	$W\sqrt{\theta}/\delta$ (lb/sec)	P_4/P_1	η_{41}	T_5 (°F)	SFC
100.0	3.640	12.53	0.812	2500	0.443
59.5	2.983	9.48	0.819	2085	0.481
30.0	2.378	7.02	0.809	1750	0.611
21.9	2.165	6.25	0.799	1650	0.713

2. $\eta_{AX} = 0.945 \eta_{AX, \text{DESIGN}}$ for AAVIGV $\neq 0^\circ$: The efficiency degradation for this case is considered to be representative of maximum loss to be expected and is estimated from GTP331-13 engine test data incorporating radial inlet guide vanes.

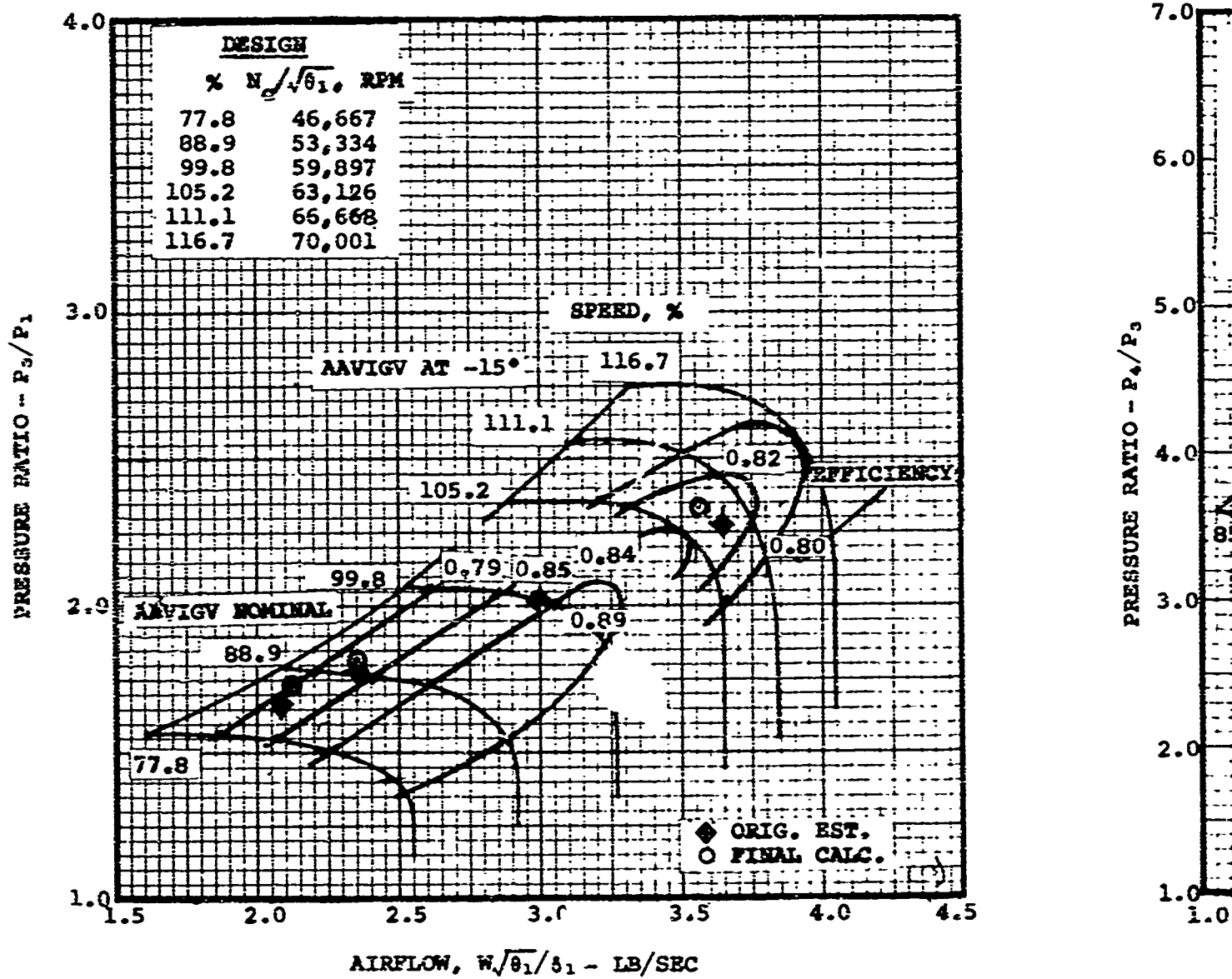
The match for this case yields an overall compressor peak efficiency of approximately 0.82 near the design point (60-percent power). The data are displayed in the three composite compressor maps (0° and -15° AAVIGV setting angles) of Figure 24.

Part A of Figure 24 displays the axial compressor characteristics and shows the effect on the 100-percent-power point of the efficiency degradation assumed for this study. Compared to Part A of Figure 22, the 100-percent-power pressure ratio is increased while the flow is decreased.

Part B of Figure 24 displays the centrifugal compressor characteristics. Comparison with Part B of Figure 22 shows the slight effect on the 20-, 30-, 60-, and 100-percent-power points due to the efficiency degradation assumed for this case. Additional matching iterations for this combination could shift the operating line toward reduced airflows and effect some increase in efficiencies over the operating range at the expense of surge margin.

Part C of Figure 24 displays the overall compressor characteristics. Comparison with Part C of Figure 23 shows the effects of a representative efficiency degradation assigned for this study to the axial compressor component for the presence of AAVIGV's at -15° setting angle (100-percent power). The only difference to be noted is at the 100-percent-power point. The assumed efficiency degradation slightly reduces the pressure ratio, flow, and corrected speed for this point.

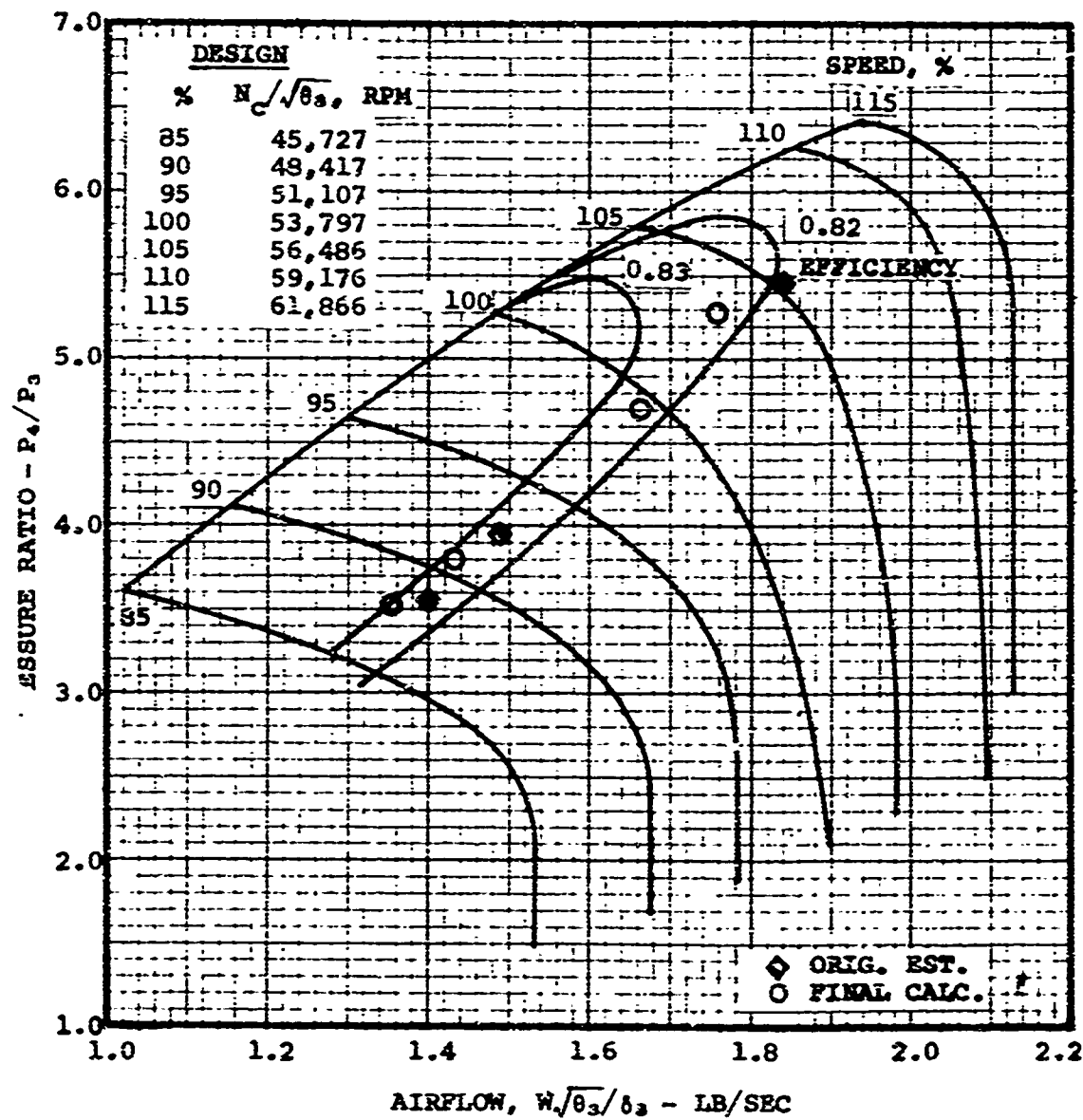
The compressor and engine SFC data for this case are given in Table IX. These values represent a performance level near the maximum potential for the compressors as designed and are considered to be achievable within a 3-year period. The slight matching improvements apparent for the centrifugal stage will be considered in the following tasks of this program.



(A) AXIAL COMPRESSOR COMPONENT: VARIABLE
 INLET GUIDE VANES, 0° AND -15°
 ($\eta_{AX} = 0.945 \eta_{AX, \text{DESIGN}}$ FOR AAVIGV AT -15°)

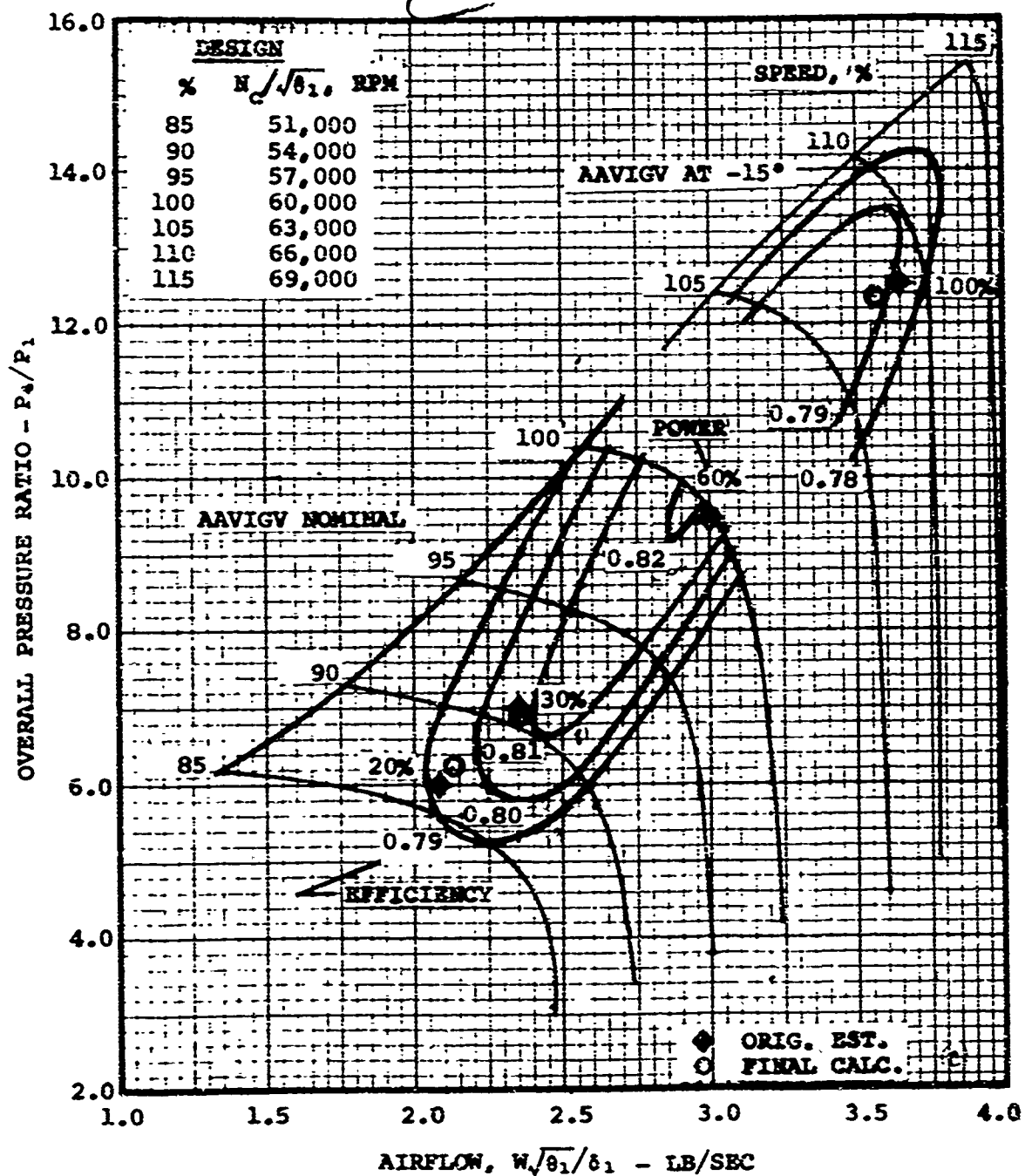
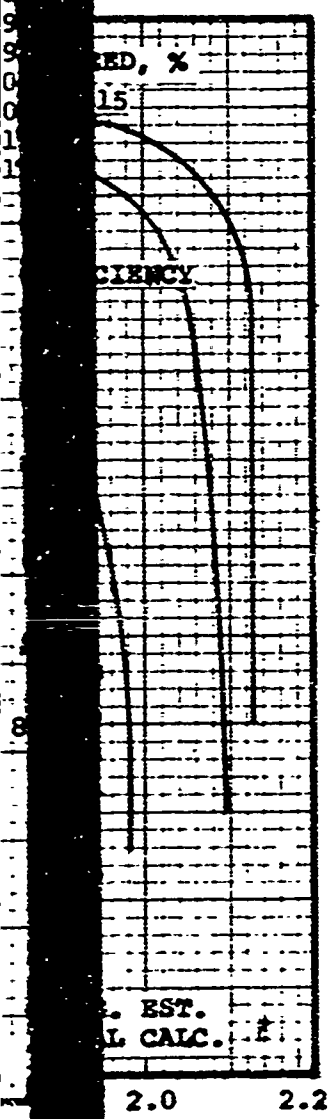
Figure 24. Estimated Performance Characteristics,
 Two-Stage Axial Plus Centrifugal Compressor
 (Includes Efficiency Degradation Due to
 AAVIGV), AAVIGV + CFG.

B



(B) CENTRIFUGAL COMPRESSOR COMPONENT: FIXED GEOMETRY

C



(C) OVERALL COMPRESSOR

TABLE IX. AAVIGV + CFG COMPRESSOR ($\eta_{AX} = 0.945 \eta_{AX, \text{DESIGN}}$ FOR AAVIGV $\neq 0^\circ$)					
Percent Power	W/δ (lb/sec)	P_4/P_1	η_{41}	T_5 (°F)	SFC
100.0	3.563	12.36	0.791	2500	0.456
60.5	2.996	9.52	0.819	2045	0.485
29.2	2.352	6.92	0.808	1700	0.629
20.8	2.129	6.11	0.797	1600	0.745

3.3.2.5 Single Spool, AAVIGV + CVIGV

A match was achieved for this case, consisting of:

1. Two-stage axial compressor component, variable inlet guide vanes (AAVIGV)
2. Single-stage centrifugal compressor component, variable inlet guide vanes (CVIGV)

This is the first of two combinations of variable compressor geometry that were evaluated in this preliminary matching study. The variable vane rows for the axial and centrifugal compressors are envisioned as axial-flow components and would be amenable to simple control linkage arrangement.

The results of this study show no advantage over the combination of compressor components employing AAVIGV's only; and in fact, for the case of representative loss assumptions for the two variable vane rows, a performance degradation is observed. The axial compressor operates at lower than optimum flows for the reduced power points, but operation at 50- and 100-percent power is near the peak efficiency points for the respective speeds. The axial compressor operates with 8- to 9-percent surge margin at 20-percent power, and additional surge margin could be gained for acceleration by actuation of the variable vane rows at reduced power.

The axial and centrifugal compressor efficiencies assumed for this study are as follows:

1. Compressor efficiencies are as estimated by the compressor preliminary design
($\eta_C = \eta_{C, \text{DESIGN}}$).

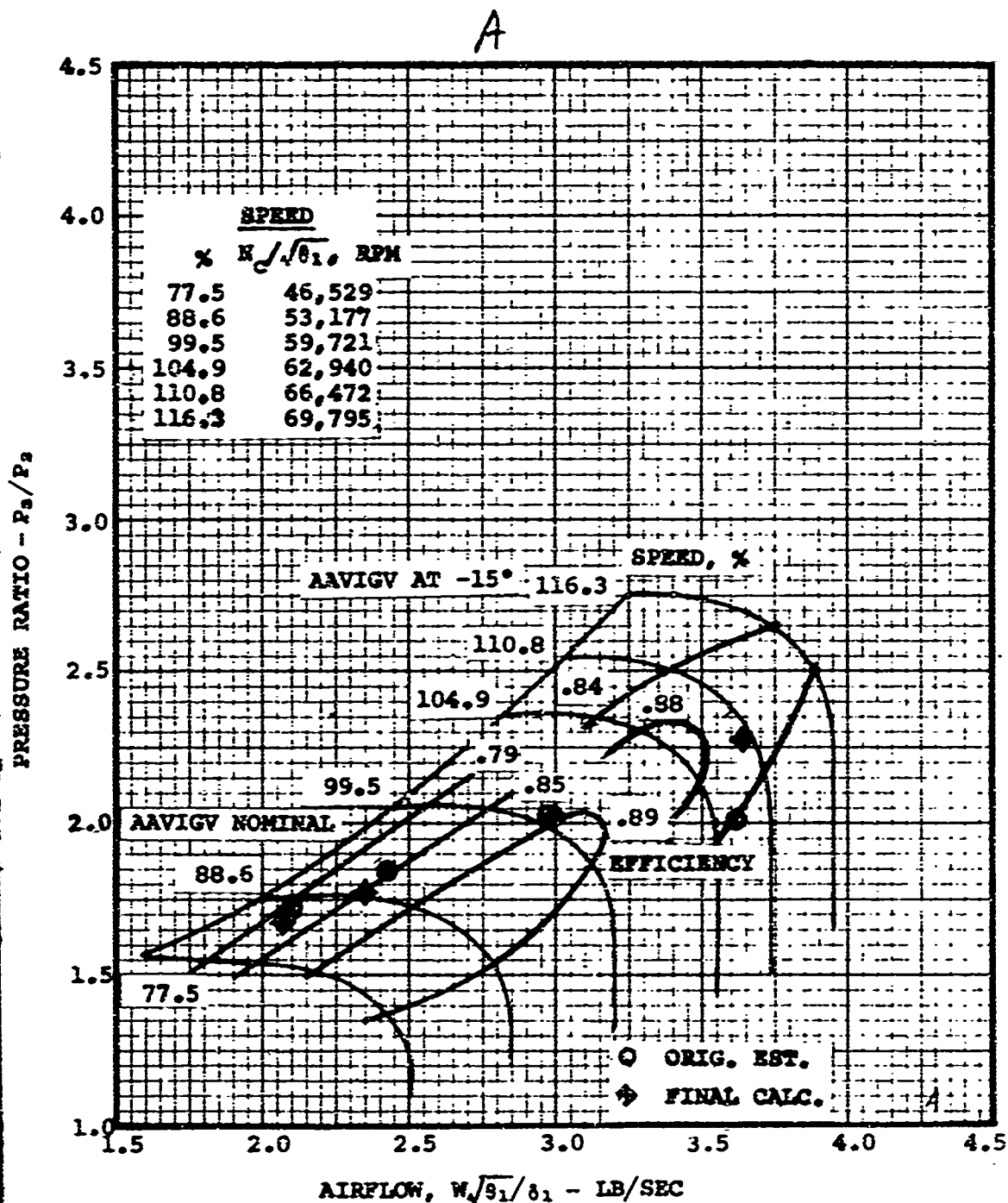
2. Compressor efficiencies are as estimated by the compressor preliminary design except that the axial and centrifugal compressor efficiencies are each degraded to 0.945 of their respective design values (or operating points) with AAVIGV's and CVIGV's actuated off 0° setting angle ($\eta_{AX-CC} = 0.945 \eta_{AX-CC, DESIGN}$ for AAVIGV and CVIGV $\neq 0^\circ$).

Based on matching iterations for this combination, AAVIGV and CVIGV angle settings were selected to be 0° for speeds up to and including 100-percent design speed, and -15° for speeds above 100 percent. Note that negative setting angles for both AAVIGV's and CVIGV's effect swirl in the direction opposite to rotor rotation.

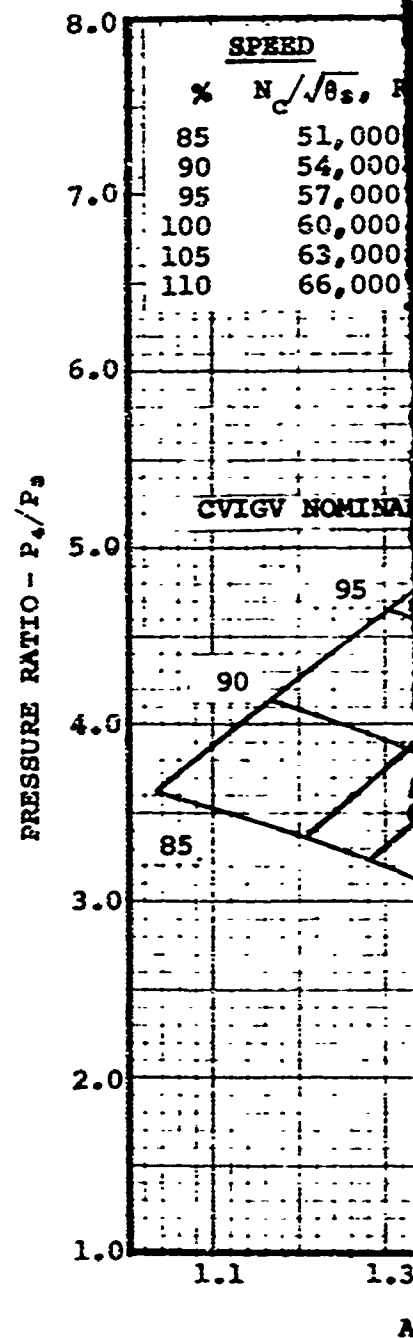
1. $\eta_C = \eta_{C, DESIGN}$: The match for this case yields the same overall compressor peak efficiency (0.82) as was observed for Combination 4, consisting of AAVIGV + CFG. The peak efficiency island occurs between the design point (60-percent power) and surge. The data are displayed in the three composite compressor maps (0° and -15° AAVIGV and CVIGV setting angles) of Figure 25.

Part A of Figure 25 displays the axial compressor characteristics and shows a match almost identical with that of Combination 4, AAVIGV + CFG, except for the 100-percent-power point, where the pressure ratio and efficiency for the axial compressor are significantly lower. The design-point efficiency for this compressor component is 0.885 compared to the 0.89+ peak efficiency. As was discussed for Combination 4, AAVIGV + CFG, the inlet guide vanes could be actuated at the low power levels to increase the surge margin without mechanical complication, but possibly with some slight increase in SFC for the low power points.

Part B of Figure 25 displays the centrifugal compressor characteristics and indicates a match almost identical with that for Combination 4, AAVIGV + CFG, except for the 100-percent-power point, where the pressure ratio is significantly higher and the efficiency is reduced.



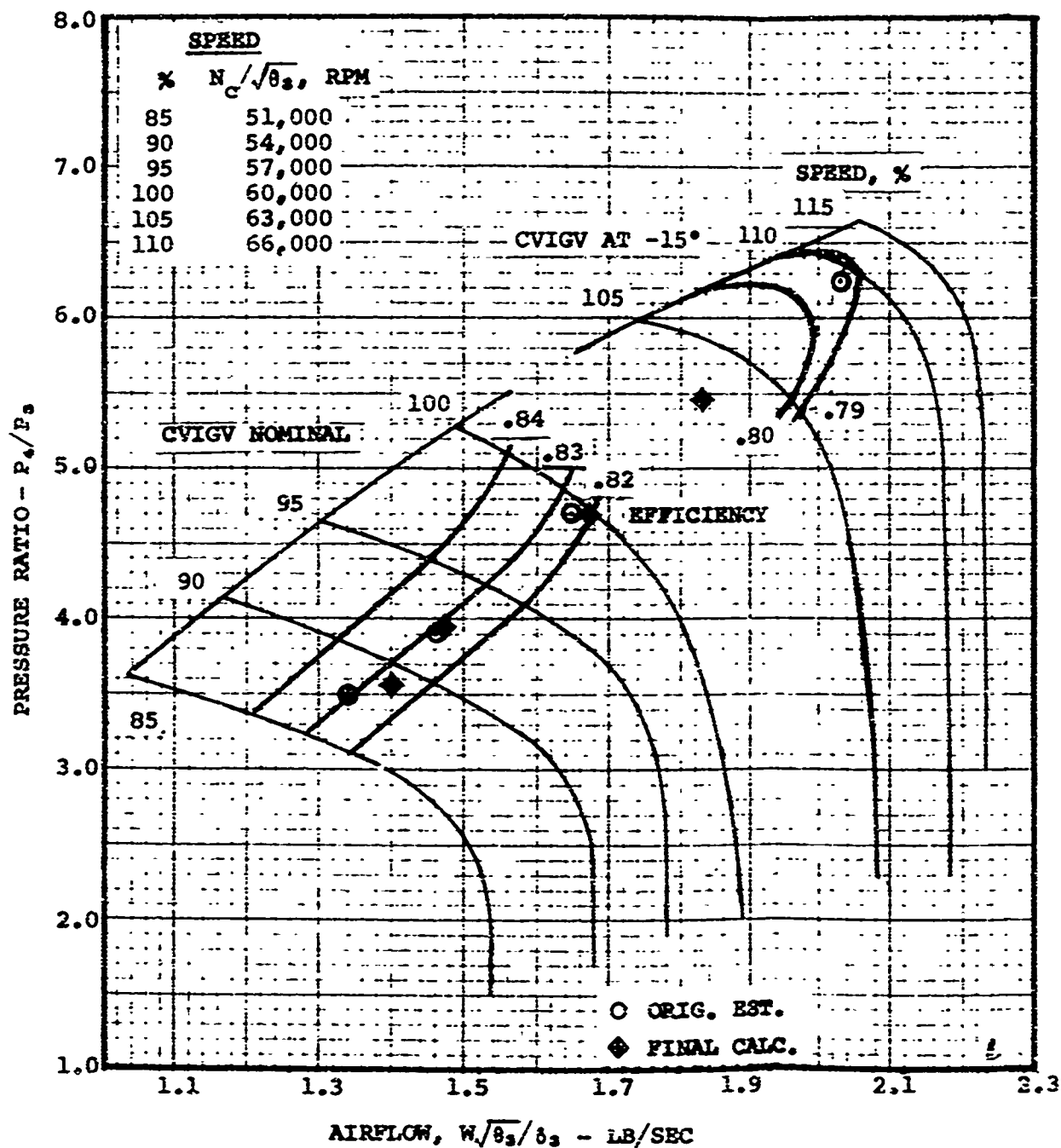
(A) AXIAL COMPRESSOR: VARIABLE
INLET GUIDE VANES, 0° AND -15°



(B)

Figure 25. Estimated Performance Characteristics, Two-Stage Axial Plus Centrifugal Compressor (Includes No Efficiency Degradation Due to AAVIGV and CVIGV), AAVIGV + CVIGV.

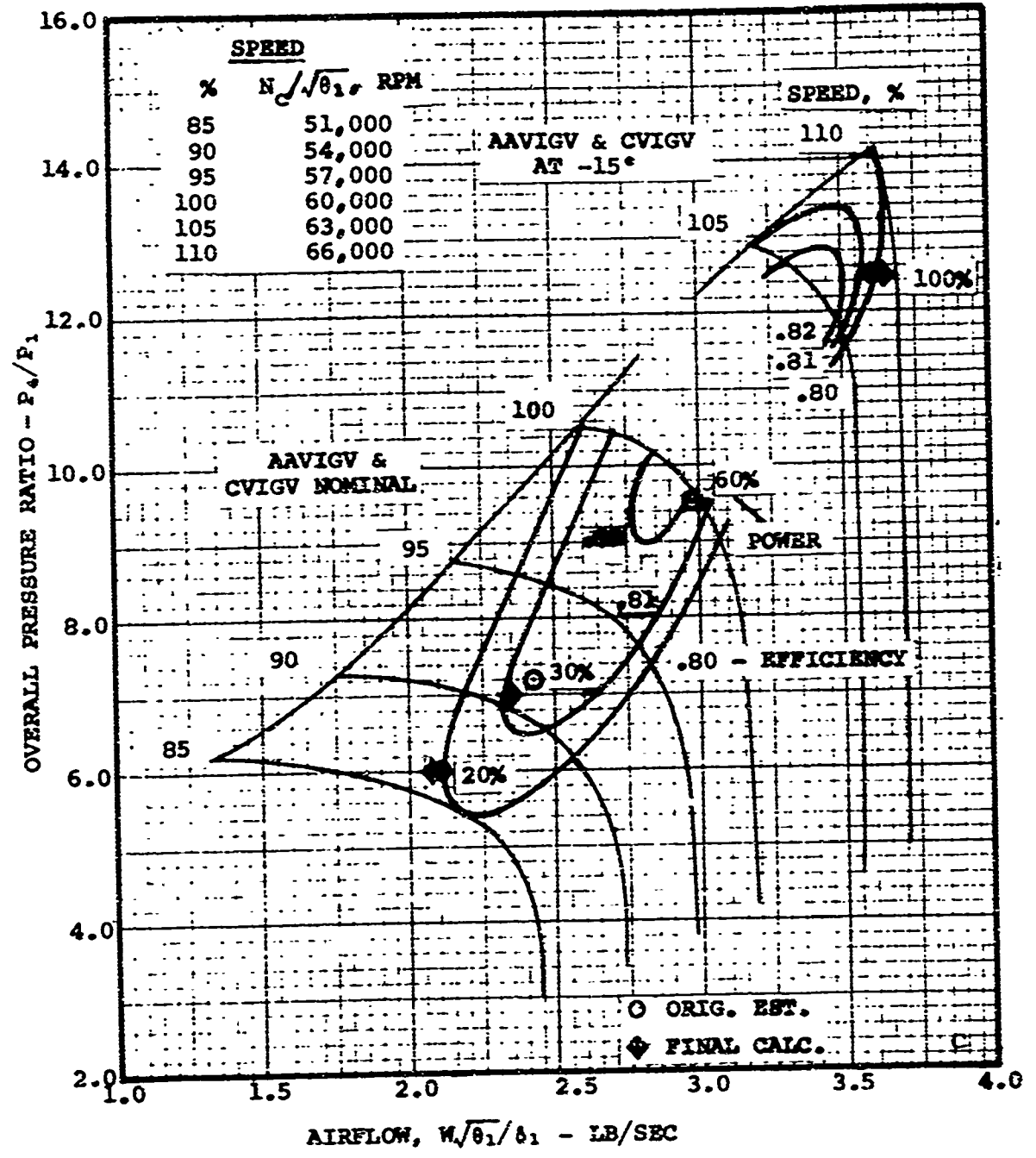
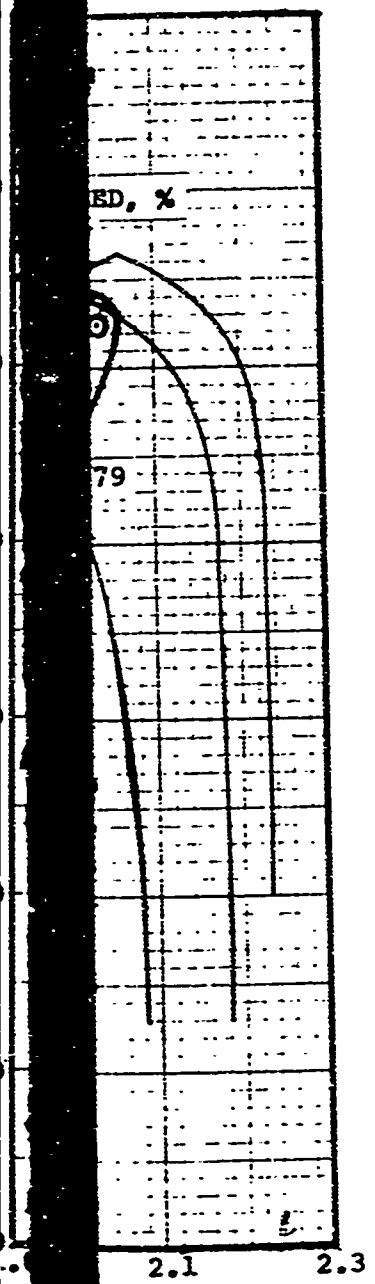
B



(B) CENTRIFUGAL COMPRESSOR: VARIABLE INLET GUIDE VANES, 0° AND -15°

tage
No
GV),

C



(C) OVERALL COMPRESSOR

Part C of Figure 25 displays the overall compressor characteristics. It shows that the operating line falls near the peak efficiency points for the various speed lines with adequate surge margin over the operating range. The design-point efficiency is approximately 0.819.

The compressor and engine SFC data for this case are given in Table X. These results reflect slightly lower performance than that reported for the $\eta_C = \eta_{C, \text{DESIGN}}$ study for Combination 4 (AAVIGV + CFG), Paragraph 3.4.2.4.

TABLE X. AAVIGV + CVIGV COMPRESSOR ($\eta_C = \eta_{C, \text{DESIGN}}$)

Percent Power	$W\sqrt{\theta}/\delta$ (lb/sec)	P_4/P_1	η_{41}	T_5 (°F)	SFC
100.0	3.615	12.49	0.805	2500	0.447
59.7	2.985	9.49	0.819	2070	0.483
31.8	2.426	7.19	0.814	1750	0.598
19.6	2.104	6.02	0.799	1600	0.759

2. $\eta_{AX-CC} = 0.945 \eta_{AX-CC, \text{DESIGN}}$ for AAVIGV + CVIGV $\neq 0^\circ$: The match for this case yields the same overall peak efficiency of 0.82 as was observed above and as was observed for Combination 4 (AAVIGV + CFG). The peak efficiency similarly occurs between the design point and the surge line. The data are displayed in the three composite compressor maps (0° and -15° AAVIGV and CVIGV setting angles) of Figure 26.

Part A of Figure 26 displays the axial compressor characteristics and shows the effect of the efficiency degradation assumed for this study on the 100-percent-power point. Comparison with Part A of Figure 25 shows that the pressure ratio is increased while the flow is decreased.

Part B of Figure 26 displays the centrifugal compressor characteristics. Comparison with Part B of Figure 25 shows the slight effect on the 20-, 30-, 60-, and 100-percent-power points due to the efficiency degradation assumed for this case.

Part C of Figure 26 displays the overall compressor characteristics. Comparison with Part C of Figure 25 shows the effects of a representative efficiency degradation as assigned for this study to the axial and centrifugal compressor components for the presence of AAVIGV's and CVIGV's at the -15° setting angle. The only difference to be noted is at the 100-percent-power point. The assumed efficiency degradation reduces the pressure ratio, flow, and corrected speed for this point.

The compressor and engine SFC data for this case are given in Table XI. These results reflect slightly lower performance than that reported in Paragraph 3.3.2.4 for Combination 4 (AAVIGV + CFG) with efficiency degradation for AAVIGV's.

TABLE XI. AAVIGV + CVIGV COMPRESSOR ($\eta_{AX-CC} = 0.945 \eta_{AX-CC, \text{DESIGN}}$ FOR AAVIGV + CVIGV $\neq 0^\circ$)					
Percent Power	$W\sqrt{\theta}/\phi$ (lb/sec)	P_4/P_1	η_{41}	T_5 ($^\circ\text{F}$)	SFC
100.0	3.496	12.21	0.777	2500	0.462
60.2	2.974	9.45	0.818	2010	0.489
31.8	2.414	7.15	0.813	1700	0.611
23.1	2.196	6.35	0.804	1600	0.713

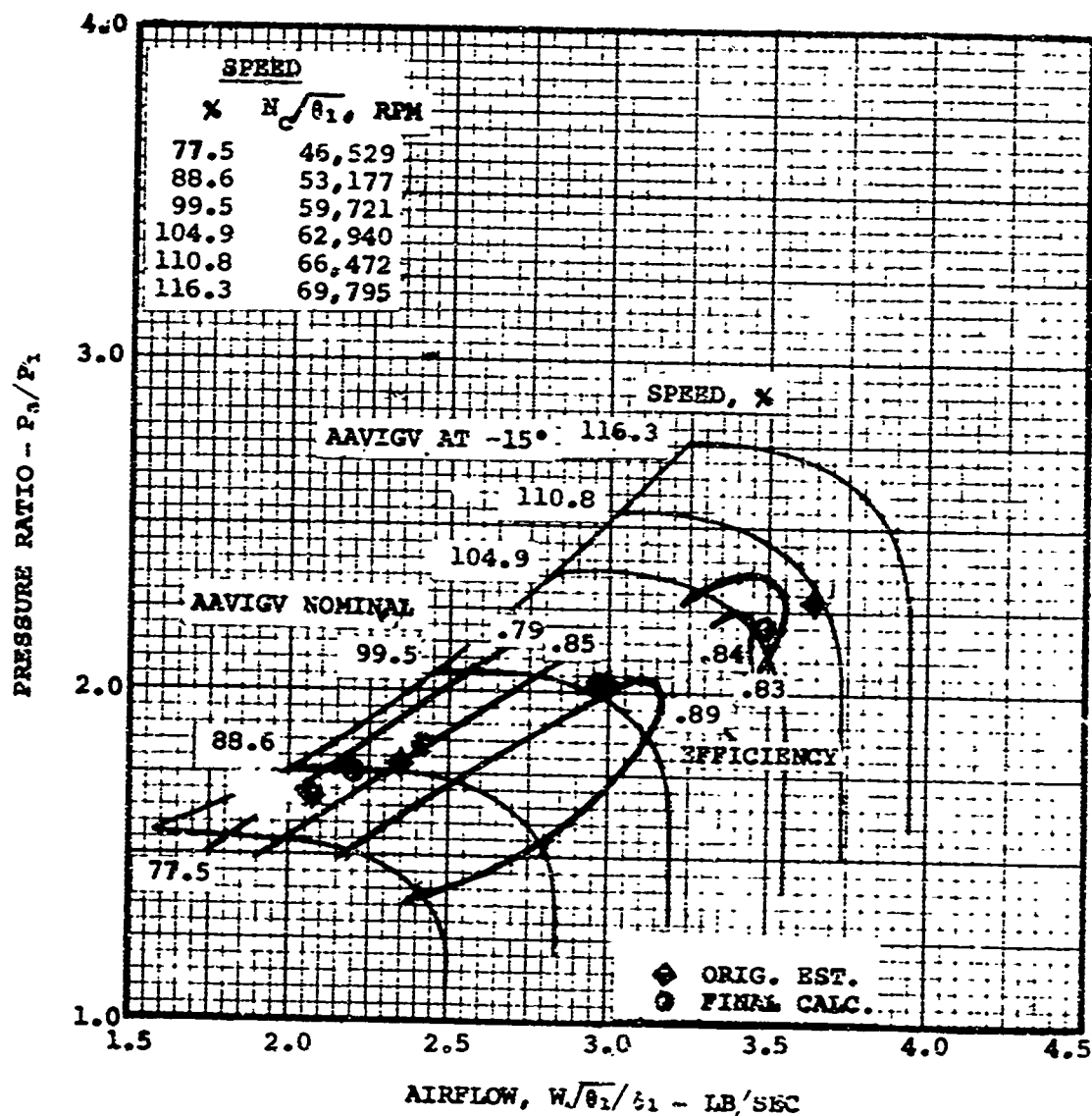
3.3.2.6 Single Spool, AAVIGV + C(VIGV + VDV)

A match was achieved for this case, consisting of:

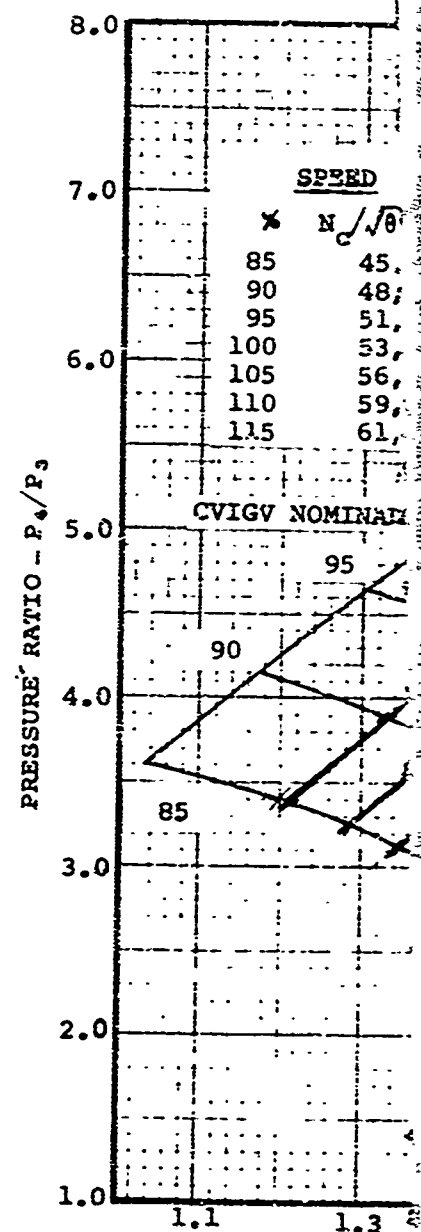
1. Two-stage axial compressor component, variable inlet guide vanes (AAVIGV)
2. Single-stage centrifugal compressor component, variable inlet guide vanes, and variable diffuser vanes C(VIGV + VDV).

This is the second of two combinations of variable compressor geometry that were evaluated in this preliminary matching study. The intent of this study was to explore the performance potential for such a system with full recognition of the mechanical complexity that would be required for operation.

A

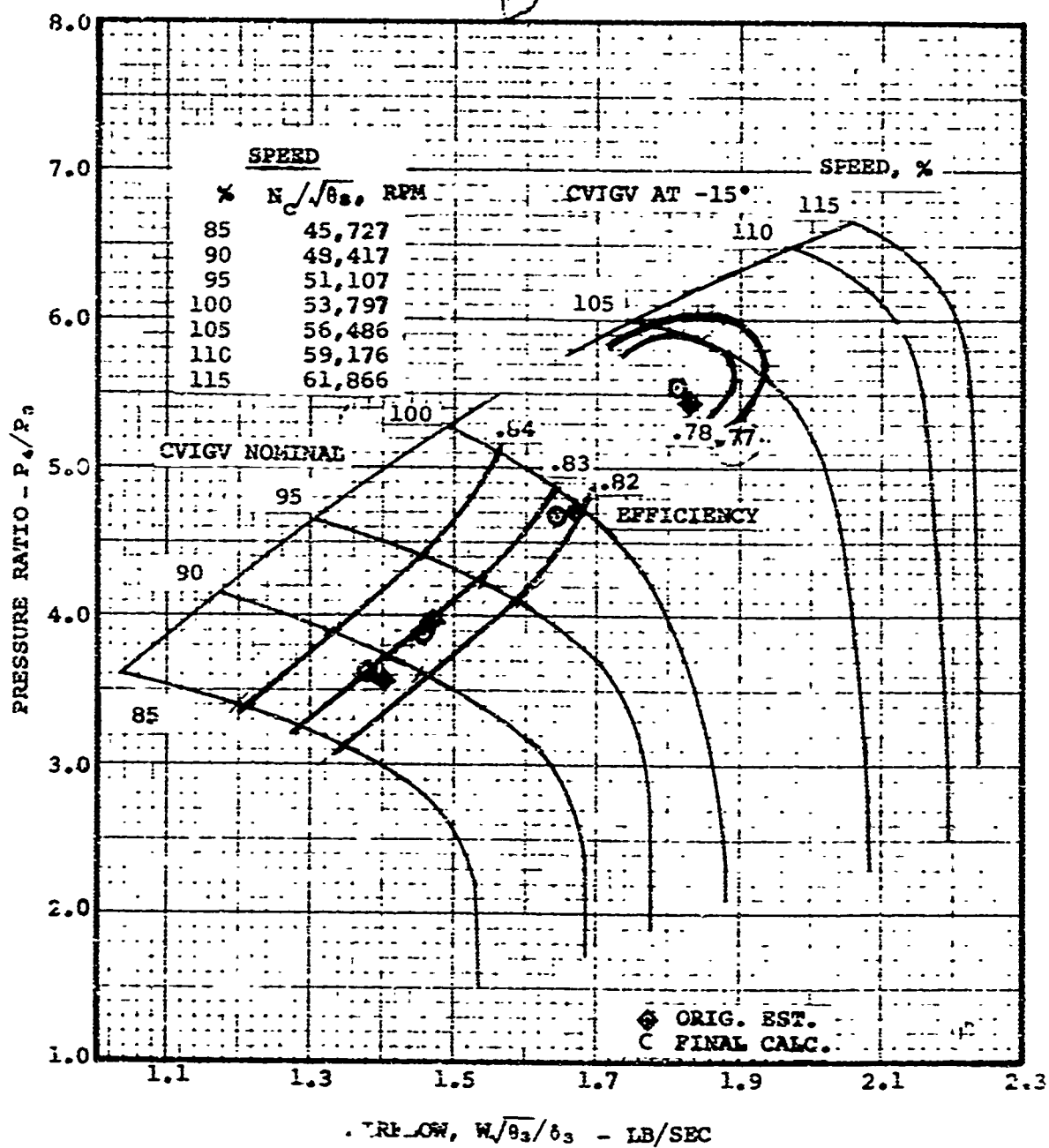


(A) AXIAL COMPRESSOR COMPONENT:
 VARIABLE INLET GUIDE VANES, 0° AND -15°
 $\eta_{AX} = 0.945 \eta_{AX, DESIGN}$ FOR AAVIGV AT -15°

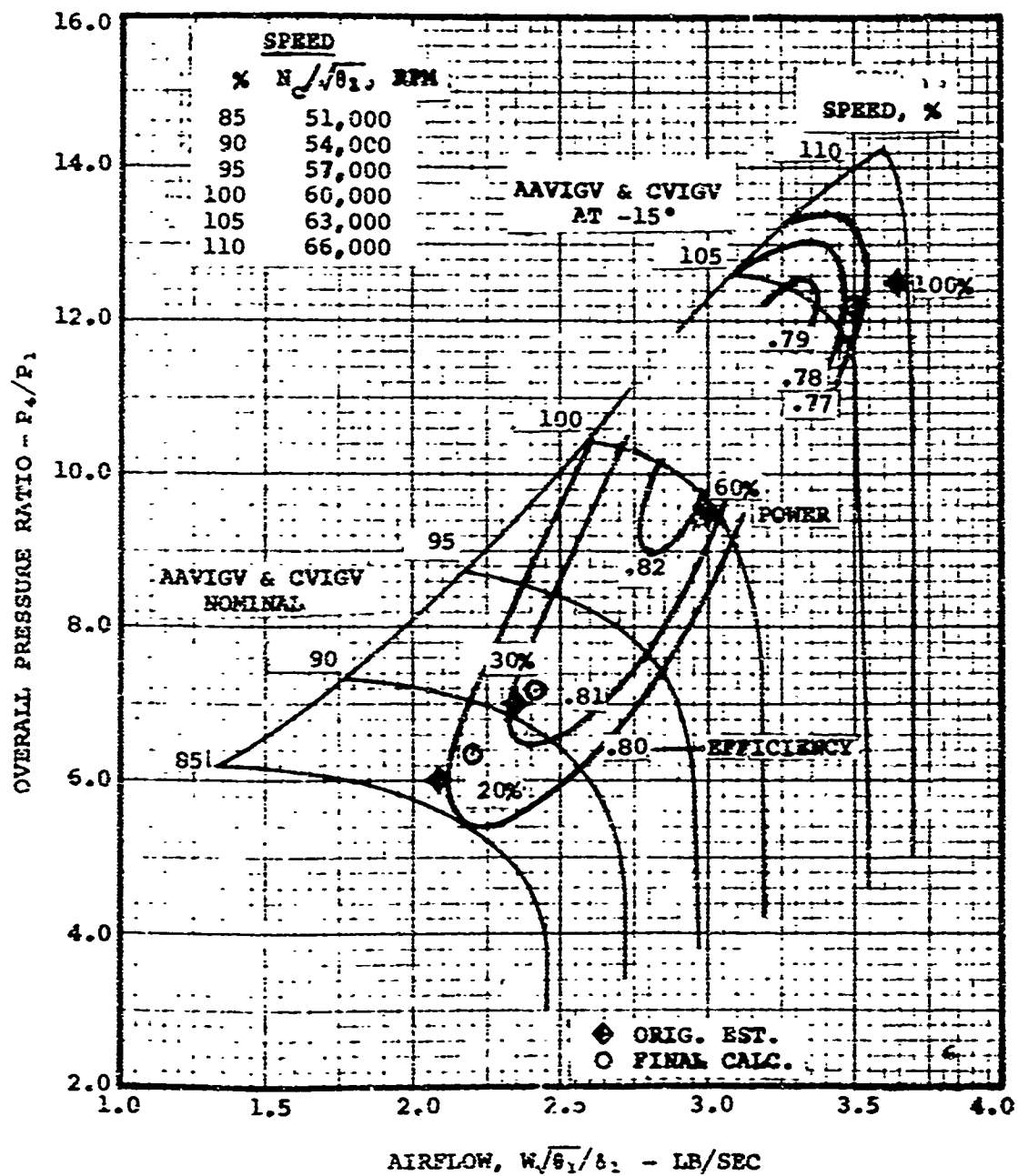
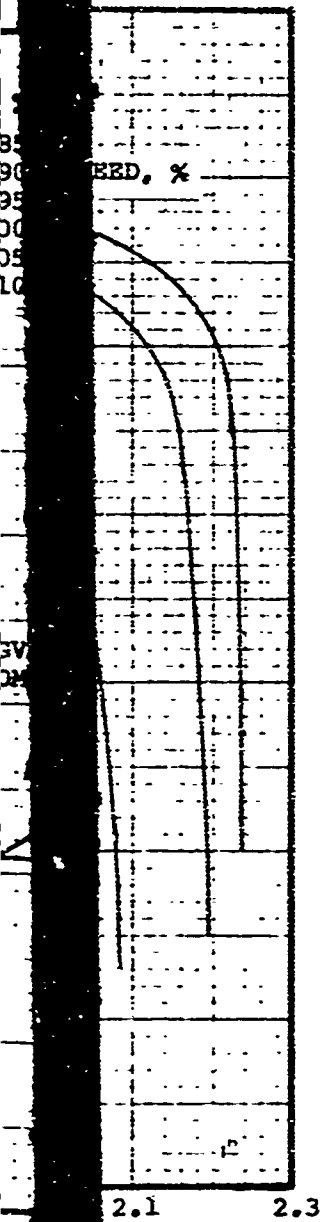


(B) CENTRIFUGAL COMPRESSOR COMPONENT:
 VARIABLE INLET GUIDE VANES
 $\eta_{CC} =$

Figure 26. Estimated Performance Characteristics, Two-Stage Axial Plus Centrifugal Compressor (Includes Efficiency Degradation Due to AAVIGV and CVIGV), AAVIGV + CVIGV.



(B) CENTRIFUGAL COMPRESSOR COMPONENT:
 VARIABLE INLET GUIDE VANES, 0° AND -15°
 ($\eta_{CC} = 0.945 \eta_{CC,DESIGN}$ FOR CVIGV AT -15°)



(C) OVERALL COMPRESSOR

The results of this study show no significant advantage over the combination of compressor components employing AAVIGV's and CVIGV's only. Similar to the previous combinations studied, the axial compressor operates at lower than optimum flows for the reduced-power points, with operation at 60- and 100-percent power near the peak efficiency points for the respective speeds. The axial compressor operates with approximately 7-percent surge margin at 20-percent power. Additional surge margin might be gained for acceleration by actuation of the variable vane rows at reduced power.

The axial and centrifugal compressor efficiencies assumed for this study are the same as those estimated by the compressor preliminary design study except that the axial and centrifugal compressor efficiencies are each degraded to 0.945 of their respective design values for operating points(s) with AAVIGV's and CVIGV's actuated off 0° setting angle ($\eta_{AX-CC} = 0.945 \eta_{AX-CC, DESIGN}$ for AAVIGV, CVIGV, and CVDV $\neq 0^\circ$). This study did not include analysis for no efficiency degradation, since data for this comparison have already been observed for Combinations 3 (AAFG + CVIGV), 4 (AAVIGV + CFG), and 5 (AAVIGV + CVIGV).

AAVIGV, CVIGV, and CVDV angle settings were selected to be 0° for speeds up to and including 100-percent design speed, and -15°, -15°, and -2°, respectively, for speeds above 100 percent. Note that negative setting angles for both AAVIGV's and CVIGV's effect swirl in the direction opposite to rotor rotation. Additionally, negative setting angles for the CVDV's effect adjustment to reduce the vane angle with respect to the radial direction and thereby increase flow.

The match for this case yields a reduced overall compressor peak efficiency of 0.81 compared to 0.82 for Combinations 4 (AAVIGV + CFG) and 5 (AAVIGV + CVIGV). The peak efficiency island coincides with the operating line at speeds slightly below the 100-percent-power speed. The data are displayed in the three composite compressor maps (0° and -15°, -15°, and -2° setting angles for AAVIGV's, CVIGV's, and CVDV's, respectively) of Figure 27.

Part A of Figure 27 displays the axial compressor characteristics. Comparison with the map for Combination 5 (AAVIGV + CVIGV), Part A of Figure 26, shows that the operating points on the axial compressor map are virtually unchanged by actuation of the diffuser vanes at 100-percent power.

Part B of Figure 27 displays the centrifugal compressor characteristics. Comparison here with the map for Combination 5 (AAVIGV + CVIGV), Part B of Figure 26, shows the effect of variable diffuser vanes, actuated for -2° at 100-percent power, on the centrifugal compressor 100-percent-power match point. The principal result as displayed is to increase the centrifugal compressor efficiency at the expense of surge margin.

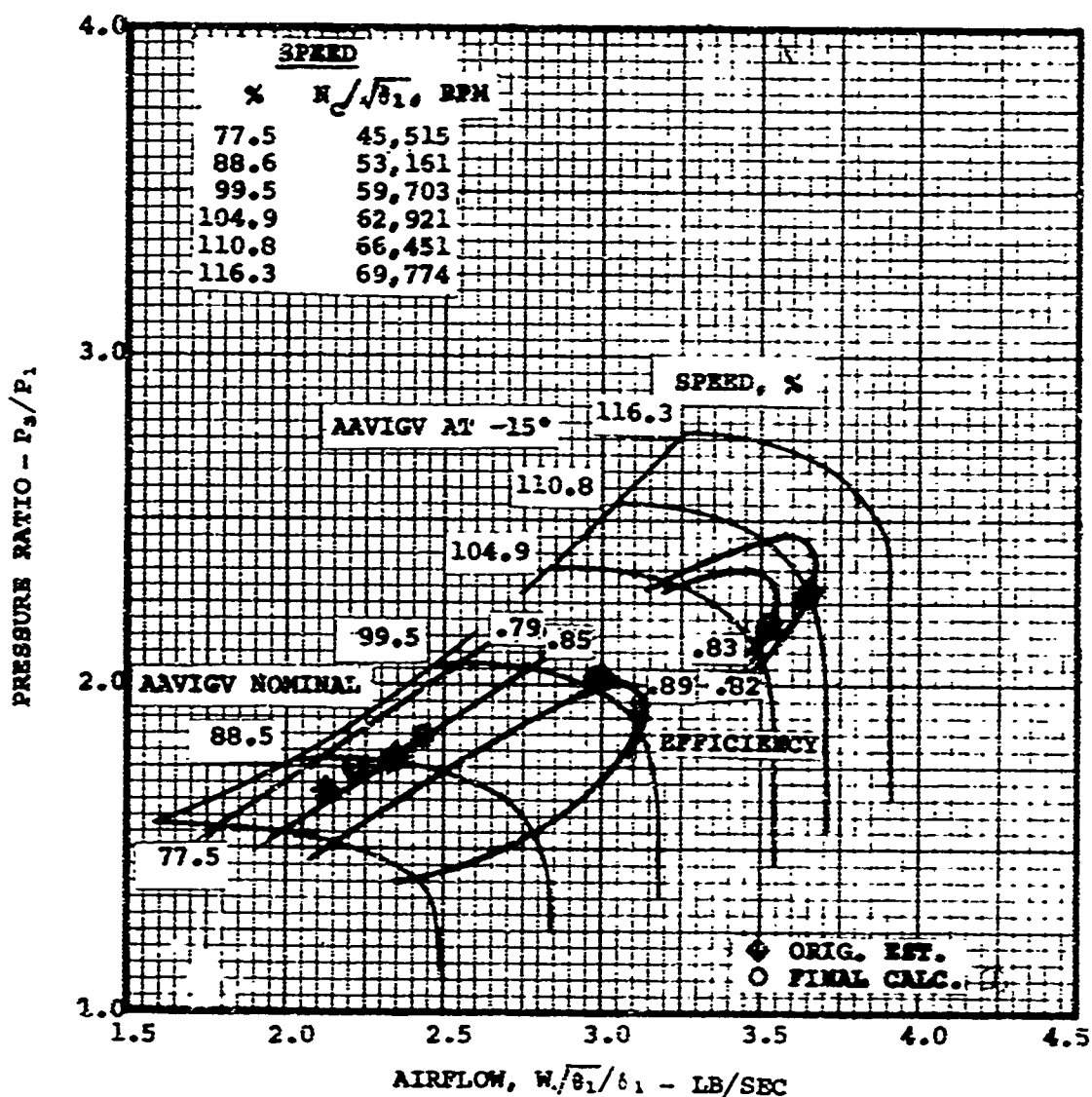
Part C of Figure 27 displays the overall compressor characteristics. From this it can be seen that the operating line falls near the peak efficiency points for the operating range. Comparison again with the respective map for Combination 5 (AAVIGV + CVIGV), Part C of Figure 26, shows that the design points are changed only slightly by actuating the diffuser vanes at the 100-percent-power point.

The increase of approximately 0.01 in centrifugal compressor efficiency compared to Combination 5 (AAVIGV + CVIGV) produces only a fractional gain in compressor overall efficiency for the 100-percent-power point due to the simultaneous loss in axial compressor efficiency and pressure ratio. Based on this, it is concluded that no significant advantage can be realized for this combination.

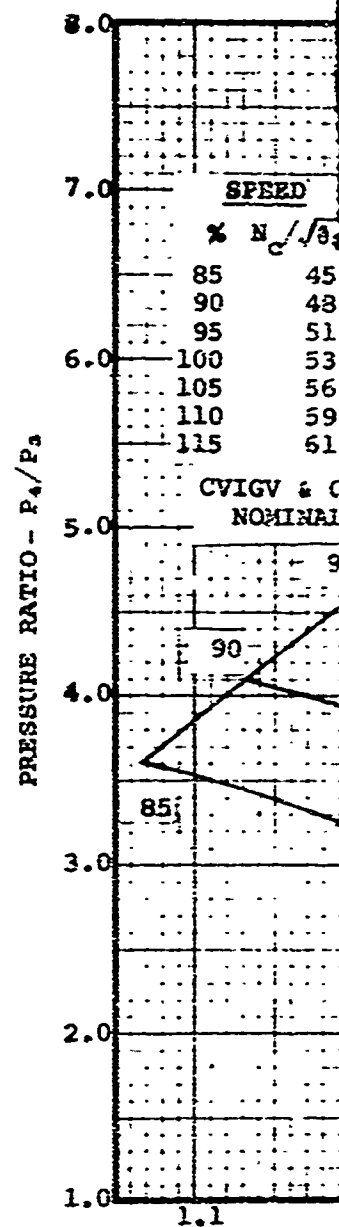
The Compressor and engine SFC data for this case are given in Table XII.

TABLE XII. AAVIGV + C (VIGV + VDV) COMPRESSOR ($\eta_{AX-CC} = 0.945 \eta_{AX-CC, \text{DESIGN}}$ FOR AAVIGV, CVIGV, AND CVDV $\neq 0^\circ$)					
Percent Power	$\dot{W}/\dot{V}/\delta$ (lb/sec)	P_4/P_1	$\eta_{4,1}$	T_5 ($^\circ\text{F}$)	SPC
100.0	3.507	12.24	0.778	2500	0.461
60.1	2.980	9.47	0.819	2010	0.489
32.0	2.424	7.18	0.815	1700	0.609
23.4	2.212	6.40	0.807	1600	0.706

A



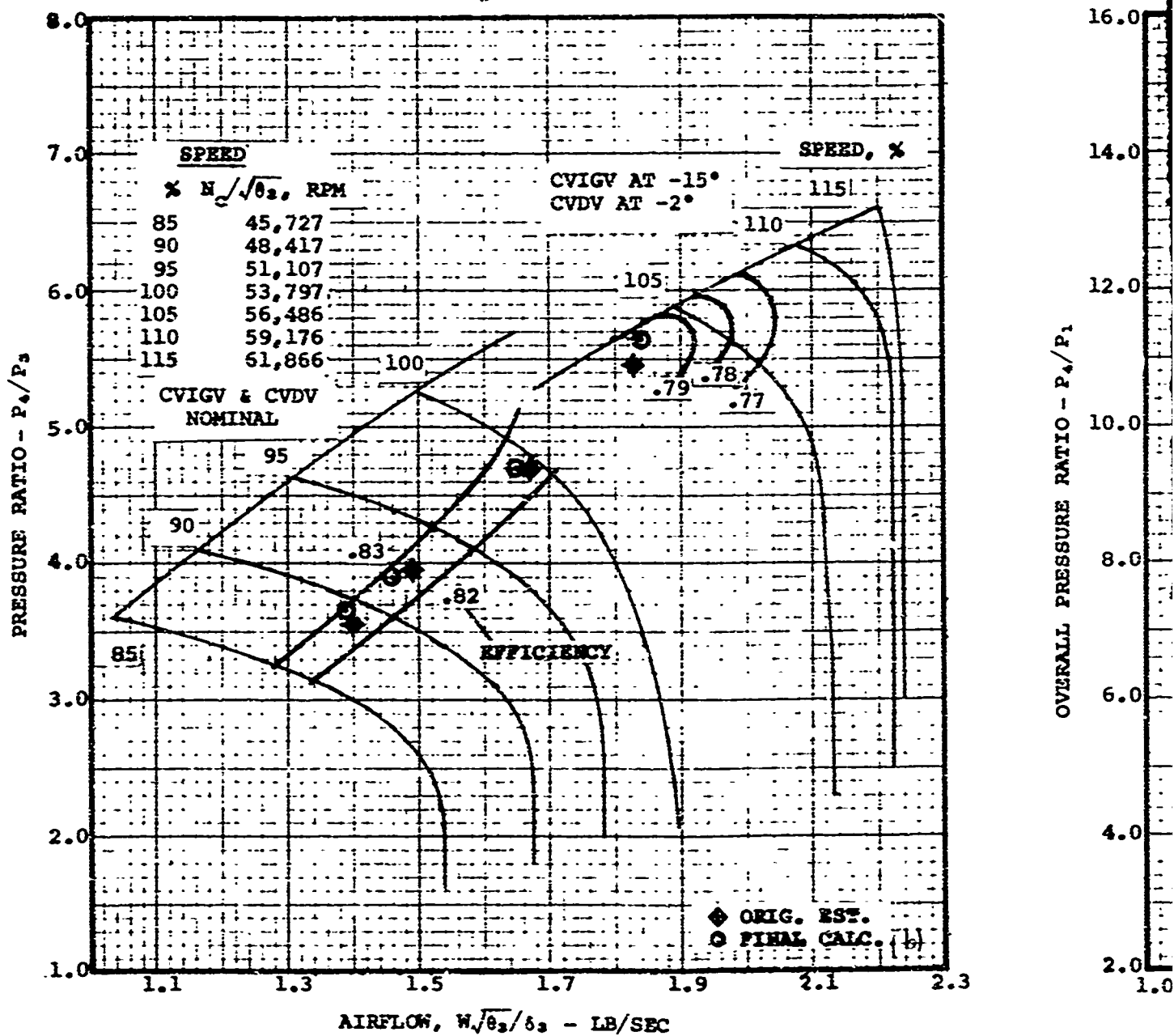
(A) AXIAL COMPRESSOR COMPONENT: VARIABLE INLET GUIDE VAKES, 0° AND -15°
 $(\eta_{AX} = 0.945 \eta_{AX, DESIG} \text{ FOR AAVIGV -15°})$



(B) CENTRIFUGAL GUIDE V.
 $(\eta_{CC} =)$

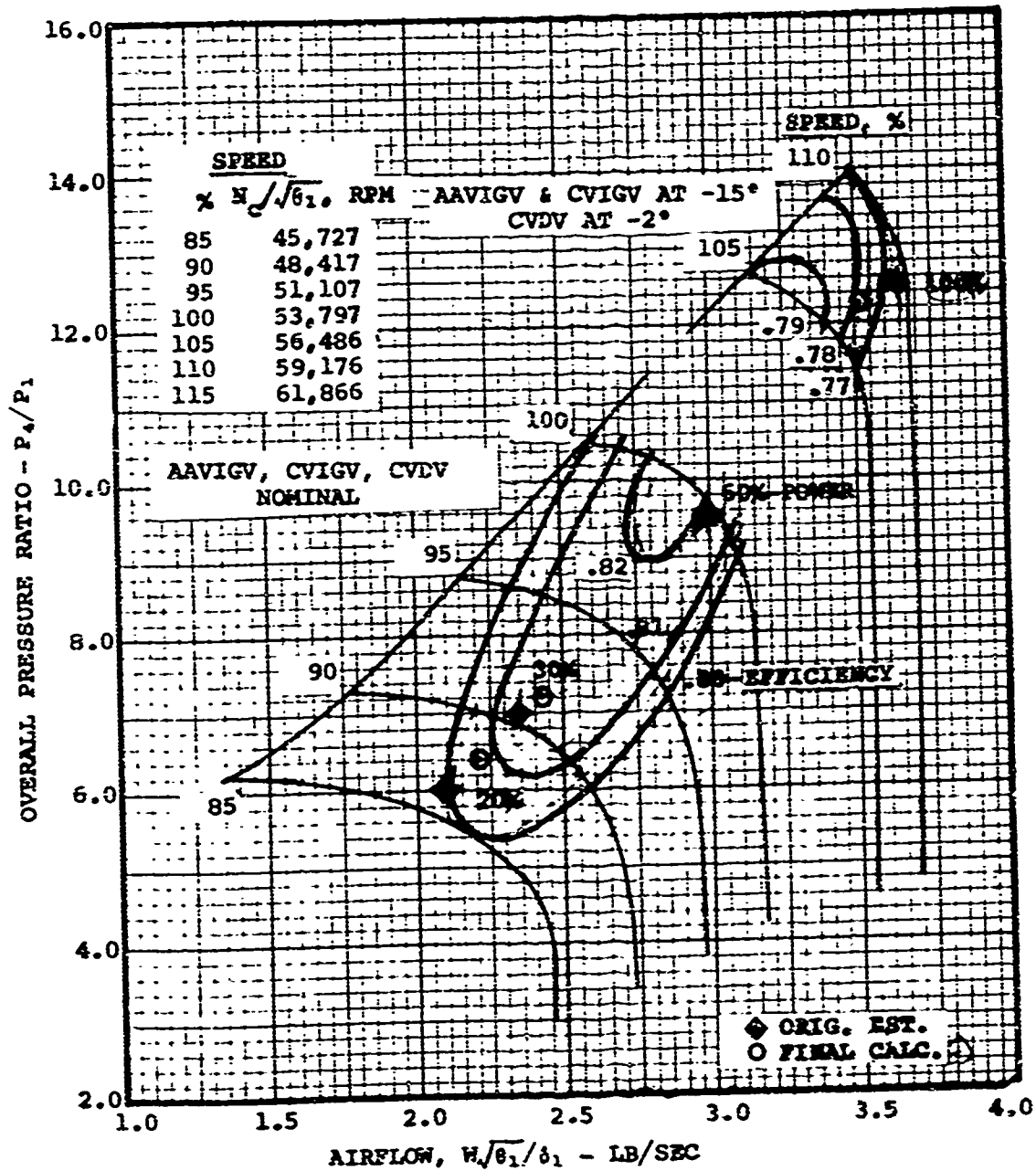
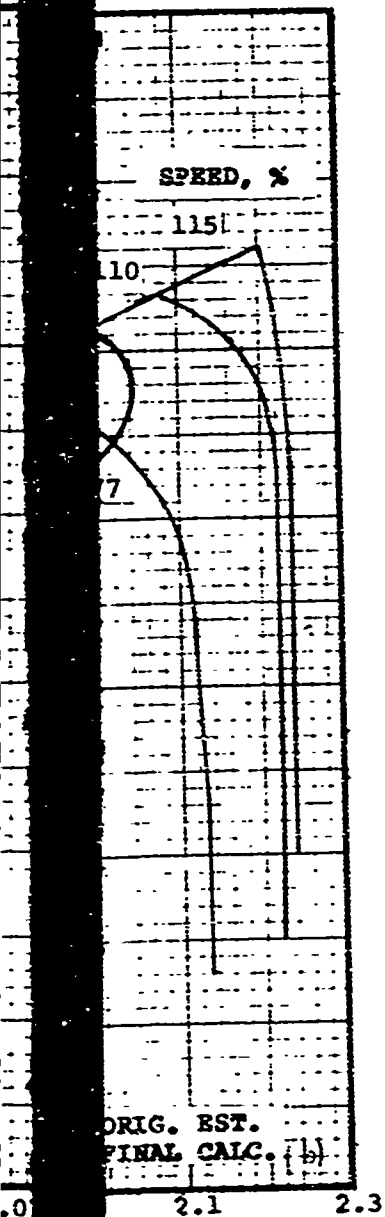
Figure 27. Estimated Performance Characteristics, Two-Stage Axial Plus Centrifugal Compressor (Includes Efficiency Degradation Due to AAVIGV + CVIGV), AAVIGV + CVIGV + CVDV.

B



(B) CENTRIFUGAL COMPRESSOR COMPONENT: VARIABLE INLET GUIDE VANES, 0° AND -15° , PLUS VARIABLE DIFFUSER
 $(\eta_{CC} = 0.945 \eta_{CC, \text{DESIGN FOR CVIGV } -15^\circ})$

C



(C) OVERALL COMPRESSOR

INLET
FUSER

3.3.2.7 Twin Spool, AAFG + CFG

Matching studies were conducted for this case, consisting of:

1. Two-stage axial compressor, fixed geometry, coupled to the second stage of a two-stage gasifier turbine (low-pressure spool)
2. Single-stage centrifugal compressor, fixed geometry, coupled to the first stage of a two-stage gasifier turbine (high-pressure spool)

The intent of this study was to explore the performance potential of twin-spool matching. Clearly, nothing less than a significant performance advantage for this case would justify its selection in light of the complexity of the mechanical arrangement that would result for the small, front-drive turboshaft engine assumed for this program. This mechanical complexity would result for either a three-coaxial-shaft arrangement or a parallel-shaft arrangement.

The results of this study show that low-pressure-spool and high-pressure-spool matches yield high compressor efficiency levels for both the axial and the centrifugal compressor. Furthermore, both compressor matches provide for adequate surge margin over the operating range from 20- to 100-percent power. However, engine cycle data show that the effect of gasifier turbine component efficiency degradation resulting for twin spooling partially offsets the high compressor performance.

The matching conducted in this study is based on axial and centrifugal compressor characteristics as estimated in the preliminary compressor design for this task and as follows:

1. Engine component efficiencies (excluding compressors) and cycle assumptions are as reported for Task IA design-point studies, Paragraph 2.2 (reference Appendix I) and off-design studies, Paragraph 2.4 (reference Appendix II). Gasifier turbine stages 1 (high-pressure spool) and 2 (low-pressure spool) each operate with the efficiency estimated for the two-stage gasifier turbine ($\eta_{HPT} = \eta_{LPT} = \eta_{GT, DESIGN}$).

2. Same as (1) except that efficiencies of the second-stage gasifier turbine (low-pressure spool) are degraded by 4 percent ($\eta_{HPT} = \eta_{LPT} = 0.96 \eta_{GT, \text{DESIGN}}$).

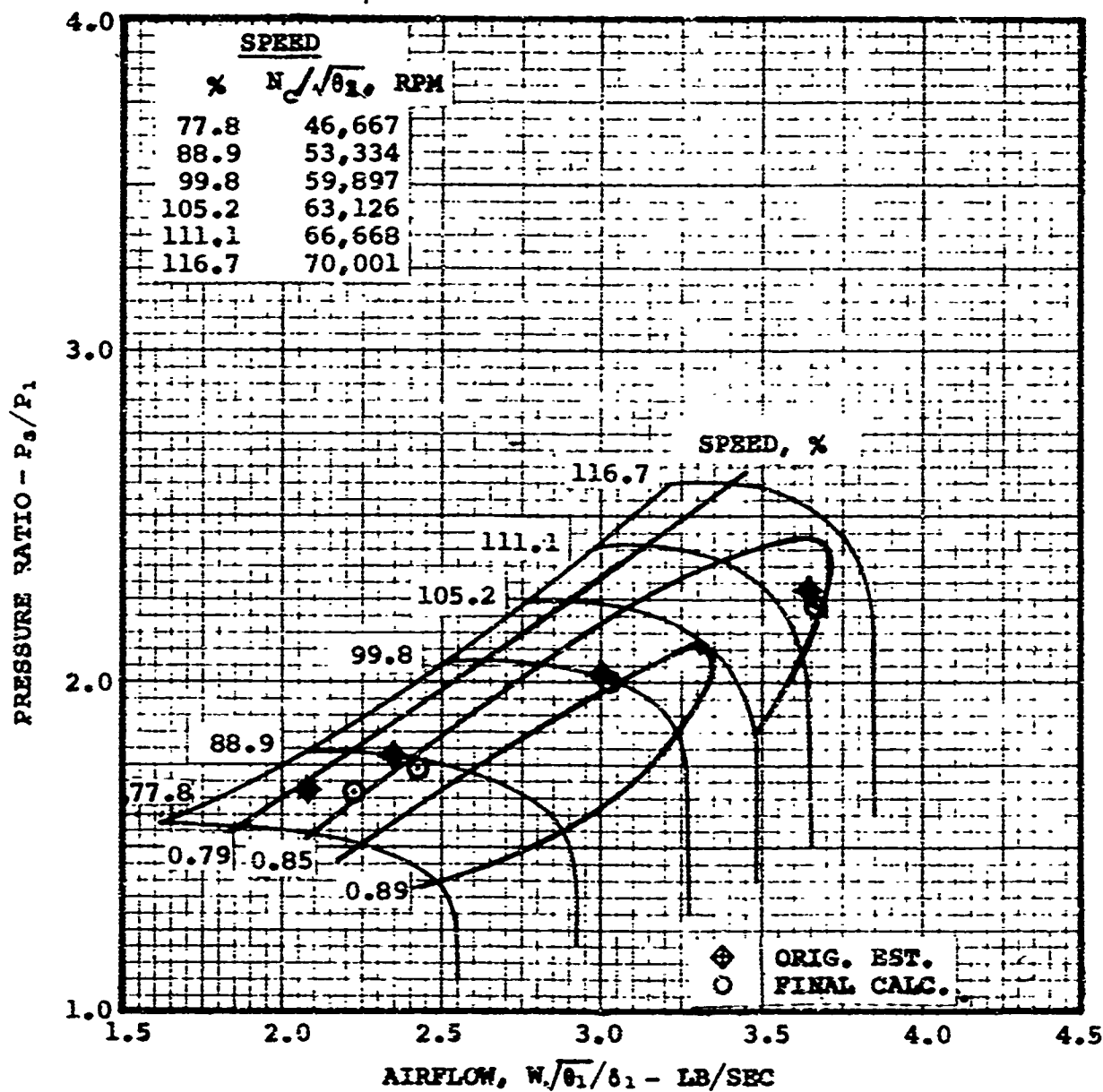
Analysis was made based on the assumptions given in (1) and (2), and results are discussed below.

1. $\eta_{HPT} = \eta_{LPT} = \eta_{GT, \text{DESIGN}}$ - The axial and centrifugal compressor characteristics for this case are identical with those displayed in Figure 28 for the case with gasifier turbine efficiency degradation. The operating points for this case would be slightly different from those shown on Figure 28.

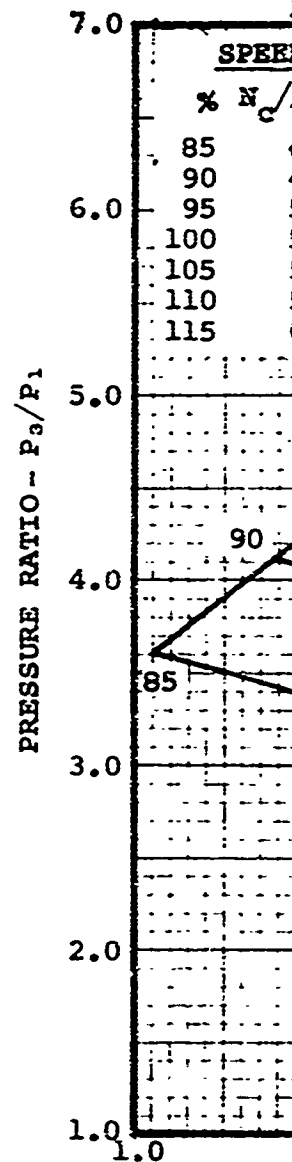
The data from this match, which are given in Table XIII show a design-point SFC of 0.483 (TIT = 2060°F) compared to design-point values for Combination 4 (AAVIV + CFG) of 0.481 (TIT = 2085°F) and 0.485 (TIT = 2045°F) with efficiency degradation. Further comparison with off-design values showed a slight advantage for twin spooling compared to the data for Combination 4 (with efficiency degradation). Clearly, no significant advantage is evidenced for this case of twin spooling, notwithstanding the fact that the twin-spool data are somewhat optimistic.

TABLE XIII. TWIN-SPOOL COMPRESSOR, AAFG + CFG ($\eta_{HPT} = \eta_{LPT} = \eta_{GT, \text{DESIGN}}$)					
Percent Power	$W\sqrt{\theta}/\delta$ (lb/sec)	P_4/P_1	η_{41}	T_5 (°F)	SFC
100.0	3.658	12.62	0.799	2500	0.449
59.5	3.020	9.56	0.819	2060	0.483
29.5	2.420	7.10	0.819	1700	0.614
22.2	2.238	6.41	0.816	1600	0.701

2. $\eta_{HPT} = \eta_{GT, \text{DESIGN}} : \eta_{LPT} = 0.96 \eta_{LPT, \text{DESIGN}}$ - The axial and centrifugal compressor characteristics for this case are shown in Figure 28.



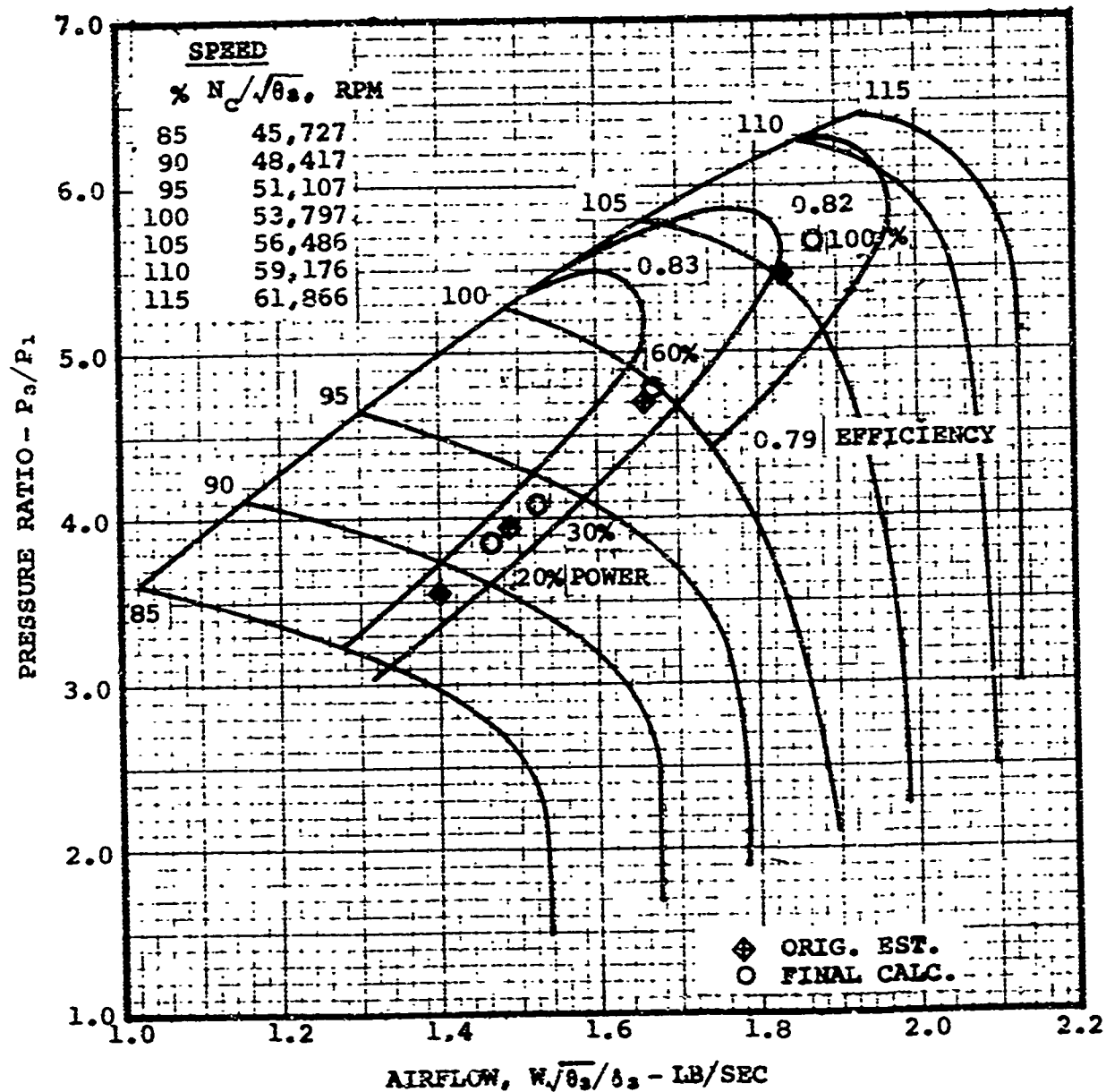
(A) TWO-STAGE AXIAL COMPRESSOR COMPONENT



(B) S

Figure 28. Estimated Performance Characteristics,
Two-Stage Axial Plus Centrifugal Compressor
(Includes No Efficiency Degradation),
Twin Spool - AAFG + CFG.

B



(B) SINGLE-STAGE CENTRIFUGAL COMPRESSOR COMPONENT

Figure 28(A) displays the axial compressor characteristics and the 20-, 30-, 60-, and 100-percent-power operating points. The design-point match (60-percent power) is very near the peak efficiency for this compressor and shows an efficiency of 0.884. Adequate surge margin is evidenced over the operating range, including approximately 19 percent at 20-percent power.

Figure 28(B) displays the centrifugal compressor characteristics and the 20-, 30-, 60-, and 100-percent-power operating points. The resultant operating line for this stage provides for adequate surge margin over the operating range, including approximately 16 percent at 20-percent power.

The compressor and engine SFC data for this task are given in Table XIV. The performance levels indicated are considered to be achievable with the gasifier turbine efficiency degradation assumed for this study. Comparison of these data with those reported for Combination 4 (AAVIGV + CFG), Paragraph 3.3.2.4, Table XIV, showed comparable performance levels, with a slight advantage for the AAVIGV + CFG combination.

TABLE XIV. TWIN-SPOOL COMPRESSOR, AAFG + CFG $\eta_{HPT} = \eta_{GT, DESIGN}$; $\eta_{LPT} = 0.96$ $\eta_{GT, DESIGN}$					
Percent Power	$W\sqrt{\theta}/\delta$ (lb/sec)	P_4/P_1	η_{41}	T_5 (°F)	SFC
100.0	3.662	12.68	0.800	2500	0.454
59.5	3.031	9.58	0.820	2060	0.489
29.4	2.436	7.10	0.819	1700	0.623
22.2	2.245	6.41	0.816	1600	0.713

3.3.2.8 Selection of Matching Scheme

The results of these matching studies are presented and compared in the above paragraphs, 3.3.2.1 through 3.3.2.7. The compressor maps presented show that the principal variations for the schemes studied are in the axial compressor match points. Except for Combination 1 with fixed geometry (AAFG + CFG), only minor differences were observed in the overall compressor efficiencies, and differences in SFC's were largely attributable to the various design-point TIT's.

A summary of comparisons is as follows:

SINGLE SPOOL

- (1) AAFG + CFG combination yields a poor design-point efficiency match and reduced-power operation of the axial compressor in stall.
- (2) AAFG + CVDV combination yields a design-point efficiency approximately 2 points below Combination 4 (AAVIGV + CFG) but shows an SFC only slightly higher due to the higher match TIT (+85°F). The axial compressor operates near stall at reduced powers.
- (3) AAFG + CVIGV combination with representative efficiency degradation yields design-point efficiency approximately 1 point below Combination 4 (AAVIGV + CFG) with correspondingly higher SFC. Axial compressor operates near stall at reduced power.
- (4) AAVIGV + CFG combination with representative efficiency degradation yields the best design-point efficiency, 0.819, and the lowest SFC, 0.435. Axial compressor operation at reduced power requires AAVIGV actuation for stall margin. Selected as the best matching scheme.
- (5) AAVIGV + CVIGV and (6) AAVIGV + C(VIGV + VDV) with representative efficiency degradation yields design-point efficiency identical with that of Combination 4 (AAVIGV + CFG) but slightly higher SFC due to lower match TIT (-35°F). Axial compressor operation at reduced power requires AAVIGV actuation for stall margin. These are mechanically

complicated compared to Combination 4 (AAVIGV + CFG).

TWIN SPOOL

- (7) AAFG + CFG combination yields design-point efficiencies identical with those of Combination 4 (AAVIGV + CFG) but SFC is slightly higher, with representative gasifier turbine efficiency degradation. Mechanically complicated front-drive shafting is required.

The selected Combination 4 (AAVIGV + CFG) shows performance values below the theoretical peak efficiency for these axial and centrifugal compressors, including 0.819 versus 0.834 for compressor efficiency and 0.485 versus 0.479 for engine SFC at 2045°F (TIT). However, additional matching iterations would effect some improvement for this case, but are not warranted for the tentative studies of this task.

3.4 COMPRESSOR DESIGN AND MATCHING, AAVIGV + CFG, $P_4/P_1 = 10.5:1$

The aerodynamic design was conducted for a two-stage axial plus centrifugal compressor for the 10.5:1-design-point pressure ratio selected in Task IA, Section 2.0. The axial and centrifugal compressors were configured for 2.06:1 and 5.1:1 design-point pressure ratios, respectively, based on the optimum work-split calculations of Task IA.

The compressors were then matched by employing the matching scheme as selected in Paragraph 3.3.2, AAVIGV + CFG. The design and matching data are displayed in the three composite maps (0° and -15° AAVIGV setting angles) of Figure 29.

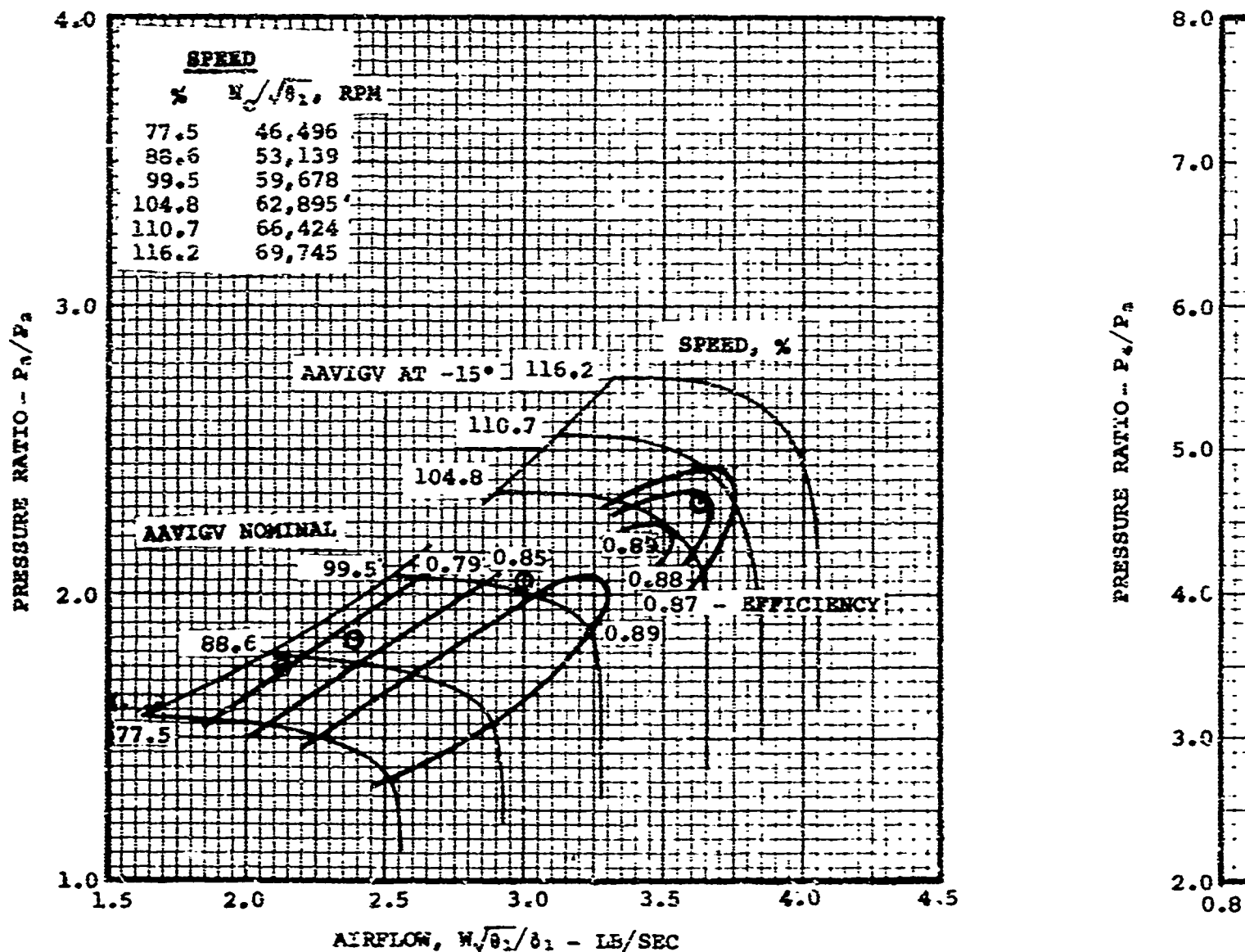
These results include no efficiency degradation for AAVIGV's and can be compared to the results for the 9.5:1-pressure-ratio compressor reported in Paragraph 3.3.2.7, Figure 25.

These compressor data, along with the data for the 9.5:1 and 11.5:1 (Paragraph 3.5) compressors, are the basis for Task IB cycle studies to determine the optimum design-point pressure ratio for the engine assumed for this program.

3.5 COMPRESSOR DESIGN AND MATCHING, AAVIGV + CFG, $P_4/P_1 = 11.5:1$

The aerodynamic design was conducted for this two-stage axial plus centrifugal compressor for the 11.5:1-design-point pressure selected in Task IA, Section 2.0. The design and matching were conducted identical with that reported in Paragraph 3.4 except that the axial and centrifugal compressors were configured for 2.09:1 and 5.5:1 design-point pressure ratios respectively.

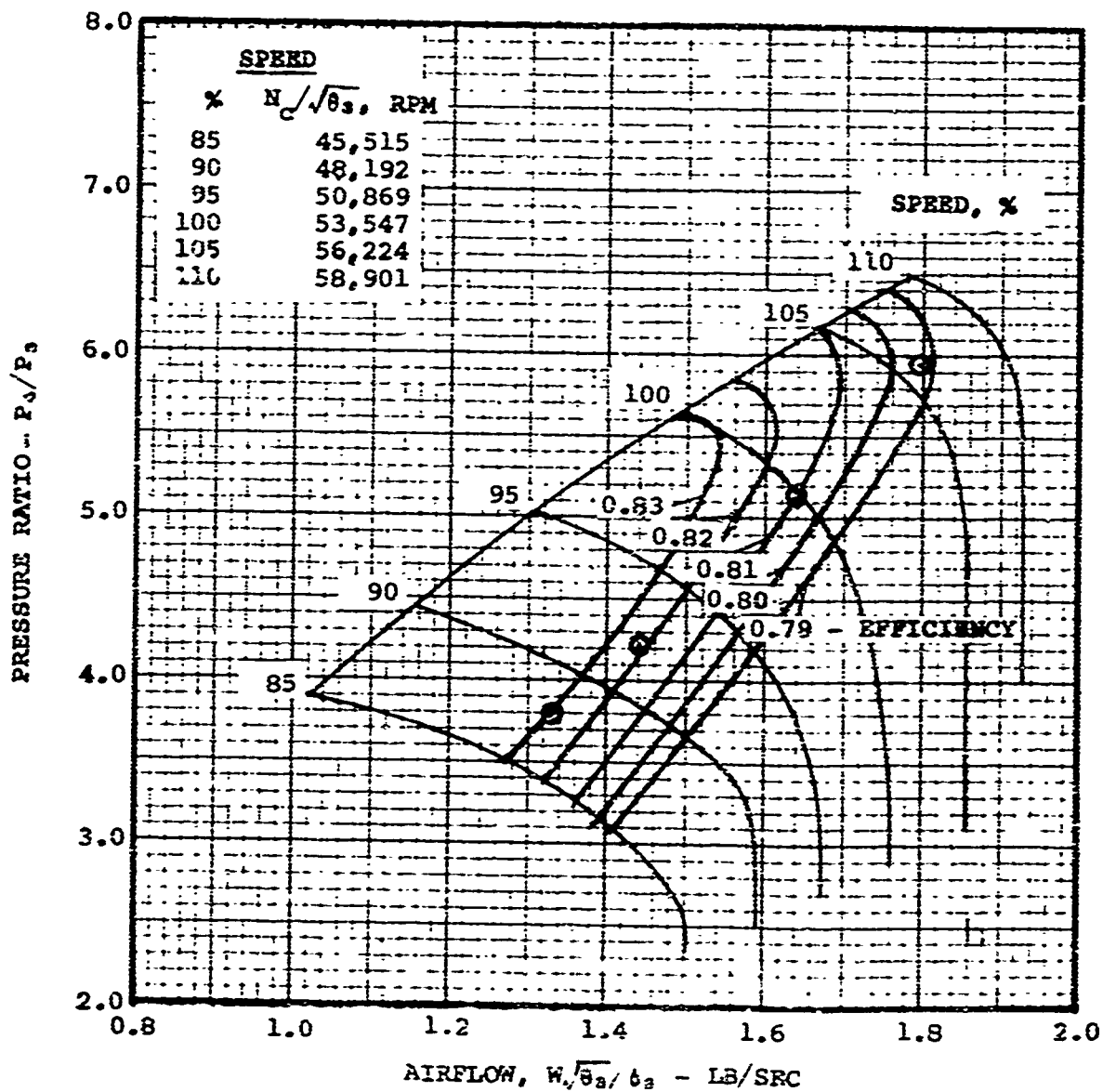
The design and matching data are displayed in Figure 30, which can be compared to Figures 29 (10:5:1) and 25 (9.5:1).



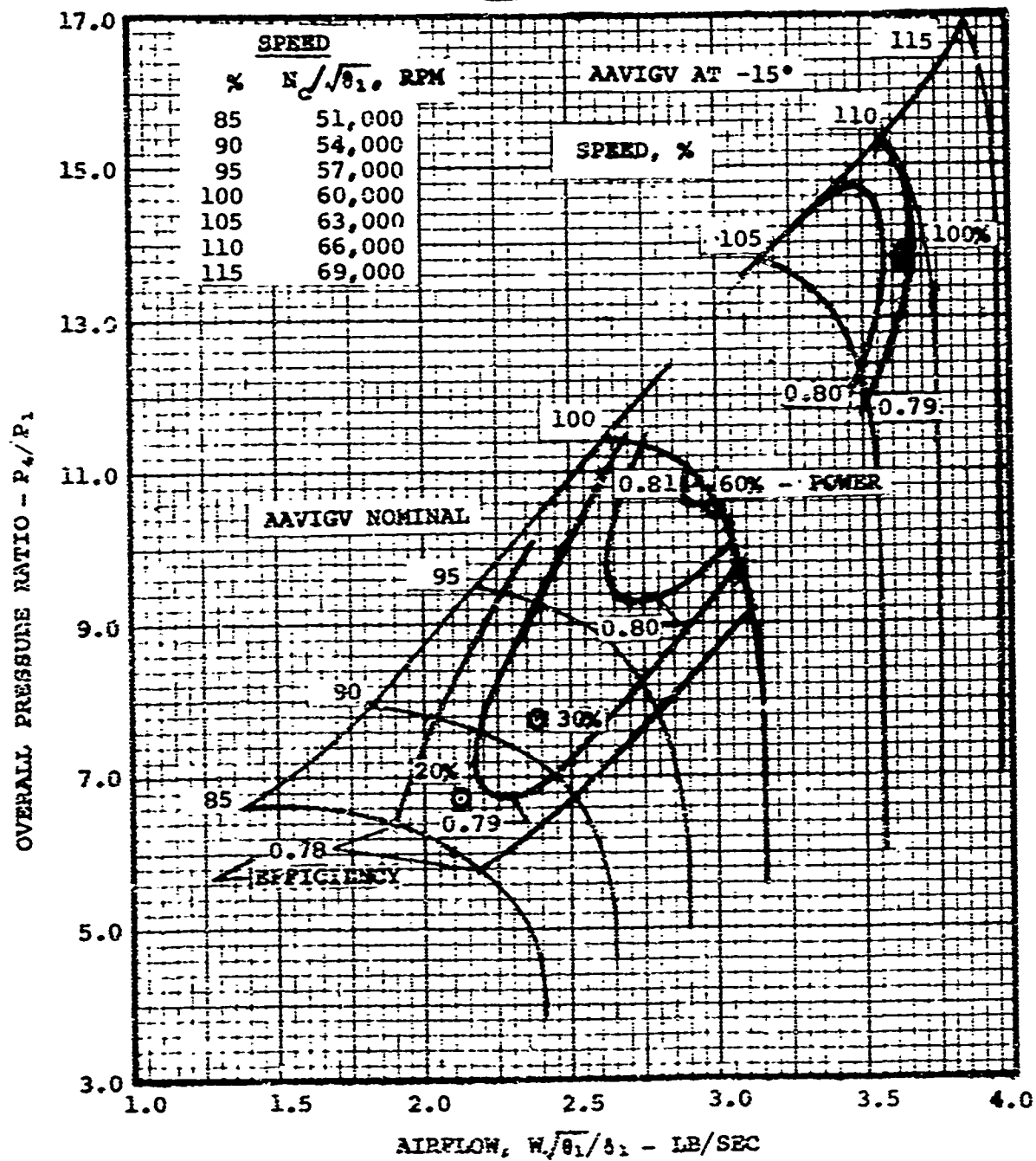
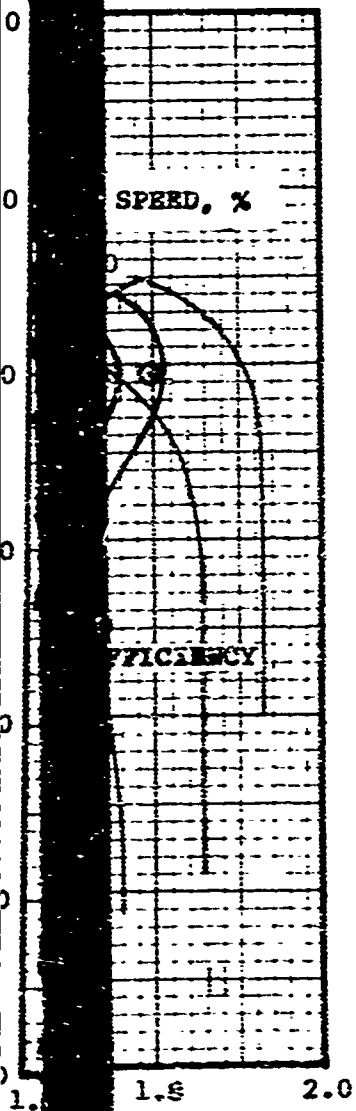
(A) AXIAL COMPRESSOR COMPONENT: VARIABLE
INLET GUIDE VANES, 0° AND -15°

Figure 29. Estimated Performance Characteristics, Two-Stage Axial Plus Centrifugal Compressor. Design-Point Overall Pressure Ratio = 10.5 (No Efficiency Degradation Due to AAVIGV), AAVIGV + CFG.

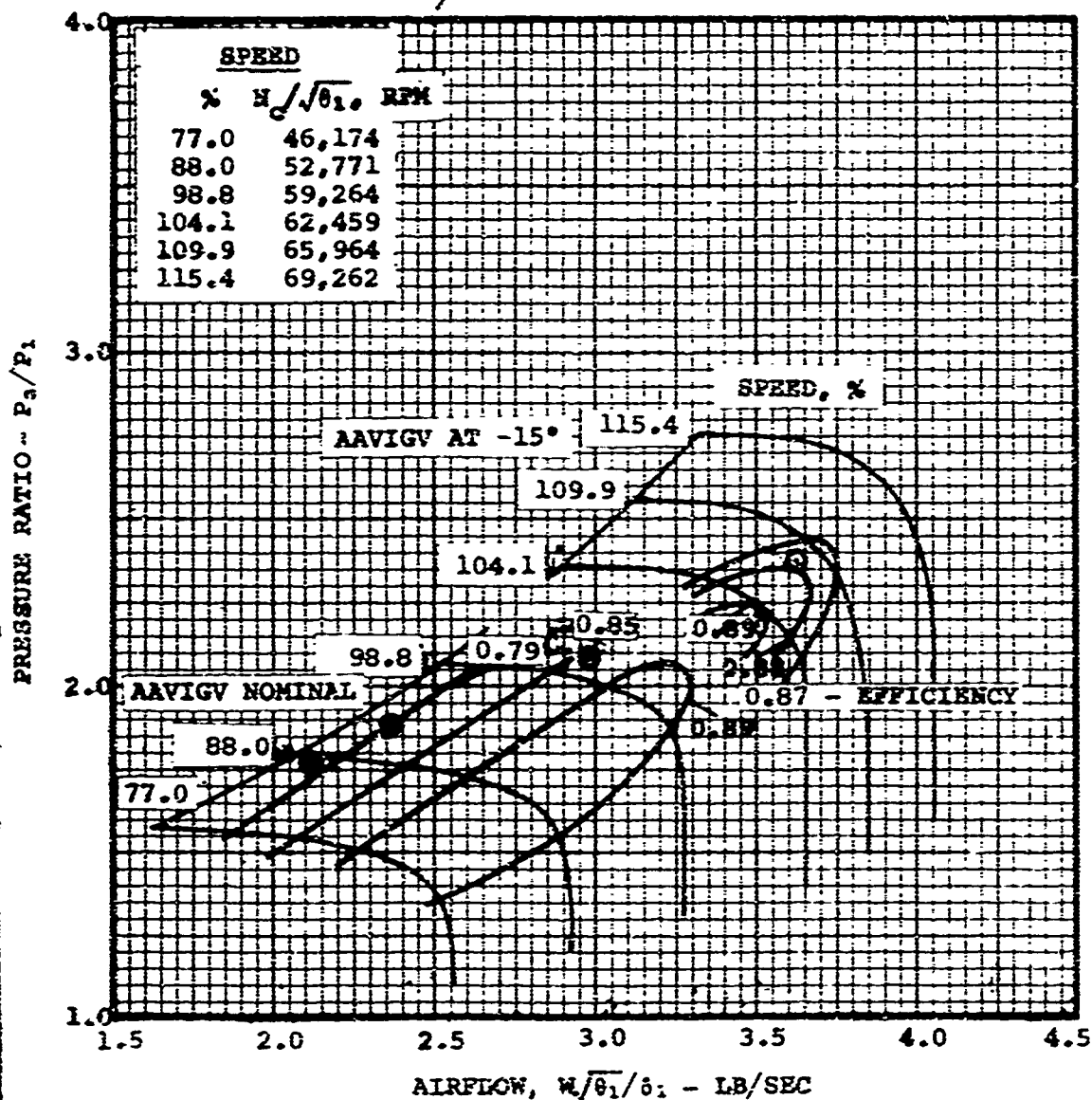
B



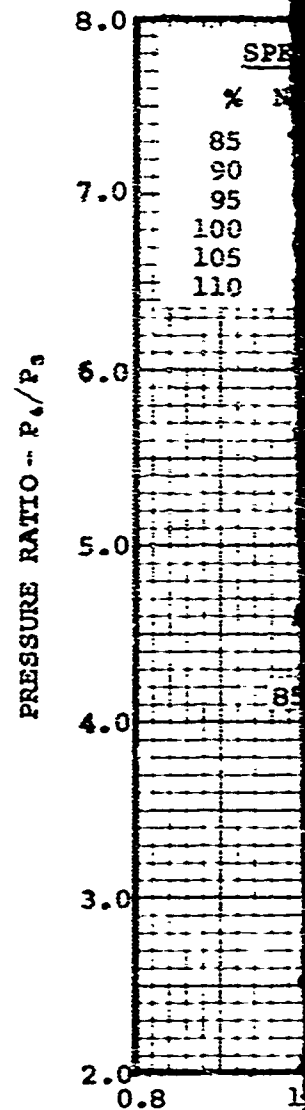
(B) CENTRIFUGAL COMPRESSOR: FIXED GEOMETRY



(C) OVERALL COMPRESSOR



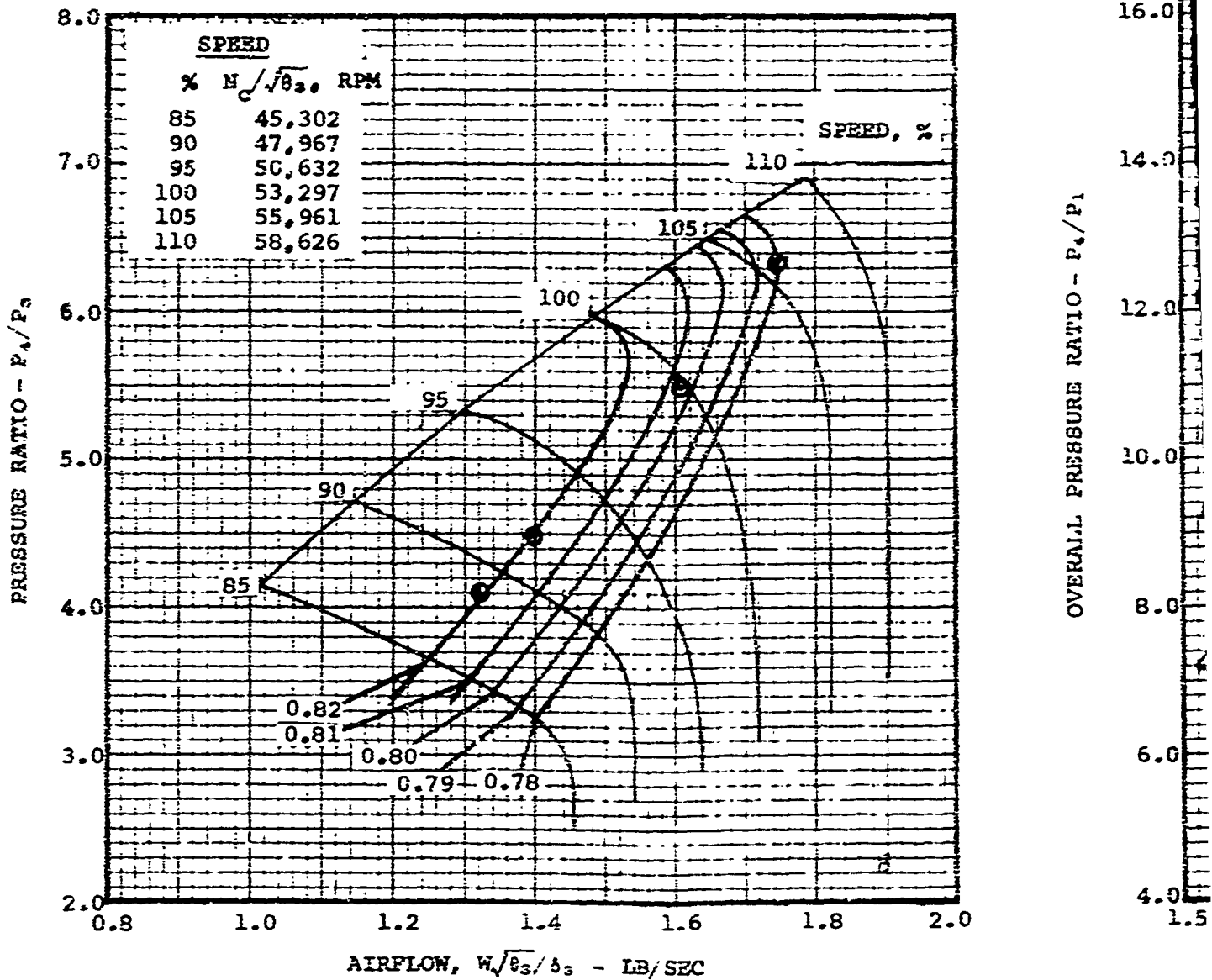
(A) AXIAL COMPRESSOR COMPONENT: VARIABLE INLET GUIDE VANES, 0° AND -15°



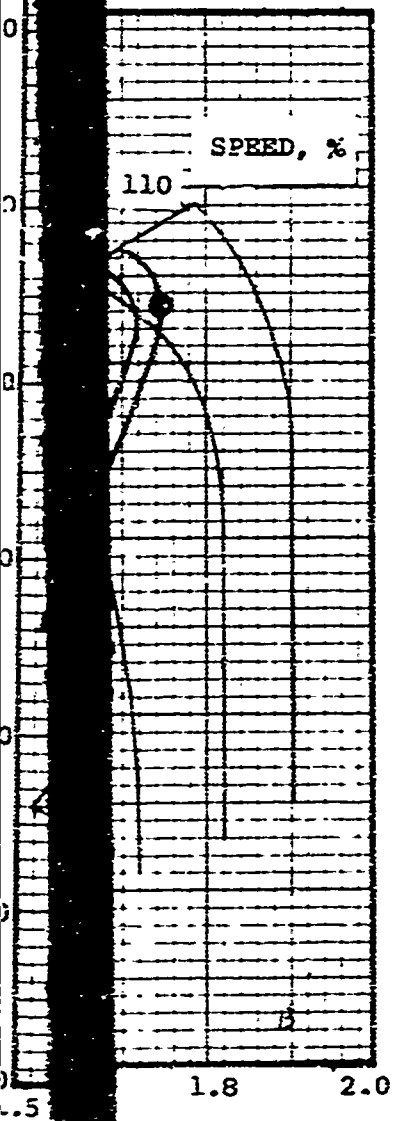
(B) CENTRIFUGAL COMPRESSOR COMPONENT

Figure 30. Estimated Performance Characteristics, Two-Stage Axial Plus Centrifugal Compressor. Design Point: Overall Pressure Ratio = 11.5 (No Efficiency Degradation Due to AAVIGV), AAVIGV + CFG.

B

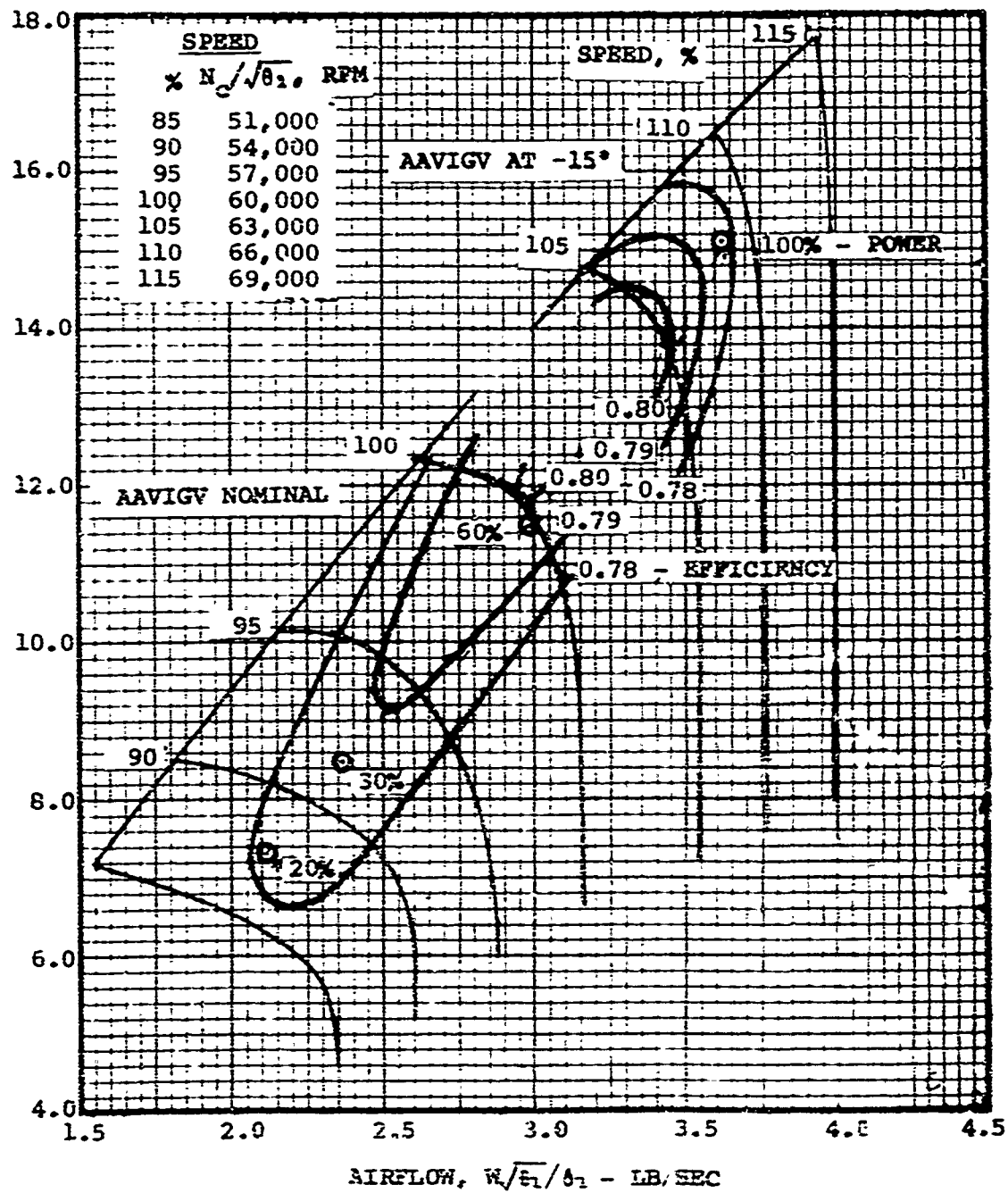


(B) CENTRIFUGAL COMPRESSOR COMPONENT: FIXED GEOMETRY



FIXED GEOMETRY

OVERALL PRESSURE RATIO - P_4/P_1



(C) OVERALL COMPRESSOR

4. TASK IB, ENGINE CYCLE ANALYSIS

4.1 GENERAL

This task was conducted to (1) produce engine performance data for the various compressor matching schemes compared in Task IIA, Section 3.0, (2) effect a firm selection of the optimum design-point pressure ratio, and (3) estimate an engine operating line to display final compressor design requirements for Task IIB.

4.2 CYCLE ASSUMPTIONS

Advanced technology component performance levels have been assumed for these analyses and are identical, except as noted, with the design and off-design assumptions reported for Task IA in Paragraph 2.2 (refer also to Appendix I) and Paragraph 2.4 (refer also to Appendix II) except for the assumed compressor performance. The various compressor performance and operating characteristics assumed in these cycle analyses are as estimated in Task IIA, Section 3.0.

4.3 COMPRESSOR MATCHING STUDIES, $P_4/P_1 = 9.5:1$

Engine cycle analyses were conducted for the various compressor matching studies conducted in Task IIA and reported in Paragraph 3.3.2. The compressor matching variations studied consisted of various matching arrangements of a two-stage axial compressor (AA) and a single-stage centrifugal compressor (C). The matching arrangements studied consisted of compressor configurations employing fixed geometry (FG), variable inlet guide vanes (VIGV's), and variable diffuser vanes (VDV's).

The performance data for these studies were reported, in part, in Paragraph 3.3.2 and are more fully presented in Table XV.

To indicate the proximity of the operating points from the multistage compressor instability (discussed in Section 3.0), the margin of the operating points from axial compressor surge is indicated in Table XV. For instance, on Table XV, what is displayed for axial compressor surge margin at 20 percent power for AAVIGV + CFG (Combination 4, 5.3 percent surge margin) is in reality the margin from the multistage compressor instability band. It will be recalled that this is a narrow range of instability for the multistage compressor and that hard surge does not occur until the centrifugal compressor surges. This is what is referred to in Table XV as overall surge margin.

Notice that the surge margins displayed for the centrifugal and multistage compressors have different values. The reason for this is that the flows for surge and the operating points on the overall compressor map must be corrected for the axial compressor discharge conditions (pressure and temperature).

The surge flow of the centrifugal compressor when corrected for the axial compressor exit conditions is $W_{S.C.} \frac{\sqrt{\theta_3}}{\delta_3}$. The value of $W_{S.C.}$ (surge flow for centrifugal compressor) comes from the centrifugal compressor map. The actual value of this surge flow is

$$\left(W_{S.C.} \frac{\sqrt{\theta_3}}{\delta_3} \right) \frac{\delta_3}{\sqrt{\theta_3}} = W_{S.C.} \frac{\sqrt{\theta_1}}{\delta_1}$$

since the compressor maps are displayed for a standard day. Similarly, for an operating point,

$$\left(W_{O.P.} \frac{\sqrt{\theta_3}}{\delta_3} \right) \frac{\delta_3}{\sqrt{\theta_3}} = W_{O.P.} \frac{\sqrt{\theta_1}}{\delta_1}$$

The value of the operating point, $W_{O.P.}$, is taken from the centrifugal compressor map. Surge margin for the operating points on the centrifugal compressor map SM_C is

$$SM_C = \frac{W_{O.P.} \left(\frac{\sqrt{\theta_3}}{\delta_3} \right)_{O.P.} - W_{S.C.} \left(\frac{\sqrt{\theta_3}}{\delta_3} \right)_{S.C.}}{W_{O.P.} \left(\frac{\sqrt{\theta_3}}{\delta_3} \right)_{O.P.}}$$

Surge margin for the operating points on the overall compressor map, SM_O is

$$SM_O = \frac{W_{O.P.} - W_{S.C.}}{W_{O.P.}} \neq SM_C$$

13

ENGINE CYCLE DATA (CALCULATED)
COMPRESSOR MATCHING STUDIES

COMPRESSOR TYPE	COMPRESSOR FLOW (CORRECTED)		COMPRESSOR PRESSURE RATIO			COMPRESSOR EFFICIENCY			COMPRESSOR SURGE MARGIN (ΔW FOR $N/\sqrt{S} = \text{CONST.}$)		
	AXIAL/ OVERALL (LB/SEC)	CENTRIFUGAL (LB/SEC)	AXIAL P_2/P_1	CENTRIFUGAL P_2/P_1	OVERALL P_2/P_1	AXIAL η_{c1}	CENTRIFUGAL η_{c1}	OVERALL η_{c1}	AXIAL (%)	CENTRIFUGAL (%)	OVERALL (%)
SINGLE SPOOL											
CENTRIFUGAL	3.698	1.89	2.22	5.63	12.57	0.865	0.805	0.793	10.5	5.9	11.8
	2.989	1.68	2.02	4.70	9.50	0.780	0.820	0.780	1.5	11.9	16.6
	2.351	1.47	1.78	3.89	6.93	0.720	0.828	0.768	-4.0	15.9	21.9
	2.080	1.35	1.70	3.48	5.92	0.680	0.828	0.762	-16.9	17.5	22.1
CENTRIFUGAL	3.725				12.61			0.793			
	3.014				9.57			0.780			
	2.391				7.10			0.769			
	2.170				6.30			0.763			
CENTRIFUGAL	3.630	1.94	2.15	5.86	12.60	0.834	0.824	0.809	16.0	2.0	1.9
	2.988	1.67	2.02	4.70	9.51	0.840	0.820	0.801	9.0	12.0	14.7
	2.389	1.48	1.80	3.93	7.08	0.775	0.827	0.788	3.6	15.5	21.4
	2.095	1.35	1.70	3.53	6.00	0.755	0.830	0.778	0.0	17.1	22.1
CENTRIFUGAL	3.644	1.975	2.08	6.02	12.53	0.880	0.810	0.802	18.5	5.2	4.6
	2.963	1.655	2.02	4.69	9.48	0.855	0.825	0.808	12.1	11.9	16.0
	2.327	1.442	1.80	3.83	6.90	0.780	0.830	0.793	5.3	15.4	24.7
	2.135	1.365	1.73	3.55	6.15	0.750	0.820	0.785	4.0	16.0	27.5
CENTRIFUGAL	3.542	1.845	2.175	5.66	12.29	0.885	0.787	0.780	16.1	7.9	6.5
	2.970	1.655	2.02	4.66	9.44	0.850	0.825	0.808	11.9	11.9	16.9
	2.408	1.480	1.81	3.75	7.18	0.795	0.830	0.796	6.6	15.5	23.3
	2.095	1.340	1.73	3.48	6.02	0.750	0.832	0.783	2.0	16.0	28.4
CENTRIFUGAL	3.640	1.820	2.28	5.50	12.53	0.881	0.820	0.812	17.6	7.7	7.6
	2.983	1.552	2.02	4.70	9.48	0.878	0.825	0.819	15.4	11.0	14.5
	2.378	1.442	1.83	3.84	7.02	0.810	0.83	0.809	7.5	16.0	22.2
	2.165	1.370	1.75	3.57	6.25	0.790	0.83	0.799	5.3	17.5	27.0
CENTRIFUGAL	3.563	1.755	2.34	5.28	12.36	0.832	0.823	0.791	14.1	8.1	7.4
	2.996	1.660	2.02	4.71	9.52	0.880	0.825	0.819	15.6	11.4	14.5
	2.352	1.432	1.82	3.80	6.92	0.810	0.830	0.808	8.9	16.3	22.9
	2.129	1.350	1.74	3.51	6.11	0.785	0.830	0.797	7.1	17.1	29.5
CENTRIFUGAL	3.615	2.030	2.0	6.25	12.49	0.840	0.788	0.805	19.1	5.2	4.5
	2.985	1.650	2.02	4.70	9.49	0.835	0.824	0.819	15.4	11.5	13.6
	2.426	1.462	1.84	3.90	7.19	0.830	0.828	0.814	11.0	15.4	22.5
	2.104	1.340	1.725	3.49	6.02	0.800	0.830	0.799	8.1	17.0	31.0
CENTRIFUGAL	3.496	1.810	2.20	5.55	12.21	0.835	0.793	0.777	16.8	7.0	8.5
	2.974	1.645	2.02	4.68	9.45	0.885	0.825	0.818	15.4	11.3	13.6
	2.414	1.455	1.84	3.88	7.15	0.830	0.830	0.813	11.0	15.4	22.5
	2.195	1.375	1.76	3.61	6.35	0.815	0.830	0.804	5.8	17.0	25.1
CENTRIFUGAL	3.507	1.842	2.17	5.65	12.24	0.830	0.790	0.778	16.8	0.5	7.3
	2.980	1.650	2.02	4.69	9.47	0.830	0.823	0.819	15.4	11.5	14.5
	2.424	1.458	1.84	3.80	7.18	0.845	0.830	0.815	12.5	14.2	20.8
	2.212	1.390	1.75	3.65	6.40	0.830	0.830	0.807	11.5	17.3	26.1
TWIN SPOOL											
CENTRIFUGAL	3.662	1.876	2.23	5.67	12.58	0.853	0.814	0.800	15.6	7.2	
	3.031	1.690	2.02	4.79	9.50	0.884	0.827	0.820	15.6	10.5	
	2.426	1.525	1.74	4.06	7.10	0.861	0.828	0.819	15.6	16.0	
	2.245	1.470	1.56	3.86	6.41	0.850	0.828	0.816	12.0	16.4	
CENTRIFUGAL	3.658	1.870	2.23	5.66	12.62	0.854	0.815	0.799			
	3.020	1.684	2.00	4.78	9.56	0.884	0.821	0.819			
	2.420	1.522	1.74	4.07	7.10	0.860	0.828	0.819			
	2.238	1.466	1.66	3.85	6.41	0.849	0.828	0.816			
TWIN SPOOL											
CENTRIFUGAL	3.651	1.867	2.23	5.64		0.856	0.816				
	3.008	1.675	2.01	4.75		0.862	0.821				
	2.412	1.514	1.75	4.04		0.857	0.828				
	2.228	1.458	1.65	3.83		0.844	0.829				
CENTRIFUGAL	3.653	1.864	2.24	5.63		0.855	0.816				
	3.017	1.675	2.01	4.75		0.881	0.821				
	2.417	1.513	1.75	4.04		0.855	0.828				
	2.234	1.457	1.67	3.82		0.843	0.829				

0.945 = η_{c1} , variable geometry / η_{c1} , fixed geometry

The surge margins are equal only if

$$\left(\frac{\sqrt{\theta_3}}{\delta_3} \right)_{O.P.} = \left(\frac{\sqrt{\theta_3}}{\delta_3} \right)_{S.C.}$$

For the model used to extrapolate for axial compressor performance to flow less than axial compressor surge, δ_3 is a constant. Therefore, since $\theta_{3SC} > \theta_{3OP}$; $SM_C < SM_O$.

Configurations 1 through 6 report the results for the various matching schemes studied for a single-spool compressor. Configuration 1 shows the trend toward higher SFC's for a reduced TIT with fixed gasifier cooling. No compressor matching advantage was gained or lost by reduced cycle temperatures. Configurations 3, 4, and 5 include data with and without efficiency degradation for compressor components utilizing variable geometry. The efficiency degradation assumed for these cases was η_C variable geometry = 0.945 η_C , fixed geometry. These are considered to be representative efficiency degradations and are based on test data.

Configuration 7 consists of fixed compressor geometry with a twin-spoiled compressor. Of the four examples shown, the first is considered to be the most representative estimate and includes cycle losses for 9-percent cooling-air bypassing both gasifier turbine stages, and includes a 4-percent degradation of the gasifier second-stage turbine due to the unfavorable work split forced on the gasifier turbine section. The case of no efficiency degradation in the gasifier turbine and the cases of 9-percent cooling air bypass around only the first gasifier turbine are reported to show sensitivity to these parameters.

4.4 SELECTION OF OPTIMUM CYCLE PRESSURE RATIO

Engine cycle analyses were conducted based on three selected design-point pressure ratios to effect selection of an optimum cycle pressure ratio. The design-point pressure ratios were 9.5:1, 10.5:1, and 11.5:1 as selected in Task IA and reported in Section 2.0. The compressor performance characteristics for these three cases included no efficiency degradation for variable geometry and were estimated in Task IIA as reported in Paragraphs 3.3.2.4 (9.5:1), 3.4 (10.5:1), and 3.5 (11.5:1).

Cycle data for the 9.5:1 design-point pressure-ratio case were reported in Paragraph 4.3, Table XV, Configuration 4 (AAVIGV + CFG), and are repeated in Table XVI as revised by additional iterative calculations to display the data more closely to the 100-, 60-, 30-, and 20-percent-power points.

Table XVI reports the calculated cycle data for the final iterations made. The results show design-point SFC values of 0.480 (9.5:1), 0.479 (10.5:1), and 0.482 (11.5:1). While these SFC levels are slightly optimistic because no efficiency degradation was included for variable compressor geometry, the trends are considered valid for selection of the optimum design-point pressure ratio.

To facilitate this selection, a cross-plot was made and is reported in Figure 31. The results are plotted with solid symbols and are displayed, along with the cycle results of Task IA, for comparative purposes. Based on the data from this task, a selection was made for a design-point pressure ratio of 10.5:1, which is in agreement with the tentative selection made in Task IA and reported in Paragraph 2.4.

4.5 ESTIMATED ENGINE OPERATING LINE

Based on the selection of the 10.5:1 design-point pressure ratio and on the selected compressor matching scheme (AAVIGV + CFG), an engine operating line was estimated. The engine operating line consists of a plot of cycle pressure ratio versus engine airflow and is based on the data reported in Paragraph 4.4, Table XVI, 10.5:1 design-point pressure ratio.

The engine operating line is shown in Figure 32 (solid symbols), along with the tentative 10.5:1 operating line estimated on Task IA, Paragraph 2.5. The Task IA data were based on the idealized compressor map assumed for that task. Comparison of these results showed that the achieved compressor match from Task IIA compares very favorably with the potential performance levels estimated in Task IA.

The engine operating line established in this task represents the compressor design requirements for the final compressor design as conducted in Task IIB, Section 5.0.

A

TABLE XVI. ENGINE CYCLE DATA (C
CYCLE PRESSURE-RATIO

CONFIGURATION*	SPECIAL REMARKS	POWER		SFC	TIT (°F)	COMPRESSOR SPEED (% DESIGN)		COMPRESSOR FLOW (CORRECTED)	
		(%)	(HP)			AXIAL/ OVERALL (%)	CENTRIF- UGAL (%)	AXIAL/ OVERALL (LB/SEC)	CENTRIF- UGAL (LB/SEC)
Single-Spool Compressor	Design Point		797.4	0.443	2500	108.0	105.8	3.640	1.820
	P ₄ /P ₁	60.2	479.7	0.480	2093	100.0	99.6	2.994	1.660
		30.0	239.2	0.611	1750	91.1	91.9	2.378	1.442
	9.5:1	20.0	159.5	0.749	1626	86.8	87.5	2.111	1.335
AAVIGV + CFG	Design Point		777.5	0.443	2500	108.3	105.8	3.635	1.795
	P ₄ /P ₁	60.0	466.0	0.479	2087	99.9	100.0	2.994	1.642
		30.0	233.0	0.612	1751	91.3	92.1	2.380	1.440
	10.5:1	20.0	155.5	0.747	1623	87.0	88.1	2.119	1.332
	Design Point		752.6	0.446	2500	108.2	106.1	3.626	1.747
	P ₄ /P ₁	60.0	451.0	0.482	2089	99.8	99.6	2.984	1.610
		30.0	226.0	0.610	1769	91.6	92.2	2.364	1.400
	11.5:1	20.0	150.5	0.756	1636	87.8	88.9	2.108	1.320

*No efficiency degradation assumed due to variable inlet guide vanes

13

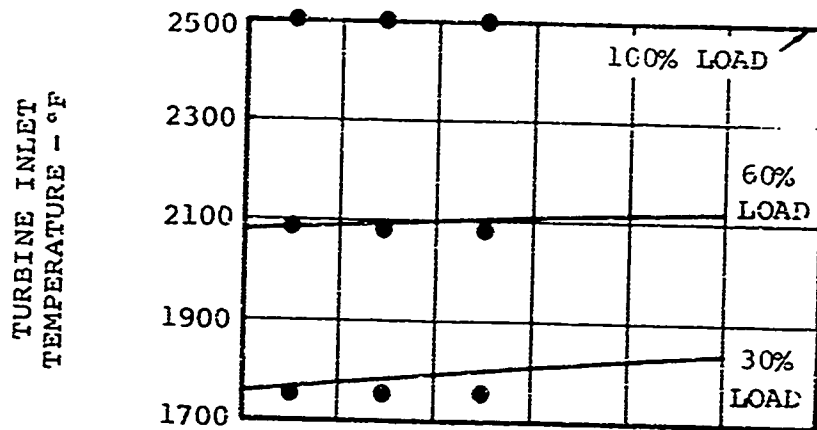
TABLE XVI. ENGINE CYCLE DATA (CALCULATED)
CYCLE PRESSURE-RATIO STUDY

COMPRESSOR SPEED (% DESIGN)		COMPRESSOR FLOW (CORRECTED)		COMPRESSOR PRESSURE RATIO			COMPRESSOR EFFICIENCY			COMPRESSOR SURGE (ΔW FOR N/V)	
AXIAL/ OVERALL (%)	CENTRIF- UGAL (%)	AXIAL/ OVERALL (LB/SEC)	CENTRIF- UGAL (LB/SEC)	AXIAL P_3/P_1	CENTRIF- UGAL P_4/P_2	OVERALL P_4/P_1	AXIAL η_{31}	CENTRIF- UGAL η_{43}	OVERALL η_{41}	AXIAL (%)	CENTRIF- UGAL (%)
108.0	105.8	3.640	1.820	2.28	5.50	12.53	0.881	0.820	0.812	17.6	7.1
100.0	99.6	2.994	1.660	2.02	4.70	9.53	0.878	0.826	0.819	15.4	11.1
91.1	91.9	2.378	1.442	1.83	3.84	7.02	0.810	0.830	0.809	7.5	16.1
86.8	87.5	2.111	1.335	1.75	3.46	6.05	0.770	0.830	0.796	5.3	17.1
108.3	105.8	3.635	1.795	2.32	5.96	13.81	0.882	0.794	0.795	17.5	5.1
99.9	100.0	2.994	1.642	2.05	5.12	10.50	0.870	0.810	0.807	14.1	8.1
91.3	92.1	2.380	1.440	1.84	4.21	7.76	0.810	0.822	0.800	7.1	15.1
87.0	88.1	2.119	1.332	1.76	3.80	6.70	0.780	0.830	0.791	4.2	16.1
108.2	106.1	3.626	1.747	2.38	6.34	15.08	0.878	0.780	0.782	15.6	3.1
99.8	99.6	2.984	1.610	2.09	5.49	11.47	0.860	0.805	0.797	11.5	8.1
91.6	92.2	2.364	1.400	1.89	4.49	8.47	0.790	0.820	0.787	4.9	13.1
87.8	88.9	2.108	1.320	1.78	4.11	7.32	0.760	0.820	0.782	3.5	15.1

the vanes

TA (CALCULATED)
RATIO STUDY

	COMPRESSOR PRESSURE RATIO			COMPRESSOR EFFICIENCY			COMPRESSOR SURGE MARGIN (ΔW FOR $N/\sqrt{g} = \text{CONST.}$)		
	AXIAL P_3/P_1	CENTRIF- UGAL P_4/P_3	OVER LL P_4/P_1	AXIAL η_{31}	CENTRIF- UGAL η_{43}	OVERALL η_{41}	AXIAL (%)	CENTRIF- UGAL (%)	OVERALL (%)
0	2.28	5.50	12.53	0.881	0.820	0.812	17.6	7.7	7.6
0	2.02	4.70	9.53	0.878	0.826	0.819	15.4	11.0	14.5
2	1.83	3.84	7.02	0.810	0.830	0.809	7.5	16.0	22.2
5	1.75	3.45	6.05	0.770	0.830	0.796	5.3	17.5	27.0
5	2.32	5.96	13.81	0.882	0.794	0.795	17.5	5.9	4.0
2	2.05	5.12	10.50	0.870	0.810	0.807	14.1	8.5	12.5
0	1.84	4.21	7.76	0.810	0.822	0.800	7.1	15.2	19.3
2	1.76	3.80	6.70	0.760	0.830	0.791	4.2	16.5	24.0
7	2.38	6.34	15.08	0.878	0.780	0.782	15.6	3.9	4.9
0	2.09	5.49	11.47	0.860	0.805	0.797	11.5	8.0	12.9
0	1.89	4.49	8.47	0.790	0.820	0.787	4.9	13.5	18.6
0	1.78	4.11	7.32	0.760	0.820	0.782	3.5	15.0	19.0



— Task IA Data Based on Idealized Map
 • Task IB Data Based on Tentative Compressor Maps (AAVIGV + CFG), Task IIA

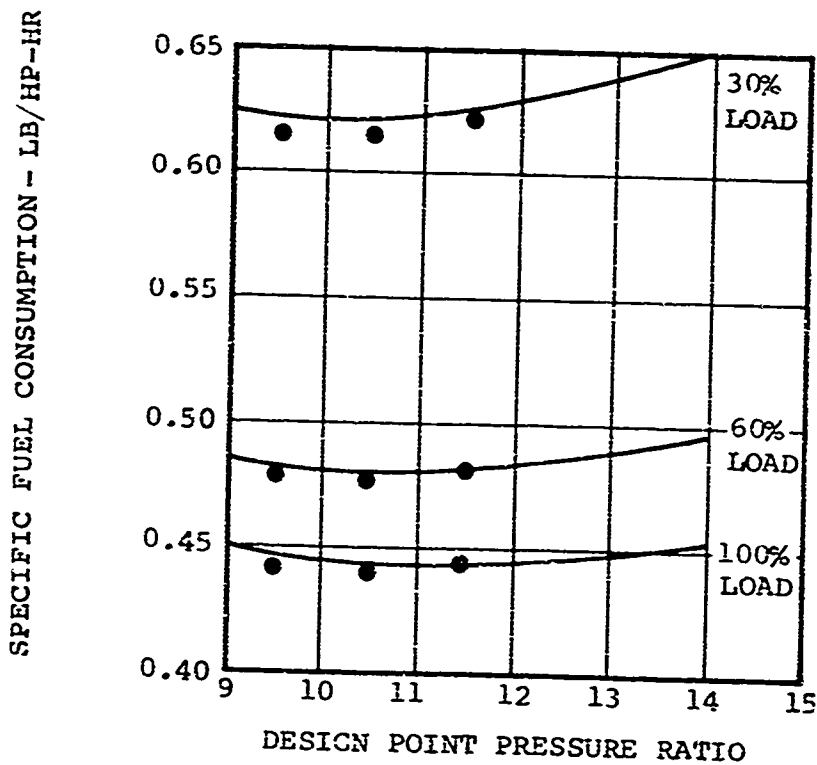


Figure 31. Engine Off-Design Performance: Specific Fuel Consumption and Turbine Inlet Temperature Versus Design Pressure Ratio.

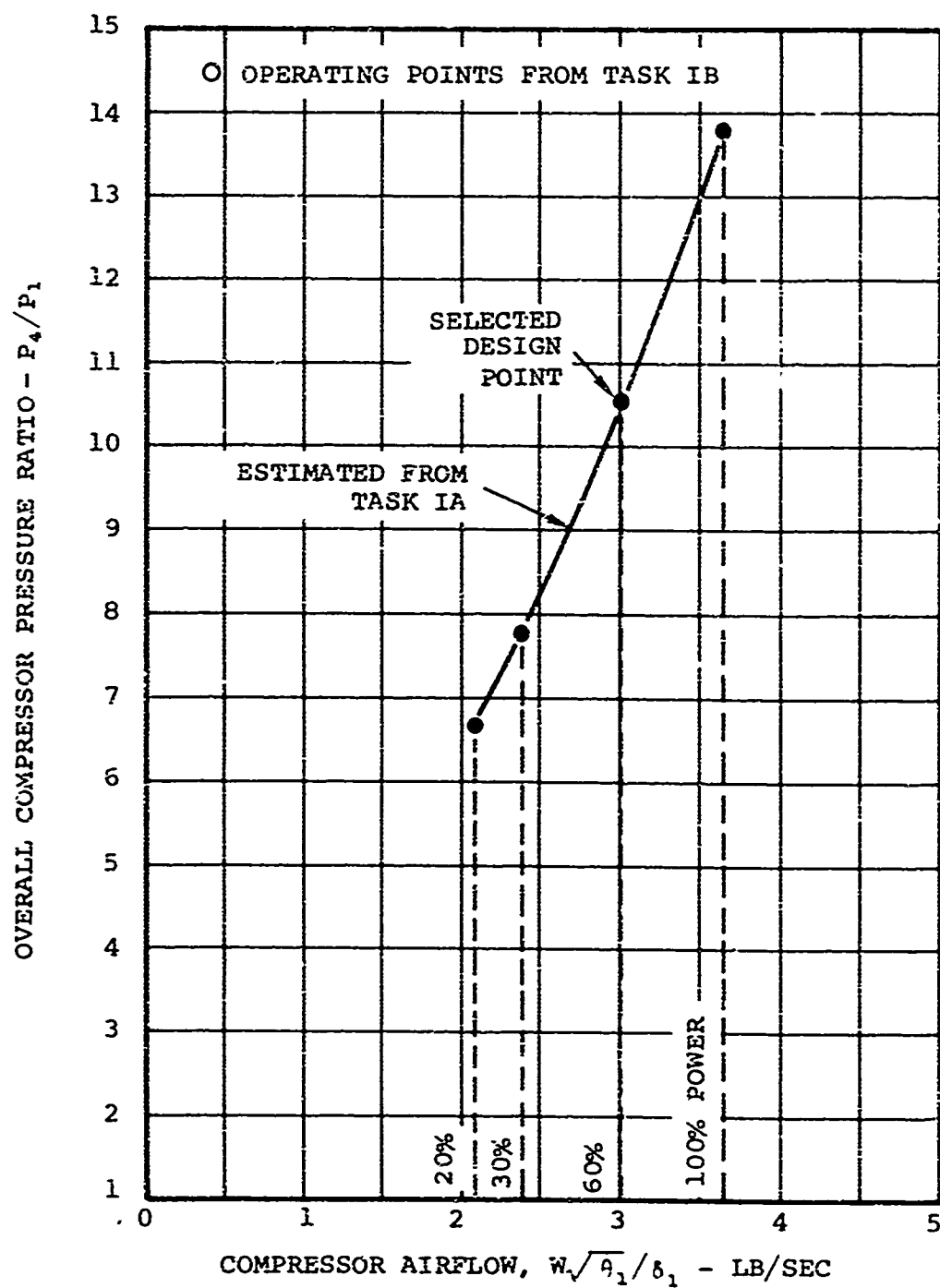


Figure 32. Engine Operating Line
(Tentative Compressor Requirements).

5. TASK IIB, COMPRESSOR DESIGN AND MATCHING

5.1 GENERAL

Preliminary designs were performed for two compressor configurations. First, the design of a compressor with two axial stages and one centrifugal stage was started in accordance with the results of TASK IIA. Results were submitted to engine conceptual design studies before the aerodynamic calculations were completed. Preliminary analysis revealed that a low critical speed for the power turbine shaft could be expected because of a long unsupported-shaft-length/shaft-diameter ratio. From five possible alternative design approaches, the decision was made to shorten the compressor length by reconfiguring for AVIGV + CFG. This task was consequently concluded with the design of a one-axial-stage and one-centrifugal-stage compressor configuration. The aerodynamic and mechanical design procedures and results are discussed below for these compressor design activities.

5.2 AERODYNAMIC DESIGN AND MATCHING. AAVIGV + CFG ($P_4/P_1 = 10.5:1$)

The aerodynamic design of the axial compressor was preceded by a study to verify that a 15° change of preswirl angle could, in fact, accomplish the changes in the compressor pressure ratio characteristic at 100-percent power that were estimated for the variable-geometry study of Task IIA. This effort was necessary since the aerodynamic design of the axial compressor depends on the magnitude of the preswirl angle change induced onto the first-stage rotor between the 60- and 100-percent-power points. Furthermore, it was observed at the conclusion of Task IIA that more IGV actuation might enable the 60- and 100-percent-power match points to be located more closely to the maximum achievable axial compressor efficiencies at their respective speeds.

Following the matching study, the aerodynamic design of the flow path and blading for the axial compressor was conducted. Fluid mechanic information is computed from a radial-equilibrium type of calculation between blade rows. The equation of motion includes the effects of curvature and entropy gradient. The loss variation at all blade row exits, except for the IGV, is computed from a loss model suggested

by Lieblein, Reference 3, and empirically extended by Swan, Reference 4. The blade camber selection and off-design turning angle characteristics are determined from NACA low-speed cascade data.

The centrifugal compressor design and performance were computed from the same analytical techniques that were described in Section 2. The empirical correlations that were used to design the compressor were applied to the compressor geometry to obtain the performance at off-design conditions. The empiricism contains correlations used to estimate rotor surge, choke, slip factor and efficiency, the friction coefficient for the vaneless diffuser, and the cascade data for the vaned diffuser.

5.2.1 Two-Stage Axial Compressor Matching

The performance characteristics of two AiResearch axial compressors were used to represent the estimated performance for the individual stages of the two-stage axial compressor. The characteristics of the individual stages were matched to each other with several shifts of the pressure-ratio characteristics of the first stage in the vicinity of the 100-percent-power match point. A number of combinations of these shifts on the first-stage were examined to arrive at a match of the two-stage compressor which would yield maximum two-stage efficiency at 60-percent power. In this matching procedure it was also necessary to make size changes on the second stage to arrive at the best possible two-stage matching.

The optimum result would, of course, be to match the highest attainable efficiencies of both stages simultaneously at the 60- and 100-percent-power points. However, to accomplish this requires a change of pressure-ratio characteristic inconsistent with the first-stage rotor pitch-line parameters which determine the flow and pressure ratio changes as a function of preswirl angle. These parameters are: the tangential rotor speed, inlet air angle, and air turning angle. Consequently, the matching study was terminated when it appeared that little or no overall two-stage efficiency could be gained with further preswirl angle change.

A point was reached at which the maximum attainable efficiencies of both stages were matched at the 100-percent-power point and nearly so at 60-percent power. The results are displayed in Table XVII.

TABLE XVII. SUMMARY OF DESIGN MATCHING RESULTS (AAVIGV)				
	60-Percent Power		100-Percent Power	
	Final Match Results	Maximum Attainable Efficiency	Final Match Results	Maximum Attainable Efficiency
First-stage efficiency	0.693	0.896	0.881	0.882
Second-stage efficiency	0.906	0.921	0.908	0.911
Overall efficiency	0.895	0.907	0.891	0.892

The match-point efficiency of the second stage is 1.5 points below the maximum that could be attained at the match-point pressure ratio. Further efforts to arrive at a better overall match did not seem to be rewarding. The study was concluded at this point.

5.2.2 Preswirl Angle Estimation

An analytical method was developed to compute the preswirl angle associated with the shift of the pressure-ratio characteristic that achieves the matching results discussed above. Reference 5 contains published test data of the effect of preswirl angle on the performance characteristics of a single-stage axial compressor. No other published reference contained as much or as systematic a set of information that could be used to estimate the change in performance characteristics with change in preswirl. Even so, there was doubt whether this information could be directly applied if the aerodynamic parameters such as rotor blade speed and rotor relative inlet air angle were different from those of Reference 5. Consequently, a theoretical approach was taken to find out the controlling parameters and to estimate performance characteristic changes with preswirl angle changes.

The problem consists of computing the change in stage pressure ratio and flow rate with a change of inlet preswirl angle. This is done by computing the meridional velocity change at a given rotor pitch-line speed. In order to obtain performance changes that come about purely as a result of the preswirl angle change, the relative inlet air angle is held constant. In an actual compressor, it is very common to have a radial shift of the streamlines from inlet to outlet of stage. To simplify the analysis, a constant streamline radial position is assumed. Meridional velocity changes also take place across an actual rotor, but the meridional velocity is assumed here to be invariant across the rotor.

The derivation of the equations is displayed in Appendix IV. In the appendix, it is shown that the stage pressure ratio can be written as

$$\frac{P_2}{P_1} = \left[1 + \frac{\frac{\eta_C U^2}{TN\beta_1 + TN\beta_s} (TN\beta_1 - TN\beta_2)}{gJC_P T_1} \right]^{\frac{\gamma}{\gamma-1}} \quad (7)$$

The pressure-ratio change from a condition of zero preswirl is obtained from

$$\frac{P_2/P_1 \big|_{IGV \neq 0}}{P_2/P_1 \big|_{IGV = 0}}$$

From the continuity equation, flow is computed from

$$W_C = \left[1 - \frac{U^2 \sec^2 \beta_s}{(TN\beta_1 + TN\beta_s)^2 2gJC_P T_1} \right]^{\frac{1}{\gamma-1}} \frac{\rho_{t_1} A_1 \lambda_1 U}{TN\beta_1 + TN\beta_s} \quad (8)$$

The flow-rate change from a condition of zero preswirl is obtained from

$$\frac{W_C \big|_{\beta_s \neq 0}}{W_C \big|_{\beta_s = 0}}$$

A plot of the pressure-ratio parameter against the flow-ratio parameter is displayed in Figure 33 for $\beta_1 = 60^\circ$, $U = 1000$ fps, and $\beta_1 - \beta_2 = 10^\circ$, 20° , and 30° . Note that maximum flow change occurs at a certain value of negative preswirl angle.

These equations were used to compute the pressure-ratio and flow-ratio parameters for the pitch-line conditions of the first-stage rotor.

In the variable-geometry study of Task IIA, the axial compressor was considered to have zero swirl at the 20-, 30-, and 60-percent-power match points and a value of -15° preswirl at 100-percent power. Actuating the guide vanes opposite rotation at full power gives a significant increase in the first rotor tip relative inlet Mach number. If the compressor is designed for 15° preswirl at the three lower power points and zero preswirl at full power, the tip relative Mach number can be minimized at full power and lowered at the other power points. This increases the stator hub inlet Mach number, but it can be accepted as long as it is below the blade section drag-rise Mach number. It was therefore decided to design the compressor with 15° preswirl at 60-percent power and zero preswirl at 100-percent power.

5.2.3 Two-Stage Axial Compressor Design ($P_3/P_1 = 2.05:1$)

To minimize the flow-path distortion of the transition section between the axial and the centrifugal stage, the axial compressor design was characterized by a specification of zero rotor hub exit relative swirl. This results in a minimum hub diameter for the axial compressor. The rotor tip speed was selected to be 1200 fps at design point. At the rotor tip speed for 20-percent power ($U = 1045$ fps), the match-point flow is 23-percent lower than the flow at maximum attainable efficiency for this speed. The data band of Figure 3 shows that at this rotor speed, the largest surge-free range from maximum efficiency obtained from test is 26.5 percent. As pointed out in Task IA, the state-of-the-art advancement is expected to come from means that achieve, through design intent, the surge-free range required of the axial compressor. This is expected as long as the design does not exceed the data band of Figure 3.

Each stage was designed for a pressure ratio of 1.432 ($\sqrt{2.05}$). A work split study was not performed for the two-stage axial compressor. It was assumed that the work split would probably be nearly equal. Identical pressure ratios in each stage do not give equal work, but it was assumed to be a close approximation. Rotor and stage efficiencies were assumed to compute the rotor pressure ratio, which was specified at each of the

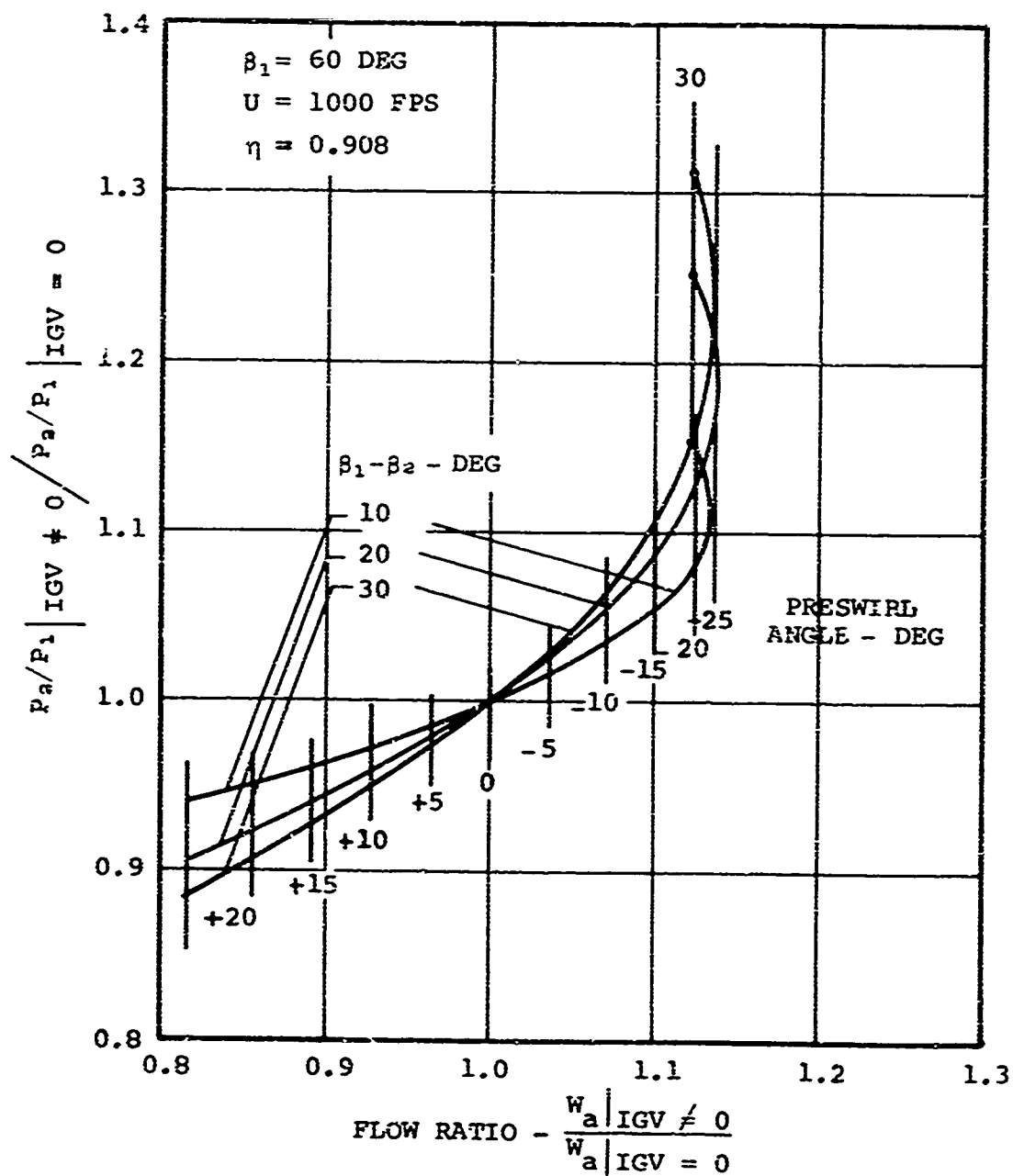


Figure 33. Pressure-Ratio/Flow-Ratio Characteristics for Various Amounts of Preswirl.

rotor exit stations. If the required overall stage pressure ratio were not obtained, these input rotor pressure ratios were iteratively adjusted. Exit air angle was specified at each of the stator exit stations. With these specifications, the computer program selected the blade sections needed to accomplish the design. These sections were selected from empirical correlations of the NACA low-speed cascade data.

After completion of the design calculations, the compressor geometry was resubmitted to the computer program to obtain the vector diagram data under the flow, speed, and preswirl conditions of the 30- and 100-percent-power match points.

Many flow-path configurations were examined in an effort to arrive at a design that would accommodate the 30-percent-power conditions without stalling one of the blade rows. The most significant contribution to this end came from using tandem blade rows in the stators and from accelerating the design meridional velocity as much as possible and still accommodating the flow at 100-percent power. The reason that a satisfactory design is difficult to achieve is the high hub loss. This stems from the fact that the off-design conditions at 30-percent power affect the hub more than the rest of the blade span.

The off-design problem at 30-percent power can be explained as follows. The rotor has its highest inlet Mach number where the air turning is lowest--at the tip. The stator has its highest inlet Mach number where the air turning is highest--at the hub. The rotor hub has generally a higher value of diffusion factor than the rotor tip but a lower inlet velocity head. The stator hub has generally a higher value of diffusion factor than the tip and a higher inlet velocity head. Furthermore, the hub solidity is generally about twice the value at the stator tip. These factors double the hub loss coefficient compared to the tip. At 30-percent-power off-design, the change in inlet air angle contributes a proportionately higher loss to the stator hub than the stator tip because of the basically larger value of design D-factor. With a higher loss at off-design at the hub than at the tip, the entropy gradient term in the equation of motion reduces the hub meridional velocity, which further contributes to increasing the diffusion factor.

The flow and speed conditions at 30-percent power are responsible for the air-angle change from 60-percent-power design conditions. A stator hub inlet vector diagram comparison is shown in Figure 34 for the 30- and 60-percent-power-point conditions. The meridional velocity is 6 percent below a value proportional to the ratio of the flows of the two power

—— 60-PERCENT POWER
- - - 30-PERCENT POWER

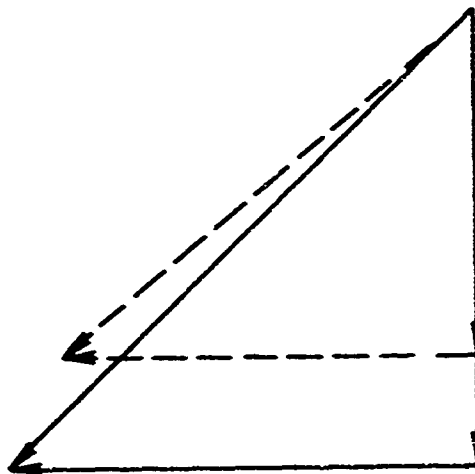


Figure 34. First-Stage Stator Hub Inlet
Vector Diagram Comparison.

points. The inlet-air-angle difference from the design value is therefore a consequence of the flow and speed values at 30-percent power. The difficulty in arriving at a convergent calculation is a result of the off-design power selected. This is an aerodynamic feature worthy of consideration when part-power percentage is specified.

Several approaches can be taken to alleviate the strength of the loss. Loss contributions from large angle-of-attack changes from design values can be diminished with a variable first-stage stator. Another means would be to retwist the blade rows such that the hub sections are biased away from the minimum loss angle of attack in order to accommodate the 30-percent-power conditions. Still another means would be to relax the specification of zero rotor hub exit relative swirl to reduce the stator hub inlet Mach number. Finally, changes could be made in hub solidity to reduce the loss coefficient.

To investigate all these possibilities would have taken much longer than estimated for the contract schedule. Furthermore, at this point in the aerodynamic design, mechanical design calculations revealed that the natural frequency of the engine shaft would be too close to the power turbine operating speed. In view of these considerations, a single-stage axial compressor configuration was designed.

Table XVIII shows a summary of the design results for the last iterations conducted for the two-stage axial compressor. The design is shown in the multistage compressor flow path presented in Figure 35.

5.2.4 Centrifugal Compressor Design ($P_4/P_3 = 5.1:1$)

The design parameter study carried out in Task IIA was considered to be applicable for the design of the centrifugal compressor. A rotor blade exit angle of 50° and an absolute air angle (relative to the radial direction) of 69° were specified. The compressor configuration is shown in Figure 35. The vaned diffuser has a tandem blade row. It is followed by a vaneless bend and an annular flare diffuser. Final diffusion to compressor exit conditions occurs at the exit of the flare.

The radial extent of the vaneless diffuser for this compressor is larger than that designed for Task IIA. A higher stage efficiency (of 0.5 point) could have been obtained at design point with a smaller vaneless diffuser. With a larger one, the inlet Mach number to the vaned diffuser at 100-percent power is below the drag-rise Mach number of the first row of vanes. Consequently, the stage efficiency is two points

TABLE XVIII. AERODYNAMIC DATA SUMMARY
FOR TWO-STAGE AXIAL COMPRESSOR

		30% POWER		60% POWER		100% POWER	
		Hub	Tip	Hub	Tip	Hub	Tip
First-Stage Rotor							
Rel. inlet Mach No.		0.505	0.984	0.598	1.087	0.767	1.315
Diffusion factor		0.382	0.464	0.284	0.385	0.427	0.419
Camber				64.8	23.2		
Rel. inlet air angle		49.7	73.2	43.4	70.0	45.8	62.5
First-Stage Rotor							
1st Row	Abs. inlet Mach No.	0.673	0.548	0.839	0.605	0.896	0.639
	Diffusion factor	0.608	0.225	0.309	0.172	0.267	0.061
	Camber			17.4	13.2		
	Abs. inlet air angle	51.9	44.9	46.9	39.8	46.6	34.3
2nd Row	Abs. inlet Mach No.	0.333	0.490	0.622	0.554	0.697	0.629
	Diffusion factor	0.635	0.172	0.364	0.206	0.371	0.213
	Camber			44.1	49.4		
	Abs. inlet air angle	37.2	30.9	35.0	30.0	34.8	29.3
Second-Stage Rotor							
Rel. inlet Mach No.		0.519	1.002	0.706	1.106	0.763	1.202
Diffusion factor		0.694	0.392	0.336	0.424	0.294	0.425
Camber				61.5	20.7		
Rel. inlet air angle		73.1	56.0	51.0	58.0	50.3	56.7
Second-Stage Stator							
1st Row	Abs. inlet Mach No.	0.470	0.628	0.780	0.694	0.877	0.756
	Diffusion factor	0.773	0.075	0.253	0.108	0.219	0.064
	Camber			25.0	8.6		
	Abs. inlet air angle	58.7	27.1	39.6	28.3	37.1	27.2
2nd Row	Abs. inlet Mach No.	0.189	0.611	0.644	0.658	0.743	0.744
	Diffusion factor	0.746	0.194	0.175	0.228	0.185	0.249
	Camber			23.4	27.6		
	Abs. inlet air angle	23.9	20.0	20.0	20.0	19.7	19.9

*Relative
**Absolute

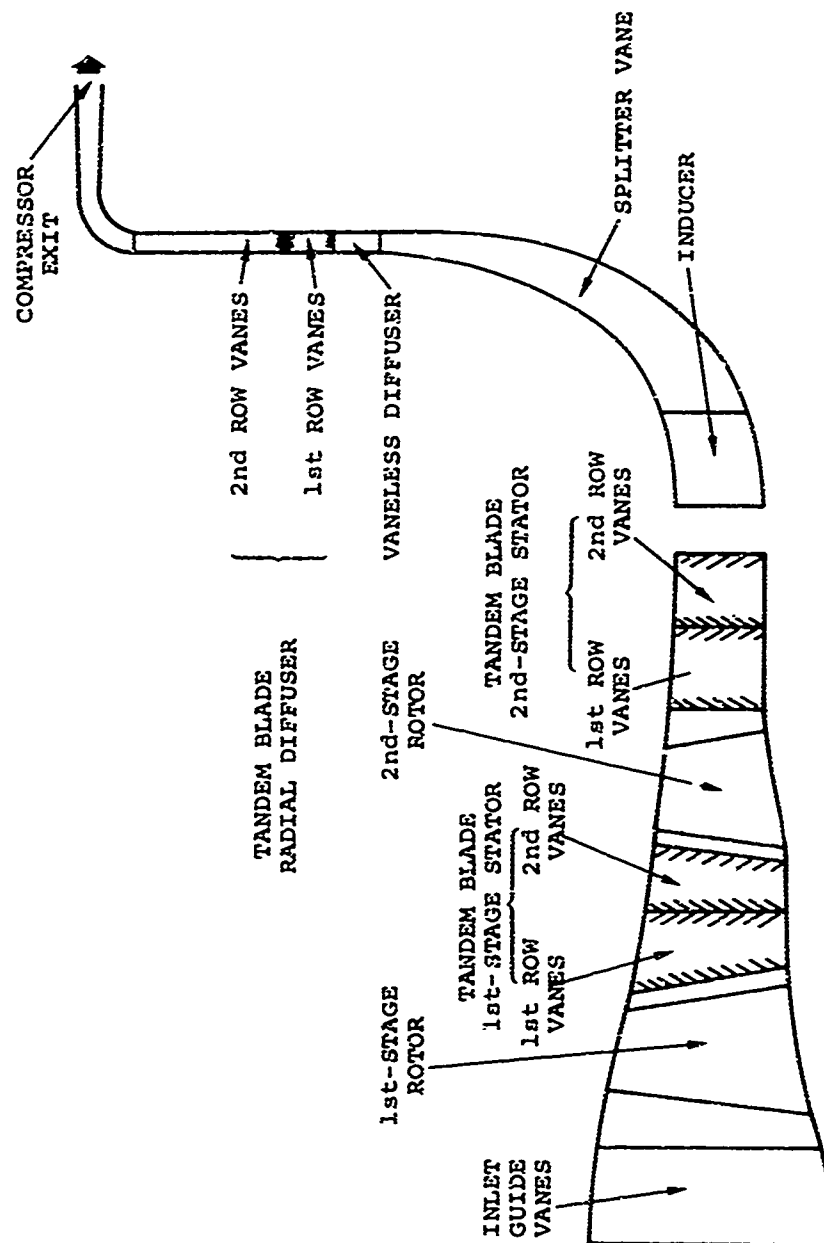


Figure 35. Compressor Flow Path, Two-Stage Axial Plus Centrifugal Compressor, AAVIGV + CFG.

higher than when no trade-off is taken at design point. This gives a lower SFC at 60-percent power because the efficiencies at these two powers are closer to each other.

A summary of the design results is displayed in Table XIX.

TABLE XIX. AERODYNAMIC DATA SUMMARY FOR A CENTRIFUGAL COMPRESSOR DESIGNED TO MATCH WITH A TWO-STAGE AXIAL COMPRESSOR			
	30% Power	60% Power	100% Power
Inducer tip rel. Mach No.	0.965	1.028	1.109
Impeller tip speed	1630.0	1770.0	1872.0
Impeller exit abs. Mach No.	0.988	1.029	1.076
Vaned diffuser inlet Mach No.	0.865	0.901	0.937
Vaned diffuser exit Mach No.	0.215	0.212	0.206
Compressor exit Mach No.	0.153	0.150	0.146

5.2.5 Compressor Matching

No axial-centrifugal compressor matching runs were made for the AAVIGV + CFG compressor since the aerodynamic design for the two-stage axial compressor was not completed. Successful conclusion of the aerodynamic design for the two-stage axial compressor could be expected to lead to axial, centrifugal, and overall compressor performance comparable to that predicted in Task IIA, displayed in Figure 29, and reported in Table XVI for the case of $P_4/P_1 = 10.5:1$. Some differences in characteristics might be expected if a variable first-stage stator row were required. However, the design-point efficiency level and SFC values would be essentially the same.

5.2.6 Engine Conceptual Design Considerations

The iterative design and matching computations for the AAVIGV + CFG compressor were based on tentatively chosen compressor flow-path configurations. The configuration for the last design calculations made for the AAVIGV + CFG compressor is shown in Figure 35.

This configuration was submitted to engine conceptual design studies, which included a preliminary critical-speed analysis for the engine shafting. This preliminary analysis showed that a low critical speed for the power turbine could be expected because of the long-unsupported-shaft-length/shaft-diameter ratio. Calculation for a simply supported power turbine quill-shaft (17.5 inches long) resulted in a power turbine shaft critical speed of approximately 35,000 rpm. Based on this, several design alternatives were apparent, including the following:

- (1) Size the power turbine for 25,000 to 30,000 rpm and accept a significant weight and size penalty.
- (2) Reconfigure the compressor for larger hub radii to accommodate larger diameter shafting.
- (3) Shorten the unsupported length of the power turbine shaft by employing an intershaft bearing.
- (4) Shorten the compressor and, hence, the unsupported length of the power turbine shaft.
- (5) Reconfigure the shafting arrangement for end-moment constraint.

It was beyond the scope of this program to explore the merits of these approaches or combinations of these approaches. While the comparison based on performance considerations as reported in Paragraph 2.2.2 shows an advantage for the AA+C combination over the A+C combination, this advantage is contingent on two basic assumptions:

- (1) The aerodynamic design of the two-stage axial compressor can be completed to achieve stall-free operation near the potential performance levels. The potential performance levels are estimated to be the same as those predicted by the preliminary design and matching studies of Task IIA and displayed in Figure 29. Engine cycle data for this case is reported in Table XVI for $P_4/P_1 = 10.5:1$.

- (2) The front drive shafting can be designed to achieve a mechanically feasible arrangement with acceptable revisions to the two-stage axial compressor.

Since neither of these assumptions could be made with confidence, a choice was made to complete the design and matching of an A+C compressor reconfigured for a shafting arrangement incorporating end-moment constraint.

5.3 Cycle Considerations for A + C Compressor

Based on the choice of an A + C compressor, a review was conducted to establish cycle requirements for this compressor.

5.3.1 Aerodynamic Design Requirements, A + C Compressor

A choice was made to design the A + C compressor for an overall pressure ratio of 10.5:1 at 60-percent power. The tentative compressor design requirements were assumed to be the same as those determined in Task IIA for an AA + C compressor, as displayed in Figure 32. This choice was made to expedite the design of the A + C compressor and to allow direct comparison with the potential performance estimated for an AA + C compressor as determined in Tasks IIA and IB and displayed in Figure 29 and Table XVI.

This choice of design requirements for the A + C compressor was considered to be a close approximation to optimum values for A + C compressors based on observations made for the AA + C compressor. The design-point pressure ratio for the AA + C compressor was selected to be 10.5:1 in Task IB, Section 4, based on cycle analyses for an AAVIGV + CFG compressor. This selection was in agreement with the tentative selection made in Task IA and reported in Paragraph 2.5, based on cycle analyses utilizing an AA + C idealized compressor map (Figure 53) and the AA + C compressor efficiency estimates displayed in Figure 7 (Curve B). Since the nondimensionalized efficiency characteristics of an A + C compressor can be expected to be similar to those estimated for an AA + C compressor (Figure 53) the major effect to be noted is the comparison of the efficiency versus design-point pressure ratios for an A + C (Figure 6) and an AA + C compressor (Figure 7). Examination of the B portion of these curves shows that the slopes for the respective speed lines are only slightly different. Since the efficiency for an A + C compressor decreases (with increasing P_4/P_1) at a slightly greater rate, it can be expected that the optimum design-point pressure ratio for an A + C compressor is slightly lower than that selected for an AA + C compressor (10.5:1).

It was decided to parallel the design and matching of the selected A + C compressor with engine cycle analyses to determine the validity of the selection for the 10.5:1 design-point pressure ratio. The results of these analyses are reported in Paragraph 5.3.1.1.

5.3.1.1 Validation Analysis for A + C Compressor, $P_4/P_1 = 10.5:1$

Engine cycle analyses were conducted for design-point pressure ratios of 9:1, 10:1, 11:1, 12:1, 13:1, and 14:1. Cycle assumptions were identical with those reported for Task IA in Paragraph 2.4 (reference Appendix II) with the following exceptions:

- (1) A + C compressor design point efficiencies were assumed to be as displayed in the B portion of Figure 6, $N/\sqrt{\theta} = 60,000$ rpm.
- (2) A + C compressor characteristics were assumed to be as displayed in the idealized compressor map of Figure 36.

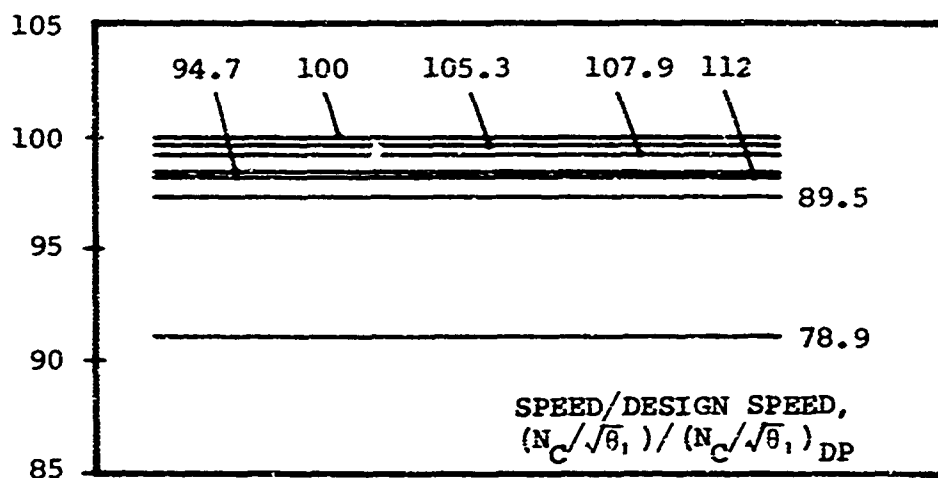
The results of these analyses are plotted in Figure 37 and are compared to the results previously shown in Figure 14. The results of this study show that for the case of an A + C compressor, the optimum design-point pressure ratio for minimum SFC at 60-percent power is 10.0:1. While this is slightly less than the 10.5:1 ratio selected for the design of an A + C compressor, the SFC characteristic is relatively flat in this range. Therefore, the engine performance levels for the AVIGV + CFG compressor represent a satisfactory evaluation of the potential for this compressor arrangement.

5.3.2 Matching Scheme, A + C Compressor

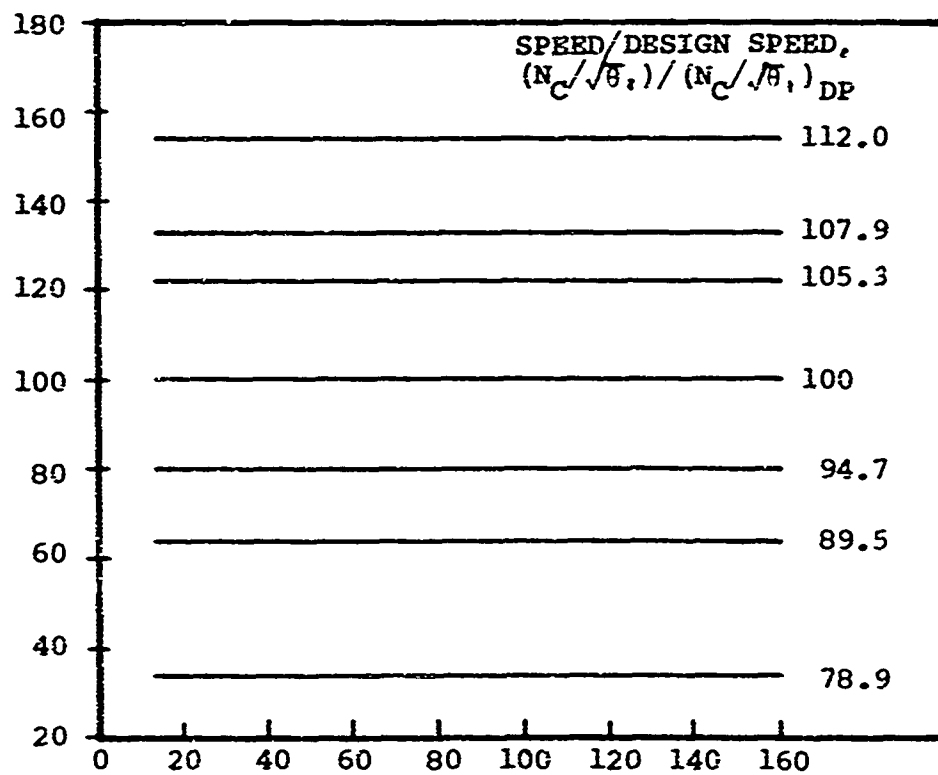
A selection was made of the best matching scheme for an A + C compressor based on the matching studies of Task IIA. The scheme selected was the same as that selected for the AA + C compressor and consists of variable inlet guide vanes ahead of the axial compressor and fixed geometry for the centrifugal compressor (AVIGV + CFG).

This selection is considered to be a valid extension of the results reported in Section 3 for the study of an AA + C compressor. The reason for this is that the speed-flow/pressure-ratio relationships as a function of power output do not change for the axial compressor component when a single-stage rather than a two-stage compressor is employed as the axial component. In either case, the use of variable inlet guide vanes provides the best solution to the matching problem.

EFFICIENCY/DESIGN EFFICIENCY
 $\eta_C / \eta_{C,DP}$ - PERCENT

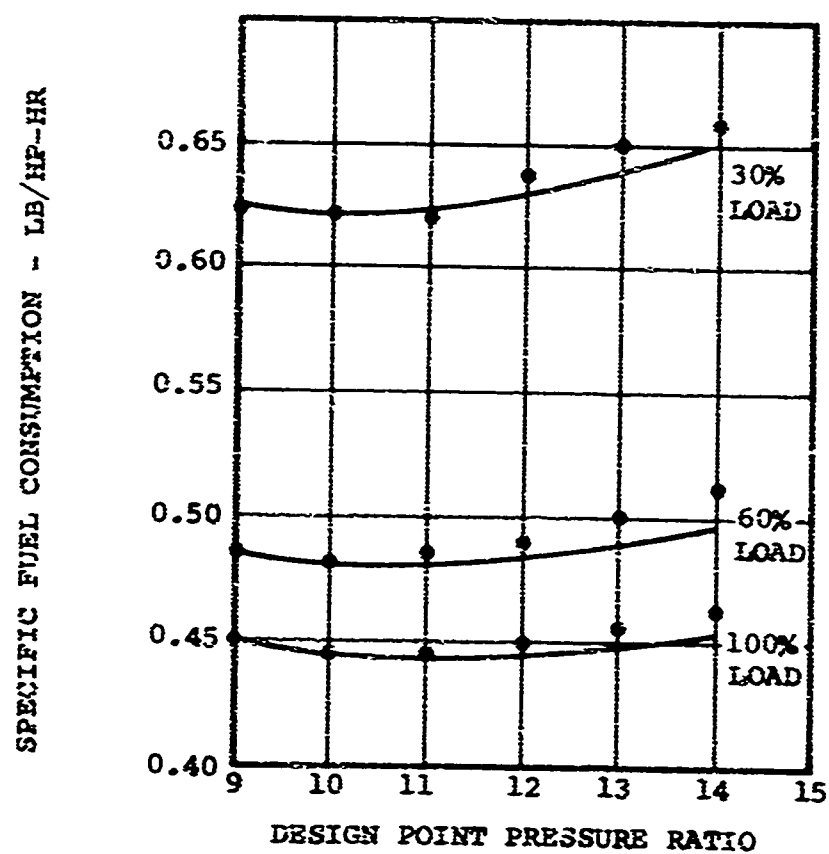
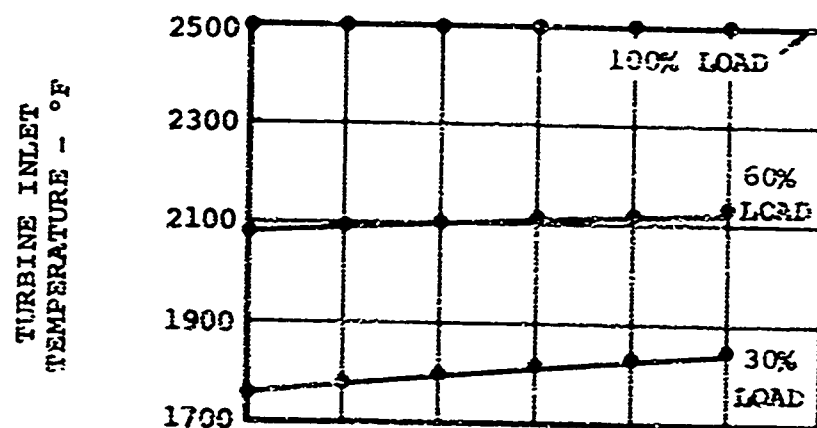


PRESSURE RISE/DESIGN PRESSURE RISE,
 $(P_4/P_1 - 1) / (P_4/P_1 - 1)_{DP}$ - PERCENT



AIRFLOW/DESIGN AIRFLOW, $(W_1 \sqrt{\theta_1} / \delta_1) / (W_1 \sqrt{\theta_1} / \delta_1)_{DP}$ - PERCENT

Figure 36. Idealized Compressor Map,
 Nondimensionalized From A + C Data.



— AA + C IDEALIZED COMPRESSOR (FIG 14)
 • A + C IDEALIZED COMPRESSOR

Figure 37. Engine Off-Design Performance: Comparison With A + C and AA + C Compressors.

This is true notwithstanding the fact that for the AAVIGV + CFG compressor, a variable stator vane row may be required in order to achieve the required surge-to-choke range for the second axial stage.

5.4 AERODYNAMIC DESIGN AND MATCHING, AVIGV + CFG ($P_4/P_1 = 10.5:1$)

The aerodynamic design and matching of this AVIGV + CFG compressor were completed based on the design requirements as discussed in Paragraph 5.3. The aerodynamic design procedures used here were described in Paragraph 5.2.

The results of Task IA show that the optimum work split for this A + C compressor, by reference to the B portion of Figure 6 ($N/\sqrt{h} = 60,000$ rpm), is for design values of $P_3/P_1 = 1.48:1$; therefore, $P_4/P_3 = 7.1:1$.

5.4.1 Preswirl Angle Estimation

The inlet-guide-vane analysis derived for this program and reported in Appendix IV was used to compute the preswirl angle associated with the shift of the pressure-ratio characteristics required for a good compressor match. The performance characteristics of an axial compressor with advanced efficiency levels for this pressure ratio were used to represent the estimated performance for this compressor. With this compressor map, computations showed that a preswirl angle change of 15 degrees would place the 60- and 100-percent-power points on the maximum efficiencies for their respective speeds. This is in agreement with the preswirl angle estimation made for the AAVIGV + CFG compressor.

Based on these results, it was decided to design the compressor with positive 15° preswirl at power levels up to 60 percent and with zero preswirl at 100-percent power. Note that positive preswirl is in the direction of rotation and therefore reduces airflow.

5.4.2 Single-Stage Axial Compressor Design ($P_3/P_1 = 1.48$)

The design completed for this axial compressor is very similar to the axial first-stage design displayed in Figure 35 ($P_2/P_1 = 1.432$) for the last iteration made for the AAVIGV + CFG compressor.

The design of this stage was dictated by a specification of zero rotor-hub exit relative swirl for minimum hub diameter and, hence, minimum flow-path distortion between the axial and centrifugal stages. The rotor tip speed was selected to be 1200 fps at the design point.

Slight modifications to the inlet hub contour of the first axial stage of the AA + C compressor as reported in Paragraph 5.3.2 were made. An aerodynamic configuration was achieved that accommodates both the 30- and the 100-percent off-design conditions with the stipulated IGV actuation.

Table XX shows a summary of the design results. The flow path is given in Figure 38.

5.4.3 Centrifugal Compressor Design, $P_4/P_3 = 7.1:1$

The design parameter study carried out in Task IIA was considered applicable for the design of this centrifugal compressor. A rotor blade exit angle of 50 degrees and an absolute air angle (measured from the radial direction) of 69 degrees were specified. Since the design-point pressure ratio of this compressor is 7.1:1 and that of Task IIA was 4.7:1, a spot check was made at another blade angle. The change in overall stage efficiency was the same as that for the compressor designed in Task IIA. No further parameter examinations were made.

As with the centrifugal compressor designed for the two-stage axial compressor configuration, the radial extent of the vaneless diffuser has been selected for good efficiency at 100-percent power. However, the overall stage efficiency is 0.8 point lower in efficiency than anticipated from the work-split study in Task IA. In that study, only changes in specific speed were considered. Application of the details of the aerodynamic design resulted in a 0.5-point increase due to clearance and 0.3 point due to increased vaneless diffuser gap compared to the centrifugal compressor designed for the two-stage axial compressor configuration. The clearance of 0.010 inch is proportionately larger, with respect to the rotor exit width for this compressor, than that of the compressor designed to mate with two axial stages.

The compressor configuration is shown in Figure 38. It features a tandem blade row for the vanned diffuser, a vaneless bend, and a vaneless flare. A summary of the design results is displayed in Table XXI.

TABLE XX. AERODYNAMIC DATA SUMMARY FOR ONE-STAGE AXIAL COMPRESSOR						
	30% Power		60% Power		100% Power	
	Hub	Tip	Hub	Tip	Hub	Tip
First-Stage Rotor						
Rel. inlet Mach No.	0.490	0.991	0.574	1.098	0.743	1.327
Diffusion factor	0.375	0.495	0.279	0.424	0.430	0.470
Camber			73.3	24.8		
Rel. inlet air angle	51.0	72.4	44.8	69.2	47.5	67.6
First-Stage Stator						
Abs. inlet Mach No.	0.700	0.550	0.880	0.610	0.970	0.633
Diffusion factor	0.477	0.266	0.311	0.204	0.266	0.115
Camber			22.9	19.5		
Abs. inlet air angle	53.7	47.0	51.7	41.8	52.5	38.2
2nd Stage						
Abs. inlet Mach No.	0.429	0.478	0.661	0.549	0.768	0.608
Diffusion factor	0.399	0.190	0.302	0.205	0.295	0.215
Camber			44.1	49.4		
Abs. inlet air angle	36.3	30.8	34.9	29.7	34.8	29.1

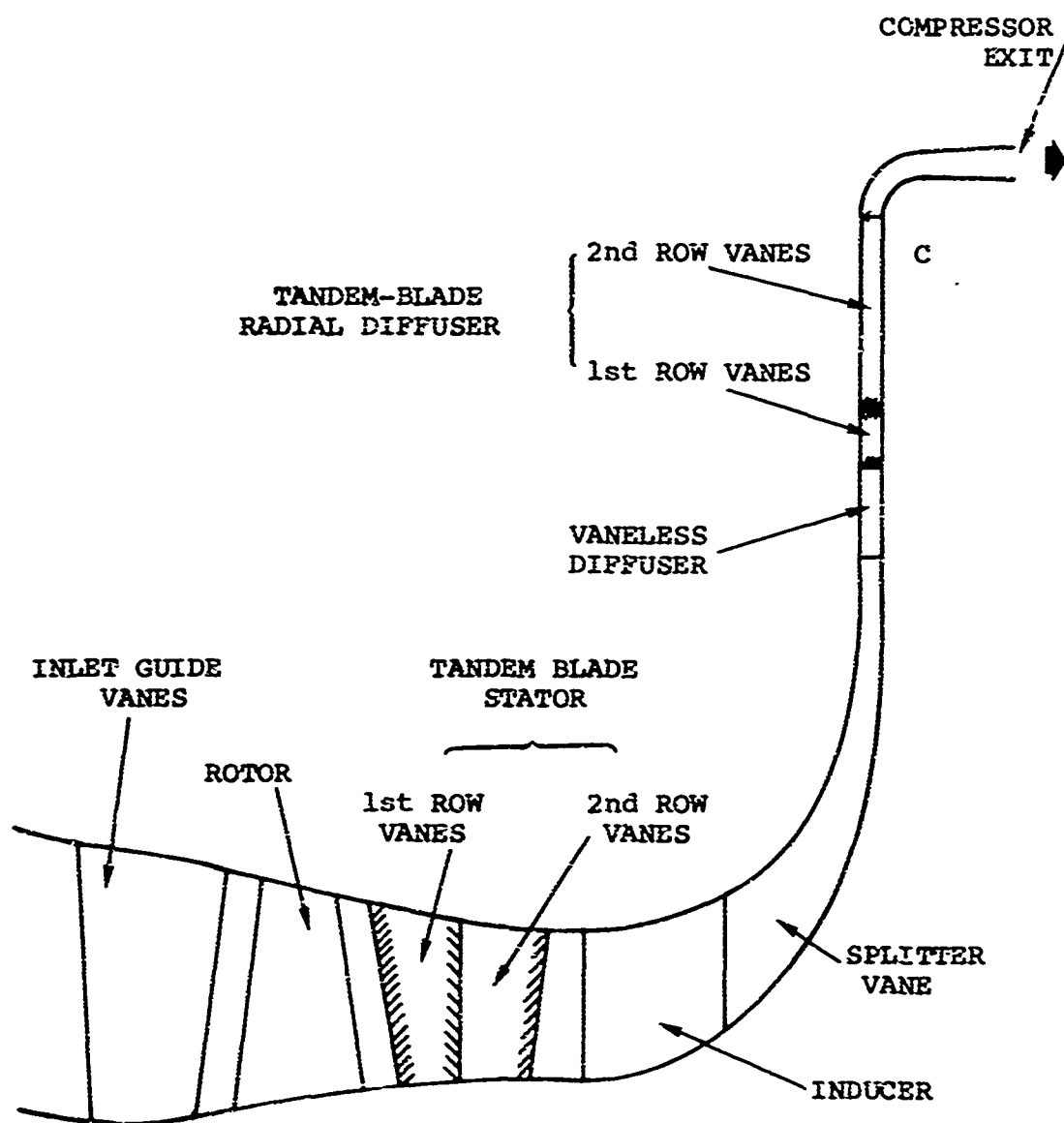


Figure 38. Compressor Flow Path, Single-Stage Axial Plus Centrifugal Compressor, AVIGV + CFG.

TABLE XXI. AERODYNAMIC DATA SUMMARY FOR CENTRIFUGAL COMPRESSOR DESIGNED TO MATCH WITH ONE-STAGE AXIAL COMPRESSOR

	30% Power	60% Power	100% Power
Inducer tip rel. Mach No.	0.985	1.092	1.175
Impeller tip speed	1840.0	2000.0	2116.0
Impeller exit abs Mach No.	1.072	1.140	1.200
Vaned diffuser inlet Mach No.	0.875	0.922	0.954
Vaned diffuser exit Mach No.	0.238	0.224	0.201
Compressor exit Mach No.	0.154	0.150	0.135

5.4.4 Compressor Matching, AVIGV + CFG

Several matching iterations were made for this final compressor arrangement based on compressor matching data and engine cycle data. A satisfactory match was achieved, and final results are displayed in Table XXII. The axial, centrifugal, and overall compressor maps for this case are presented in Figure 44 and discussed in Section 6.

5.5 CONCEPTUAL DESIGN OF COMPRESSOR AND ENGINE

Based on the aerodynamic design of the compressor as configured for this task (AVIGV + CFG, $P_4/P_1 = 10.5:1$) and reported in Paragraph 5.3, a conceptual layout shows a mechanical arrangement for the compressor as it might be incorporated in an engine power section. The layout consists of a cross-section view of a front-drive, turboshaft-engine power section, including a free turbine, and is presented in Figure 39.

The envelope of the gasifier section is 12.6 inches in diameter by 14 inches long, while the power turbine as shown adds 12 inches to the length to complete the power section. The engine diameter is set by the 7.1:1-pressure-ratio centrifugal-

A

TABLE XXII. ENGINE CYCLE DATA (CA
AVIGV + CFG COMPRESSOR MATCHING

CONFIGURATION	SPECIAL REMARKS	POWER		SFC	TIT (°F)	COMPRESSOR SPEED (% DESIGN)		COMPRESSOR FLOW (CORRECTED)		AXIAL P ₃ /P ₁
		(%)	(HP)			AXIAL/ OVERALL (%)	CENTRIF- UGAL (%)	AXIAL/ OVERALL (LB/SEC)	CENTRIF- UGAL (LB/SEC)	
SINGLE-SPOOL COMPRESSOR AVIGV + CFG	DESIGN	100	757.2	.452	2500.	107.5	105.2	3.634	2.355	1.67
	POINT	60	454.7	.491	2096.	100.	100.	3.00	2.16	1.48
	P ₄ /P ₁	30	226.	.630	1760.	91.7	91.8	2.4	1.8	1.41
	10.5:1	20	150.5	.77	1620.	87.9	88.2	2.15	1.64	1.37

B

TABLE XXII. ENGINE CYCLE DATA (CALCULATED),
IGV + CFG COMPRESSOR MATCHING RESULTS

COR N)	COMPRESSOR FLOW (CORRECTED)		COMPRESSOR PRESSURE RATIO			COMPRESSOR EFFICIENCY			COMPRESSOR SURGE MARGIN (ΔW FOR $N/\sqrt{R} = \text{CONST}$)		
	AXIAL/ OVERALL (LB/SEC)	CENTRIF- UGAL (LB/SEC)	AXIAL P_3/P_1	CENTRIF- UGAL P_4/P_3	OVERALL P_4/P_1	AXIAL η_{31}	CENTRIF- UGAL η_{43}	OVERALL η_{41}	AXIAL (%)	CENTRIF- UGAL (%)	OV
7.2	5.2	3.634	2.355	1.675	8.249	13.817	0.892	0.775	.778	17.	4.2
8.0	9.0	3.00	2.16	1.48	7.125	10.545	0.91	0.786	.788	18.4	10.2
1.8	2.4	1.8	1.415	5.548	7.85	0.83	0.795	.7836	9.7	13.3	
7.2	2.2	2.15	1.64	1.37	4.964	6.80	0.79	0.795	.7805	4.6	15.0

C

ATED),
TS

COMPRESSOR PRESSURE RATIO		COMPRESSOR EFFICIENCY			COMPRESSOR SURGE MARGIN (ΔW FOR $N/\sqrt{h} = \text{CONST.}$)		
CENTRIF- UGAL P_4/P_3	OVERALL P_4/P_1	AXIAL η_{31}	CENTRIF- UGAL η_{43}	OVERALL η_{41}	AXIAL (%)	CENTRIF- UGAL (%)	OVERALL (%)
8.249	13.817	0.892	0.775	.778	17.	4.2	6.4
7.125	10.545	0.91	0.786	.788	18.4	10.2	12.0
5.548	7.85	0.83	0.795	.7836	9.7	13.3	16.0
4.964	6.80	0.79	0.795	.7805	4.6	15.0	17.0

A

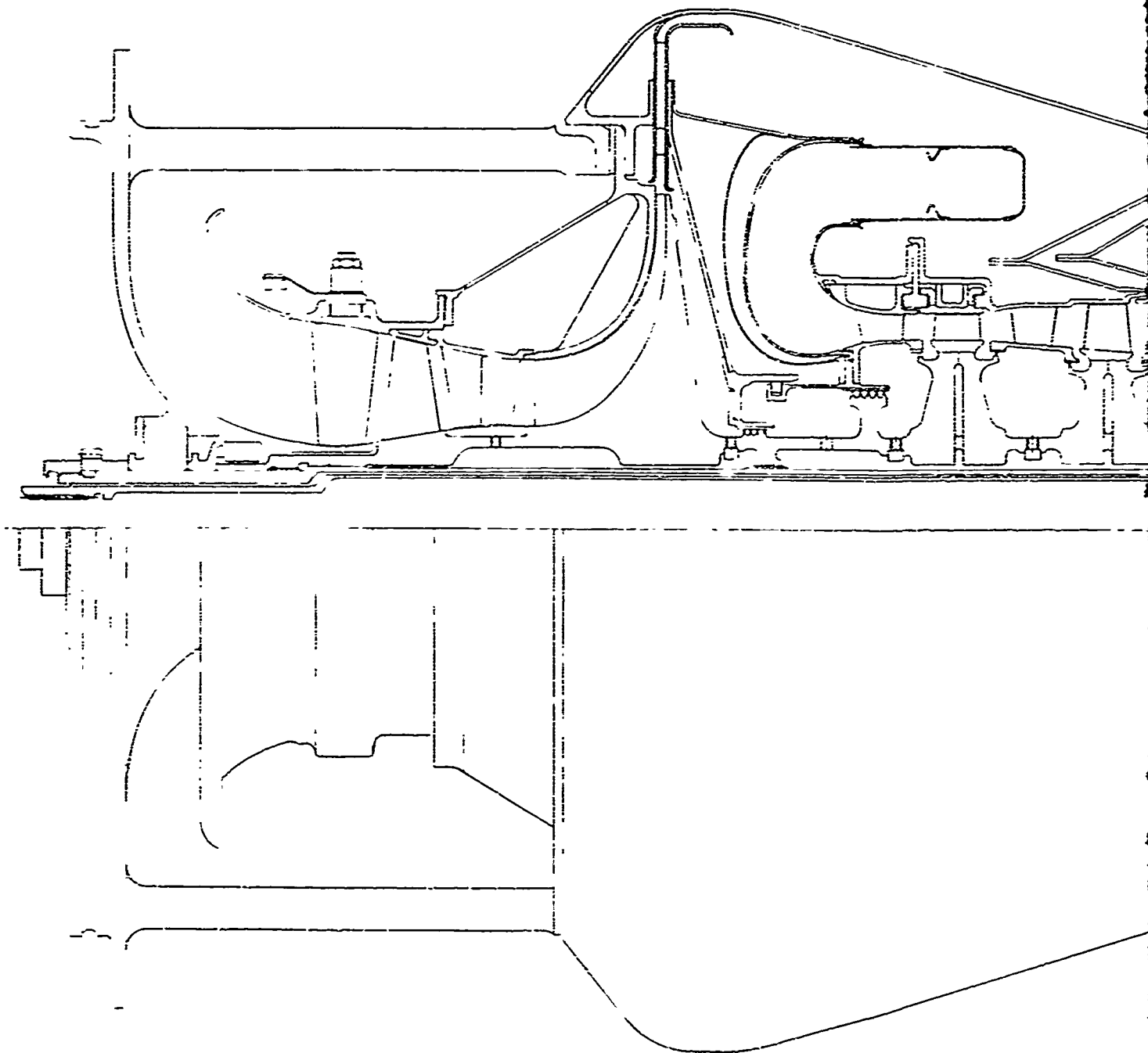
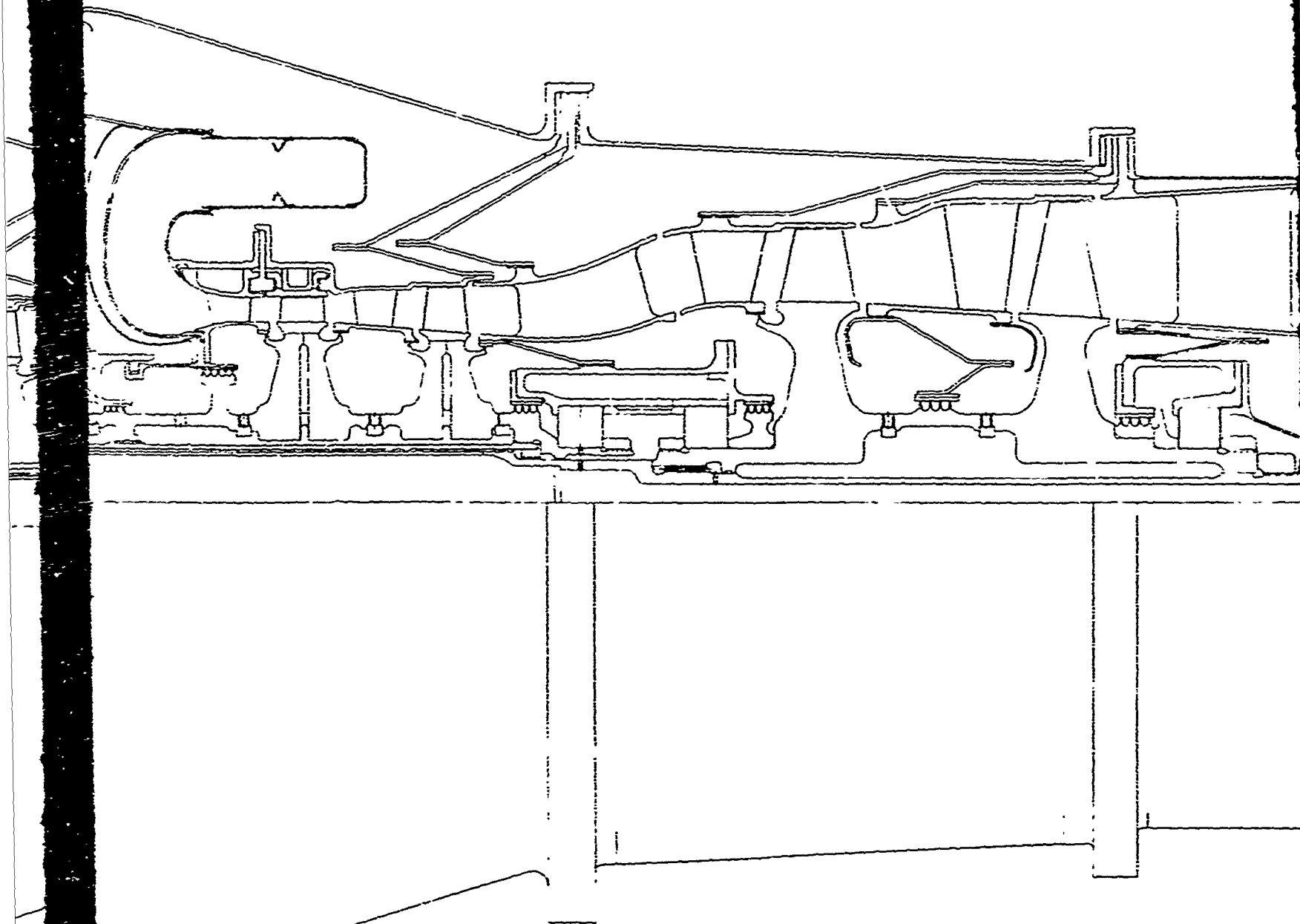


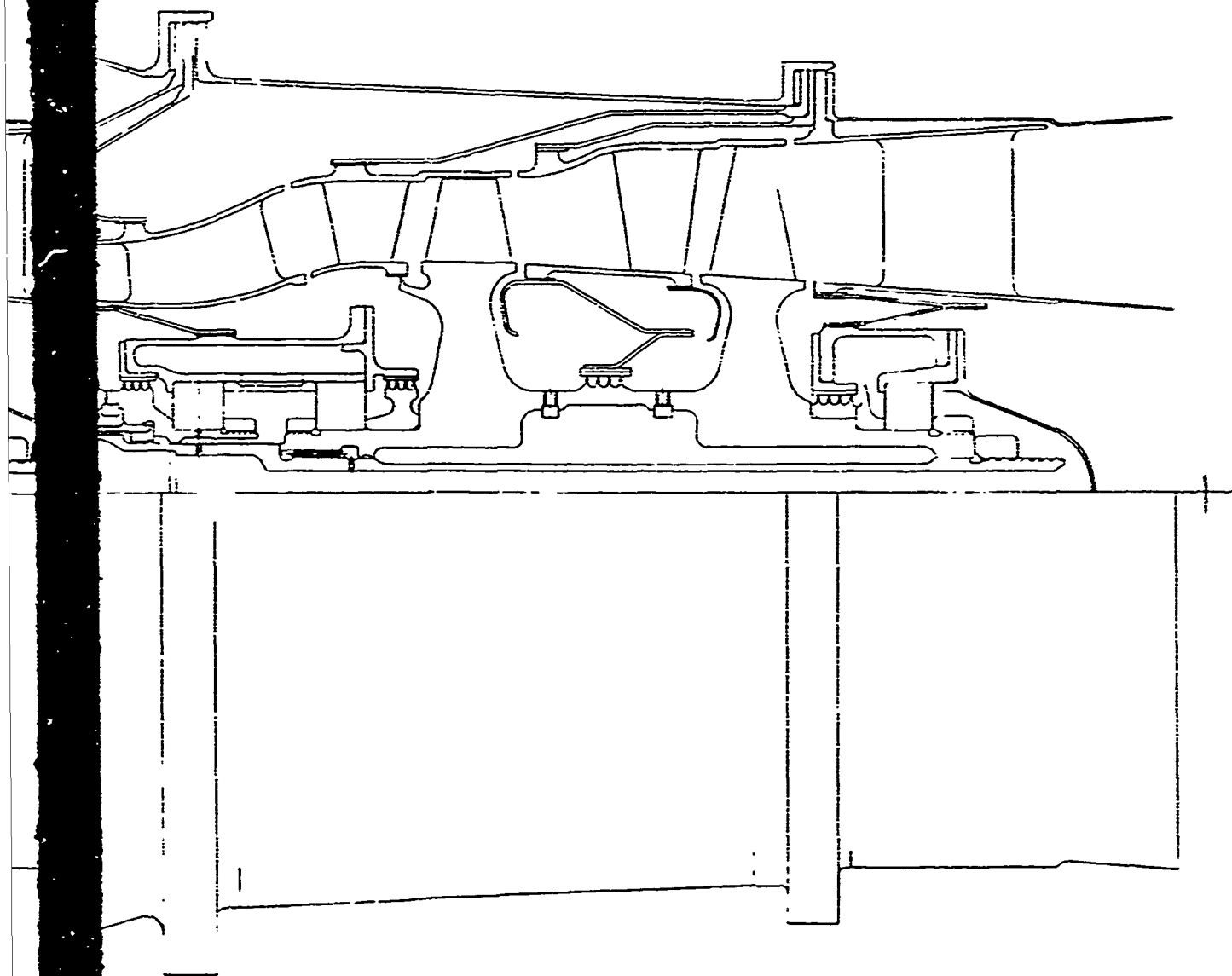
Figure 39. Engine Conceptual Layout.

B



B

C



compressor stage. This diameter is obviously larger than the combustor and/or turbine sizing dictates. Additional compressor design studies might be expected to achieve a reduction in this diameter but are beyond the scope of this program.

5.5.1 Mechanical Analyses for Compressor Rotors

Stress and displacement analyses for both the axial and the centrifugal rotors were performed with use of the finite-element method. The elemental model is shown in Figure 40. The method used permits a good evaluation of displacements at the hub and shroud line. This is an essential feature if such displacements are to be minimized to permit running with the smallest possible axial and radial clearances.

An extension of the analysis with existing programs could investigate the inelastic behavior of the components.

A summary of values obtained is given in Table XXIII.

The detailed results for selected elements are given in Table XXIV to illustrate the depth of the analysis conducted for the rotors.

The stress levels in the axial rotor are observed to be moderate and within the range for a conventional design. The stress levels obtained in the bore of the centrifugal rotor are higher than would be acceptable in a current production rotor. However, they represent the initial state of a design, and subsequent design iterations would in the normal course reduce stress levels and disk flowering to acceptable limits and improve the burst margin.

The temperature range is suitable for the material chosen (annealed titanium, 90 Ti-6Al-4V). Should a creep problem persist in the centrifugal rotor, then a change to titanium Ti-6Al-2Sn-4Zr-2Mo would be needed.

5.5.2 Mechanical Analyses for Engine Shafting

The gasifier section is straddle-mounted and incorporates conventional shafting. Because of the well-established mechanical integrity of this type of system, no analyses were considered necessary to affirm the mechanical feasibility of this rotating group.

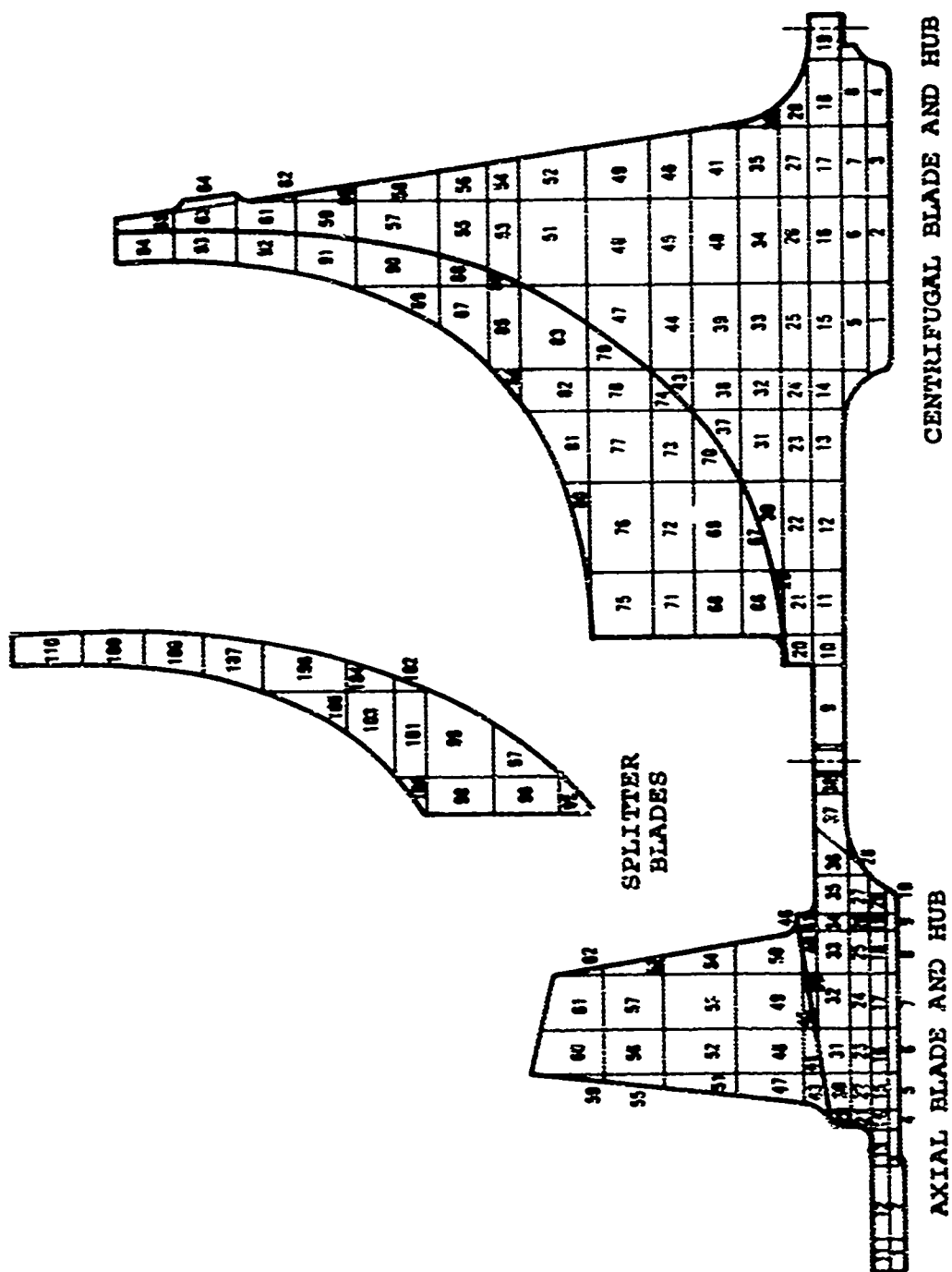


Figure 40. Elemental Model of Axial and Centrifugal Compressor Rotors.

TABLE XXIII. MECHANICAL ANALYSIS FOR COMPRESSOR ROTORS		
Description	Axial Rotor	Centrifugal Rotor
Average tangential stress, ksi	27.1	71.7
Maximum blade stress, inlet, ksi	47.4	19.8
Maximum blade stress, splitter, ksi	-	7.3
Maximum bore stress, ksi	44.1	122.4
Maximum rim stress, ksi	34.8	37.0
Minimum burst speed, rpm	126,000	69,400 (1154)
Blade tip growth, inlet, radial, inches	0.0072	0.0057
Blade tip growth, exit, radial, inches	0.0053	0.0224
Blade tip axial movement, inch	0.0010	0.0186
Hub weight, pounds	0.481	4.517
Blade weight, pounds	0.139	0.351
All values at 66,000 rpm.		
Minimum burst speed assumes minimum properties (minus 35) and a burst factor of 0.9.		

The power turbine is straddle-mounted and includes an integral tie-bolt and power turbine drive shaft. This arrangement was chosen to effect higher critical speeds for the power turbine drive shaft than would result for a simply supported quill shaft as examined and reported in Paragraph 5.2.5.

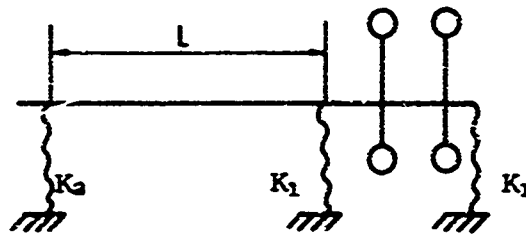
Analyses were made for this mechanical arrangement, and results are displayed in Figure 41 for the power turbine shaft critical speeds. The design as finalized (see Figure 39) resulted in a power turbine drive shaft unsupported length of 16.6 inches.

TABLE XXIV. MECHANICAL ANALYSIS DATA FOR SELECTED ELEMENTS OF COMPRESSOR ROTORS							
Stage		Element	Stress (in ksi)				
			Radial	Tan- gential	Axial	Shear	Equivalent
Axial	Blade	47	39.55	0	0.40	4.46	40.09
Axial	Disk	20	1.32	34.41	-2.02	-1.08	34.93
Radial	Blade	70	13.47	0	-3.93	-9.06	22.27
Radial	Splitter	94	3.12	0	-0.97	-1.19	4.23
Radial	Disk	38	10.33	51.92	2.38	4.12	46.62
Displacements for a typical element, node are:							
Element 65, (centrifugal rotor rim)				radial axial	0.0224 inch -0.0186 inch		
All values at 66,000 rpm.							

Figure 42 displays the calculated data for power-shaft radial spline and bearing loads. The power turbine configured for this task was sized for 40,000 rpm. The indicated bearing loads for this case and for an unsupported shaft length (L) of 16.6 inches show that resultant bearing loads are feasible for long-life operation.

Figure 41 shows that the critical speeds and more importantly the acceptable operating regime is relatively insensitive to shaft length from 16 to 19 inches. Similarly, Figure 42 shows that the radial loads for the spline and bearings are acceptable for shaft length of 17, 18, and 19 inches. Based on this analysis for the A+C compressor it is clear that an AA+C compressor could be designed for this application and would present no significant mechanical problems.

A



$$K_1 = 200,000 \text{ LB/IN.}$$

$$K_2 = 10,000 \text{ LB/IN.}$$

①	—	23,32
②	- - -	49,86
③	—	50,33
④	- - -	100,64

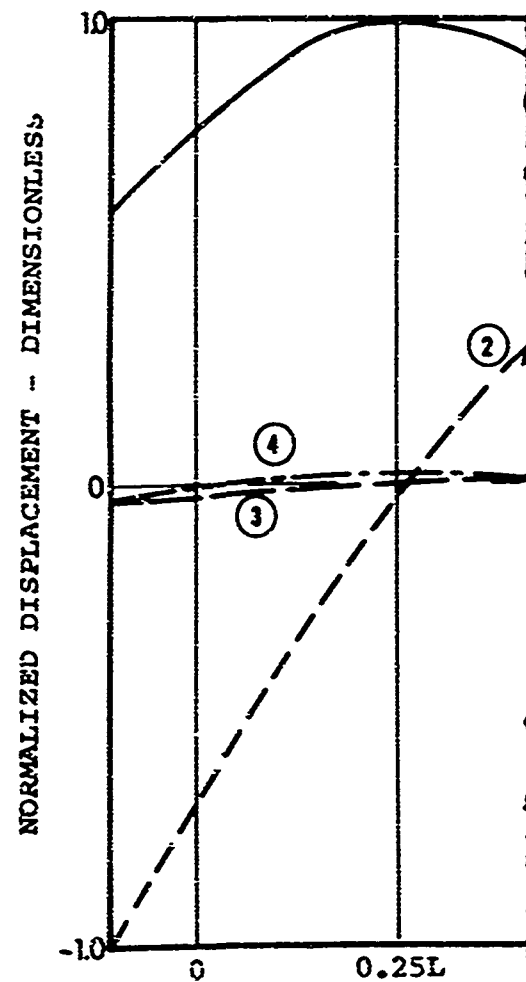
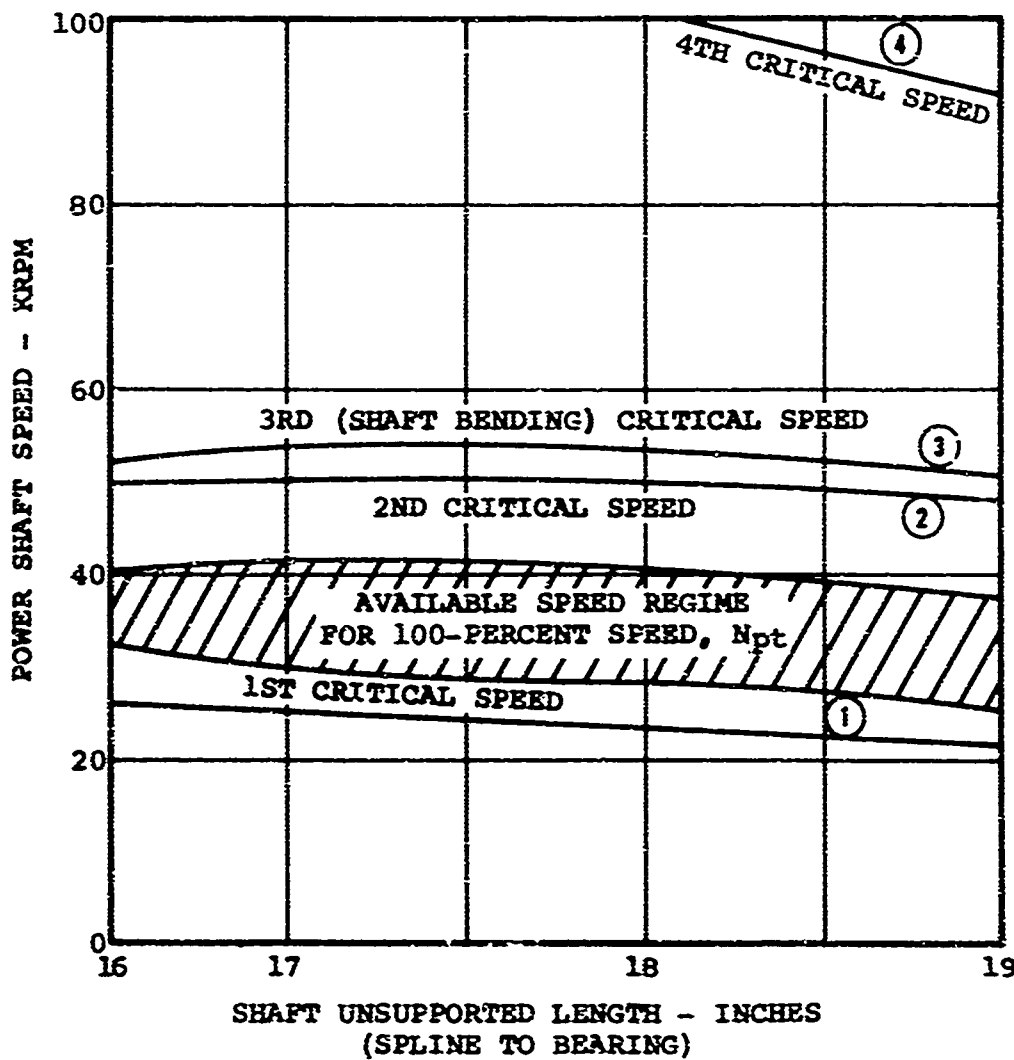
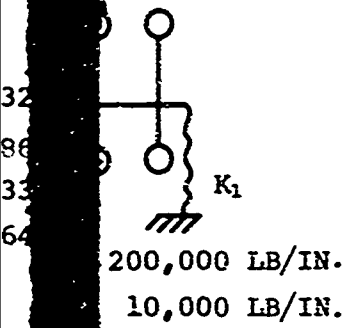
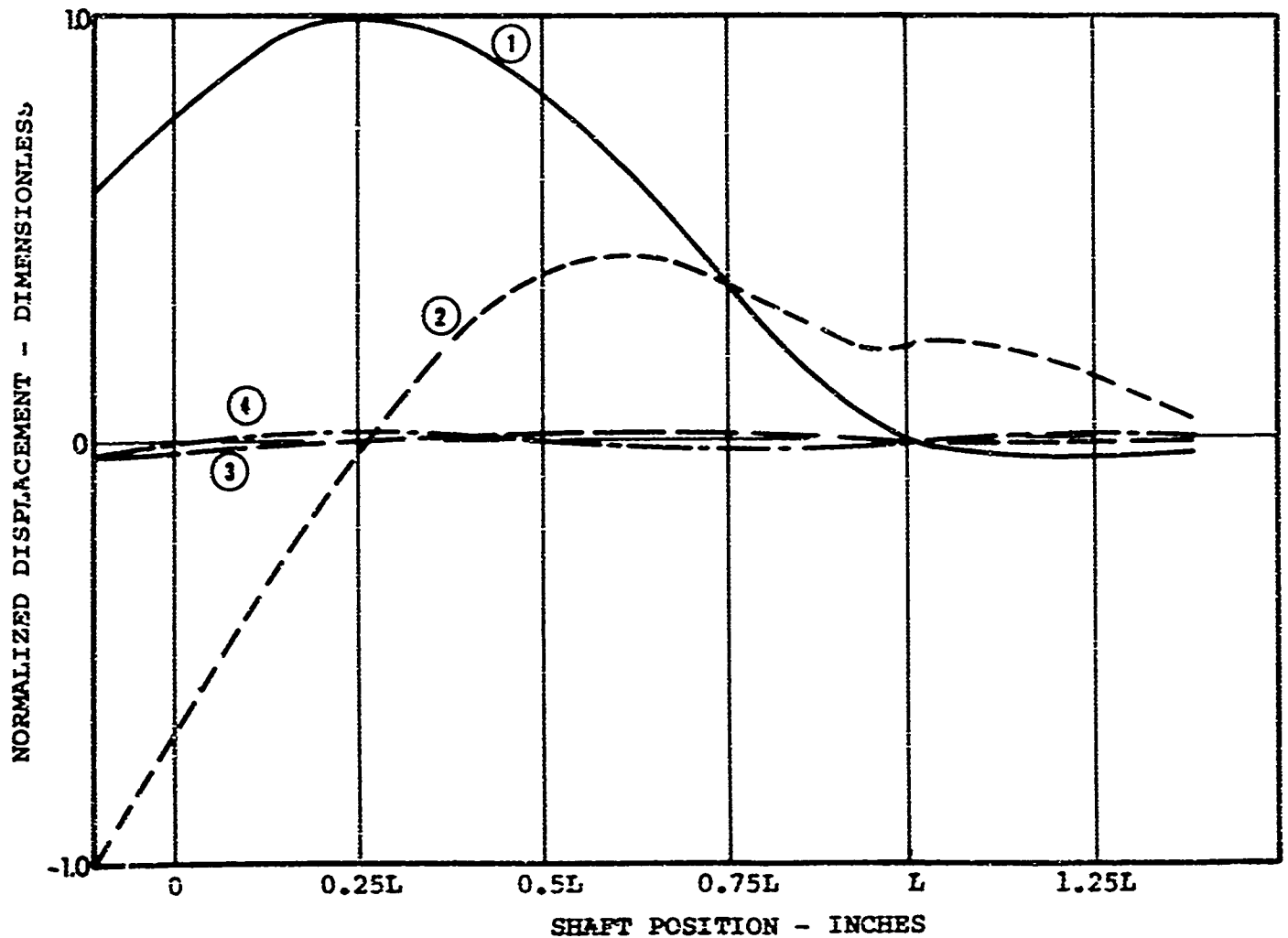
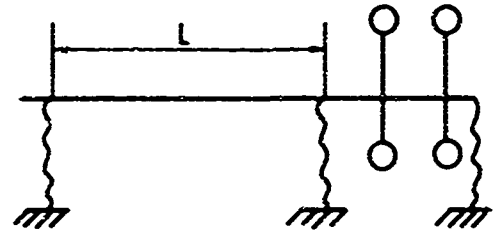


Figure 41. Power-Shaft Dynamic Analysis.

B

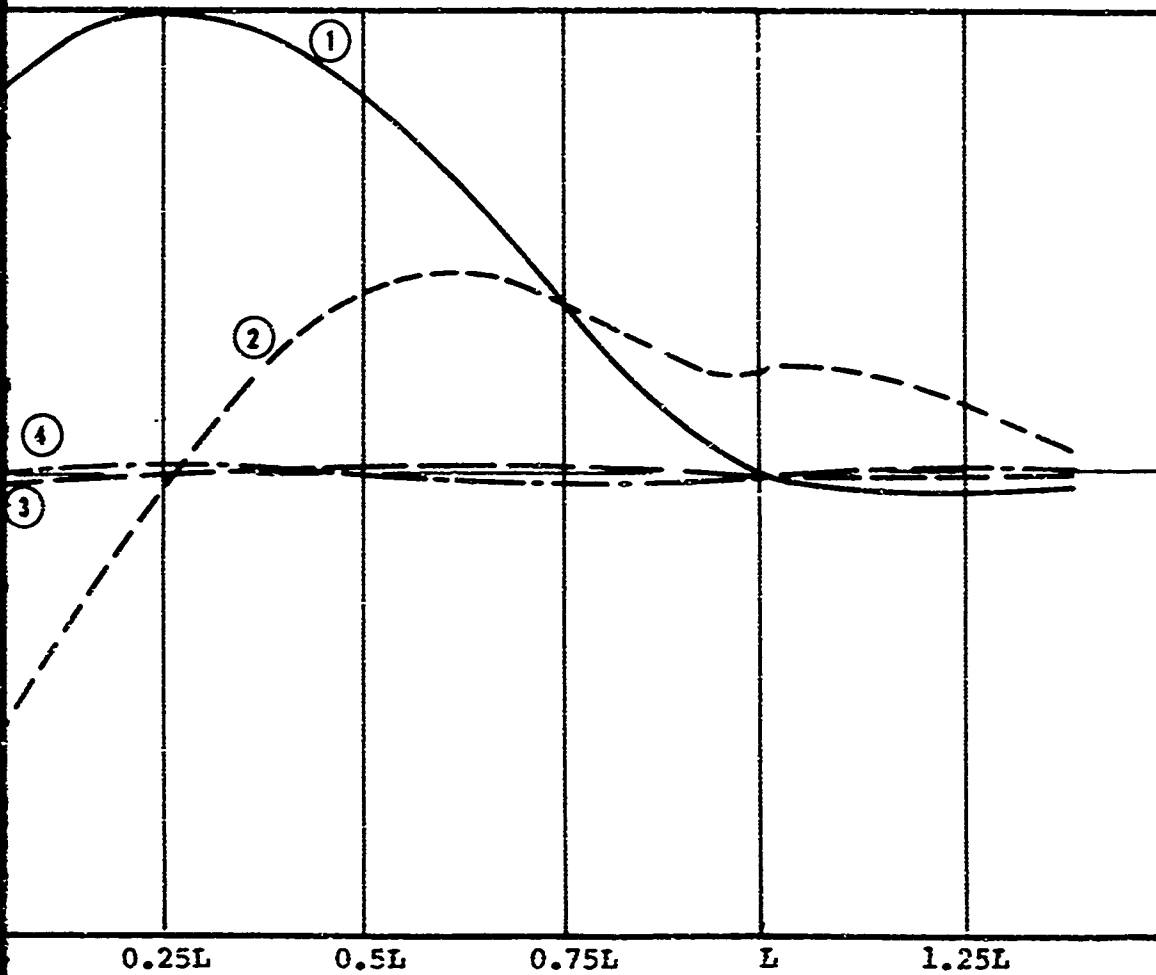
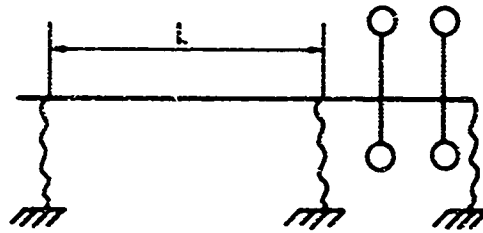


- ① ————— 23,329 RPM
- ② - - - - - 49,864 RPM
- ③ ————— 50,332 RPM
- ④ - - - - - 100,641 RPM



NORMALIZED MODE SHAPES

— 23,329 RPM
 - - 49,864 RPM
 — 50,332 RPM
 - - 100,641 RPM



SHAFT POSITION - INCHES

NORMALIZED MODE SHAPES

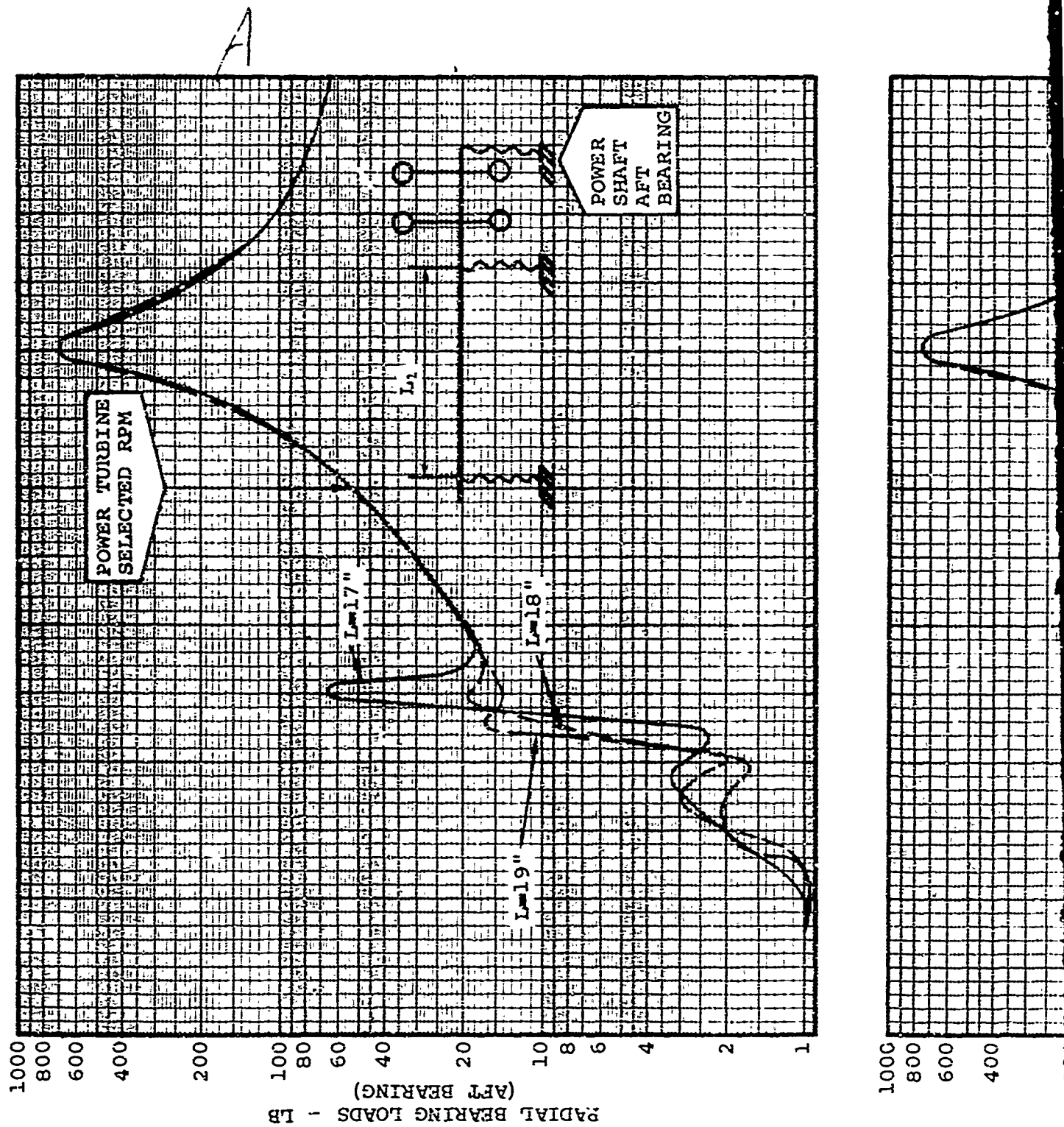
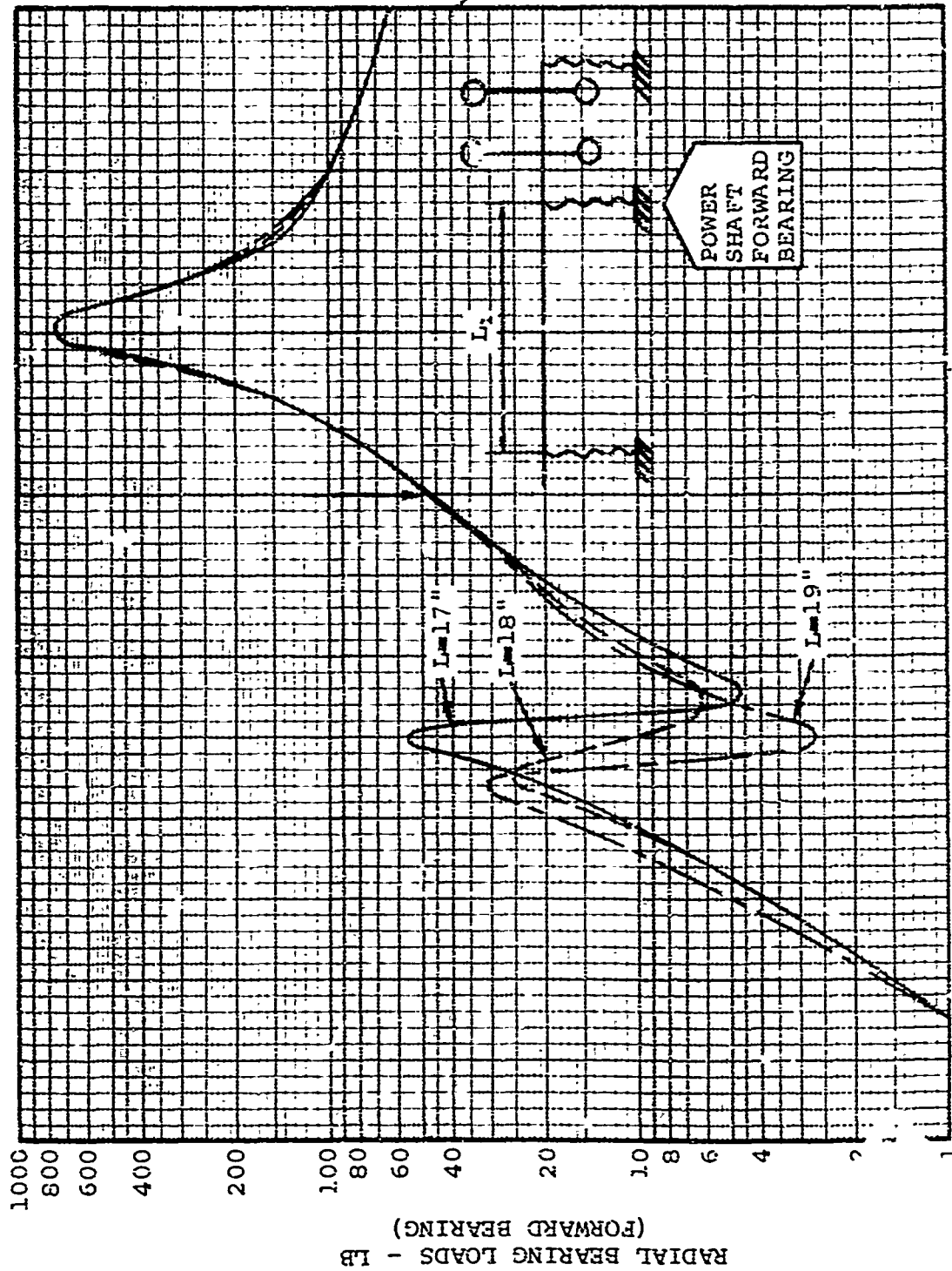


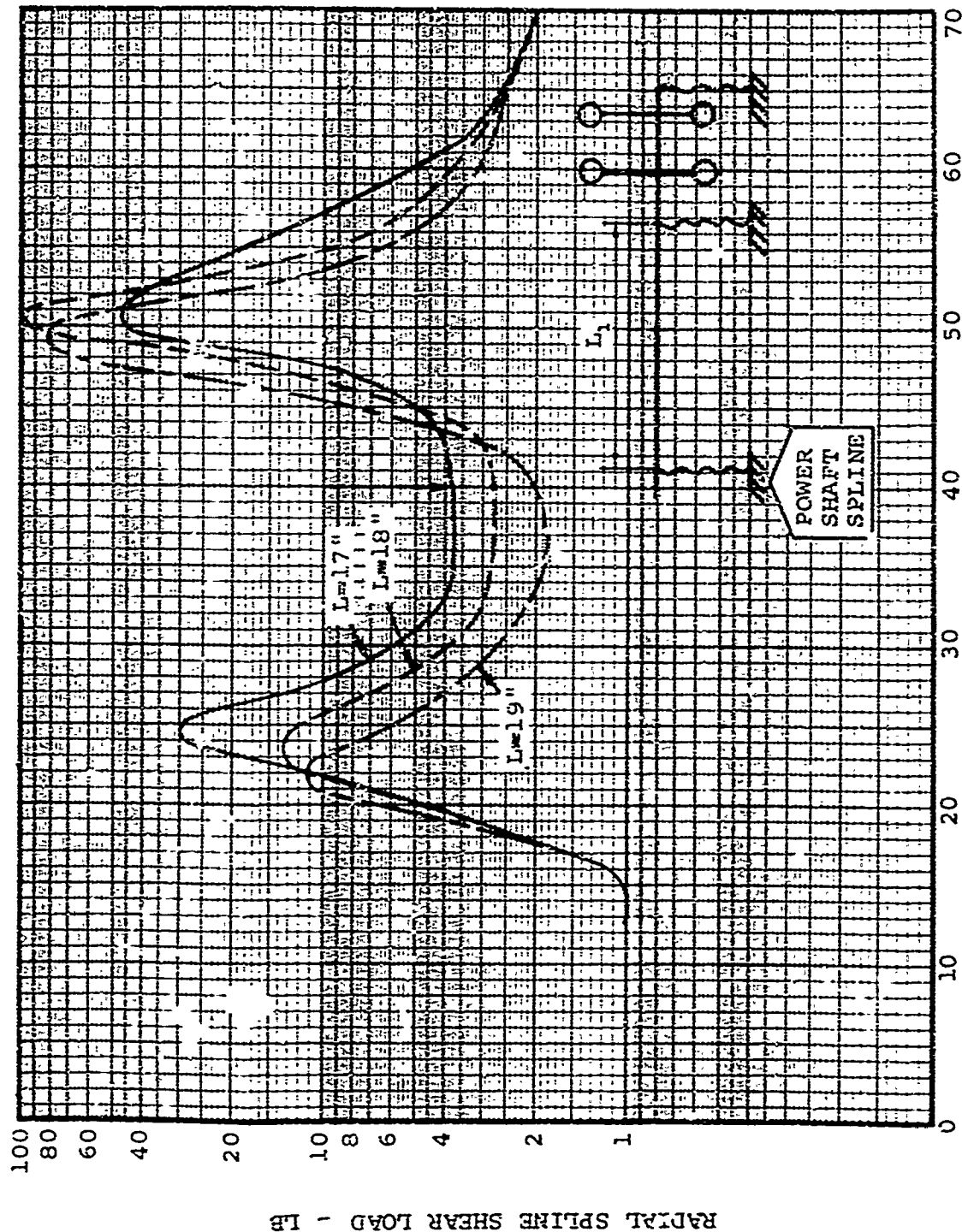
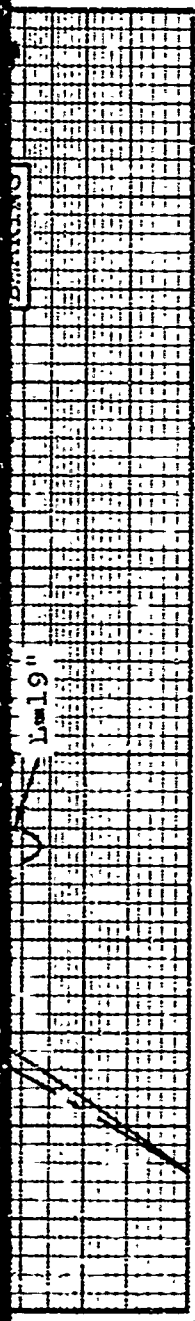
Figure 42. Power-Shaft Radial Spline and Bearing Loads.

B



RADIAL BEARING LOADS - LB
(FORWARD BEARING)

ing Loads.



SHAFT SPEED - KRPM

RADIAL SPLINE SHEAR LOAD - LB

6. TASK III, COMPRESSOR PERFORMANCE PREDICTION

6.1 DATA DISPLAY

The final compressor flow path is displayed in Figure 43. The specification of zero rotor hub exit swirl, combined with a transonic inducer-tip relative Mach number, has eliminated the usual transition section length. As the axial compressor design was finally configured, the rotor exit hub swirl is actually slightly negative. The inducer-tip relative Mach number is 1.092 at 60-percent power.

The estimated compressor performance characteristics are displayed in Figure 44. The axial compressor performance is a combination of the efficiency of an existing AiResearch compressor with the range indicated by the upper end of the data band in Figure 2. The centrifugal compressor performance was computed from the same analytical techniques that were used in the compressor design and which were described in Section 3. The empirical correlations that were used to design the compressor were applied to the compressor geometry to obtain the performance at off-design conditions. The empiricism contains correlations used to estimate rotor surge, choke, slip factor and efficiency, the friction coefficient for the vaneless diffuser, and the cascade data for the vaned diffuser.

Included in Figure 43 is the identification of the locations at which vector diagram data are presented. The vector diagrams are displayed in Figures 45, 46, and 47 for the 30-, 60-, and 100-percent-power points, respectively.

6.2 DISCUSSION

The flow range from surge to choke on the centrifugal compressor and the broadness of the efficiency islands are a result of the combined contribution of the rotor, with its backward-leaning blades, and the tandem cascade of the vaned diffuser. The feature of backward-leaning rotor blades allows the maximum rotor efficiency to occur at or near the engine operating line. In this way, the rotor-diffuser system can be matched to obtain the highest possible stage efficiency. For the vaned-diffuser inlet Mach numbers that resulted from the design study, only the tandem-cascade type of vaned diffuser has experimentally demonstrated at AiResearch the flow range displayed for the centrifugal compressor.

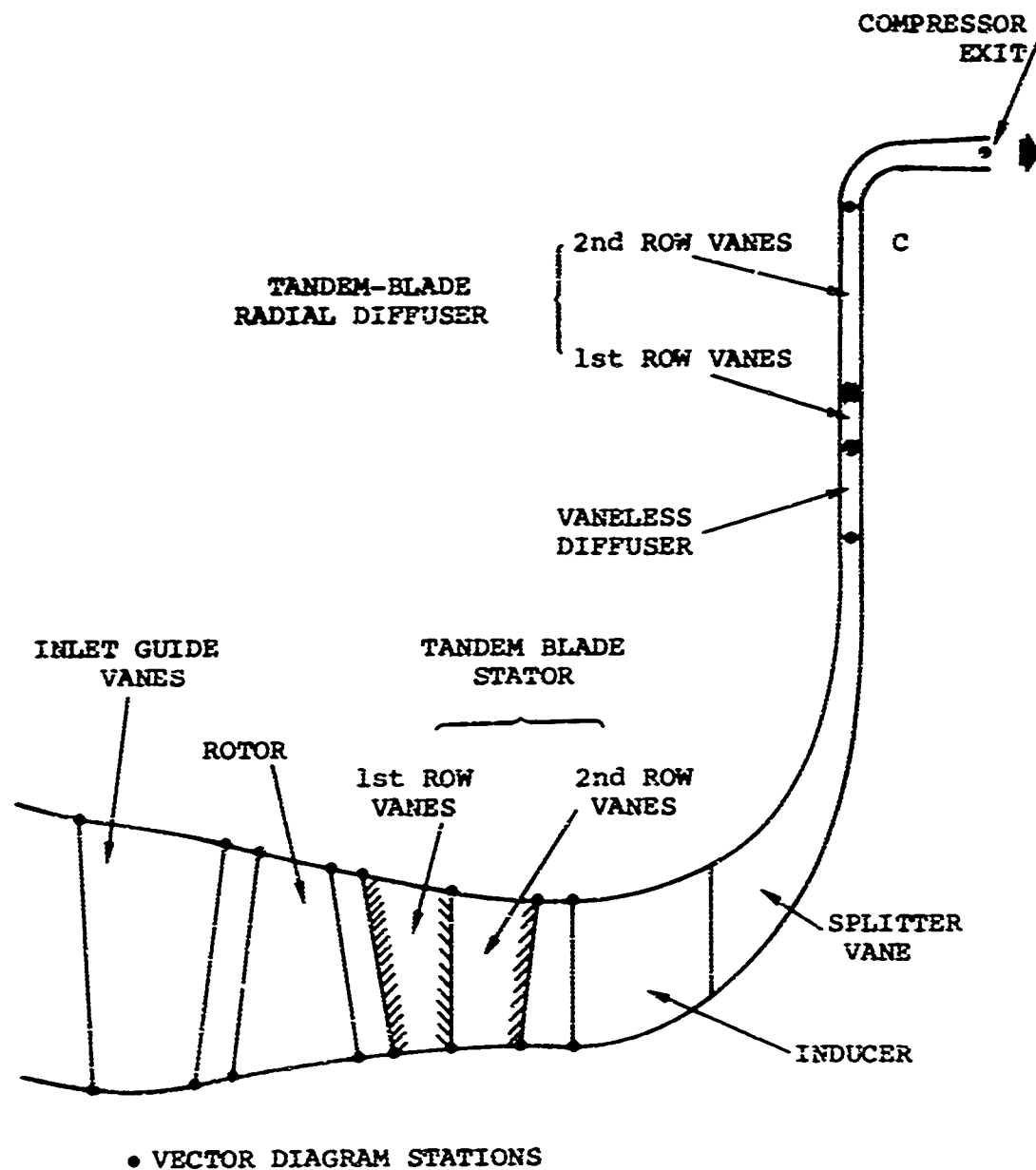
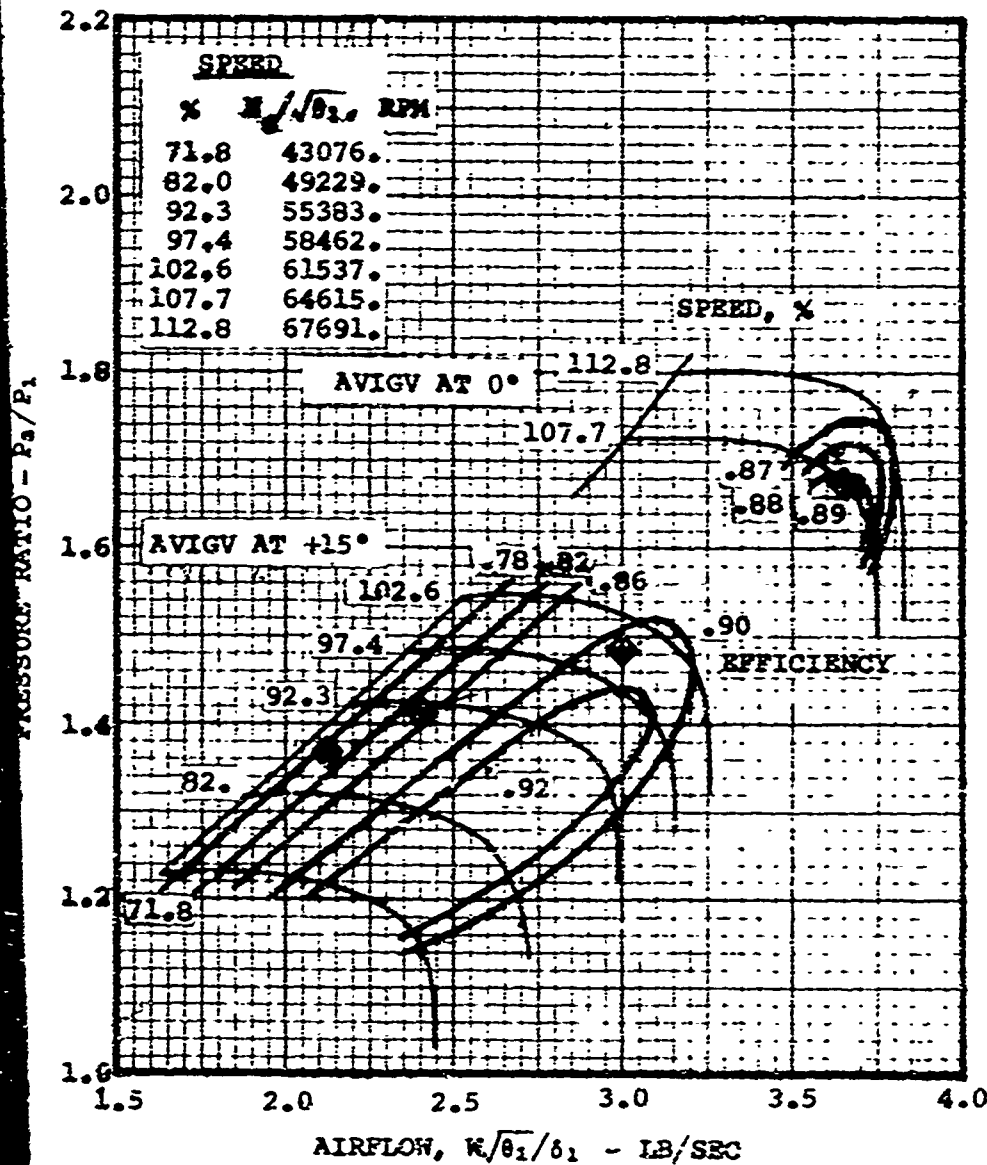
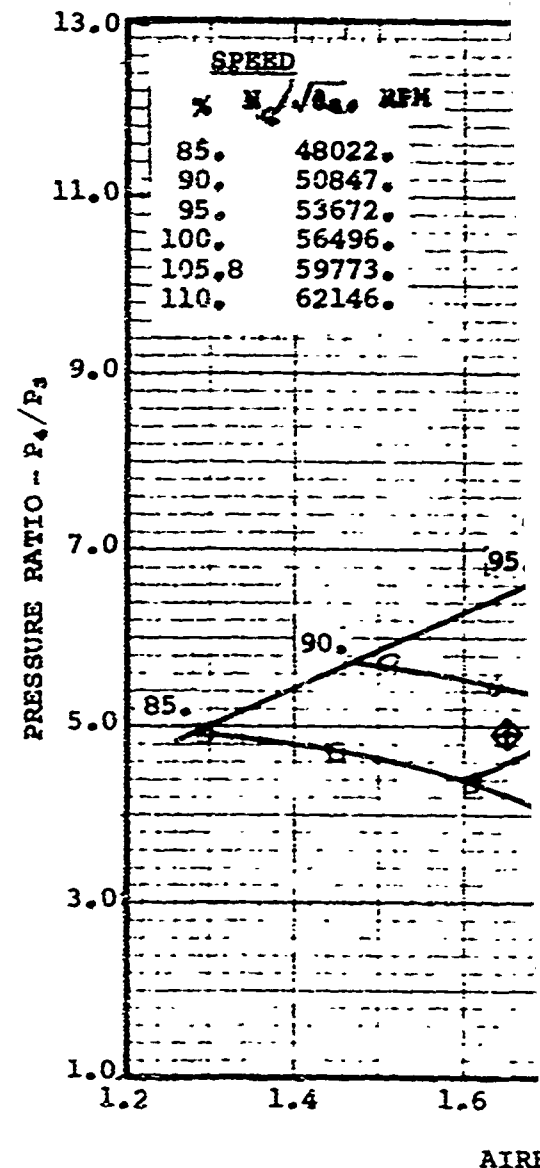


Figure 43. Compressor Flow Path, Single-Stage Axial Plus Centrifugal Compressor, AVIGV + CPG.

A



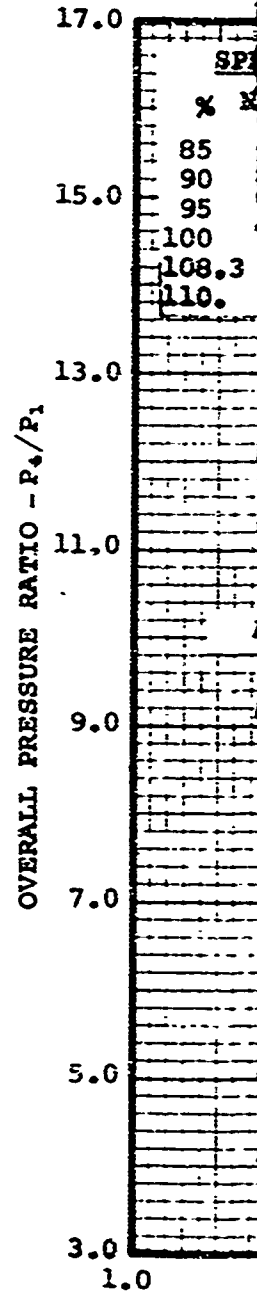
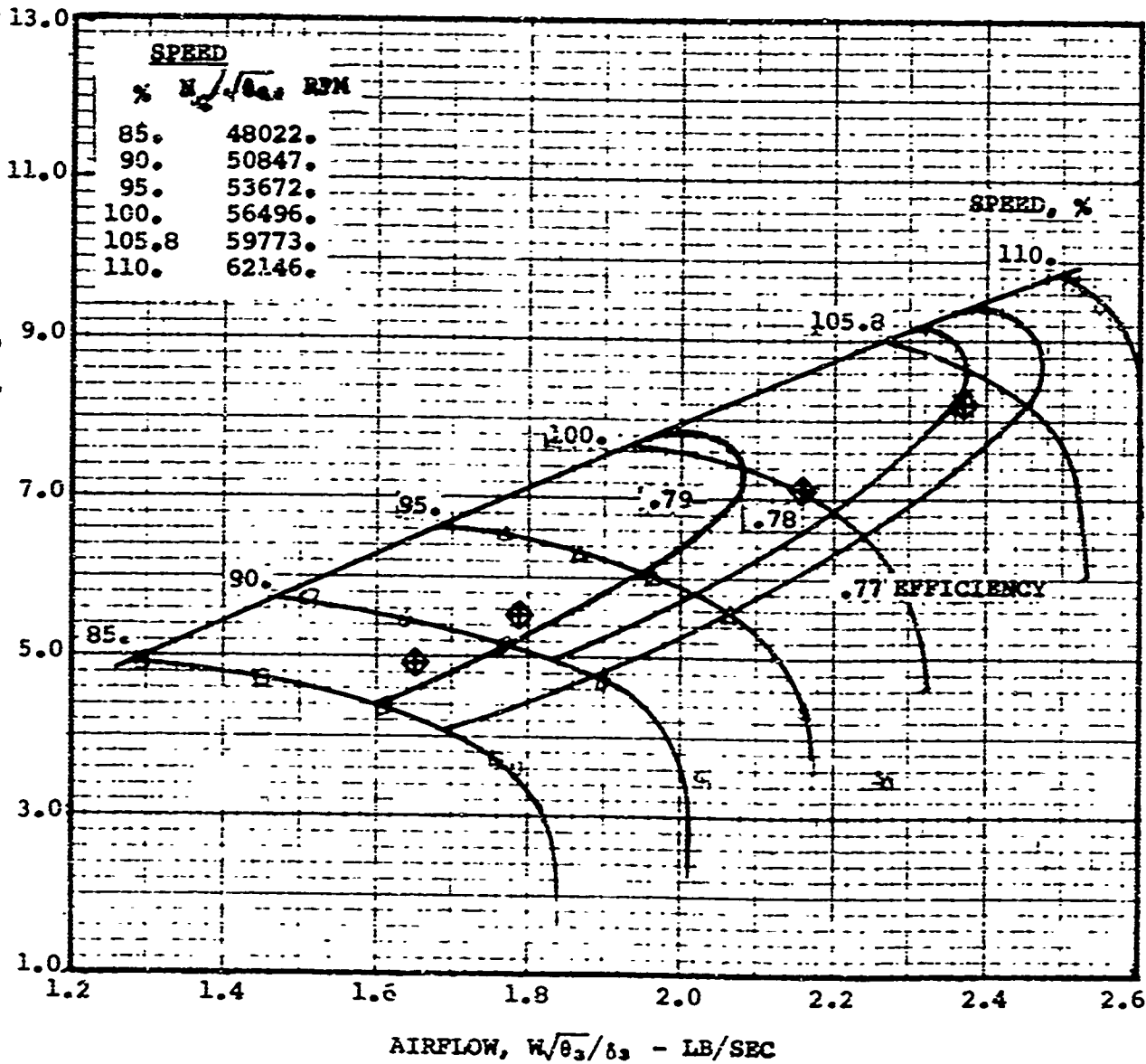
(A) AXIAL COMPRESSOR: VARIABLE INLET GUIDE VANES



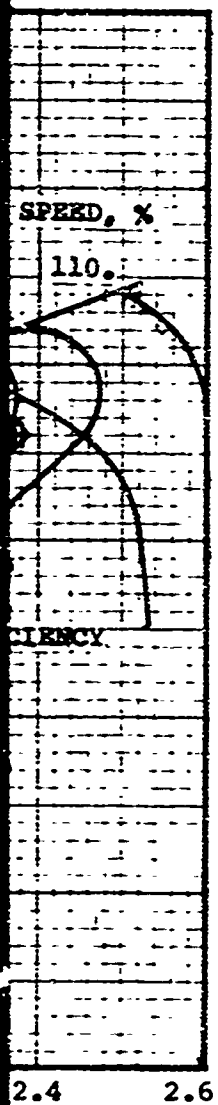
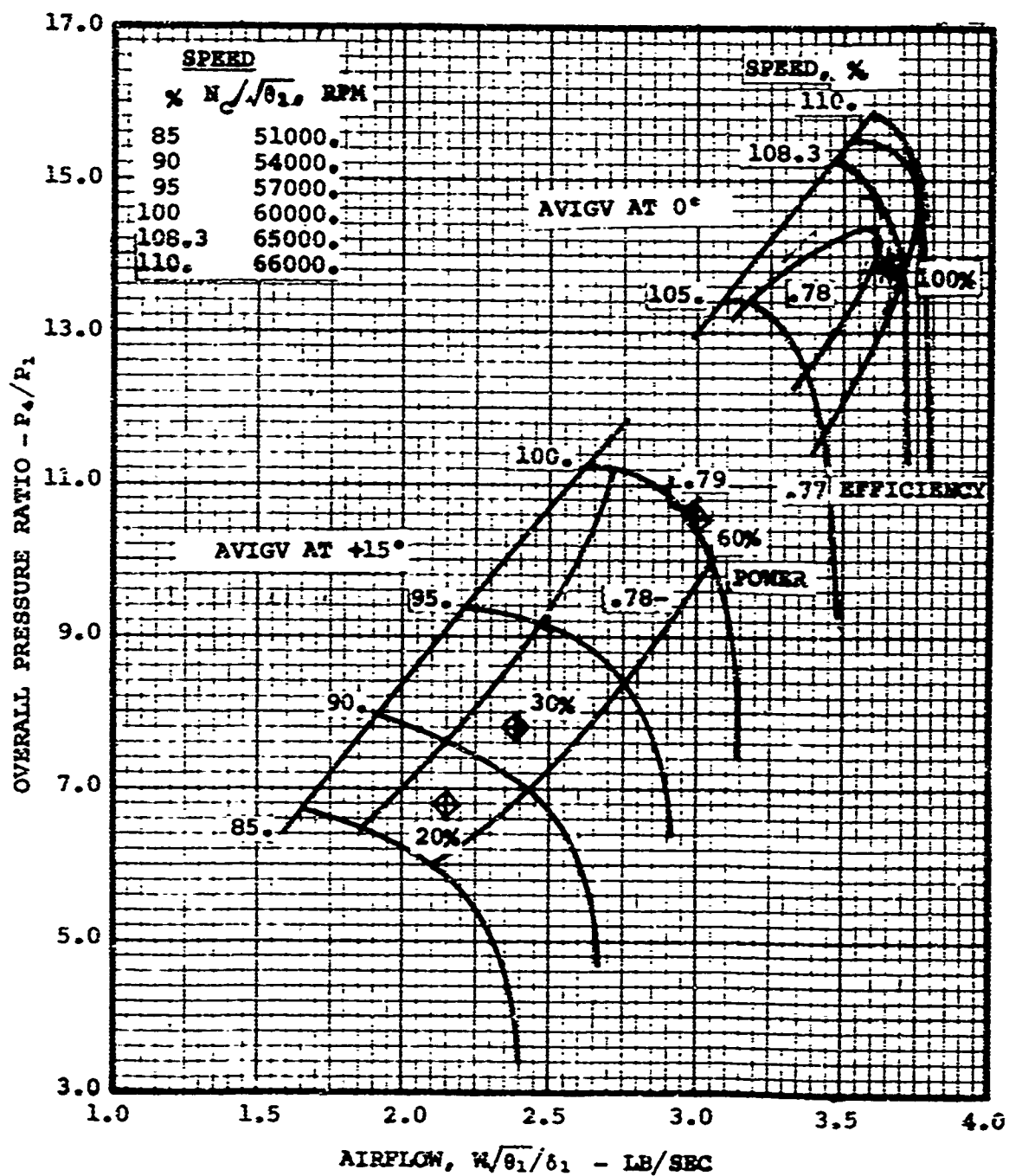
(B) CENTRIFUGAL

Figure 44. Estimated Performance Characteristics, One-Stage Axial Plus Centrifugal Compressor, AVIGV + CFG.

B

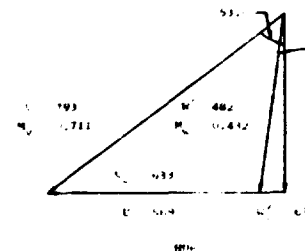
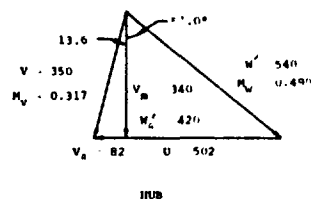
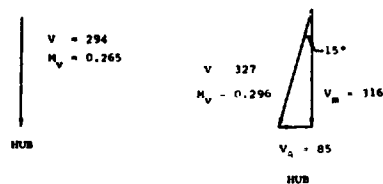
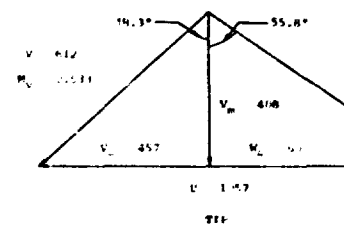
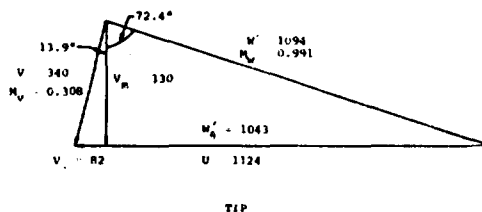
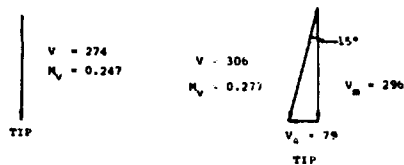


(2) CENTRIFUGAL COMPRESSOR: FIXED GEOMETRY



A

AXIAL COMPRESSOR



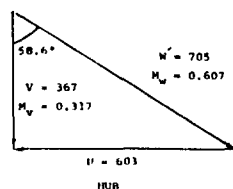
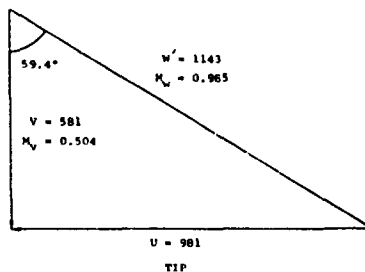
GUIDE VANE INLET
30-PERCENT POWER

GUIDE VANE OUTLET
30-PERCENT POWER

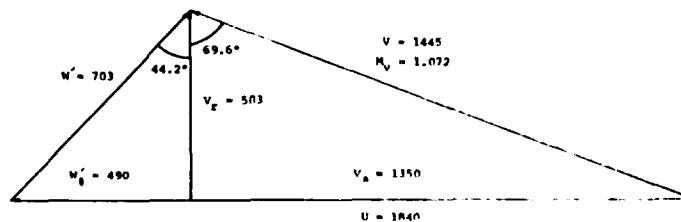
ROTOR INLET
30-PERCENT POWER

ROTOR OUTLET
30-PERCENT POWER

CENTRIFUGAL COMPRESSOR



INLET INLET
30-PERCENT POWER

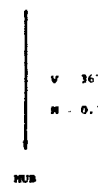
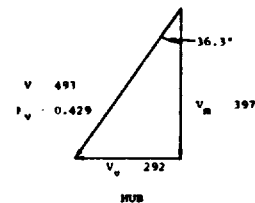
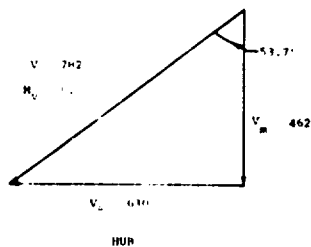
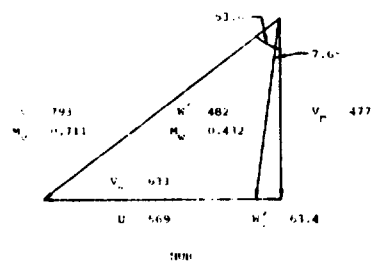
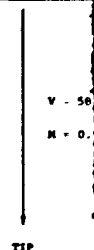
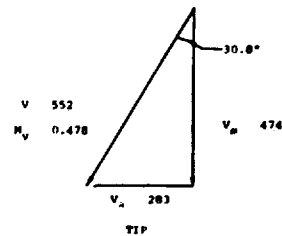
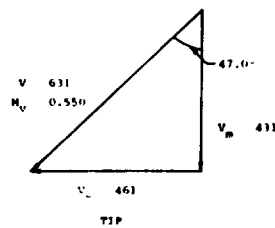
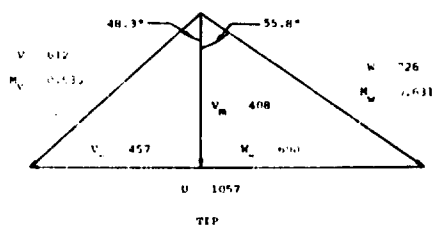


CENTRIFUGAL ROTOR EXIT
30-PERCENT POWER

Figure 45. Compressor Vector Diagrams, 30-Percent Power.

B

AXIAL COMPRESSOR



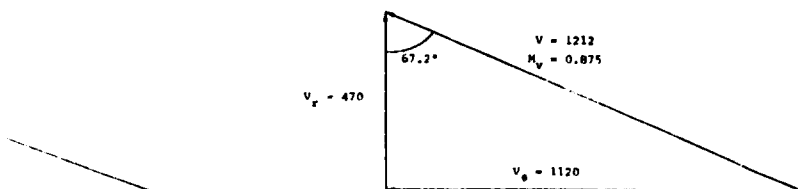
HUB-OUTLET
10-PERCENT POWER

FIRST STATOR INLET
30-PERCENT POWER

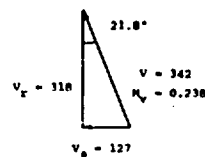
SECOND STATOR INLET
10-PERCENT POWER

SECOND STATOR INLET
30-PERCENT POWER

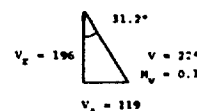
CENTRIFUGAL COMPRESSOR



VANED DIFFUSER INLET

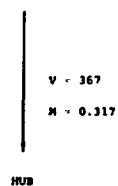
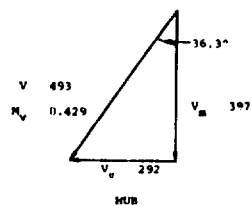
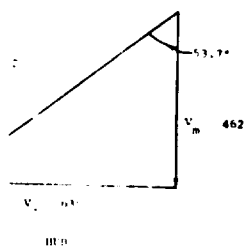
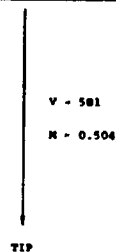
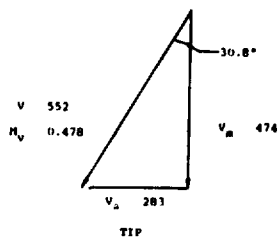
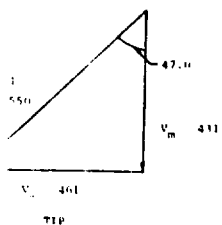


VANED DIFFUSER EXIT
10-PERCENT POWER



COMPRESSOR EXIT
30-PERCENT POWER

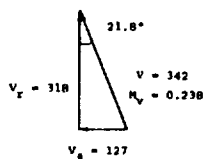
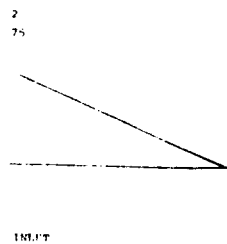
C



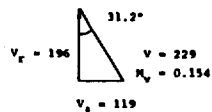
FIRST STATOR INLET
30-PERCENT POWER

SECOND STATOR INLET
30-PERCENT POWER

SECOND STATOR INLET
30-PERCENT POWER



VANED DIFFUSER EXIT
30-PERCENT POWER



COMPRESSOR EXIT
30-PERCENT POWER

A

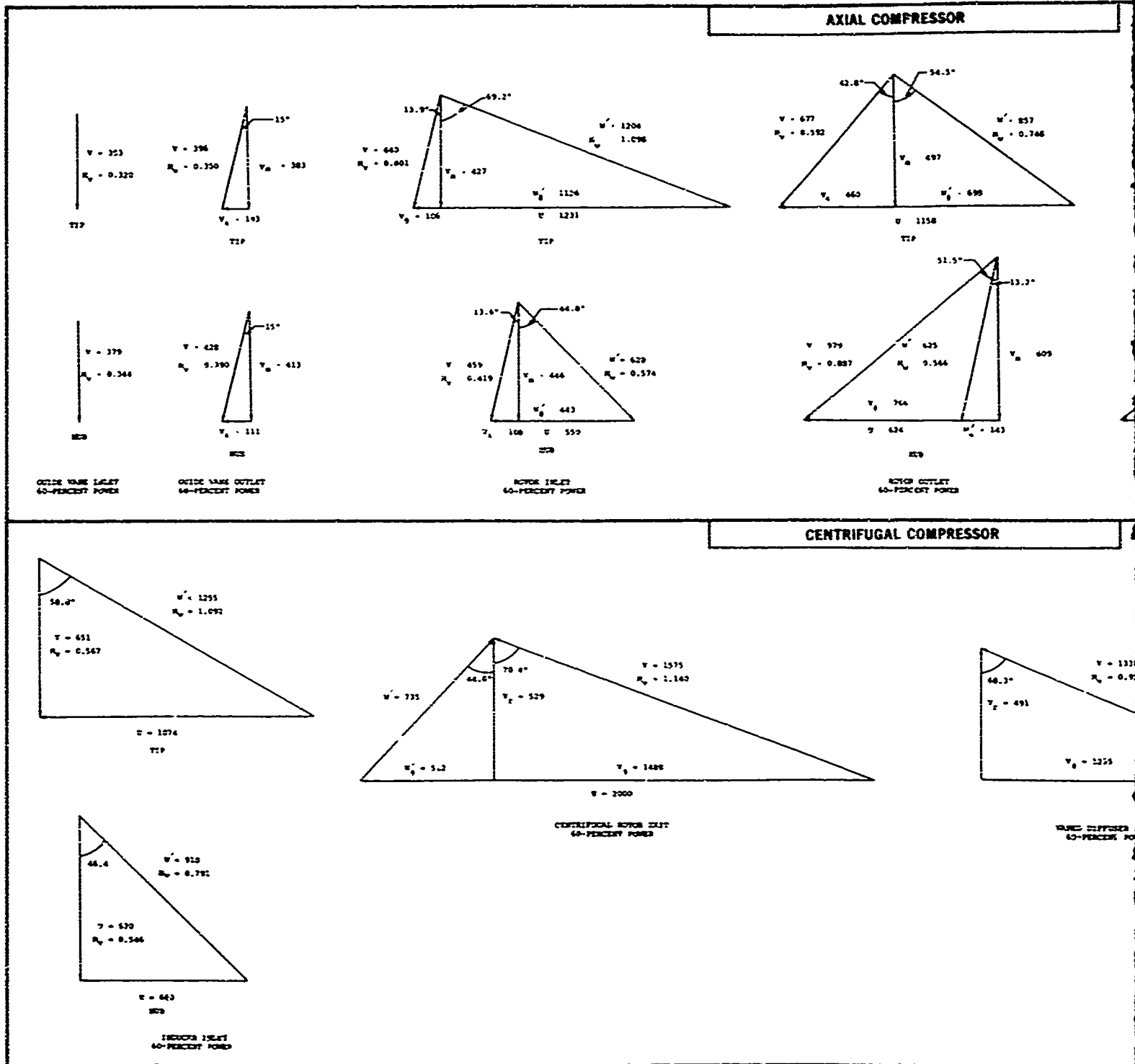
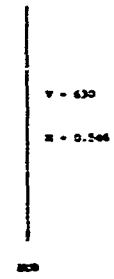
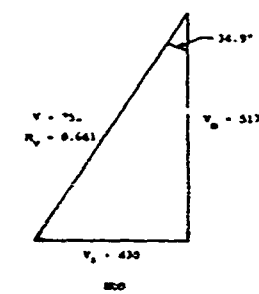
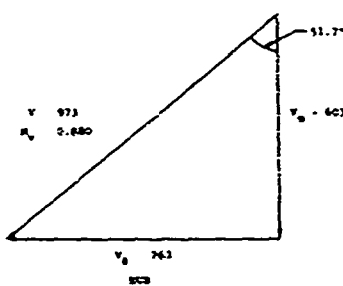
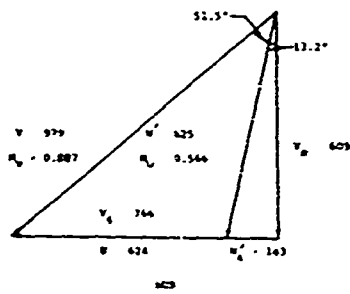
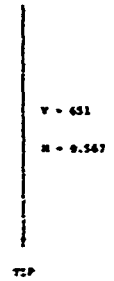
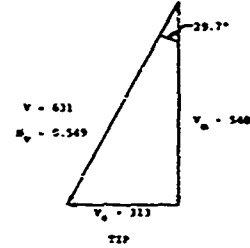
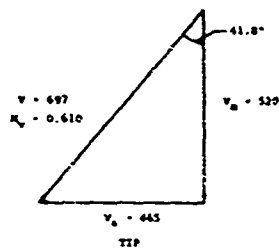
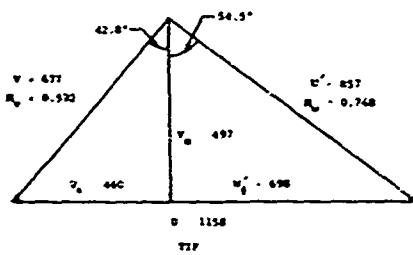


Figure 46. Compressor Vector Diagrams, 60-Percent Power.

B

AXIAL COMPRESSOR



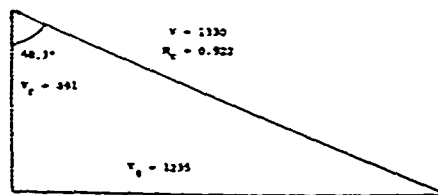
MOTOR INLET
60 PERCENT POWER

FIRST STATOR INLET
60 PERCENT POWER

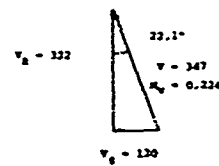
SECOND STATOR INLET
60 PERCENT POWER

SECOND STATOR OUTLET
60 PERCENT POWER

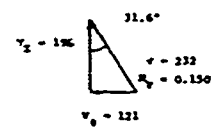
CENTRIFUGAL COMPRESSOR



WARD OFFICE INLET
60 PERCENT POWER



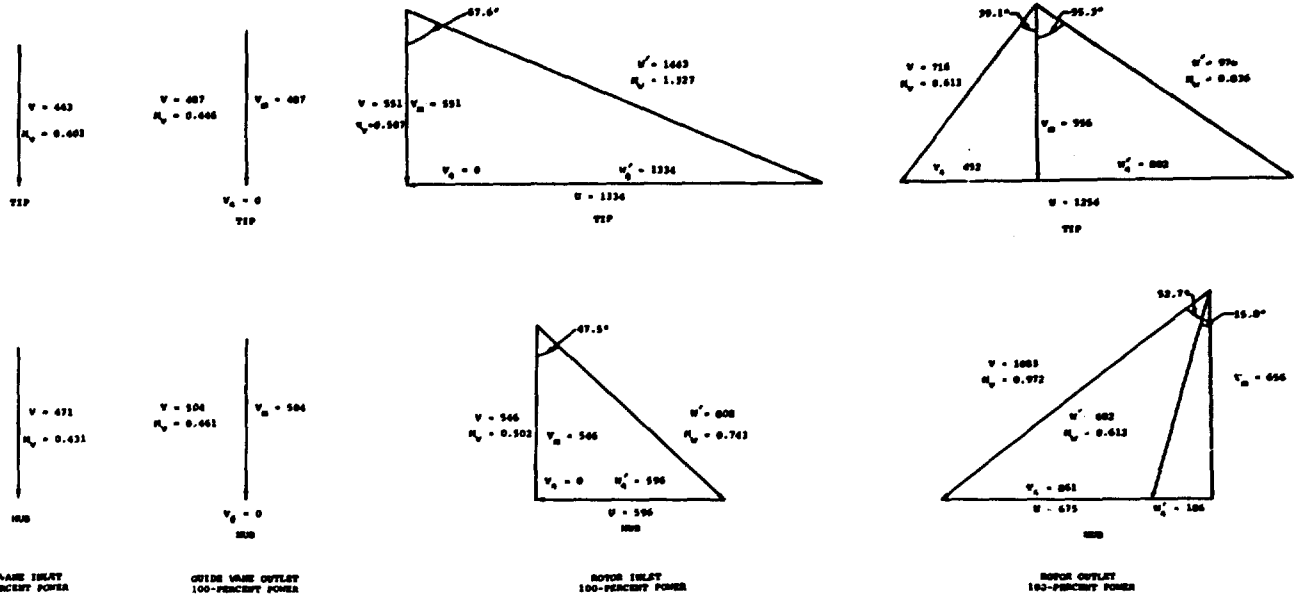
WARD OFFICE INLET
60 PERCENT POWER



WARD OFFICE INLET
60 PERCENT POWER

A

AXIAL COMPRESSOR



CENTRIFUGAL COMPRESSOR

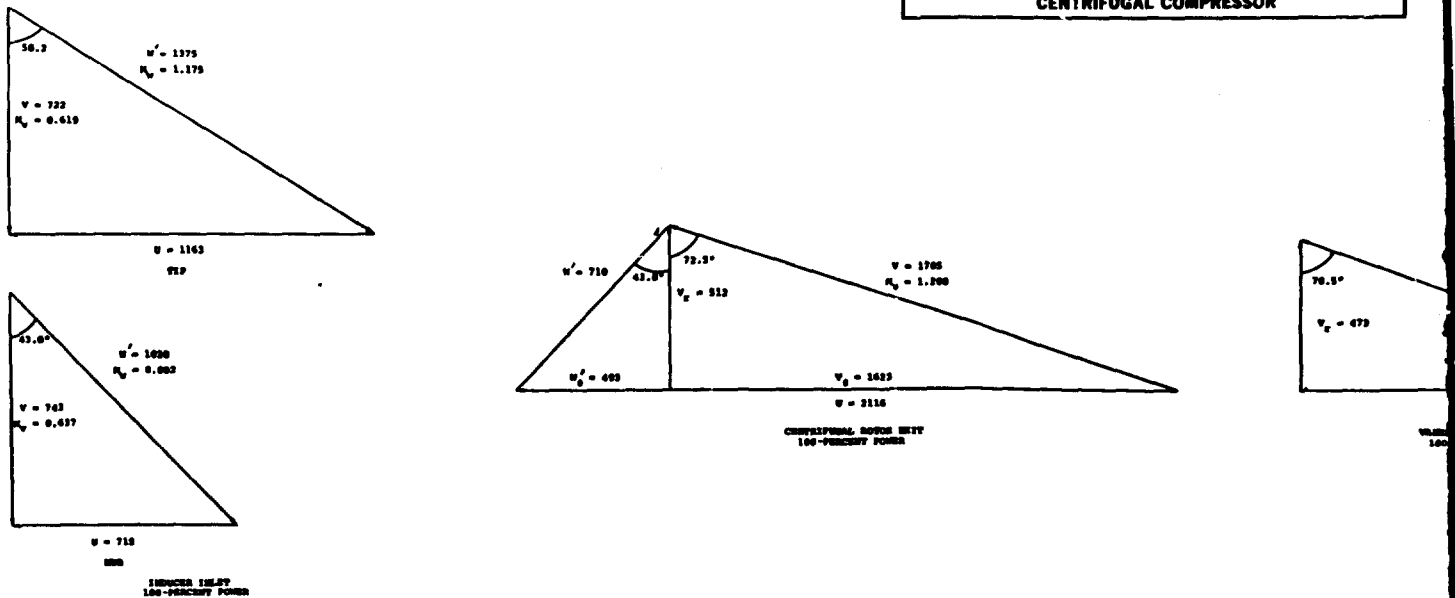
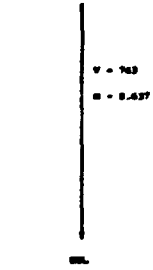
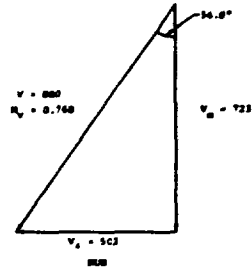
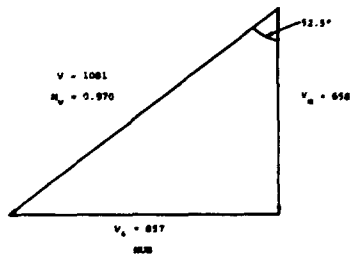
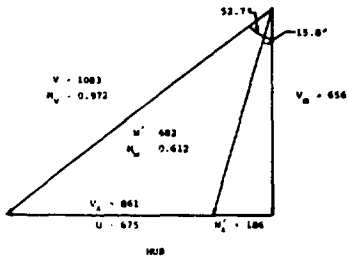
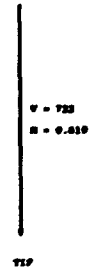
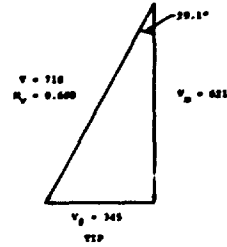
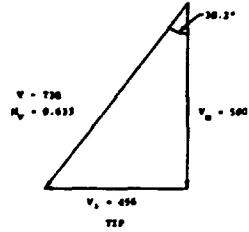
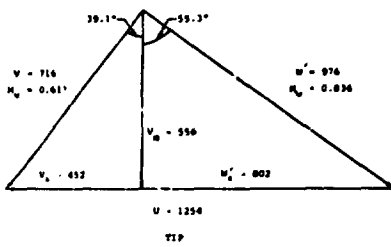


Figure 47. Compressor Vector Diagrams, 100-Percent Power.

13

AXIAL COMPRESSOR



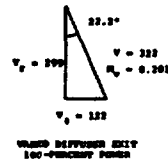
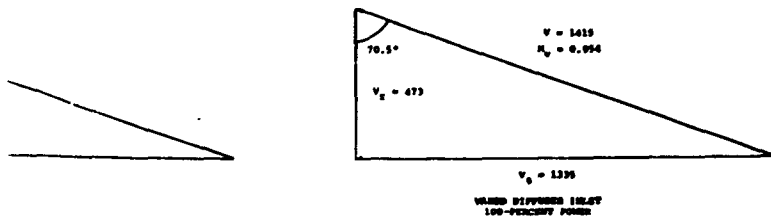
ROTOR OUTLET
100-PERCENT POWER

FIRST STATOR INLET
100-PERCENT POWER

SECOND STATOR INLET
100-PERCENT POWER

SECOND STATOR OUTLET
100-PERCENT POWER

CENTRIFUGAL COMPRESSOR



The surge-to-choke flow range of the centrifugal compressor is basically a result of data correlations from existing in-house compressor rotors and tandem-bladed vaned diffusers. As such, it represents a system of components that have been tested extensively. There are, however, other system components that could provide the range for the particular operating line of this program for the case of a centrifugal compressor preceded by an axial compressor. Reference 2, page 5, shows a compressor map on Figure 175, and Reference 6 shows a compressor map on Figure 19 that could provide adequate range. Both these compressors use radial-bladed rotors. In Reference 2, the vaned diffuser is a rectangular passage diffuser (vane island); and in Reference 6, the diffuser is conical (pipe diffuser).

Figure 48 shows a dimensionless comparison of the compressor map estimated for this study and those taken from References 2 and 6. Included on the comparison are the four operating points from the final cycle results. The surge line of the Boeing compressor parallels that of the AiResearch-estimated map. The Pratt and Whitney surge line needs more development work in the vicinity of the 100-percent-power point. However, on the whole, it is clear that high-pressure-ratio centrifugal compressors can be designed with adequate surge margin for the conditions (match with axial compressor, free power turbine, etc.) of this study. The emphasis on state-of-the-art advancement lies on improving the efficiency level.

The efficiency levels displayed in Part B of Figure 44 represent values expected to be achieved in a 3-year development period. The range required at the 60-percent power point at an efficiency of 0.76 at the design-point pressure ratio of 7.1:1 have been demonstrated. Development of the compressor was not completed, but examination of the test results showed 1.0 percentage point lost because the diffuser design diffusion was not achieved. With proper redesign and the use of a parametric study as outlined in Section 3.2 to determine the rotor exit blade for optimum system efficiency, a design-point efficiency of 0.786 is achievable. Figure 16 shows a 1.5-percentage-point increase in efficiency between a stage with a radial-bladed rotor and one with a blade exit angle of 50 degrees.

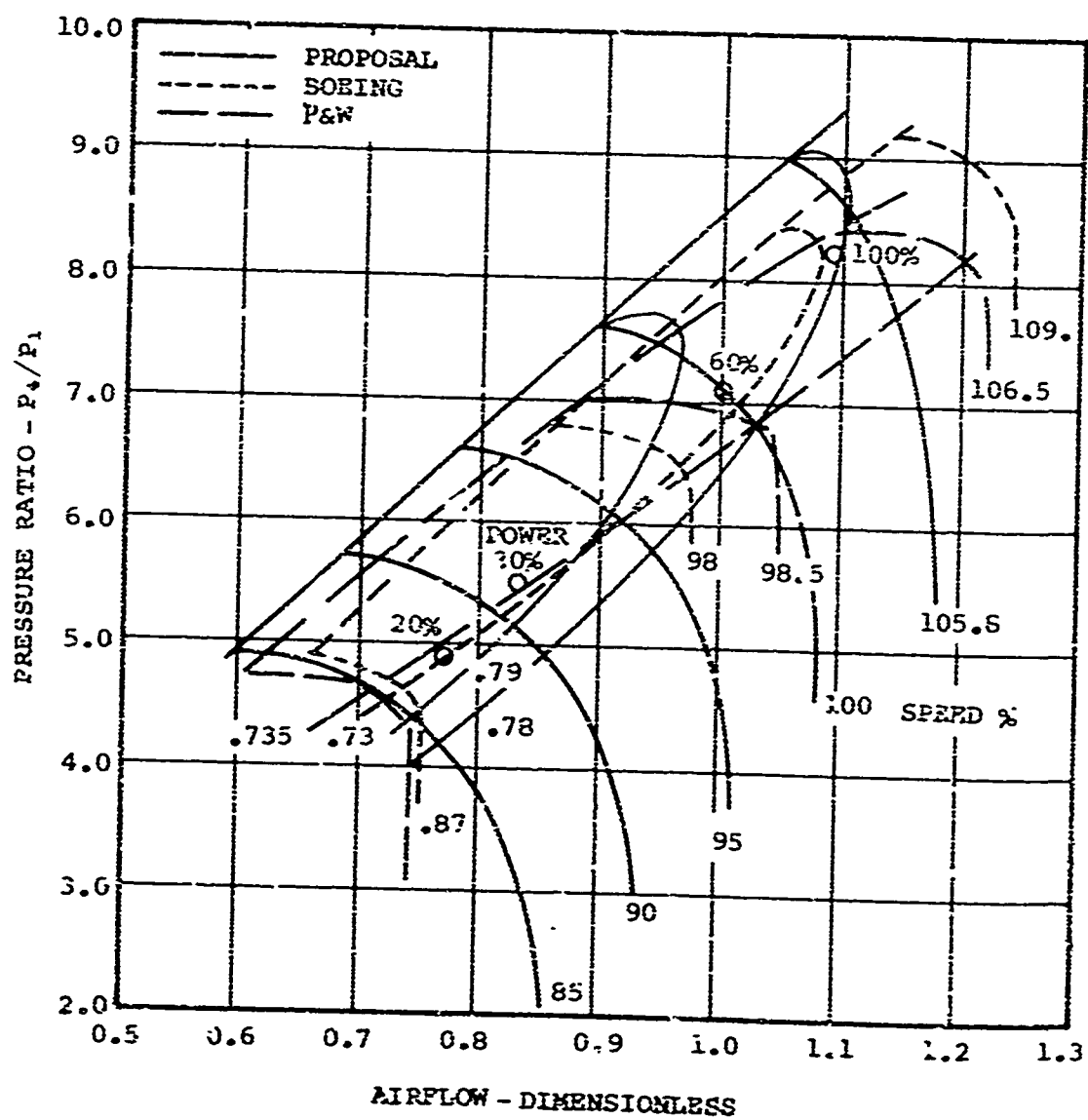


Figure 48. Compressor Map Comparison.

The matching studies conducted on this program reveal the need for an extended range of surge-free operation for 20-percent-power operation. This is close to the maximum achieved experimentally but is not an established design capability. This is the technological achievement required of the axial compressor in order for the inlet guide vane to be the only variable blade row. Otherwise, a variable stator may be required. This is true whether the axial compressor has one or two stages. It is possible that the range of surge-free operation could be achieved by examining influences such as blade loading, aspect ratio, and solidity. This was not undertaken in the design procedure, since it was considered to be beyond the scope of a preliminary design task.

In summary, the axial compressor requires a design capability for a wide range of surge-free operation, the shift of the pressure-ratio characteristics with 15° of preswirl change needs to be established, and the efficiency predicted for the centrifugal compressor has to be validated. An alternate configuration to achieve the overall compressor matching would be a two-stage centrifugal compressor. No variable geometry would be required, since the range of surge-free operation is well within centrifugal compressor technology. This is especially true of compressors with rotors having backward-leaning blades.

7. TASK IV, ENGINE PERFORMANCE PREDICTION

7.1 GENERAL

A compressor consisting of two axial stages and one centrifugal stage was selected for continuing study as a result of Task IA. Very satisfactory performance, showing a close approach to idealized values, was calculated for this compressor combination with use of variable inlet guide vanes during the study conducted under Task IIA. When preliminary engine layouts were attempted during Task IIB, difficulty was encountered in achieving a satisfactory mechanical design for an engine employing a concentric power-output shaft. The inlet hub diameter of the two-stage axial compressor proposed for this engine was too small, in combination with the unsupported shaft length required, to achieve (at first analysis) an acceptable shaft design with the use of the materials and technology anticipated to be available in 3 years.

The larger shaft diameter and shorter length provided by a single-stage axial compressor offered an immediate solution to the shafting problem. A modified two-stage axial compressor design, in conjunction with more detailed shaft analysis and mechanical design ingenuity, might be expected to solve the problem, but since preliminary cycle analysis had indicated only a small (0.004) increase in SFC with a single-stage axial and a single-stage centrifugal compressor, this combination was selected for final analysis within the contracted work.

7.2 CALCULATION PROCEDURE

Engine performance calculations were conducted for a single-spool gas generator operating with a design-point pressure ratio of 10.5:1. A single-stage axial compressor incorporating variable inlet guide vanes (AVIGV) and a fixed-geometry single-stage centrifugal compressor (CFG) were used in a direct-coupled combination. Cycle calculations were made for 50° decrements in TIT from 2500°F to 1500°F. A TIT of 2090°F was also used because this temperature was expected to yield 60-percent power, the design point. The cooling air, 9 percent of the compressor airflow, was assumed to re-enter the cycle upstream of the power turbine.

7.3 OVERALL COMPRESSOR PERFORMANCE

The trend of the overall compressor adiabatic efficiency as a function of power output (Figure 49) illustrates that the primary objective of the compressor matching study--obtaining maximum efficiency at 60-percent power--has been achieved. The maximum efficiency predicted for the actual matched AVIGV + CFG compressor having adequate surge margin is 0.788 compared to the maximum value of 0.804 predicted in Task IA cycle studies. The compressor efficiency decreases by approximately one point at both 20-percent power and at 100-percent power, which indicates good performance over the required power range.

The airflow ratio of about 1.21 required between 60- and 100-percent power can be achieved by 15° of inlet guide vane actuation, opening as speed and power increase to 100 percent and closing as speed and power decrease to 60 percent. As illustrated on Figure 49, the corrected airflow at 100 percent power is 3.53 pounds per second--about 21 percent greater than the design airflow of 3.0 pounds per second.

The decrement of 1.6 points in overall compressor efficiency is significantly greater than was anticipated between the use of single-stage and two-stage axial compressors. The greater decrement resulted from the detailed examination which the centrifugal compressor required to produce a pressure ratio of 7.1:1 while being supercharged. Greater losses were calculated than anticipated in the diffuser, both in the vaneless space and in the vanes.

7.4 GASIFIER TURBINE PERFORMANCE

Since the turbine driving the compressors operates at only one value of corrected flow, work coefficient, and corrected speed over most of the required power turbine output range, it was to be expected that the gasifier turbine efficiency would remain essentially constant at approximately 0.872 (Figure 49). The actual speed varies from about 52,700 rpm to 64,600 rpm as the power turbine output increases from 20 to 100 percent.

At 60-percent power, the gasifier turbine inlet temperature decreases about 410° from the maximum value of 2960°R (2500°F) selected for 100-percent-power operation. This temperature change is in close agreement with cycle calculations conducted during Task IA, which employed simplified and idealized component characteristics for preliminary predictions.

7.5 POWER TURBINE PERFORMANCE

A maximum efficiency of 89.0 percent is obtained at 60-percent power (Figure 49). A decrease of 4 points is predicted as power output is increased to 100 percent, and a decrease of 12 points as power output is decreased to 20 percent. Although other design-point selections could have been made to improve efficiency at 20-percent power, a sacrifice in performance at 60- and 100-percent power would have resulted.

7.6 ENGINE PERFORMANCE

The SFC calculated at 60-percent power is 0.491; the 30- and 100-percent power point SFC's are 0.630 and 0.452 respectively. For the 60- and 100-percent power points, the SFC values are approximately 0.012 point or 2.5 percent greater than estimated during the Task IA preliminary cycle analysis. At the design point, the power calculated for a 3-pound-per-second-airflow engine is 454.7 horsepower for a specific power of 151.5 horsepower per pound per second. At full power, the corresponding values are 757.2 horsepower and 208.0 horsepower per pound per second. The predicted performance is believed to be very good for an engine of this small airflow and power.

The primary reason for the greater SFC calculated for this engine compared to the preliminary cycle studies is the lower overall efficiency obtainable with this AVIGV + CFG compressor compared to the AAVIGV + CFG compressor. Even if the mechanical design problem can be solved, and it probably can, an evaluation of the trade-offs between performance and complexity and diameter versus length will be required before the best choice of compressor for an engine of this size can be made.

A

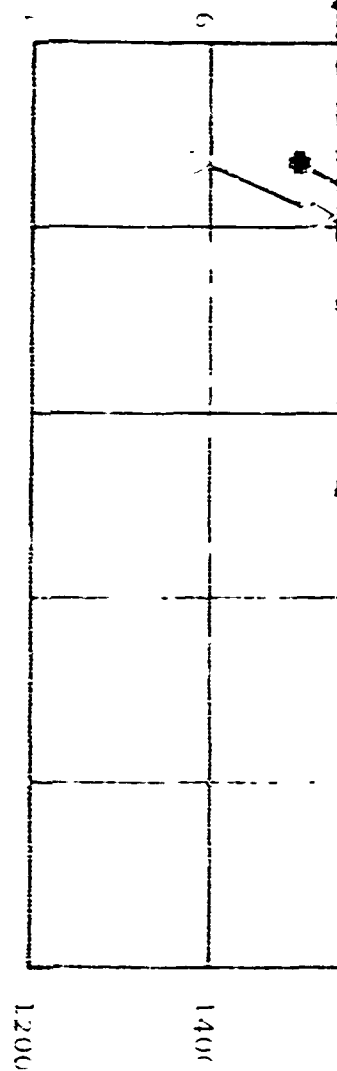
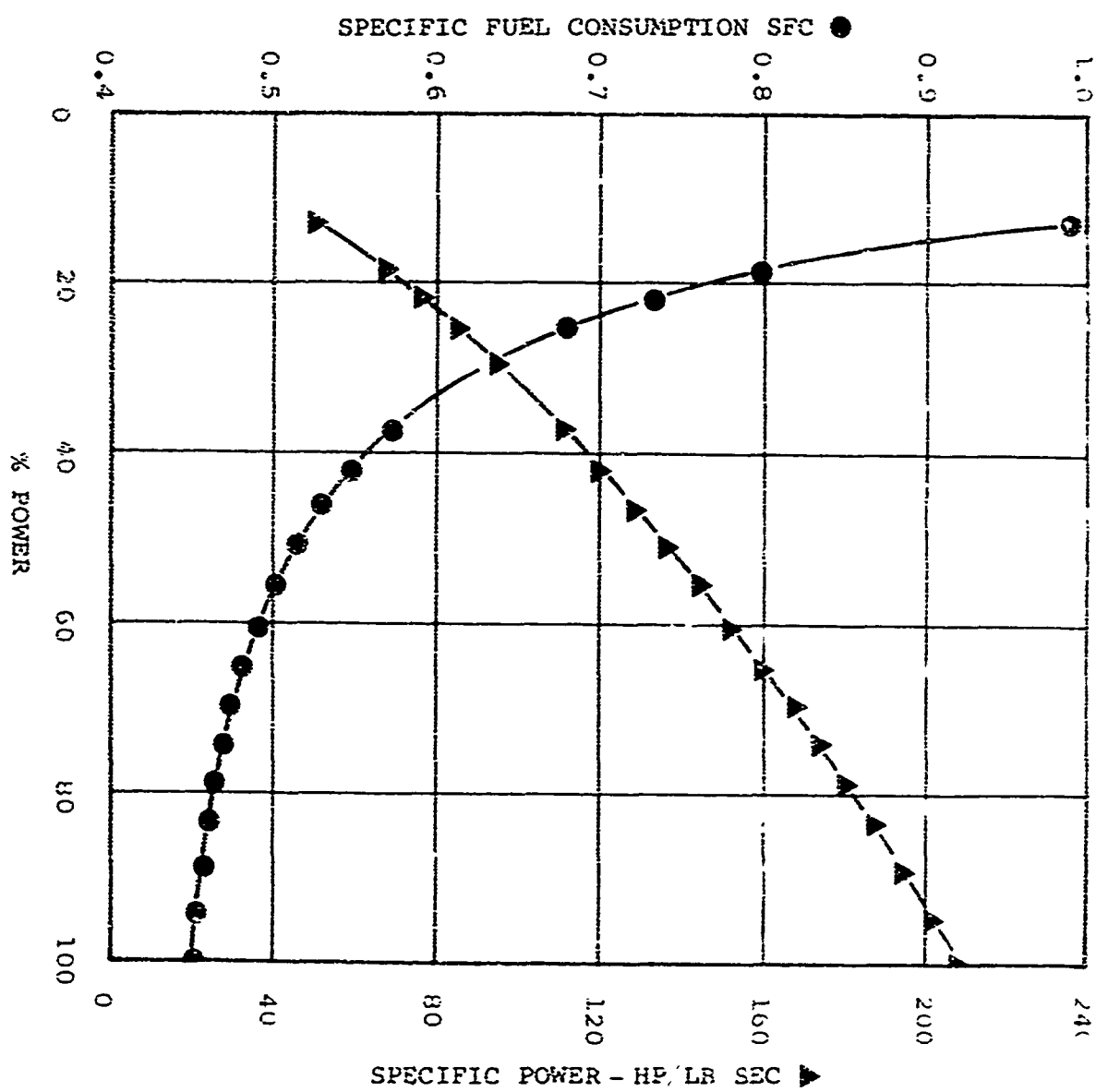
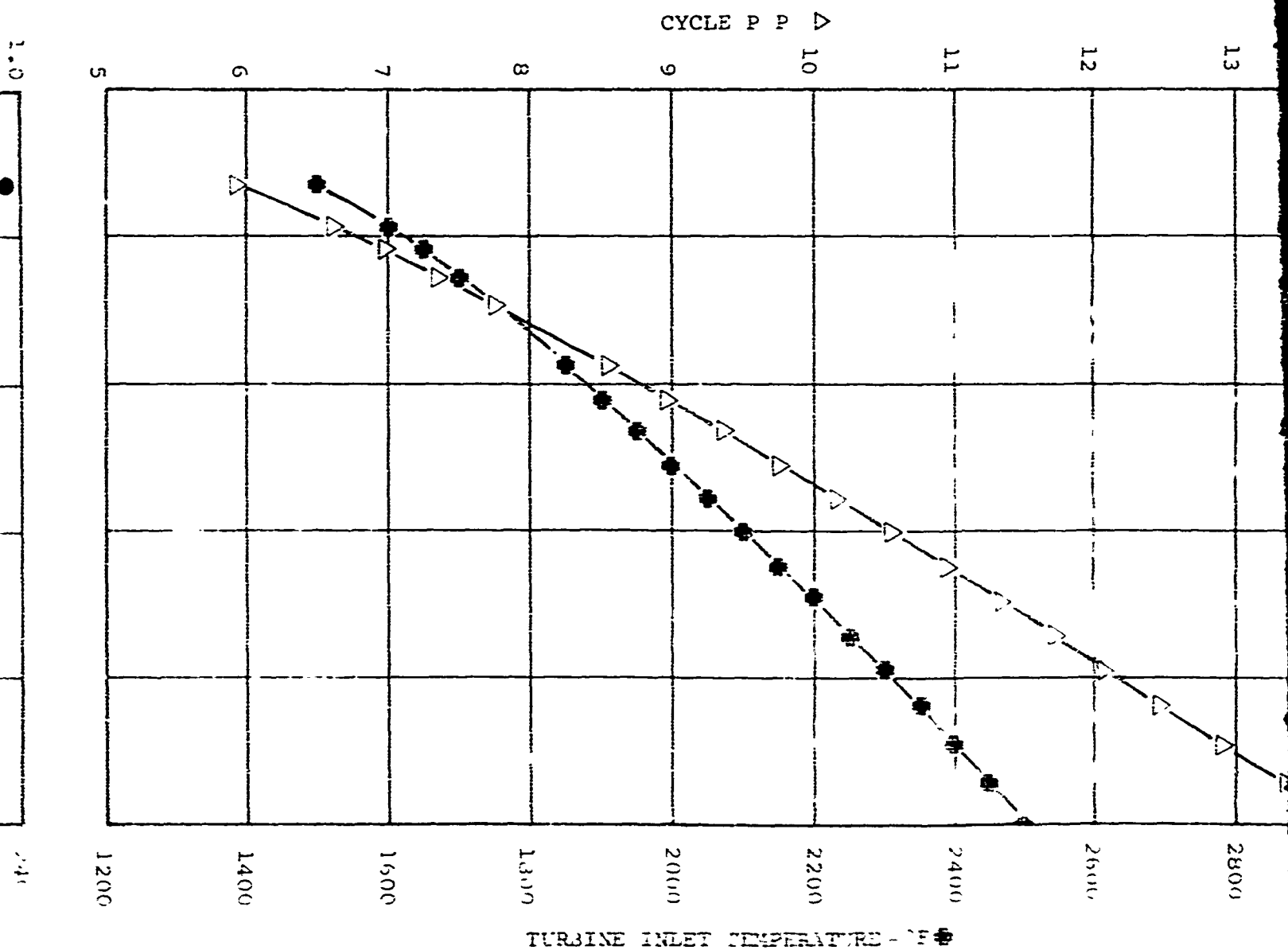
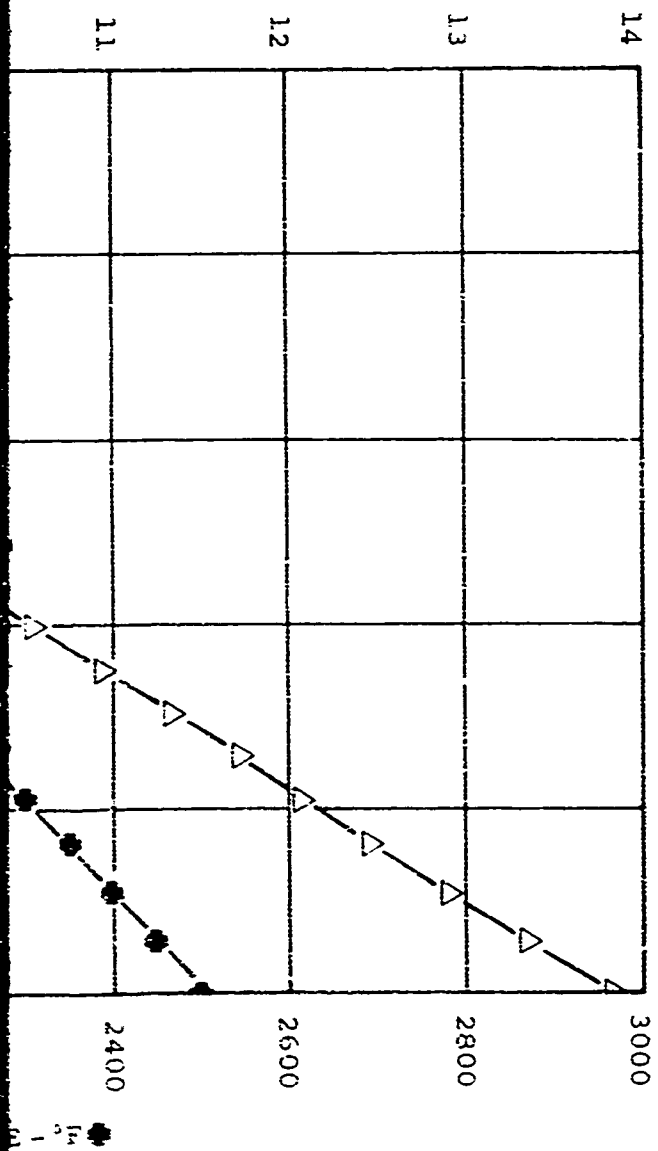
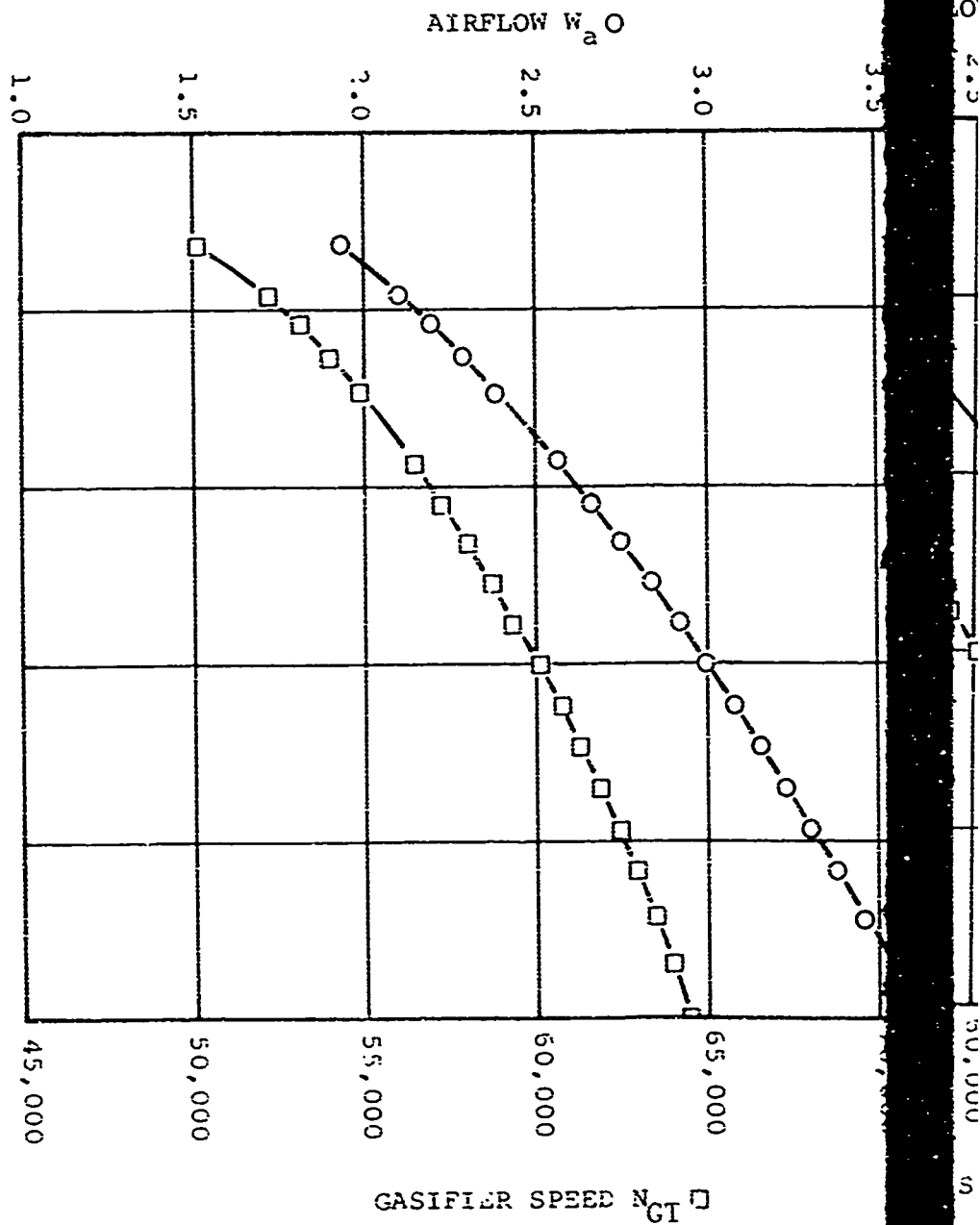
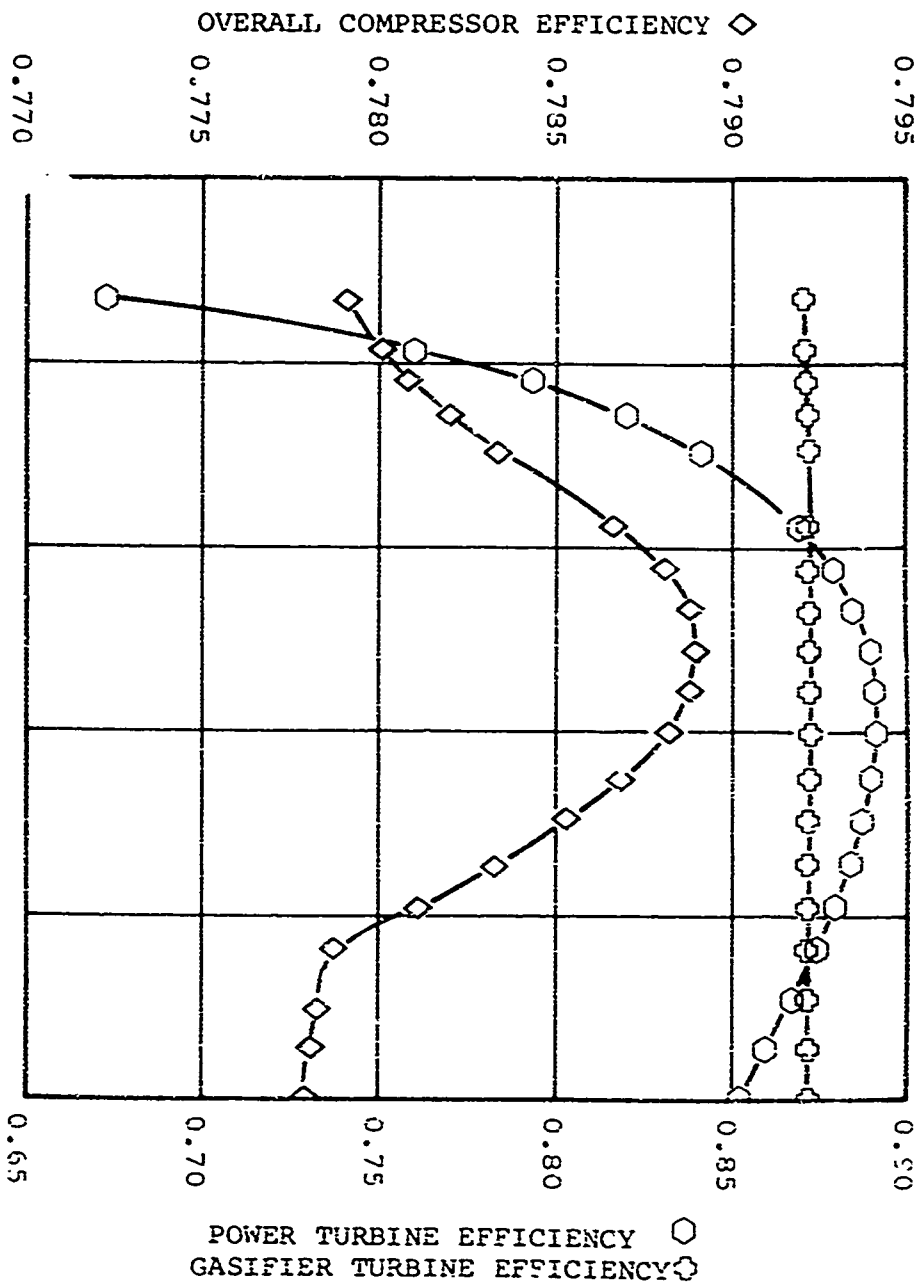


Figure 49. Engine Performance Parametric Plots.

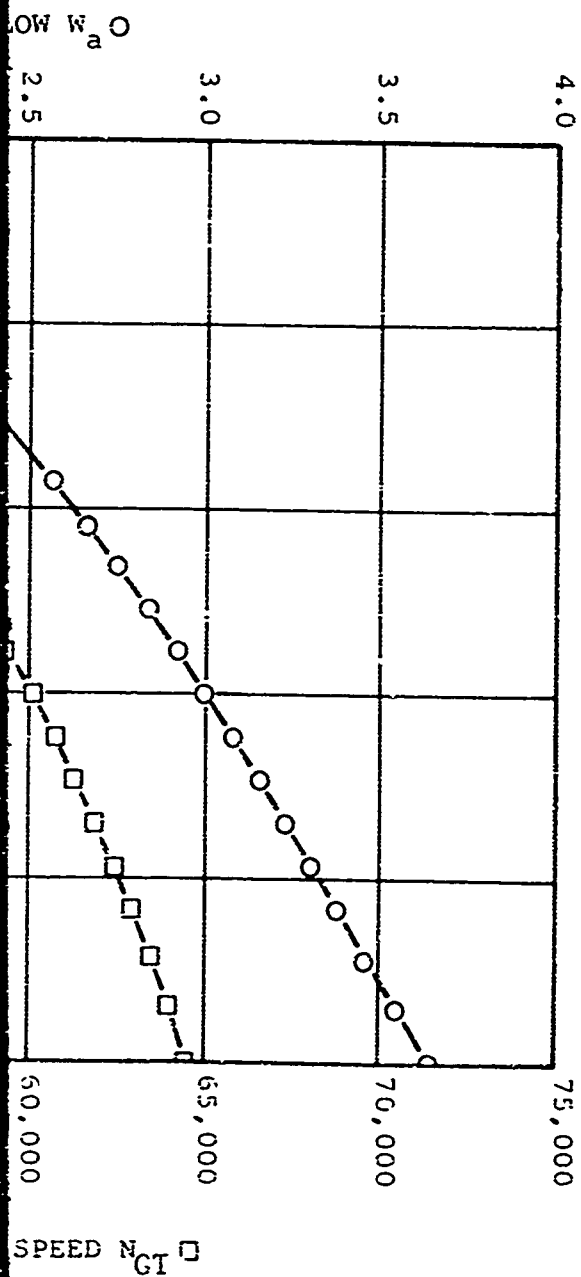


C





7



8. CONCLUSIONS AND RECOMMENDATIONS

8.1 GENERAL

This study program has been conducted to explore the compressor matching considerations appropriate to achieve a useful combination of axial and centrifugal compressors for small gas turbine engines (2 to 5 pounds per second). A representative engine was defined to facilitate this study and is characterized as follows:

1. The turboshaft engine has a front drive.
2. All engine component performance levels are advanced but considered to be achievable within a 3-year development period. Components are optimized for design-point operation, defined as 60-percent power, and sized for 3.0 pounds per second flow at the design point.
3. The compressor is a combination of axial stages (one or two) and a centrifugal stage.
4. The turbine consists of a gasifier section, cooled to allow 100-percent-power operation at 2500°F (TIT), and a free power turbine.
5. The engine operating range is 20- to 100-percent power, and performance emphasis is on SFC at 60-percent power (first priority) and 30-percent power (second priority).

The conclusions and recommendations presented below are based on the compressor matching study made for the representative engine as defined.

8.2 CONCLUSIONS

1. The best matching arrangement of a single-spool compressor for part-load SFC and surge-free operation was selected to be a combination of variable inlet guide vanes for the axial compressor and fixed geometry for the centrifugal compressor.
 - a. A fixed-geometry arrangement yields a poor match for the axial compressor, resulting in poor performance and axial compressor stall at part load.

- b. The other cases of variable geometry studied, including combinations of variable geometry, offer no advantage over the selected arrangement.
- 2. Twin spooling with fixed geometry yields a good compressor match for part-load performance and for surge-free operation over the operating range.
 - a. Front-drive requirement complicates this arrangement to a degree that it could not be justified.
- 3. A single-spool compressor incorporating either a single- or a two-stage axial compressor can be configured to be compatible with the front-drive requirement.
 - a. A two-stage axial compressor offers a performance advantage due to 1.5 points higher potential compressor efficiency.
- 4. A useful combination of axial and centrifugal compressors can be configured and matched for this engine to achieve the following performance levels:
 - a. Single-stage axial SFC at 60-percent power, 0.491.
 - b. Two-stage axial SFC at 60-percent power, 0.479.
- 5. Requirements for compressor state-of-the-art advancements are identified to be:
 - a. Develop axial compressor for a broad choke-to-surge range when combined with variable inlet guide vanes.
 - b. Develop centrifugal compressor for increased efficiency levels while maintaining broad choke-to-surge range.
- 6. The optimum 60-percent power pressure ratio for an engine having 2500°F TIT at 100-percent power is as follows:
 - a. AA + C compressor, 10.5:1
 - b. A + C compressor, 10.0:1

8.3 RECOMMENDATIONS

1. Conduct limited studies to complement the results of this program as follows:

- (a) Complete the preliminary design, matching analyses, and engine layout studies for a two-stage axial plus centrifugal compressor (AAVIGV + CFG). These studies should provide for direct comparison with the results reported herein for an AVIGV + CFG compressor, $P_4/P_1 = 10.5:1$.

- (b) Conduct preliminary design, matching analyses, and engine layout studies for a two-stage centrifugal compressor with fixed geometry.

The study should provide for direct comparison with the AAVIGV + CFG compressor in accordance with (a) above and with the AVIGV + CFG compressor as reported herein.

Select the best compressor combination for the engine defined for these studies. If an axial-centrifugal compressor combination is selected, then conduct development programs as set forth in Recommendations 2 and 3 below.

2. It is recommended that a program be conducted to develop a two-stage axial compressor meeting the requirements of the 10.5:1-pressure-ratio engine cycle. Variable inlet guide vanes and variable stators should be employed in the developmental test vehicle to permit economical stage matching for design and off-design conditions.
3. If further study with the two-stage axial compressor configuration indicates more variable geometry is needed than with the single-stage configuration, it is recommended that a development program be conducted to verify experimentally the single-stage axial plus centrifugal compressor combination with the variable inlet guide vanes.

9. LITERATURE CITED

1. Muller, C.H., and Sabatink, A., The Development of Supersonic Axial Compressor Boost Stages for Small Gas Turbines, Curtiss-Wright Corporation; ASME Paper No. 69-GT-44, March 1969.
2. Welliver, A. D., and Acurio, J., Design and Development of Small, Single-Stage Centrifugal Compressor, The Boeing Company; USAAVLABS Technical Report 67-47, U.S. Army Aviation Materiel Laboratories, Fort Eustis, Virginia, September 1967, AD 385595L.
3. Lieblein, S., ANALYSIS OF EXPERIMENTAL LOW-SPEED LOSS AND STALL CHARACTERISTICS OF TWO-DIMENSIONAL COMPRESSOR BLADE CASCADES, NACA RM E57A28, 1957.
4. Swan, W. C., A PRACTICAL METHOD OF PREDICTING TRANSONIC COMPRESSOR PERFORMANCE, Journal of Engineering for Power, Trans. ASME, Series A, Vol. 83, pp. 322-330, 1961.
5. Davis, James V., ADVANCEMENT OF SMALL GAS TURBINE COMPONENT TECHNOLOGY, ADVANCED SMALL AXIAL COMPRESSORS, Continental Aviation and Engineering Corporation; Defense Documentation Center, Cameron Station, Alexandria, Virginia, Report No. 1033, December 1966, AD 386098.
6. Morris, R. E., and Kenny, D. P., HIGH PRESSURE RATIO CENTRIFUGAL COMPRESSORS FOR SMALL GAS TURBINES, United Aircraft of Canada Limited, Document No. 6, prepared for the 31st Meeting of the Propulsion and Energetics Panel of AGARD "Helicopter Propulsion Systems," Ottawa, Canada, June 1968.

APPENDIX I
CYCLE ASSUMPTIONS
FOR
ENGINE DESIGN-POINT ANALYSIS

Component efficiencies and other required cycle performance parameters assumed for the design-point engine analysis are listed.

- (a) Lower heating value: 18,400 Btu per lb
- (b) Sea-level, standard-day performance
- (c) Accessory horsepower: 1.5 hp per lb per sec of mass flow
- (d) Combustion efficiency: 0.99
- (e) Combustor pressure loss: $\Delta P/P = 0.04$
- (f) Mechanical efficiency: 0.98
- (g) Compressor leakage flow: $\frac{W_L}{W_C} = 1.5$ percent
- (h) Transition duct loss between the gas generator turbine and the power turbine: $\Delta P/P = 0.02$
- (i) Compressor efficiency: A two-stage axial plus single-stage centrifugal compressor was assumed. The overall efficiency-versus-pressure-ratio characteristics are as shown in Figure 7 of the main body of this report. As listed in Figure 7, the 60,000-rpm rotational speed line was selected for the design-point analysis.
- (j) Gasifier-turbine component efficiency: Efficiency variance for the two-stage gasifier turbine is from 88.7 percent for a pressure ratio of 8:1 to 81.5 percent for a pressure ratio of 20:1. The gasifier turbine efficiency, on a total-to-total basis, was varied as a function of compressor pressure ratio as shown in Figure 50.
- (k) Power turbine efficiency: The total-to-static efficiency is 89.0 percent for the pressure-ratio range of consideration.

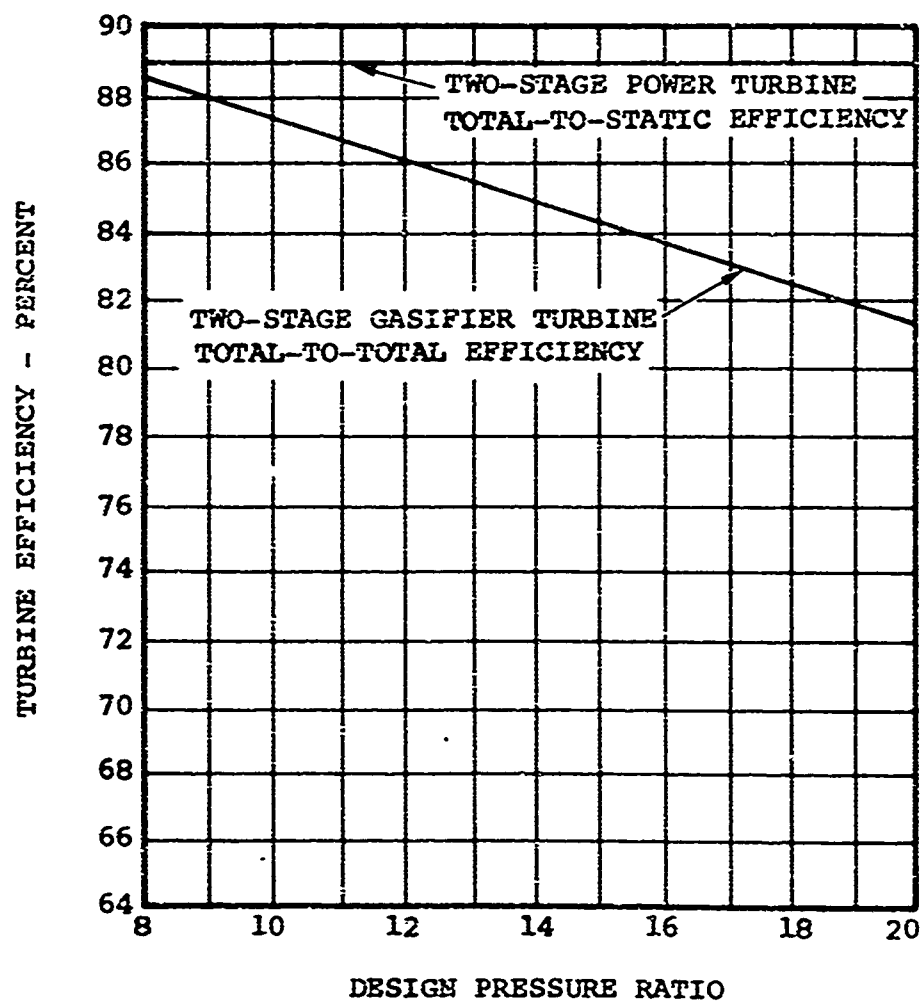


Figure 50. Turbine Design-Point Efficiency Versus Engine Cycle Pressure Ratio.

APPENDIX II

CYCLE ASSUMPTIONS FOR ENGINE OFF-DESIGN ANALYSIS

Component performance and other required cycle parameter data assumed for the engine off-design analysis are presented in this appendix.

TURBINE COMPONENT MAPS

Maps for the gasifier turbine are presented in Figure 51 and show, respectively, (a) efficiency ratio ($\eta_T/\eta_{T,DP}$) versus

isentropic head ratio ($\frac{\Delta H/T_s}{\Delta H/T_{s,DP}}$) and (b) corrected airflow ($W_s\sqrt{\theta_s}/\delta_s$) versus turbine pressure ratio (P_8/P_7).

Similar maps for the power turbine are presented in Figure 52.

These maps relate off-design component performance to design values. Design values for component efficiency have been estimated for various cycle pressure ratios and are presented in Appendix I. The combined data represented in these plots were used to fully define the turbine component performance for the engine analysis (off-design) as conducted in Task 1A and reported in Section 2.

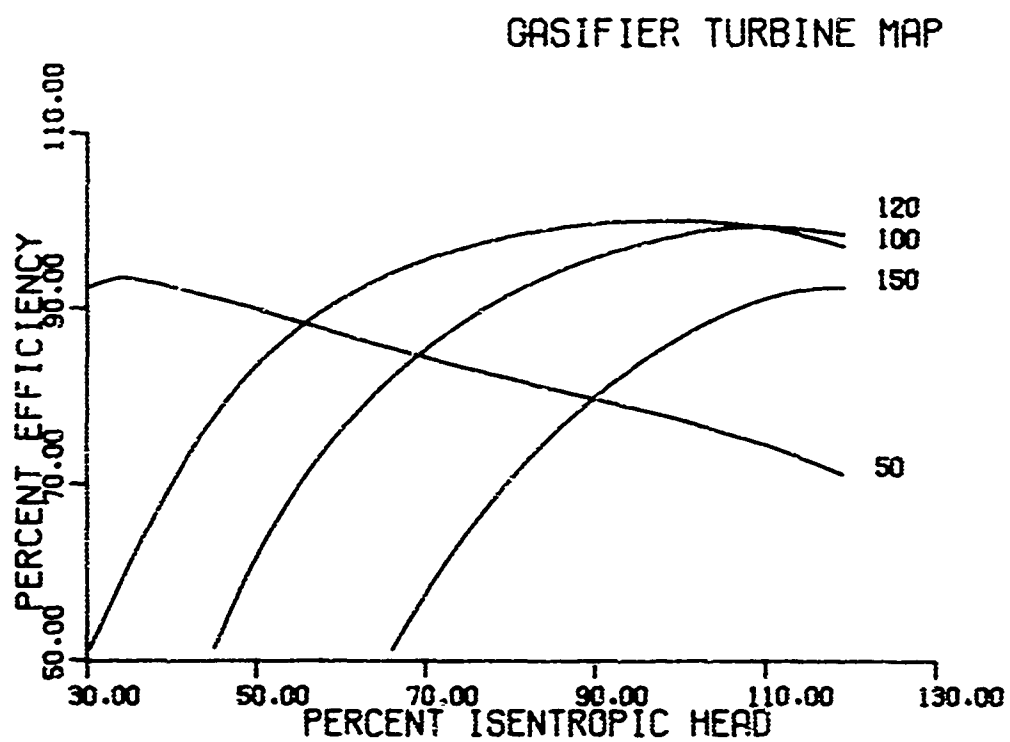
IDEALIZED COMPRESSOR MAP

A two-stage axial compressor map was matched with a representative centrifugal compressor map, and an overall compressor map was determined. Based on this, an idealized compressor map was plotted by noting the maximum pressure ratio and maximum efficiency for the various speed lines. These values were plotted without limiting range versus flow.

The idealized compressor map was then nondimensionalized and is presented in Figure 53. In this figure, efficiency ratio ($\eta_C/\eta_{C,DP}$) and pressure-rise ratio $[(P_4/P_1)-1]/[(P_4/P_1)-1]_{DP}$

are plotted versus corrected flow ratio $\frac{W_N\sqrt{\theta_1}/\delta_1}{W_N\sqrt{\theta_1}/\delta_1}_{DP}$ with

speed ratio $\frac{N_C\sqrt{\theta_1}}{N_C\sqrt{\theta_1}}_{DP}$ as a parameter.



GASIFIER TURBINE MAP

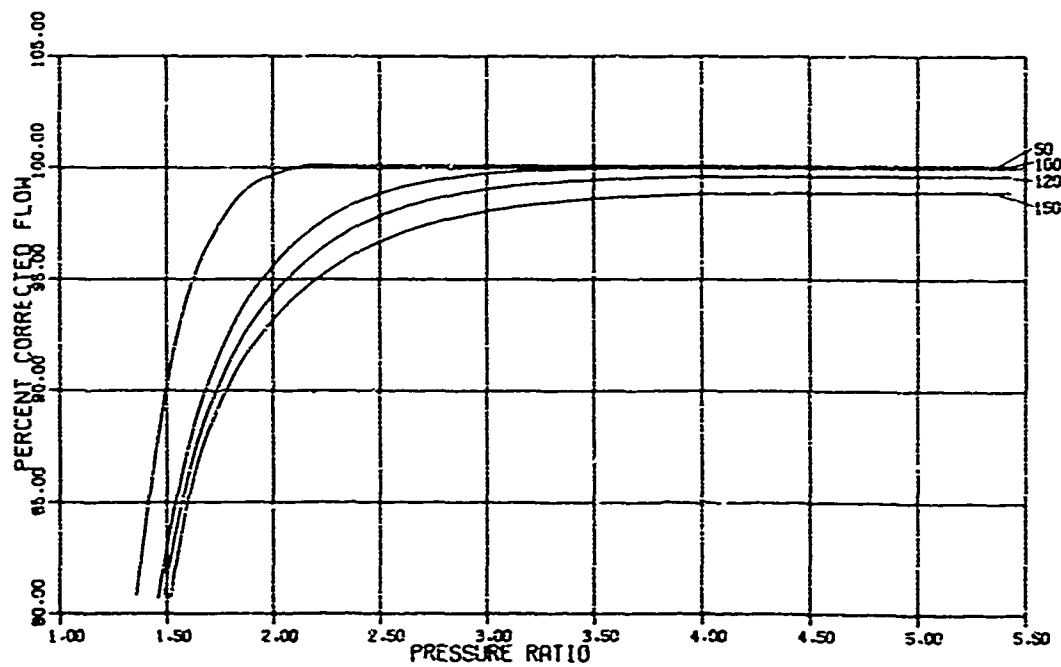
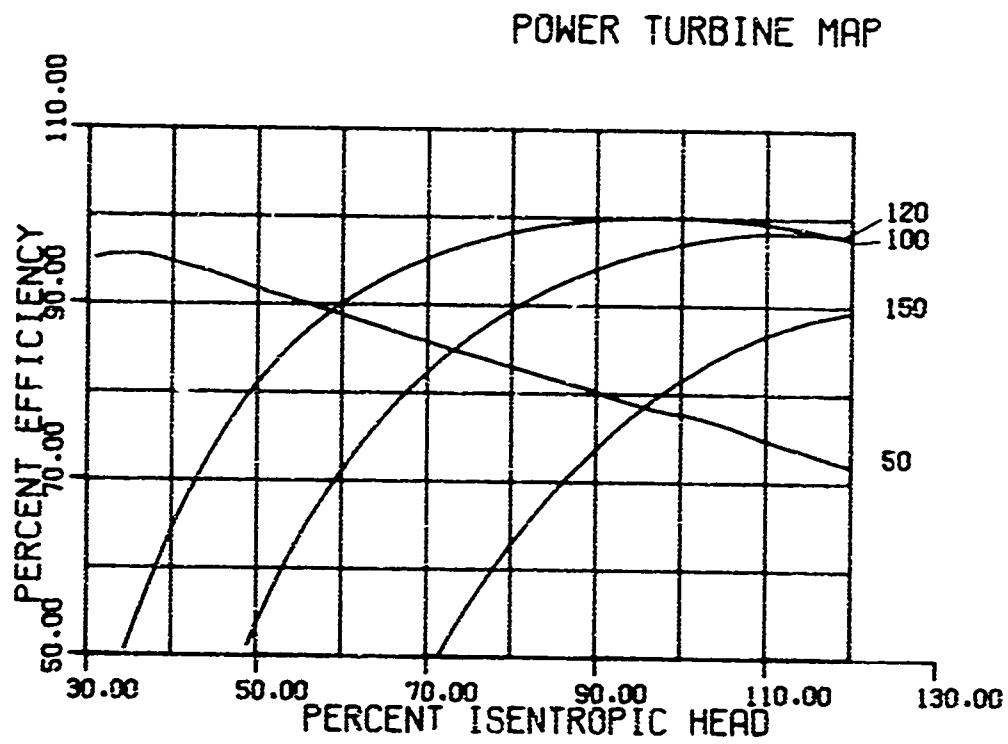


Figure 51. Gasifier Turbine Map.



POWER TURBINE MAP

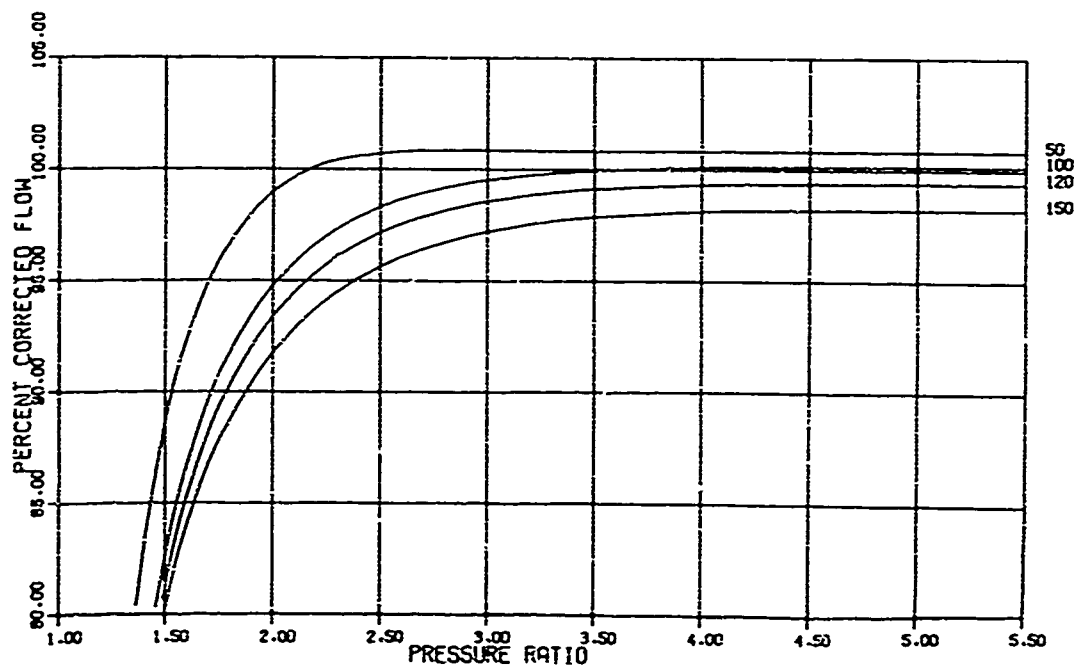
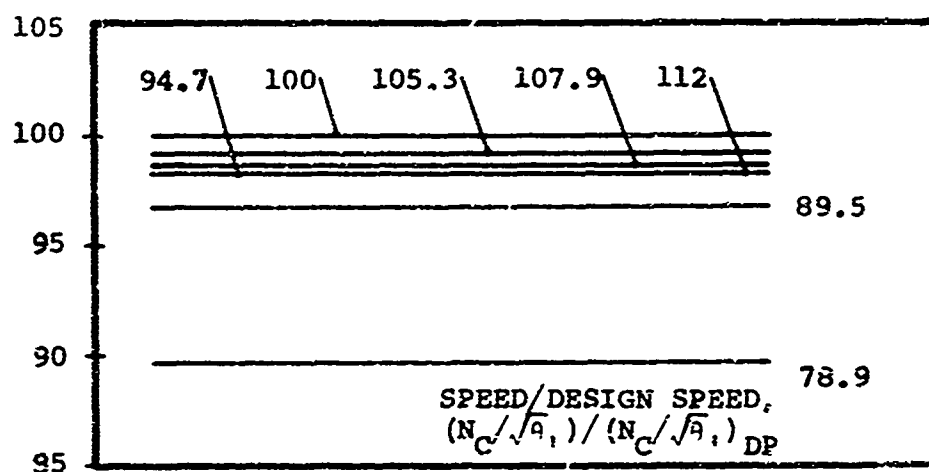
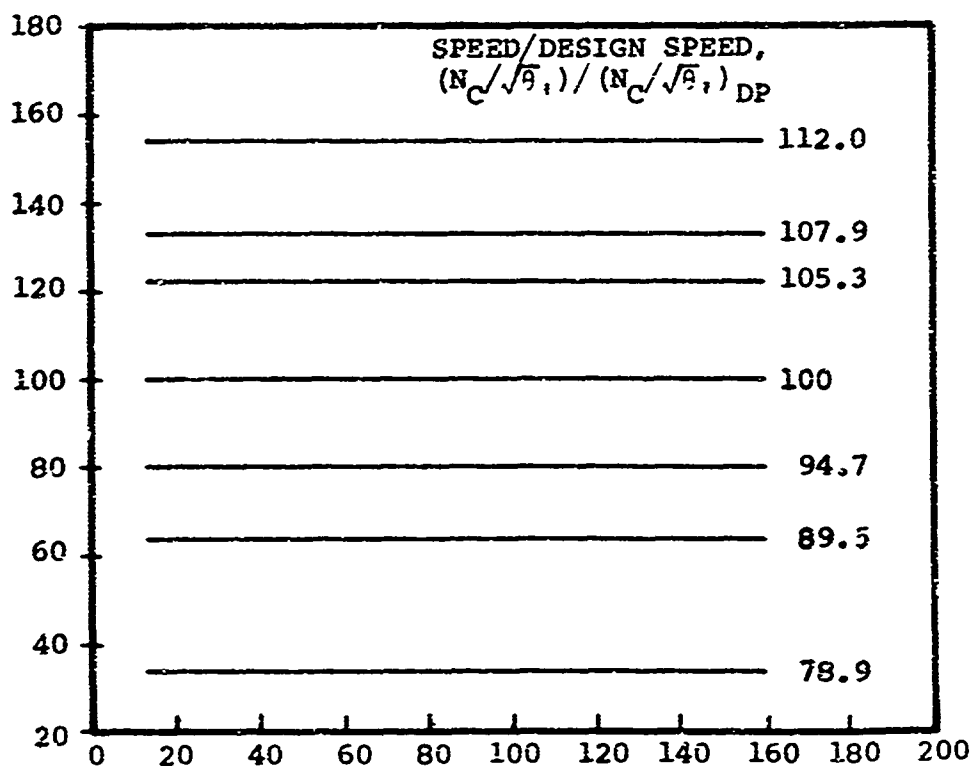


Figure 52. Power Turbine Map.

EFFICIENCY/DESIGN EFFICIENCY,
 $\eta_C/\eta_{C,DP}$ - PERCENT



PRESSURE RISE/DESIGN PRESSURE RISE,
 $(P_4/P_1-1)/(P_{4,DP}/P_1-1)$ - PERCENT



AIRFLOW/DESIGN AIRFLOW, $(W_1\sqrt{\theta_1}/\delta_1)/(W_{1,DP}\sqrt{\theta_1}/\delta_1)_{DP}$ - PERCENT

Figure 53. Idealized Compressor Map.
 Nondimensionalized From
 AA + C Data.

This map relates off-design component performance to design values. Design values for component efficiency have been estimated for various cycle pressure ratios and are presented in Appendix I.

The variation of efficiency and pressure-rise ratio with speed in accordance with this map is considered to be representative of the peak efficiency and corresponding pressure-rise ratio of a real two-stage axial plus centrifugal compressor configuration.

ENGINE ANALYSIS ASSUMPTIONS (OFF-DESIGN)

The engine off-design analysis was based on the following assumptions:

- (a) Cooling flow was fixed at 9 percent of the compressor through-flow and was assumed to bypass the gasifier turbine while producing work in the power turbine consistent with the cooling-air temperature.
- (b) Accessory horsepower was varied as a function of the gasifier speed in accordance with the following:
 $HP_{acc} = CN^2$.
- (c) Combustion efficiency was varied as a function of $\frac{P^2/W_{4A}}{(P^2/W_{4A})_{DP}}$ in accordance with Figure 54.
- (d) Combustor pressure loss was varied as a function of combustor inlet corrected flow in accordance with the following:

$$(\Delta P/P_4)_{combustor} = C_1 \left(\frac{W_{4A} \sqrt{\theta_4}}{\delta_4} \right)^2 (5.9 + T_5/T_4).$$

- (e) Pressure loss for the transition duct between the gasifier and the power turbines was varied as a function of duct inlet corrected flow in accordance

$$\text{with the following: } (\Delta P/P_7)_{duct} = C_2 \left(\frac{W_7 \sqrt{\theta_7}}{\delta_7} \right)^2.$$

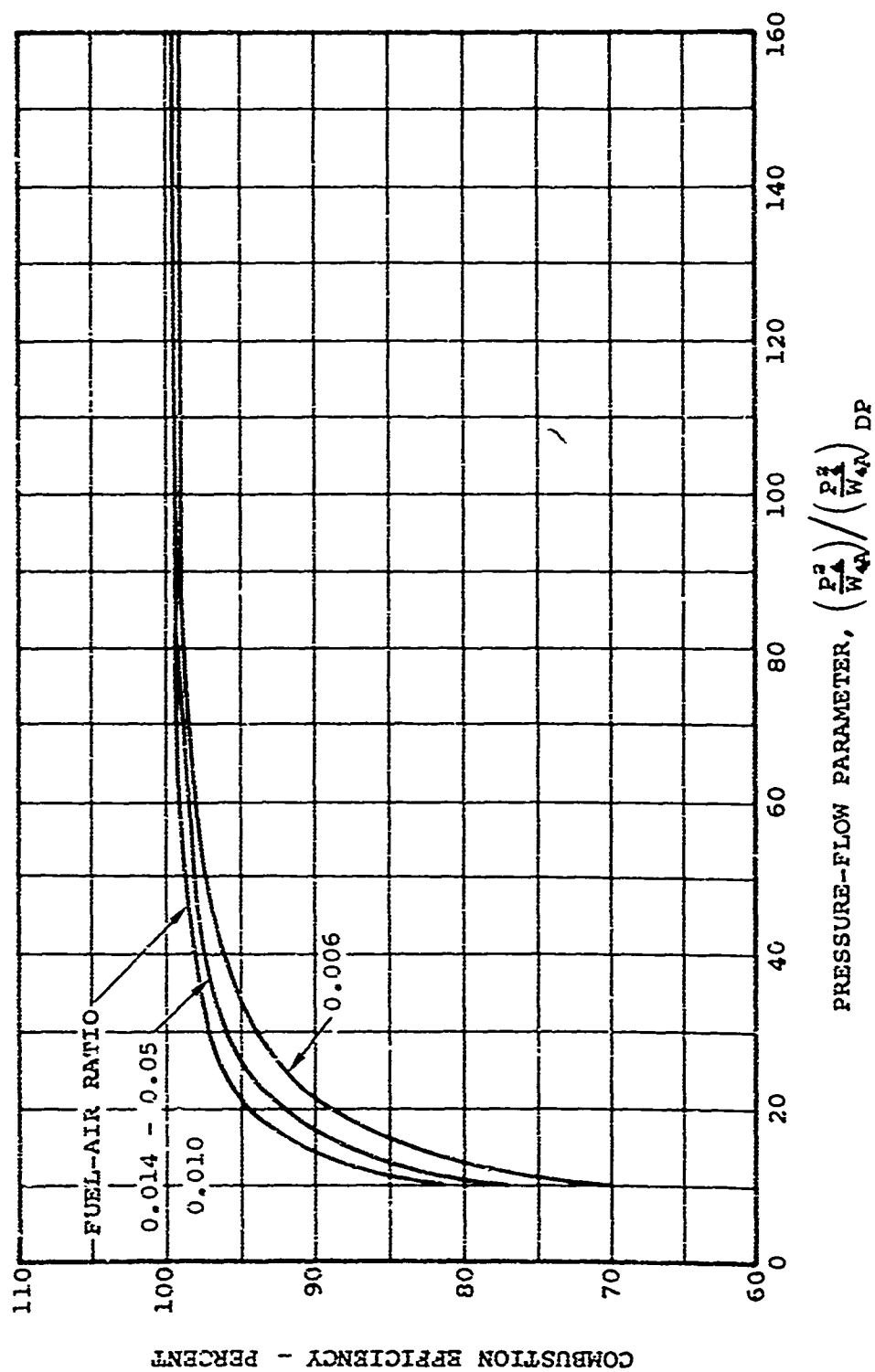


Figure 54. Combustion Efficiency Map, Nondimensionalized.

APPENDIX III

ENGINE CYCLE RELATIONSHIPS

INTRODUCTION

The matching of an axial compressor (single-stage or multi-stage) to a centrifugal compressor depends on the link between cycle requirements at design point and some off-design reference. Sometimes this link is simply between the maximum rated power at design point and a surge margin requirement at an off-design condition at some speed below design. In the case of the present matching study, besides providing for low-speed surge margin, the compressor match must be such that the engine power at design speed and flow is 60 percent of the power achievable at some speed above design at a TIT of 2500°F. To achieve a match that satisfies the cycle requirements, the compressors must be mated in a way that achieves the pressure ratios, flows, and speeds at the 60- and 100-percent-power points.

The objective of the study is to achieve as small an SFC as possible at 60-percent power without sacrificing performance at full power or stable operation at low power. A necessary condition for this achievement is the attainment of the highest possible overall compressor efficiency at the 60- and 100-percent-power points. A match that satisfies the pressure ratio, flow, and speed requirements at the two power points with fixed turbine geometry may not yield the maximum possible overall compressor efficiency at the two power points or adequate surge margin at low power points (30 percent, 20 percent). The cycle requirements may force a match at the high power points, which occurs off of peak efficiency on both the axial and the centrifugal compressor, and which forces low-power operation near the surge line of one of the compressors. Variable compressor geometry is then needed to achieve the desired match.

This section discusses the problems involved in the USAAVLABS axial/centrifugal compressor matching study and the use of variable inlet guide vanes, variable centrifugal compressor diffuser vanes, and twin spooling to satisfy all the cycle requirements.

ENGINE CYCLE ANALYSIS

The gasifier turbine has two stages which are connected together for the single-spool compressor configuration and which are separated for the twin-spool configuration. In the latter case, the first turbine drives the centrifugal

compressor and the second drives the axial compressor. Nine percent of the compressor flow is used for cooling in the gasifier turbine unit. The power turbine is free to rotate independently of the gasifier turbine; it rotates at a constant physical speed, since the engine is to be used for helicopter application. At the 60- and 100-percent-power points the gasifier and power turbines are choked.

It can be shown that, because the turbines are choked and because of the desirability of operating the gasifier turbine at peak efficiency, the pressure ratio across the gasifier turbine and its corrected flow and work remain invariant over the power range from 60 to 100 percent. The constancy of the gasifier corrected work contributes to determining the physical speed ratio that influences the compressor match. The pressure ratio and flow required of the match at 100-percent power depend on the percentage of power and compressor pressure ratio at the design point and the TIT at 100-percent power. The proof is shown in the following paragraphs.

Combustor loss, fuel flow, and leakage are neglected in this simplified analysis. If gasifier and power turbines are choked, then with cooling flow passing back into the flow path in front of the power turbine,

$$\frac{W_T \sqrt{T_5}}{P_5 A_5} = \frac{W_C \sqrt{T_7}}{P_7 A_7} = \text{Constant} \quad (9)$$

Consequently,

$$\frac{P_5}{P_7} = \frac{A_7}{A_5} \sqrt{\frac{T_5}{T_7}} \frac{W_T}{W_C} \quad (10)$$

Now the gasifier turbine pressure ratio can be expressed in terms of its actual temperature ratio and polytropic efficiency; namely,

$$\frac{P_5}{P_7} = \left(\frac{T_5}{T_7} \right)^{\frac{\gamma}{(\gamma-1)\eta_p}} \quad (11)$$

Equating (10) to (11) and rearranging,

$$\frac{W_T}{W_C} \frac{A_7}{A_6} = \left(\frac{T_6}{T_7} \right)^{\frac{\gamma}{(\gamma-1)\eta_p} - \frac{1}{2}} \quad (12)$$

If the turbine geometry is constant, if the polytropic efficiency is independent of T_6 , and if the percentage of cooling flow is constant, then

$$\frac{T_6}{T_7} = \text{constant and } \frac{P_6}{P_7} = \text{constant} \quad (13)$$

Turbine adiabatic efficiency varies with applied pressure ratio, as shown in Figure 55.

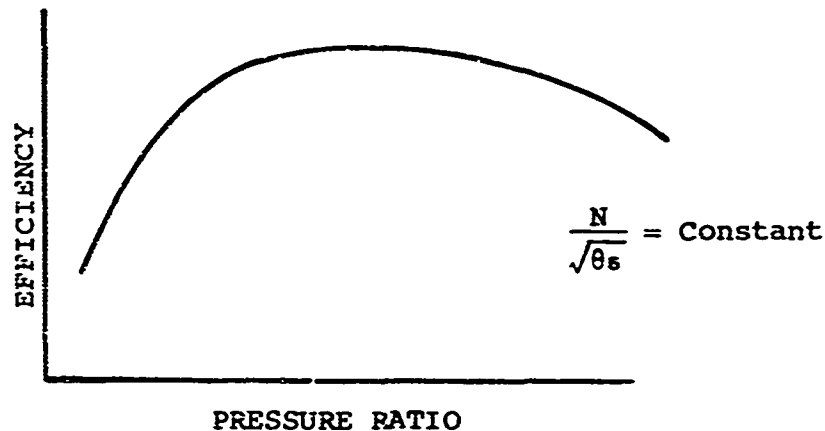


Figure 55. Typical Turbine Efficiency/Pressure Ratio Characteristic.

A similar plot can be shown for the variation of efficiency with corrected speed for a given pressure ratio. At peak efficiency,

$$\left. \frac{\partial \eta_T}{\partial (P_5/P_7)} \right|_{\frac{N}{\sqrt{\theta_5}} = \text{Const.}} = \left. \frac{\partial \eta_T}{\partial (N/\sqrt{\theta_5})} \right|_{P_5/P_7 = \text{Const.}} = 0$$

In fact, the efficiency curves are flat within experimental error over a small range of pressure ratios and speeds. If an increase in T_5 attempts to move the operating point to another place on the turbine map, the adiabatic and, hence, the polytropic efficiency can remain constant over a certain range of pressure ratios and speeds. But if the polytropic efficiency does not change, then for fixed turbine geometry, the temperature ratio across the turbine is invariant according to Equation (12). The gasifier turbine pressure and temperature ratios are therefore invariant with changes in T_5 as long as both turbines are choked and the operating point is on peak efficiency. When the gasifier turbine is choked, the corrected flow $W_{T_5} \sqrt{\theta_5/\delta_5}$ is constant and must be satisfied as T_5 changes.

The changes in compressor performance as T_5 changes determine the positions of the operating point on the turbine map. The statements of the previous paragraph are equivalent to saying that

$$\left(\frac{\Delta H}{\theta_5} \right)_{GT} = \text{constant} \quad (14)$$

Even though this is true, the values of work coefficient and rotational speed that combine to give this constant depend on the compressor work.

The compressor and turbine works can be expressed by

$$W_C \Delta H_C = W_C K_C N_C^2 \quad (15)$$

$$W_T \Delta H_T = W_T K_T N_T^2 \quad (16)$$

where K_C and K_T are kinds of work coefficients based on rotational speed. Equating the left sides of Equations (15) and (16) and using Equation (14),

$$\Delta H_C = (W_T/W_C) (\Delta H_T/T_5) T_5 \quad (17)$$

Hence, the ratio of compressor work at 100-percent power to that at 60-percent power is

$$\frac{\Delta H_{C100}}{\Delta H_{C60}} = \frac{[(W_T/W_C) T_5]_{100}}{[(W_T/W_C) T_5]_{60}} \quad (18)$$

Combining Equations (15) and (18),

$$N_{100} = N_{60} \sqrt{\frac{(W_T/W_C)_{100}}{(W_T/W_C)_{60}}} \sqrt{\frac{T_5_{100}}{T_5_{60}}} \sqrt{\frac{K_C_{60}}{K_C_{100}}} \quad (19)$$

For constant percentage of cooling flow and compressor work coefficients, the compressor rotational speed changes proportionately with the square root of the TIT. However, as compressor efficiency falls off, the less the difference is between N_{100} and N_{60} . For constant gasifier corrected work

[Equation (14)], turbine work coefficient must be increased as speed decreases. This can also be observed by equating the right sides of Equations (15) and (16):

$$\sqrt{W_C/W_T} N_C/N_T = \sqrt{K_T/K_C} \quad (20)$$

For constant percentage of cooling flow, and since

$$N_C/N_T = 1 \quad (21)$$

then

$$K_T/K_C = \text{constant} \quad (22)$$

Hence, as the compressor work coefficient increases, so does the turbine work coefficient.

To complete the determination of the speed ratio in Equation (19), it is necessary to determine the TIT ratio. It can be shown that this is a function of the compressor efficiency variation with speed and the selection of the design-point power ratio.

The power ratio, PR, is the power at design point (DP) divided by maximum power (100).

$$PR = \frac{\Delta H_{PTDP} W_{DP}}{\Delta H_{PT100} W_{100}} \quad (23)$$

The compressor specific work can be expressed in terms of its pressure ratio and polytropic efficiency, η_{CP} , as

$$\Delta H_C = \left[\left(\frac{P_4}{P_1} \right)^{\frac{\gamma-1}{\gamma \eta_{CP}}} - 1 \right] C_{P_1} T_1 \quad (24)$$

The gasifier turbine pressure ratio can be expressed in terms of the compressor work. From Equations (24) and (17),

$$\begin{aligned} \frac{P_6}{P_7} &= \left(\frac{T_6}{T_7} \right)^{\frac{\gamma}{(\gamma-1)\eta_{TP}}} = \left[1 + \frac{\Delta H_{GT}}{C_{P_7} T_7} \right]^{\frac{\gamma}{(\gamma-1)\eta_{TP}}} \\ &= \left[1 + \frac{C_{P_1} T_1 W_C}{C_{P_7} T_7 W_T} \left(\left(\frac{P_4}{P_1} \right)^{\frac{\gamma-1}{\gamma \eta_{CP}}} - 1 \right) \right]^{\frac{\gamma}{(\gamma-1)\eta_{TP}}} \end{aligned}$$

The pressure ratio across the power turbine at design-point power is

$$\begin{aligned}
 \left(\frac{P_7}{P_8}\right)_{DP} &= \frac{\left(\frac{P_4}{P_1}\right)_{DP}}{\left(\frac{P_5}{P_7}\right)_{DP}} \\
 &= \frac{\left(\frac{P_4}{P_1}\right)_{DP}}{\left[1 + \frac{C_{P_1} T_1 W_C}{C_{P_7} T_7 W_T} \left\{ \left(\frac{P_4}{P_1}\right)^{\frac{\gamma-1}{\gamma \eta_{CP}}} - 1 \right\}\right]_{DP}^{\frac{\gamma}{(\gamma-1) \eta_{TP}}}}
 \end{aligned} \tag{25}$$

The power turbine enthalpy change at design-point power is

$$\Delta H_{PTDP} = \left[\left(\frac{P_7}{P_8}\right)_{DP}^{\frac{\gamma-1}{\gamma} \eta_{TP}} - 1 \right] \left(C_{P_7} T_7 \right)_{DF} \left(\frac{T_8}{T_7} \right)_{DP} \tag{26}$$

Since it has just been shown above that

$$\left(\frac{P_6}{P_7}\right)_{DP} = \left(\frac{P_6}{P_7}\right)_{100}$$

then

$$\left(\frac{P_7}{P_8}\right)_{100} = \frac{\left(\frac{P_4}{P_1}\right)_{100}}{\left(\frac{P_6}{P_7}\right)_{DP}} \tag{27}$$

Substituting Equations (25) and (26) into Equation (23), we get

$$PR = \frac{\left\{ \left[\frac{(P_4/P_1)_{DP}}{1 + \left(\frac{C_{P_1} T_1 W_C}{C_{P_7} T_7 W_T} \right)} \left(\left(\frac{P_4}{P_1} \right)_{DP}^{\frac{\gamma-1}{\gamma} \eta_{TP}} - 1 \right) \right]^{\frac{\gamma}{(\gamma-1) \eta_{TP}}} \right\}^{\frac{\gamma-1}{\gamma} \eta_{TP}} - 1 \left(C_{P_7} T_7 W_7 \right)_{DP} \left(\frac{T_8}{T_7} \right)_{DP}}{\left\{ \left[\frac{(P_4/P_1)_{100}}{1 + \left(\frac{C_{P_1} T_1 W_C}{C_{P_7} T_7 W_T} \right)} \left(\left(\frac{P_4}{P_1} \right)_{100}^{\frac{\gamma-1}{\gamma} \eta_{TP}} - 1 \right) \right]^{\frac{\gamma}{(\gamma-1) \eta_{TP}}} \right\}^{\frac{\gamma-1}{\gamma} \eta_{TP}} - 1 \left(C_{P_7} T_7 W_7 \right)_{100} \left(\frac{T_8}{T_7} \right)_{100}} \quad (28)$$

Since the turbines are choked, and using Equation (13),

$$\frac{W_{DP}}{W_{100}} \sqrt{\frac{T_{7DP}}{T_{7100}}} = \frac{W_{DP}}{W_{100}} \sqrt{\frac{T_{8DP}}{T_{8100}}} = \frac{(P_4/P_1)_{DP}}{(P_4/P_1)_{100}} \quad (29)$$

$$\begin{aligned} \frac{\left(\frac{T_8}{T_7} \right)_{DP}}{\left(\frac{T_8}{T_7} \right)_{100}} &= \frac{\left(\frac{P_8}{P_7} \right)_{DP}^{\frac{\gamma-1}{\gamma} \eta_{TP}}}{\left(\frac{P_8}{P_7} \right)_{100}^{\frac{\gamma-1}{\gamma} \eta_{TP}}} \\ &= \frac{\left[\frac{P_8/P_7}{P_4/P_1} \right]_{DP}^{\frac{\gamma-1}{\gamma} \eta_{TP}}}{\left[\frac{P_8/P_7}{P_4/P_1} \right]_{100}^{\frac{\gamma-1}{\gamma} \eta_{TP}}} \end{aligned}$$

Since

$$\left(\frac{P_8}{P_7} \right)_{DP} = \left(\frac{P_8}{P_7} \right)_{100}$$

$$\frac{\left(\frac{T_6}{T_7}\right)_{DP}}{\left(\frac{T_6}{T_7}\right)_{100}} = \frac{\left(\frac{P_4}{P_1}\right)^{\frac{\gamma-1}{\gamma}} \eta_{TP}}{\left(\frac{P_4}{P_1}\right)^{\frac{\gamma-1}{\gamma}}_{DP} \eta_{TP}} \quad (30)$$

Again, from Equation (13),

$$T_{7100} = T_{7DP} \left(\frac{T_{6100}}{T_{6DP}} \right) \quad (31)$$

Since

$$T_7 = \frac{T_6}{\left(\frac{T_6}{T_7}\right)} = \frac{T_6}{1 + \frac{C_{P1}}{C_{P7}} \frac{T_1}{T_7} \left[\left(\frac{P_4}{P_1}\right)^{\frac{\gamma-1}{\gamma} \eta_{CP}} - 1 \right] \left(\frac{W_C}{W_T}\right)}$$

then

$$T_{7DP} = T_{5DP} - \frac{C_{P_1} T_1}{C_{P_7 DP}} \left\{ \left(\frac{P_4}{P_1} \right)_{DP}^{\frac{\gamma-1}{\gamma \eta_{CP}}} - 1 \right\} \left(\frac{W_C}{W_T} \right)_{DF} \quad (32)$$

Equation (31) becomes, after substituting (32),

$$T_{7100} = \left[T_{5DP} - \frac{C_{P_1} T_1}{C_{P_7 DP}} \left\{ \left(\frac{P_4}{P_1} \right)_{DP}^{\frac{\gamma-1}{\gamma \eta_{CP}}} - 1 \right\} \left(\frac{W_C}{W_T} \right)_{DF} \right] \frac{T_{5100}}{T_{5DP}} \quad (33)$$

Substituting Equations (29), (30) and (33) into Equation (28), we get

$$\left[\frac{(P_4/P_1)_{DF}}{1 - \frac{C_{P_1} T_1 \left\{ \left(\frac{P_4}{P_1} \right)_{DP}^{\frac{\gamma-1}{\gamma \eta_{CP}}} - 1 \right\} \left(\frac{W_C}{W_T} \right)_{DF}}{C_{P_7 DP} \left[\left(\frac{T_{5DP}}{T_{5100}} \right) T_{5100} - \frac{C_{P_1} T_1}{C_{P_7 DP}} \left\{ \left(\frac{P_4}{P_1} \right)_{DP}^{\frac{\gamma-1}{\gamma \eta_{CP}}} - 1 \right\} \left(\frac{W_C}{W_T} \right)_{DF} \right]}} \right]^{\frac{\gamma-1}{\gamma} \tau_{TP}} - 1 \quad (34)$$

$$\left[\frac{(P_4/P_1)_{100}}{1 - \frac{C_{P_1} T_1 \left\{ \left(\frac{P_4}{P_1} \right)_{DP}^{\frac{\gamma-1}{\gamma \eta_{CP}}} - 1 \right\} \left(\frac{W_C}{W_T} \right)_{DF}}{C_{P_7 DP} \left[\left(\frac{T_{5DP}}{T_{5100}} \right) T_{5100} - \frac{C_{P_1} T_1}{C_{P_7 DP}} \left\{ \left(\frac{P_4}{P_1} \right)_{DP}^{\frac{\gamma-1}{\gamma \eta_{CP}}} - 1 \right\} \left(\frac{W_C}{W_T} \right)_{DF} \right]}} \right]^{\frac{\gamma-1}{\gamma} \tau_{TP}} - 1$$

Combining Equations (18) and (24), we get

$$\frac{T_{s_{DP}}}{T_{s_{100}}} = \frac{\left[\left(\frac{P_4}{P_1} \right)_{DP}^{\frac{\gamma-1}{\gamma \eta_{CP}}} - 1 \right] \left(\frac{W_T}{W_C} \right)_{100}}{\left[\left(\frac{P_4}{P_1} \right)_{100}^{\frac{\gamma-1}{\gamma \eta_{CP}}} - 1 \right] \left(\frac{W_T}{W_C} \right)_{DP}} \quad (35)$$

Equations (34) and (35) show that the compressor pressure ratio at 100-percent power is a function of the compressor pressure ratio at design-point power, the TIT at 100-percent power, and the fraction of compressor flow used for turbine cooling at design point and 100-percent power, under the assumptions of negligible differences in C_p and the component polytropic efficiencies over the power range. For the matching study,

$$W_C/W_T = \text{constant}$$

Therefore, the compressor pressure ratio is fixed for specified values of power fraction at design point and TIT at 100-percent power. In consequence, the TIT ratio between design point and full power is determined [Equation (35)], as is also the flow ratio [Equation (29)]. For the present study, the power percentage at design point is 0.60 and the TIT at 100-percent power is 2500°F.

Note that the pressure ratio, TIT, and flow ratios between design point and 100-percent power are the same whether the compressor is single- or twin-spoiled. The speed relationship in Equation (21), however, is true only for a single-spool compressor. In the case of the twin-spool configuration, the flow and pressure-ratio fractions will determine the speed ratio. The axial compressor has a larger corrected flow difference than the centrifugal compressor between 60- and 100-percent powers. Consequently, the axial compressor speed ratio will increase with twin spooling. The

centrifugal compressor corrected flow ratio depends on the inducer inlet conditions. The axial compressor pressure ratio will not change with spool configuration, but the efficiency can change as a result of the speed ratio. If the match is near peak efficiency, the change will be small, and, hence, the centrifugal compressor speed ratio will change very little with change in spool configuration.

The power ratio can be written as

$$PR = \frac{\left[\left(\frac{P_7}{P_3} \right)_{DP}^{\frac{\gamma-1}{\gamma}} \eta_{TP} - 1 \right] \left(C_{P_7} T_7 W_C \right)_{DP} \left(\frac{P_4}{P_1} \right)_{100}^{\frac{\gamma-1}{\gamma}} \eta_{TP}}{\left[\left(\frac{P_7}{P_3} \right)_{DP} \left(\frac{P_6/P_1}{P_4/P_1} \right)_{DP} \frac{100}{100} \right]^{\frac{\gamma-1}{\gamma}} \eta_{TP} - 1} \left(C_{P_7} T_7 W_C \right)_{100} \left(\frac{P_4}{P_1} \right)_{DP}^{\frac{\gamma-1}{\gamma}} \eta_{TP}$$

Assuming constant specific heat, substituting Equations (29) and (35), and rearranging, we get, for constant cooling-flow fraction,

$$PR = \frac{\left(\frac{P_6}{P_1} \right)_{DP}^{\frac{\gamma-1}{\gamma}} \eta_{TP} \left(\frac{P_4}{P_1} \right)_{100} \left[\left(\frac{P_4}{P_1} \right)_{100}^{\frac{\gamma-1}{\gamma} \eta_{CP}} - 1 \right]^{1/2} \left[\left(\frac{P_7}{P_3} \right)_{DP}^{\frac{\gamma-1}{\gamma}} \eta_{TP} - 1 \right]}{\left(\frac{P_4}{P_1} \right)_{100}^{\frac{\gamma-1}{\gamma}} \eta_{TP} \left(\frac{P_4}{P_1} \right)_{DP} \left[\left(\frac{P_4}{P_1} \right)_{DP}^{\frac{\gamma-1}{\gamma} \eta_{CP}} - 1 \right]^{1/2} \left[\left(\frac{P_7}{P_3} \right)_{DP} \left(\frac{P_6/P_1}{P_4/P_1} \right)_{DP} \frac{100}{100} \right]^{\frac{\gamma-1}{\gamma}} \eta_{TP} - 1} \quad (36)$$

If the right side of Equation (36) were constant or changed very little with power turbine pressure ratio, the ratio of the compressor pressure ratio at the two power points would be constant or would change very little. The power turbine pressure ratio at design point depends on the TIT at design point. A fixed ratio of pressure was assumed, and the right side of Equation (36) was evaluated at four TIT's: 1600°F, 1800°F, 2000°F, and 2200°F. The ratio of the value of the right side of Equation (36) at 2000°F to that value at any other temperature is plotted in Figure 56. The plot shows that the right side of Equation (36) is approaching a constant value at temperatures above 2000°F. In fact, it varies ± 3 percent

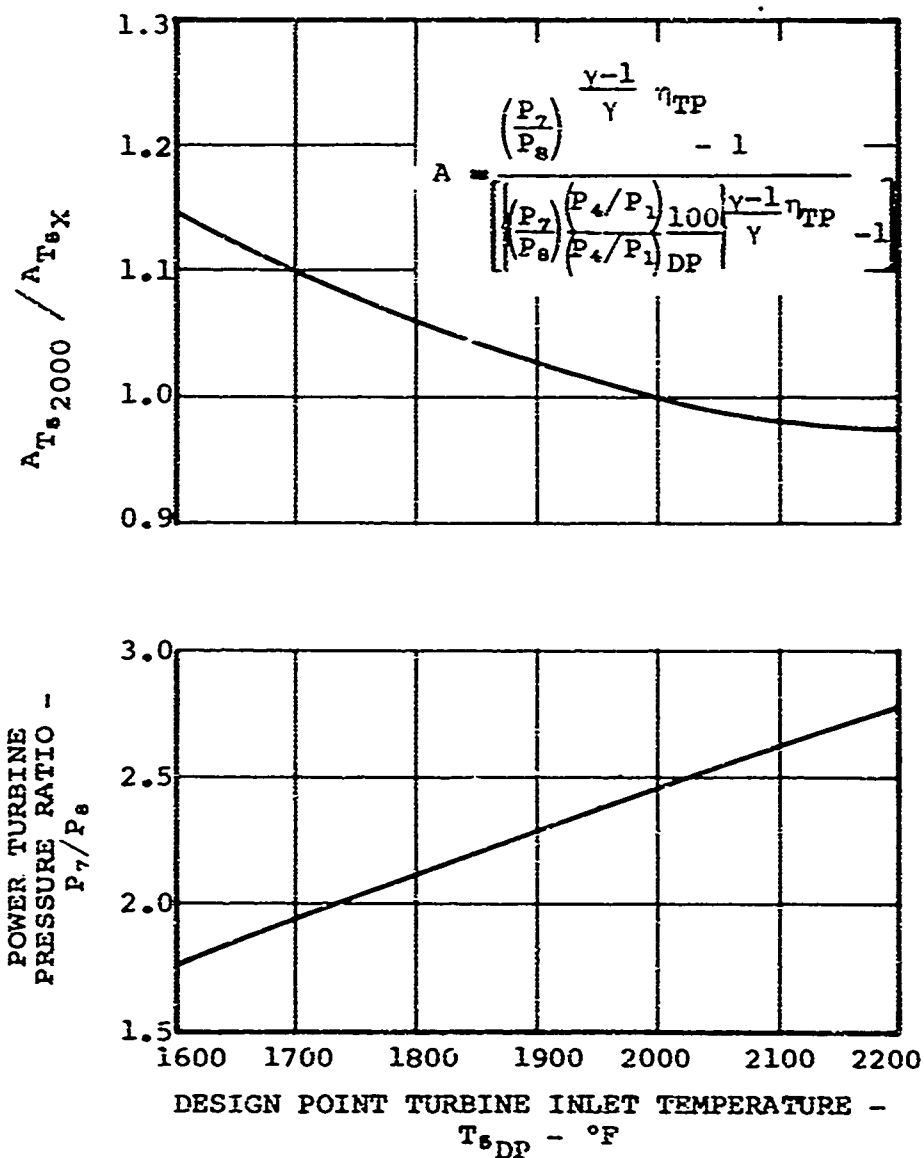


Figure 56. Variation of the Rotor of Power Turbine Work Ratio at $T_s = 2000^\circ\text{F}$ to Work Ratio at $T_s = X$ With Design Point Turbine Inlet Temperature for $1600^\circ\text{F} < x < 2200^\circ\text{F}$

between 1900°F and 2200°F. To a first approximation, then, the change in pressure ratio between design point and full power is determined by the power ratio. This, in turn, means that the flow and TIT ratios are set by the power ratio. To a very close approximation, then, for design-point TIT above 2000°F, the flow, compressor pressure-ratio, and TIT ratios are determined by the specification of design-point power fraction.

Equation (36) can then be rewritten as

$$\frac{\left(\frac{P_4}{P_1}\right)_{100}^{1-\frac{\gamma-1}{\gamma}} \eta_{TP} \left[\left(\frac{P_4}{P_1}\right)_{100}^{\frac{\gamma-1}{\gamma \eta_{CP}}} - 1 \right]^{1/2}}{\left(\frac{P_4}{P_1}\right)_{DP}^{1-\frac{\gamma-1}{\gamma}} \eta_{TP} \left[\left(\frac{P_4}{P_1}\right)_{DP}^{\frac{\gamma-1}{\gamma \eta_{CP}}} - 1 \right]^{1/2}} \approx \frac{\text{CONSTANT}}{\text{PR}} \quad (37)$$

Equation (37) shows that the compressor pressure-ratio difference increases as power ratio decreases. Thus, the lower the specified design-point power fraction is, the more difficult the compressor matching becomes. Relative flow and pressure-ratio values between design point and 100-percent power increase; thus, available flow range from surge to choke is taken up. The TIT at design power decreases; thus, SFC for a given design-point pressure ratio is raised.

If the compressor polytropic efficiency change from design point to 100-percent power is very small, Equation (37) shows that the pressure ratio at 100-percent power is primarily a function of design-point power ratio for a given value of design-point pressure ratio. Under the same assumption, Equation (35) shows that the TIT ratio is determined by the design-point and 100-percent power-point pressure ratios. Therefore, the temperature ratio is also determined primarily by the power ratio. Consequently, the speed ratio in Equation (19) is primarily determined by the design-point power ratio, for fixed percentage of cooling flow and compressor work coefficients between design point and 100-percent power. Finally, Equation (29) shows that under the same logic, the flow ratio is also determined from the selection of design-point power ratio.

APPENDIX IV

INLET GUIDE VANE ANALYSIS

The purpose of this appendix is to derive and display the relationships that were used to shift the pressure ratio air-flow characteristics of the axial compressor with the application of preswirl. The theory is applied to aerodynamic conditions at the mean line of the axial compressor rotor. Two-dimensionality (constant streamline radius) is assumed, along with the constancy of the axial velocity across the rotor. The equations are derived for a reference condition of the same inlet air angle (relative to the rotor) at the zero preswirl reference point and the nonzero preswirl point of interest.

The stage pressure ratio can be written in terms of the temperature for the ideal enthalpy rise and stage efficiency.

$$\begin{aligned} \frac{P_2}{P_1} &= \left(\frac{T_2}{T_1} \right)^{\frac{\gamma}{\gamma-1}} = \left[1 + \frac{C_p \Delta T'}{C_p T_1} \right]^{\frac{\gamma}{\gamma-1}} = \left[1 + \frac{\eta_c \Delta H}{C_p T_1} \right]^{\frac{\gamma}{\gamma-1}} \\ \frac{P_2}{P_1} &= \left[1 + \frac{\eta_c U \Delta W}{g J C_p T_1} \right]^{\frac{\gamma}{\gamma-1}} \\ &= \left[1 + \frac{\eta_c U V_z (T_{N\beta_1} - T_{N\beta_2})}{g J C_p T_1} \right]^{\frac{\gamma}{\gamma-1}} \end{aligned} \quad (38)$$

The axial velocity can be written as

$$V_z = \frac{U}{T_{N\beta_1} + T_{N\beta_2}} \quad (39)$$

Substituting Equation (39) into Equation (38), we get

$$\frac{P_2}{P_1} = \left[1 + \frac{\frac{\eta_c U^2}{TN\beta_1 + TN\beta_s} (TN\beta_1 - TN\beta_s)}{gJC_p T_1} \right]^{\frac{\gamma}{\gamma-1}} \quad (40)$$

The flow change is computed from the continuity equation.

$$\begin{aligned} W_C &= \rho_{s1} V_z A_1 \lambda_1 = \left(\frac{\rho_s}{\rho_t} \right)_1 \rho_{t1} V_z A_1 \lambda_1 \\ &= \left(\frac{t}{T} \right)_1^{\frac{1}{\gamma-1}} \rho_{t1} V_z A_1 \lambda_1 = \left[1 - \frac{\Delta T}{T_1} \right]^{\frac{1}{\gamma-1}} \rho_{t1} V_z A_1 \lambda_1 \\ W_C &= \left[1 - \frac{V_z^2 \sec^2 \beta_s}{2gJC_p T_1} \right]^{\frac{1}{\gamma-1}} \rho_{t1} V_z A_1 \lambda_1 \\ &= \left[1 - \frac{U^2 \sec^2 \beta_s}{(TN\beta_1 + TN\beta_s)^2 2gJC_p T_1} \right]^{\frac{1}{\gamma-1}} \frac{\rho_{t1} A_1 \lambda_1 U}{TN\beta_1 + TN\beta_s} \quad (41) \end{aligned}$$

Equations (40) and (41) were used to compute the following ratios:

$$\begin{array}{ccc} \frac{P_2}{P_1} \Big|_{\beta_s \neq 0} & \frac{P_2}{P_1} \Big|_{\beta_s \neq 0}^{-1} & \frac{W_C}{W_C} \Big|_{\beta_s \neq 0} \\ \hline \frac{P_2}{P_1} \Big|_{\beta_s = 0} & \frac{P_2}{P_1} \Big|_{\beta_s = 0}^{-1} & \frac{W_C}{W_C} \Big|_{\beta_s = 0} \end{array}$$

SUPPLEMENTARY

INFORMATION



DEPARTMENT OF THE ARMY
U. S. ARMY AIR MOBILITY RESEARCH & DEVELOPMENT LABORATORY
EUSTIS DIRECTORATE
FORT EUSTIS, VIRGINIA 23604

ERRATUM

USAAVLABS Technical Report 70-34, October 1970

TITLE: A Small Axial-Centrifugal Compressor Matching Study Program

Make the following pen and ink change:

Figure 4, page 11 - The ordinate values shown on Figure 44 are in error by 5 percentage points. The ordinate should be changed to encompass efficiencies of 75 to 100 percent rather than 70 to 95 percent as now shown.